ABSTRACT

Title of Dissertation: **AN EXPERIMENTAL INVESTIGATION OF THE FLEXURAL RESISTANCE OF HORIZONTALLY CURVED STEEL I-GIRDER SYSTEMS**

Joseph Lawrence Hartmann, Doctor of Philosophy, 2005

Dissertation Directed By: **Professor Emeritus Pedro Albrecht and Affiliated Associate Professor Chung Fu, Department of Civil and Environmental Engineering**

In 1998 the Federal Highway Administration (FHWA) began executing the experimental component of a multi-year program investigating horizontally curved steel I-girder bridges. This experimental program consists of full-scale testing to determine the effects of horizontal curvature on the structural performance of I-girders subject to moment and shear, to investigate moment/shear interaction, and to assess the behavior and ultimate capacity of a composite bridge.

The experiments that are the focus of this dissertation are the component tests designed to determine the bending strength of horizontally curved steel I-girders. These tests were conducted at full-scale using a 3-girder system in order to eliminate concerns with modeling and scaling of the results. Also, the boundary conditions supplied to the components by the full-scale 3-girder system are considered to be comparable if not equal to those produced on real bridges.

The seven bending component tests were designed to examine the influence of compression flange slenderness, web slenderness and transverse stiffener spacing on bending capacity. The components were loaded within a constant moment region of the test frame eliminating applied vertical shear loads from affecting their performance. For each test, an attempt was made to capture the strains due to installation of the component into the test frame and the strain due to dead-load deflection, as well as the strains due to the applied loading.

AN EXPERIMENTAL INVESTIGATION OF THE FLEXURAL RESISTANCE OF HORIZONTALLY CURVED STEEL I-GIRDER SYSTEMS

By

Joseph Lawrence Hartmann

Dissertation submitted to the Faculty of the Graduate School of the
University of Maryland, College Park, in partial fulfillment
of the requirements for the degree of
Doctor of Philosophy
2005

Advisory Committee:
Professor Emeritus Pedro Albrecht, Chair
Affiliated Associate Professor Chung Fu, Co-Chair
Professor Amde Amde
Professor Amr Baz, Dean's Representative
Professor Emeritus Bruce Donaldson

© Copyright by
Joseph Lawrence Hartmann
2005

Preface

This report is one of several that will include data and analyses specific to the Curved Steel Bridge Research Project conducted at the Federal Highway Administration's Turner-Fairbank Highway Research Structures Laboratory. This multi-year project investigated the effects of horizontal curvature on steel I-girder systems during erection, subject to uniform moment, subject to moment-shear interaction, and in composite construction. This report is specific to the experimental results of the investigation on uniform moment.

The Curved Steel Bridge Research Project was a pooled-fund effort. In addition to the Federal Highway Administration, the following state Departments of Transportation contributed funding to this project: Alabama, Arkansas, California, Florida, Georgia, Iowa, Illinois, Kansas, Kentucky, Louisiana, Minnesota, Missouri, Nebraska, Nevada, New Hampshire, New Jersey, New York, North Carolina, Oklahoma, Tennessee, Texas, Utah, Virginia, Wisconsin, and Wyoming.

Dedication

To my wife, Tracy, and daughters, Sara and Hannah.

Acknowledgements

The author wishes to gratefully acknowledge the contributions made to this report by his advisor, Professor Emeritus Pedro Albrecht, and co-advisor, Affiliated Associate Professor Chung Fu. In particular, the author would like to thank Dr. Albrecht for the steadfast support and encouragement he has provided during 15 years of graduate school advisement.

The author would also like to recognize the direct and indirect contributions made to this report by Dr. William Wright (Federal Highway Administration), Professor Donald White (Georgia Institute of Technology), and Mr. Michael Grubb (BSDI Ltd.). The author is pleased to be able to refer to these gentlemen as mentors, colleagues and friends.

Finally, the author wishes to thank his colleagues at the Turner-Fairbank Highway Research Center Structures Laboratory who were a part of the Curved Steel Bridge Research Project for their contributions to this report; Mr. Zuhan Xi, Dr. Hernando Chandra and Dr. Fassil Beshah. Without their professionalism and participation, these experiments and this report would not have been a success.

Table of Contents

List of Tables

List of Figures

List of Abbreviations

A	=	I-girder cross-sectional area
AF	=	1^{st} order lateral flange bending stress amplification factor
Bi	=	bimoment
C_b	=	moment gradient correction factor
C_w	=	warping constant
D	=	web depth
D_c	=	depth of web in compression in the elastic range
E	=	modulus of elasticity of steel
E_{st}	=	strain hardening modulus
F_{bs}	=	critical average flange stress
F_{cr}	=	critical average flange stress or critical compressive longitudinal stress in the web for the Guide Specifications; critical buckling stress for the Unified Design Method
F_{cr1}	=	critical average flange stress calculated from reduction factors
F_{cr2}	=	critical average flange stress determined from partial yielding
F_n	=	nominal flexural resistance in terms of stress
F_{nc}	=	nominal flexural resistance of the compression flange in terms of stress
$F_{nc(FLB)}$	=	nominal flexural resistance of the compression flange based on flange local buckling in terms of stress
$F_{nc(LTB)}$	=	nominal flexural resistance of the compression flange based on lateral torsional buckling in terms of stress
F_{nt}	=	nominal flexural resistance of the tension flange in terms of stress
F_y	=	specified minimum yield strength of steel
F_{yc}	=	specified minimum yield strength of compression flange steel
F_{yt}	=	specified minimum yield strength of tension flange steel
F_{yw}	=	specified minimum yield strength of web plate steel
I_x	=	moment of inertia about the x-axis
I_y	=	moment of inertia about the y-axis
L_b	=	unbraced length
L_p	=	lateral bracing limit for flexural capacity governed by plastic bending
L_r	=	lateral bracing limit for flexural capacity governed by inelastic lateral torsional buckling
M_{lat}	=	lateral flange bending moment
M_n	=	nominal vertical bending moment
M_x	=	moment about x-axis
M_x^{yield}	=	moment about x-axis that will cause yield in the compression flange
M_y	=	moment about y-axis
P_z	=	axial force in the z-direction
R	=	girder radius; minimum girder radius within a panel or over a specified length
R_b	=	flange-stress reduction factor to account for load shedding from web buckling
R_h	=	flange-stress reduction factor to account for load shedding from hybrid web yielding

S_{xc}	=	section modulus with respect to the compression flange
W_n	=	normalized unit warping
b	=	minimum flange width
b_f	=	flange width
b_{fc}	=	compression flange width
b_{ft}	=	tension flange width
d_o	=	actual distance between transverse stiffeners
d_s	=	distance between longitudinal stiffener and compression flange
f_b	=	calculated factored average flange stress at the section under consideration
f_{bu}	=	flexural flange stress due to primary bending from factored loads
f_{l1}	=	1st order lateral flange bending stress
f_l	=	2nd order lateral flange bending stress or 1st order lateral flange bending stress corrected with AF
k	=	coefficient of web bend-buckling
l	=	unbraced length
r_t	=	radius of gyration of the compression flange taken about the vertical axis
t_f	=	flange thickness
t_{fc}	=	thickness of the compression flange
t_s	=	transverse web stiffener thickness
t_t	=	thickness of the tension flange
t_w	=	web thickness
x	=	normal distance to the x-axis
y	=	normal distance to the y-axis
y_{NA}	=	distance from web mid-depth to neutral axis
y_{SC}	=	distance from neutral axis to shear center
ε	=	longitudinal strain
ε_{eng}	=	engineering strain
ε_{st}	=	strain at the onset of strain hardening
ε_{true}	=	true strain
ε_u	=	strain at tensile strength
λ_f	=	compression flange slenderness parameter
λ_{pf}	=	limiting slenderness parameter for compact flange local buckling behavior
λ_{rf}	=	limiting slenderness parameter for non-compact flange local buckling behavior
ρ_b	=	curvature factor for non-compact flange strength
ρ_w	=	curvature factor for non-compact flange strength
ρ_{w1}	=	curvature factor for non-compact flange strength
ρ_{w2}	=	curvature factor for non-compact flange strength
$\bar{\rho}_b$	=	curvature factor for compact flange strength
$\bar{\rho}_w$	=	curvature factor for compact flange strength
σ_{eng}	=	engineering stress
σ_{sy}	=	static yield strength
σ_{true}	=	true stress
σ_u	=	tensile strength

σ_z	=	stress in the z-direction
$\sigma_{0.2\%}$	=	offset yield strength
φ_f	=	resistance factor for flexure

Chapter 1. Introduction

1.1 Background/Problem

Horizontally curved girder bridges represent approximately 30% of the steel bridge market in the United States today. The current market share is a significant increase from 25 years ago when these types of structures represented only a single digit percentage of the market. The increased use of this bridge type reflects the significant attention that is now given to land usage, aesthetics, and complex roadway and viaduct alignments that are mostly found in and around urban centers.

The first significant investigations into the design and analysis of horizontally curved steel I-girder bridges began in 1969. At that time, the Federal Highway Administration (FHWA) formed the Consortium of University Research Teams (CURT). This group consisted of researchers from Carnegie-Mellon University, the University of Pennsylvania, the University of Rhode Island, and Syracuse University. CURT's analytical and experimental work, combined with research efforts conducted at the University of Maryland, formed the basis for the American Association of State Highway and Transportation Officials' (AASHTO) Guide Specification for Horizontally Curved Highway Bridges (herein referred to as the Guide Specifications). This document was first issued in 1980 and was subsequently updated in 1993 and 2003. However, the document was never adopted by AASHTO as a full or standard specification because of knowledge gaps that existed in the entire design and analysis processes for this type of bridge.

In the early 1990s, the *Curved Steel Bridge Research Project* (CSBRP) was initiated. This project focuses on the area of horizontally curved steel girders. The research project participants include the FHWA, the Transportation Research Board (TRB), and the participating states of the Highway Planning and Research (HP&R) study. The primary objective of this research study is to better define the behavior of such bridges. The study involves theoretical work leading to the development of refined predictor equations and to the verification of those equations through linear and non-linear analyses and experimental testing.

The CSBRP effort was largely based on recommendations of the Structural Stability Research Council's (SSRC) Task Group 14 [SSRC (1991)]. Several priorities were identified for research by the SSRC group:

- develop an understanding of construction issues including fabrication and erection
- determine nominal bending and shear strengths
- understand the behavior of diaphragms, cross-frames, and lateral bracings
- define the effect of lateral loads
- determine the level of analysis needed for analyzing curved girders
- determine serviceability issues

The goals of the CSBRP were to address these knowledge gaps, to generate enough information to improve the current Guide Specifications, and to incorporate curved steel girder design provisions into the AASHTO LRFD Bridge Design Specifications (herein referred to as the LRFD Specifications).

The Guide Specifications is the only consensus document available to the bridge community that supports the design and construction of horizontally curved steel I-girder bridges. In its current form, the guide is disjointed and difficult to follow. The commentary in the guide is incomplete and lacks the necessary details needed to explain the development of many of the provisions. Many of the original key references are not available to most designers. And when the references are available, they require a great deal of interpretation. The general lack of comprehensible support material available for understanding and clarifying the Guide Specifications can lead to misinterpretation of its provisions. This misinterpretation may result in overly conservative and uneconomical structures or in the development of bridges that do not meet the intended safety levels. This economic and safety uncertainty on structures that represent 30% of the steel bridge market is significant.

In 1994, AASHTO published the first edition of the LRFD Specifications. These provisions introduced the load and resistance factor design method for the design of tangent girder bridges to the bridge engineering community. Since then, AASHTO, through the National Cooperative Highway Research Council (NCHRP), has been broadening the scope of the LRFD Specifications to make a fully integrated specification for the design of all common bridge types. The FHWA mandated that beginning in 2007 all bridges that are built with Federal Aid money must use the LRFD Specifications as the governing design provisions. To incorporate the horizontally curved girder bridge design into the LRFD Specifications, statistically significant data are needed to produce calibrated and refined predictor equations. Calibrated equations will produce a uniform

level of safety across bridge types and will improve the community's ability to design and build economic structures.

A review of the existing experimental data reveals a lack of appropriate results for inclusion into the statistical models. Figure 1-1 shows flange and web slenderness combinations from all previous experimentation that produced a flexure or flexure-shear combination failure. Figure 1-2 restricts the previous experimental data to just those tests performed in uniform bending. Figure 1-3 eliminates tests performed with unrealistic boundary conditions from the Figure 1-2 data. All of these figures show the design limits for both web and flange compact and non-compact behavior. The limited data shown in Figure 1-3 represent two points with slenderness combinations far from those that represent current best practice. These data cannot realistically be used to anchor the large analytical parametric study needed to produce statistically relevant information for use in the formulation and calibration of predictor equations for the LRFD Specifications.

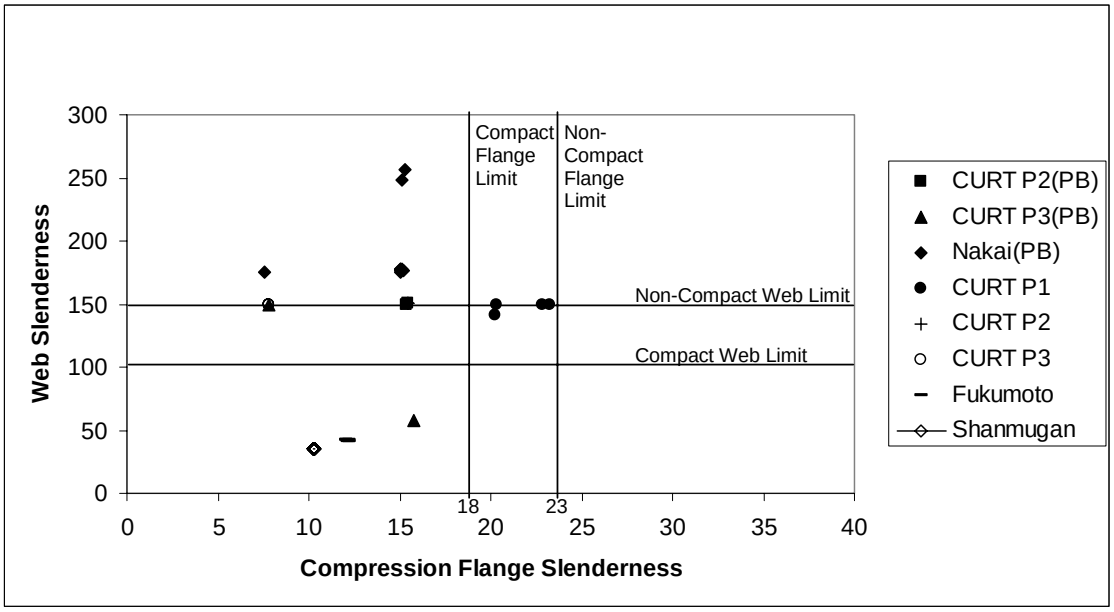

Figure 1-1: All Previous Experimental Slenderness Combinations

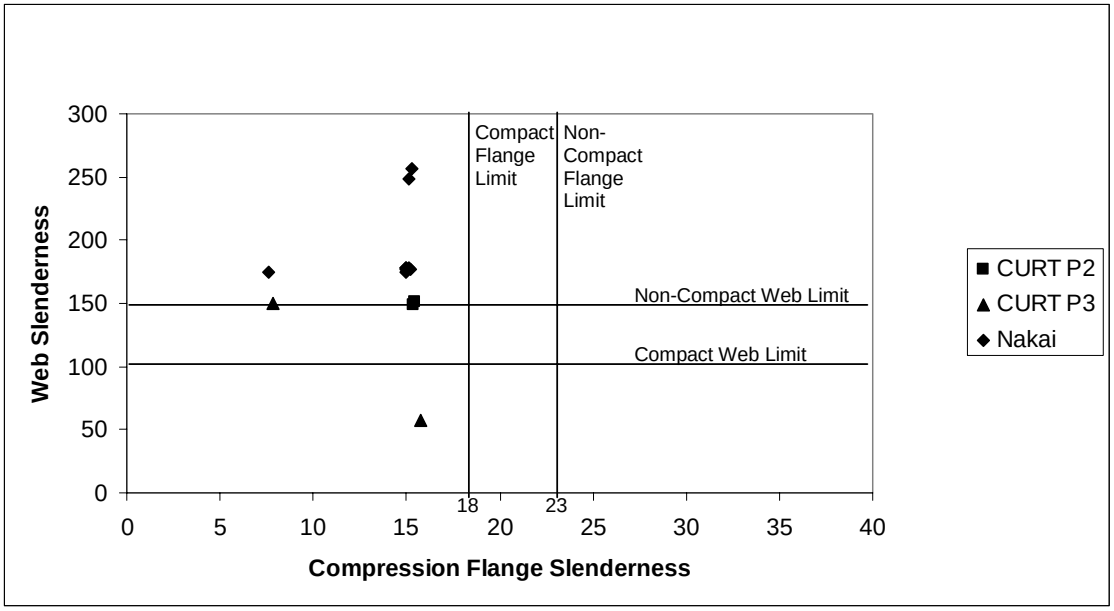

Figure 1-2: Slenderness Combinations From All Previous Uniform Bending Experiments

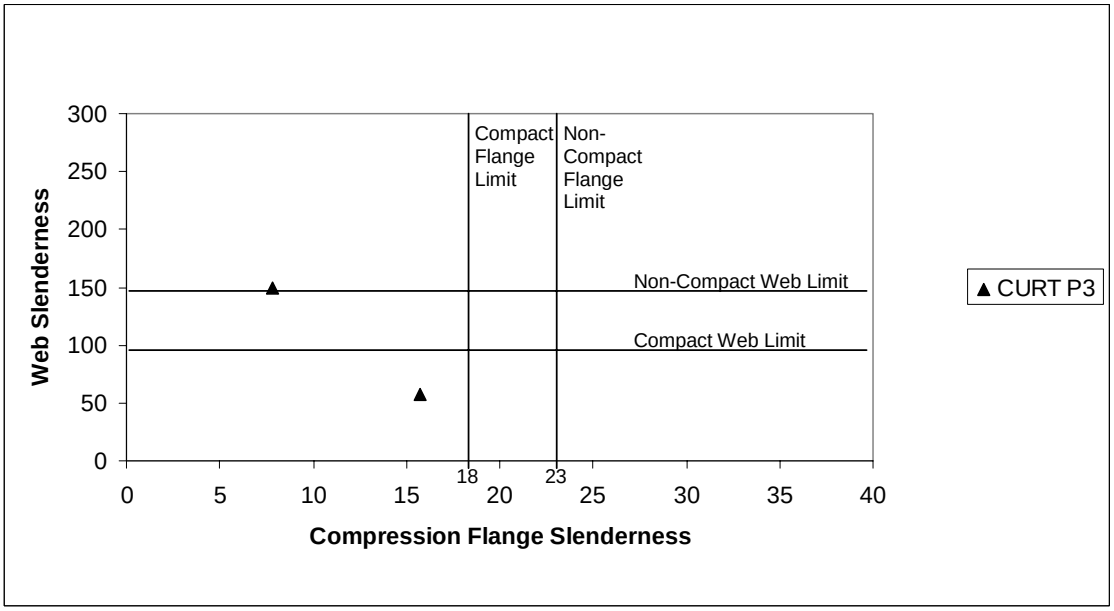

Figure 1-3: All Previous Uniform Bending Experiments with Realistic Boundary Conditions

A large suite of experimental tests with the appropriate parameters would obviously be cost prohibitive for the community. Therefore, a focused and deliberate experimental effort is needed to supply significant and sufficient physical results to anchor a finite element based study.

1.2 Objective and Scope

The objective of this experimental effort is to determine the flexural resistance of a variety of full scale horizontally curved girder components with realistic boundary conditions. The test matrix will examine the influence of (i), compression flange slenderness, (ii), web slenderness, and (iii), web stiffening on moment capacity. These results will be used to validate a computer model similar to that used to produce the hundreds of virtual test results that form the statistical basis of the recently developed predictor equations by White et al. (2001), herein referred to as the Unified Design Method.

1.3 Previous Experimental Work

With a few exceptions, previous investigations have focused on single, scaled, doubly-symmetric horizontally curved I-sections tested with artificial torsional restraint provided at the ends. In some cases, this restraint was full fixity of the end. In other cases, a sole restraint against lateral movement provided at the end was used. In either case, the end conditions of the girders in these investigations did not accurately represent the conditions produced by a horizontally curved girder bridge.

Recently, several researchers [Linzell (1999), White et al. (2001), Grubb and Hall, Zureick et al.(1994)] reviewed, critiqued, and synthesized most of the previous work in this area as part of the FHWA CSBRP. The following sections will highlight previous experimental work performed on horizontally curved steel I-girders. An emphasis is placed on those individual experiments from each investigation that produced a bending capacity type failure.

1.3.1 CURT Tests

Culver and Mozer at Carnegie Mellon University performed most of the experimental testing done for the CURT Project. These tests are documented in great detail in Mozer and Culver (1975); Mozer, Ohlson and Culver (1975); and Mozer, Cook and Culver (1975). A total of 22 failure load tests on 11 plate I-girder specimens are described in the CURT Project. Twelve of these experiments produced information on moment or moment-shear capacity of horizontally curved girders (refer to Table 1-1 for a list of selected parameters). Data are presented comparing observed elastic behavior and ultimate load capacity with prediction calculations based on analytical methods developed as part of the CURT Project. These investigations included very limited computer aided modeling analyses because neither the finite element method software nor the microcomputer were reliable or available tools to the researchers at that time.

Specimen ID	Curvature $\frac{R}{l}$	Compression Flange Slenderness $\frac{b_{fc}}{t_{fc}}$	Web Slenderness $\frac{D}{t_w}$	Overall Depth, mm (in.)
CURT P1 Tests (1970)				
C8(2)	18.6	20.3	141	474.7 (18.69)
C9(2)	6.3	20.3	150	476.0 (18.74)
D13	7.4	23.4	150	474.5 (18.68)
D14	7.4	23.0	149	476.0 (18.74)
CURT P2 Tests (1971)				
L1(A)	9.9	15.2	149	473.7 (18.65)
L2(A)	10.1	15.4	151	475.2 (18.71)
L2(B)	10.1	15.4	151	475.2 (18.71)
L2(C)	10.1	15.4	151	475.2 (18.71)
CURT P3 Tests (1973)				
GI(3)	10.0	7.82	150	482.1 (18.98)
GI(4)	10.0	7.82	150	482.1 (18.98)
GI(5)	10.0	7.82	150	482.1 (18.98)
GO(8)	10.6	15.7	58	476.8 (18.77)
Fukumoto and Nishida Tests (1980)				
AR1	13.6	12.1	45	268.2 (10.56)
AR2	29.8	12.2	44	268.5 (10.57)
AR3	99.8	12.1	44	268.5 (10.57)
BR1	12.1	12.0	45	267.0 (10.51)
BR2	25.8	12.1	44	268.2 (10.56)
BR3	172	12.0	45	267.0 (10.51)
Nakai et al. Tests (1985)				
M1		15.0	178	824.0 (32.44)
M2	14.7	15.2	177	821.4 (32.34)
M3	12.3	15.0	178	821.7 (32.35)
M4	5.2	15.0	177	821.7 (32.35)
M5	5.3	15.1	248	824.0 (32.44)
M6	5.4	15.3	257	821.4 (32.34)
M7	5.3	15.1	178	824.0 (32.44)
M8	4.7	7.6	175	824.0 (32.44)
M9	4.5	15.0	175	824.2 (32.45)
Shanmugan et al. Tests (1995)				
CB1	5.3	10.27	35.3	306.6 (12.07)
CB2	7.9	10.27	35.3	306.6 (12.07)
CB3	13.2	10.27	35.3	306.6 (12.07)
CB4	19.7	10.27	35.3	306.6 (12.07)
CB5	39.5	10.27	35.3	306.6 (12.07)
CB6	18.9	10.27	35.3	306.6 (12.07)
CB7	2.0	10.27	35.3	306.6 (12.07)
WB1	5.3	10.33	35.25	306.1 (12.05)
WB2	13.2	10.33	35.25	306.1 (12.05)
WB3	39.5	10.33	35.25	306.1 (12.05)

Table 1-1: Summary of Previous Experimental Work That Produced Flexural or Flexural/Shear Failures

Mozer and Culver (1975) contains the results from static load tests on seven scaled, doubly symmetric, welded plate girders (herein referred to as the P1 tests). The primary focus of this investigation was to determine the influence that a variety of geometric and stress parameters had on flange local buckling for this type of girder. However, only three of these tests produced that failure mode. One experiment displayed a moment/shear interaction failure while the remaining investigations produced shear failures.

The test components had radii that ranged from 115.2 m (378 ft) to 339.2 m (1,113 ft) and were either heat curved or cut curved to produce their final horizontal geometry. Flange and web steels were ASTM A36 and AISI 1008, respectively. Other geometric variables included compression flange slenderness, web slenderness, and transverse stiffener spacing. Table 1-1 contains a specimen matrix of limit geometric parameters for the specimens from this set of tests that exhibited flexural or flexure-shear interaction failure.

The P1 test girders had 3.0 m (10 ft) arc length spans that were supported on radial aligned rollers at both ends. The girder ends were also restrained from lateral translation and twisting by radial aligned bracing. Load was applied eccentrically at mid-span to produce a desired combination of warping and primary bending stresses in the compression flange. All specimens had 1.5 m (5 ft) unbraced lengths.

The results of the P1 tests that failed as a result of local flange buckling compared favorably with predictions made using equations based on the Elastic Beam theory developed by Culver and McManus (1971). The authors concluded that the contemporaneous compression flange slenderness limitations for straight girder design can be conservatively used for horizontally curved girder design if the flanges are cut

curved, and first yield is defined at the flange tip where the primary bending and warping stresses are additive. If the design preference was to neglect consideration of warping stresses, then the authors recommended limiting curved girder compression flange slenderness to the contemporaneous straight girder compact section requirements.

Mozer, Ohlson, and Culver (1975) investigated two horizontally curved I-girders, each tested with three separate loading arrangements (herein referred to as the P2 tests). The primary difference between the two specimens, designated as L1 and L2, was the transverse stiffener detail that was used. One focus was to determine the effects of partial versus full depth stiffeners on flexural resistance. Each specimen was failed using three loading regimes, A, B, and C. The A regime consisted of 4 point loading applied at the third points along the 4.6 m (15 ft) arc length of each simple span girder. The arrangement was designed to produce a flexural failure in the compression flange within the constant moment region of the girder. The B regime and C regime were nearly identical, involving a single point load located eccentrically similar to the P1 tests to produce a desired ratio of warping to bending stress. These tests were done with a 3 m (10 ft) arc length simple span leaving a 1.5 m (5 ft) overhang at one end of the overall 4.6 m (15 ft) girder. All tests had 1.5 m (5 ft) unbraced lengths. The experiments were designed to produce either a shear failure (L1 series) or a flexure-shear interaction failure (L2 series) in the girder panel adjacent to the load.

The P2 tests used bearing, bracing, and load details consistent with those employed for the P1 tests. The P2 girders had a 15.2 m (50 ft) radius. Relevant girder properties are tabulated in Table 1-1 for the four tests in which flexural was involved in failure.

The author's P2 test conclusions for flexural resistance supported those conclusions made in the P1 tests. The conclusions also indicated that adequately braced compact compression flanges were capable of developing significant post-yield bending capacity.

Mozer, Cook, and Culver (1975) investigated a pair of doubly symmetric I-girders that were concentrically curved, transversely spaced at 0.9 m (3 ft), and connected by five rigid cross frames and two rigid end diaphragms (herein referred to as the P3 tests). The P3 test frame had a centerline span of 4.7 m (15.5 ft) and a radius of curvature of 15.7 m (51.5 ft). The girder ends were held down to prevent unpredictable uplift during testing. Eight individual test results are reported, six of which detail a capacity failure. Tests 5 and 8 used third point loading to produce a constant moment region over an approximate 1.5 m (5 ft) unbraced length and local flange buckling failures in the inside (GI) and outside (GO) girders respectively. The remaining tests used a single applied load at mid-span. Tests 3 and 4 produced flexure-shear interaction failures at different locations of the inside girder. Test 1 and Test 2 produced shear failures on different panels of the inside girder.

The P3 test program included the following objectives:

- determining the bending strength of a curved plate girder in a curved bridge system
- monitoring the inelastic redistribution of load within the bridge system
- determining the capacity of curved web plates
- monitoring the influence of transverse stiffeners on web behavior

Among other conclusions, the researchers stated that cross-frames play a major role in curved I-girder bridge behavior when the structure is an open grid, the Culver-McManus

equations [Culver and McManus (1971)] are conservative when used to calculate flexural resistance, and that a considerable degree of reserve strength above initial yield exists in curved plate girders with compact compression flanges.

To prove their analytical methods and the computer analysis program developed as part of the CURT program, Brennan and Mandel (1971, 1974) built and elastically tested small-scale similitude structures. These small-scale structures were used to develop influence lines for deflection, moment, and shear for each girder of the structures modeled. The experimental results were compared with the computer generated results with good agreement reported by the researchers.

Shore and Lapore (1975) built several very small curved girder and curved bridge models that were exercised elastically to produce data that would support their numerical efforts. Their report details the experimental work and results as well as the work being done to develop a finite element approach to curved girder analysis. However, the report does not draw conclusions. The researchers planned to report comparisons and conclusions in a follow-up effort.

1.3.2 University of Maryland Tests

Contemporaneous to the CURT program, several experimental studies were conducted at the University of Maryland on the behavior of curved I-girders, box-girders, and systems as part of a large experimental and analytical program titled *The Design of Curved Viaducts*. This program was co-sponsored by the Maryland State Highway Administration and the FHWA. The program's objectives were to produce analytical tools for the design and evaluation of curved girder bridges. A series of progress and

interim reports were issued to the sponsoring agencies detailing the individual experimental and analytical efforts of the larger program.

Spates and Heins (1968) used four individual elastic loadings to evaluate the behavior of a single curved beam cold rolled to a 15.2 m (50 ft) radius. The arc length of the span was 9.1 m (30 ft), and the ends were designed to be fixed with respect to bending and torsion. The steel section used, S180x22.8 (S7x15.3), had a nominal yield strength of 207 MPa (30 ksi). Load was applied by radially cantilevering lead weight off the beam at mid-span. Strain and deflection information was compared with analytical predictions from equations developed for single girders.

The major problem encountered during this investigation was the experimental control or establishment of the desired end conditions. Even with extensive effort, the experimental data showed that truly fixed ends were not achieved. The investigators' reduction of data and analytical comparisons lead them to conclude that end conditions can be very significant on curved girder plane bending behavior of a single girder.

In the analytical portion of their investigation, Spates and Heins demonstrated how predictor equations developed for a line girder design were very conservative when used to design the individual girders of a curved bridge system.

Kuo and Heins (1971) conducted experimental testing to determine the torsional rigidity, warping behavior, and failure mode of composite I-girders subject to torsion. Four experiments were performed on 5.5 m (18 ft) single composite girders with varying end conditions and slab thickness. Torsion was applied at one end of the girder using a force couple while the other girder end was either pinned or fixed. All tests utilized a 0.3

m (1 ft) deep wide flange section and a 0.9 m (3 ft) wide composite slab with a 51 mm (2 in.), 76 mm (3 in.), 102 mm (4 in.), or 152 mm (6 in.) thickness.

In all four tests, the results indicated that the concrete slab dominates torsional behavior and that warping effects were negligible for the slab, but were very significant for the girder. Rupture of the concrete slab due to diagonal tension was the reported cause of failure for each experiment. Analytical comparisons using the Thin-Walled theory yielded excellent correlation with experimental results.

The main objective of Colville (1972) was to develop appropriate design criteria for welded stud shear connectors in curved composite sections. The experimental program consisted of four individual tests on 5.4 m (17.75 ft) arc length horizontally curved and composite concrete slabs and I-beams. Test parameters included radius of curvature, girder size, number of shear connectors per section, and type of loading.

Colville concluded that the effects of torsion and warping are not significant on the shear connectors and can be neglected if the source of the effects is from vertical loads acting on curved members. However, the design procedure developed does consider the transverse shear forces that result from the bending and warping of the composite section. The design procedure does converge to the straight girder procedure when the radius becomes large. The reader is also reminded that the data used to develop the design procedure were generated from composite slabs in compression; therefore, the results may not be valid in negative moment regions.

1.3.3 Japanese Tests

Two major experimental programs were conducted in Japan to support the Hanshin Expressway Corporation's *Guidelines for the Design of Horizontally Curved Girder*

Bridges. These guidelines and the Guide Specifications are the only two specifications for horizontally curved steel bridges in the world. While most of the literature associated with these programs is published in Japanese, other researchers [Linzell (1999), White et al. (2001), Grubb and Hall] have reviewed this work.

Fukomoto and Nishida (1981) tested six simple-span scaled doubly symmetric I-girders that had laterally restrained ends that were fabricated out of steel with an approximate 235 MPa (34 ksi) yield strength. Load was supplied with a gravity simulator at mid-span; although, the details of the system used were not reported. These specimens had a nominal compression flange slenderness of 12 and web slenderness of 45, which is very unrepresentative of bridge girders. The girders had an overall depth of less than 279 mm (11 in.) and had radii of 23.2 m (76 ft) to approximately 483 m (1,584 ft). Table 1-1 contains parameters for individual specimens. The experimental results showed good agreement to both the theoretical solution presented and the approximate solution proposed.

Nakai et al. tested nine scaled doubly symmetric components. Parameters for all specimens, M1 through M9, are included in Table 1-1. The girders were tested for flexural capacity in near uniform negative bending with the ends completely restrained from translation or out-of-plane rotation. All but one of these specimens had a compression flange slenderness of 15, and most had a web slenderness of approximately 175. Specimen M8 had a compression flange slenderness of 7.6. Two specimens, M5 and M6, had a web slenderness of approximately 250. One of these pair of specimens employed a longitudinal stiffener to stabilize the web while the other did not in an effort to quantify the effect of that web attachment on bending capacity. A reduction in capacity

compared with an equivalent straight girder analytical prediction was reported for these tests.

While the Nakai tests were conducted with girders of appropriate slenderness combinations and section depths for bridges, the specimens had a span to depth ratio of approximately 2.5. At this ratio, an assumption is made that the highly restrained girder ends affected the demonstrated flexural resistance. At the very least, the configuration tested relates poorly to bridge girder realties.

1.3.4 Other Experimental Testing

Shanmugam et al. (1995) compared experimental results with predictions made with a refined finite element model. The experimental program consisted of 10 tests to failure of single simple-span curved girders with various unsupported lengths and end conditions fabricated out of steel with a nominal strength of approximately 276 MPa (40 ksi). The primary focus of the testing was to contrast the difference in behavior between hot-rolled beams and welded plate girders. All specimens were cold-bent into their final horizontal curvature and had load applied at a single point. These girders were very small with an overall depth of about 305 mm (12 in.).

Daniels et al. (1979) at Lehigh University primarily investigated fatigue issues on horizontally curved steel I-girders. Nakai and Kotoguchi tested a pair of horizontally curved I-girders for systematic lateral buckling. Also, nearly a dozen field test studies have reported mostly limited elastic behavior data acquired primarily during the construction of horizontally curved steel I-girder bridges or from structures already in service.

1.4 Strength Predictor Equations

The current Guide Specifications (2003) uses governing equations for flange stress that are slight modifications of the original work by Culver and McManus (1971) that was sponsored by the CURT program. Culver and McManus built on the First-Order theory for determining the stresses and deformations in horizontally curved beams loaded normal to their plane of curvature. This theory was first developed by Vlasov (1961) and Dabrowski (1968). The derivation of the Culver-McManus equations was based on doubly-symmetric and prismatic curved I-girders with compact and non-compact compression flanges that were braced at a uniform spacing and subject to a constant vertical bending moment. The Guide Specifications' equations have been extended to be valid for singly symmetric I-girders by Hall and Yoo (1998). The Guide Specifications' provisions that apply to the design of non-composite I-girders in flexure are summarized in Appendix B.

The strength of the Guide Specifications' provisions is that an engineer is only required to produce a first order analysis of the structure for design. Second order effects are accounted for by the ρ-factors defined in Appendix B. Culver and McManus developed the ρ-factors by performing approximate second order elastic analyses on a range of I-girder geometric parameters, subtracting first order behavior from the results, and fitting a curve through the findings.

The ρ-factors are also the weakness of the Guide Specifications. Their derivation includes many assumptions that cannot be uncoupled from the results. A predictor equation is also used for tangent girder lateral torsional flange buckling (Equation B-3 in Appendix B) that has since been replaced in the AASHTO Standard Specifications for

the Design of Highway Bridges and LRFD Specifications for straight girder design with a more accurate formulation. The ρ-factor equations fail to recognize the amount of rigor employed in the structural analysis process forcing a common design procedure for all levels of investigation. Also, a careful review of the ρ-factor formulations by Hall et al. (1999) has revealed some inaccuracies in how warping stresses are accounted for resulting in an unintended doubling of their effect. Finally, the ρ-factor equations do not converge to any resemblance of the tangent girder design equations when the radius of curvature becomes very large. They also include a step discontinuity in behavior between compact and non-compact flanged sections.

The Proposed Unified Design Method provisions are also summarized in Appendix B. This design method has several advantages. First, the provisions are independent of the analysis method used. Second, they can be used to design for lateral loading from all sources, not just vertical loading on horizontally curved girders. Third, the design equations reduce to the tangent girder design equations when the radius is large. Finally, this method has eliminated the step discontinuity between non-compact and compact behavior.

Chapter 2. Experiment Design

A very detailed and complete chronology on the philosophy behind the Curved Steel Bridge Research Project (CSBRP) including the development of the experiment design was reported by Grubb and Hall. A review of the limited curved girder experimentation to date demonstrates the significant challenges inherent with producing relevant capacity data for this very complex structure type. As previously mentioned most documented experimental investigations have been tests on individual, doubly symmetric I-sections with proportions or scale that do not represent the family of girders typically used for bridges. Also, these investigations generally assumed some level of restraint for the ends of the test girder and at bracing or loading locations that does not replicate the structural behavior of a bridge system.

Full scale testing eliminates scaling issues. In many of the previous tests described above, girders were fabricated from very thin plate and sometimes from sheet steel. Steels in this thickness range retain very high levels of residual stress and distort significantly out-of-plane as a result of the high heat that they are subjected to as part of any welding process. These stresses and distortions can cause premature yielding or buckling that can decrease the ultimate capacity of a section. Also, many structural relationships are not linearly dependent. For instance, in dynamic tests, dead load—often called compensatory loading—needs to be added to a scaled bridge system without adding stiffness to produce a representative ratio of dead-load to live-load stresses in the girders or for added inertia. In static structural experimentation, the desired moment/shear

capacity ratios are difficult to maintain using scaled geometric properties. The full-scale structure used for this experimental program mitigates all of these concerns.

2.1 Test Frame Concept

The feasibility of single girder testing was considered for the CSBRP. Considerable analytical effort was focused on designing a set of bracing, loading and bearing details that could mimic the boundary conditions and internal load sharing of a bridge system, particularly the distribution of lateral flange bending moment. These analyses demonstrated the highly non-linear behavior of the post-peak single girder. In the final analysis of the project team, testing of a three-girder system was necessary to avoid the limitations and weaknesses of previous work and to safely produce the quantity and type of physical data needed within the financial means provided.

The CSBRP team employed the following philosophy to develop the test frame: The test frame needed to be flexible enough to accommodate testing components that would be subjected to a constant moment (pure bending) and moment-shear interaction, and the test frame had to be adaptable for a composite bridge test. The method for both sets of component tests was to insert a test specimen into the exterior test frame girder and connect it to the test frame with bolted splices and cross-frames. The test frame girders and the cross-frames were proportioned using a variety of materials and sections to remain elastic while providing realistic interaction to the test component as it experienced significant inelastic deformation. Once a test was finished, the component was replaced and the process was repeated until the series was complete.

The CSBRP team developed the three-girder bridge system shown in Figures 2-1 and 2-2. The span of the test frame was limited to 27.4 m (90 ft) because the FHWA

conducted additional unrelated experimental research in the Structures Laboratory during the tenure of the CSBRP. A radius and unbraced length of 61.0 m (200 ft) and 4.57 m (15 ft) respectively, measured along the centerline of the middle girder were selected to test the upper range of the practical limits of $\frac{l}{R}$ for a structure of this span. Once a span, radius and unbraced length were determined, the project team solved for an overall girder depth for the test frame using best practice design tools. Figure 2-3 shows the test frame in the FHWA Structures Laboratory configured for one of the bending component tests.

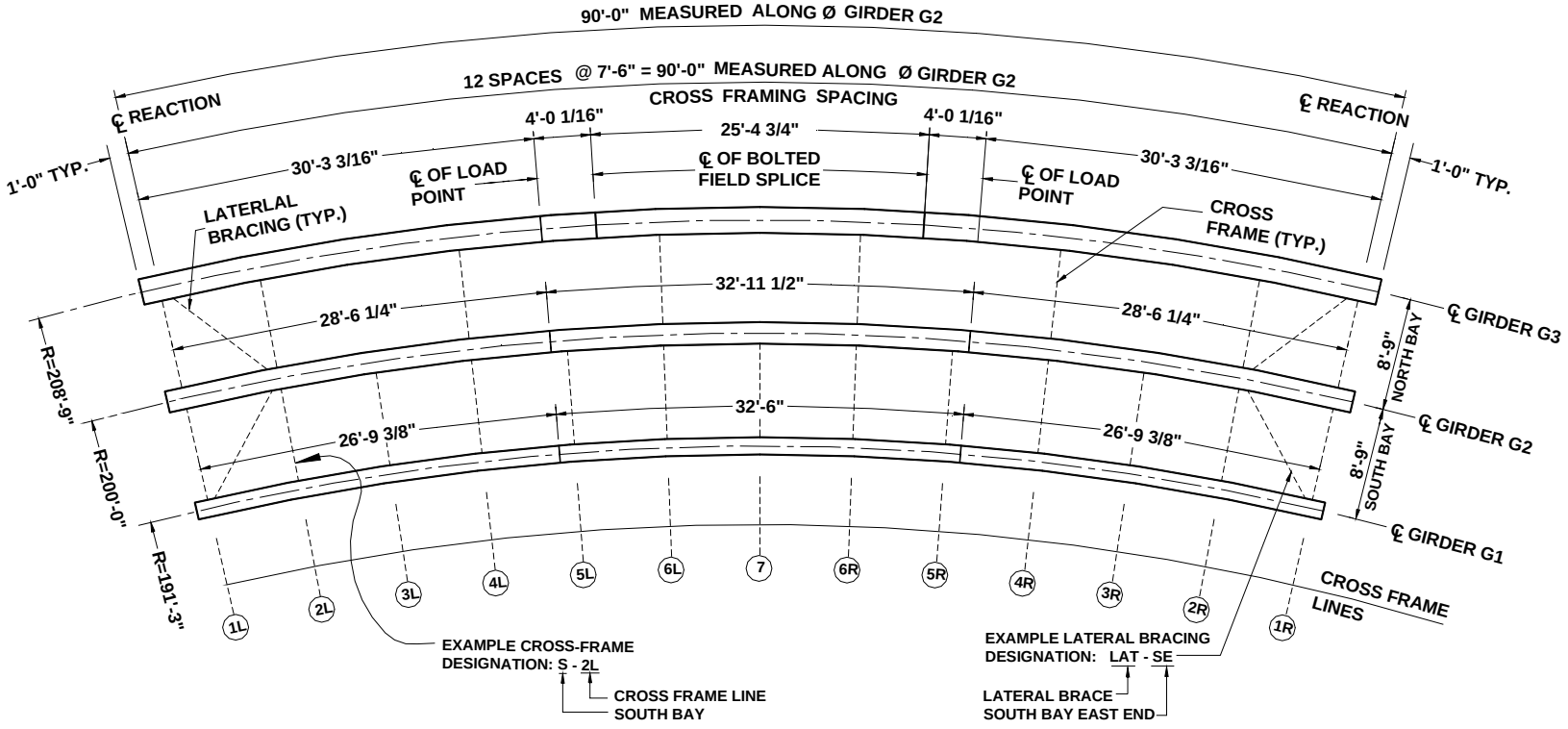

Figure 2-1: Plan View of Test Frame

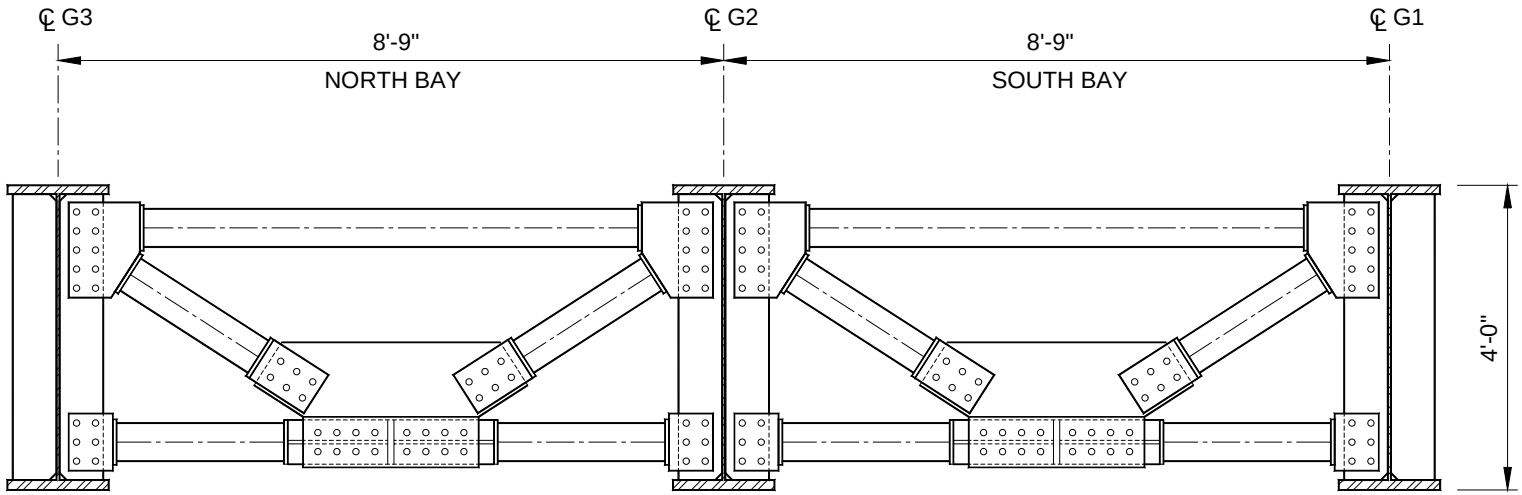

Figure 2-2: Cross-Section of Test Frame at a Cross Frame Location 6L

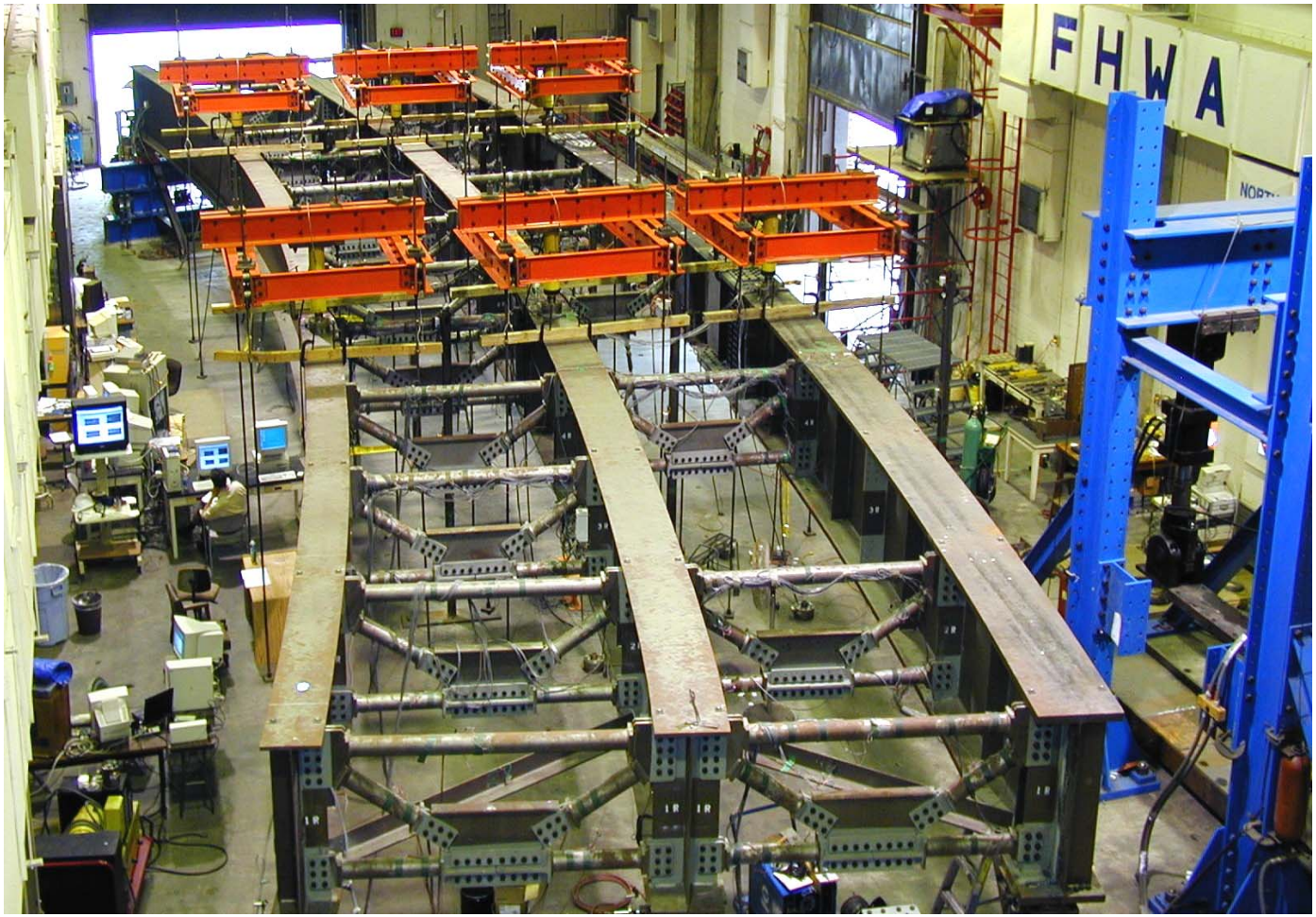

Figure 2-3: The Test Frame in the FHWA Structures Laboratory

The exterior girder on the inside radius of the test frame is herein referred to as G1. G1 is doubly symmetric and prismatic with flange plates measuring approximately 27 mm x 406 mm (1 1/16 in. x 16 in.) and a web plate measuring approximately 11 mm x 1,219 mm (7/16 in. x 48 in.).

The interior girder of this three-girder system, referred to as G2, is also doubly symmetric and prismatic. The flange plates are approximately 30 mm x 508 mm (1 3/16 in. x 20 in.), and the web plate is approximately 13 mm x 1219 mm (½ in. x 48 in.).

The exterior girder on the outside radius of the test frame, G3, is made up of three doubly symmetric and prismatic sections connected by two bolted splices. The flange plates of G3 measure approximately 57 mm x 610 mm (2 1/4 in. x 24 in.), and the web plate is approximately 13 mm x 1219 mm (½ in. x 48 in.). This girder was fabricated in three sections so that the center section could be replaced with each of the bending or moment-shear interaction components. The splices were designed to develop the full plastic moment of the strongest bending component (component B6) without slip.

With the overall depth of the girders established, the matrix of test specimens was easily developed for both the bending component and moment-shear interaction component series. The tested parameter combinations were selected to best fulfill the objective and to provide a broad enough set of information on which the analytical work could be based. Figure 2-4 shows how the slenderness combinations for the bending component series of tests compare with the current Guide Specifications compact and non-compact limits. The selected slenderness combinations slightly exceed the limits in the figure because the Guide Specifications slenderness limits were altered in 2003 while the test matrix was originally designed using the 1993 version of this document.

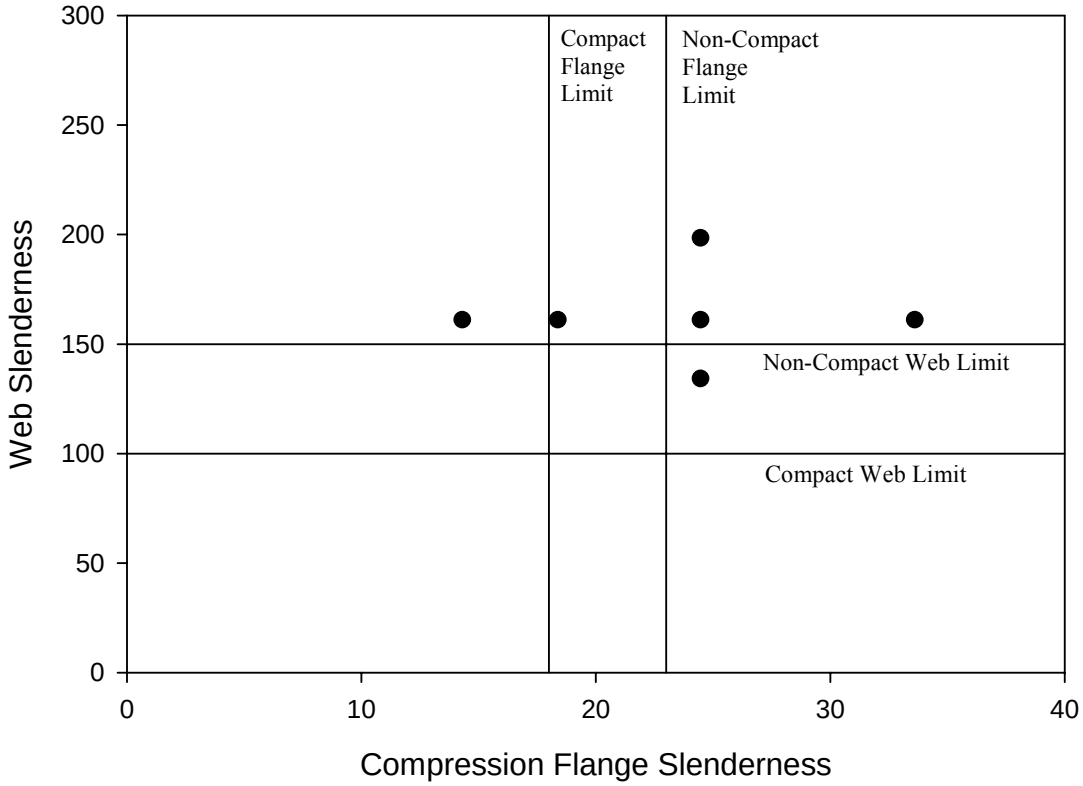

Figure 2-4: Bending Component Test Matrix

The test frame utilized the "K-type" cross-frame and diaphragm shown in Figure 2-2. However, to reduce the instrumentation demand and to ease interpretation of results, the single-leg angles that typically are used to make up horizontal and inclined legs of the cross-frames and diaphragms were replaced with round structural steel tubing. The tubing used had a nominal outside diameter of 127 mm (5 in.) and a wall thickness of 6 mm (¼ in.). This tubing size was selected because its flexural capacity approximated that of the members used in a more conventional design.

Use of the test frame also provides for redundancy in the analysis of the inelastic behavior of the test components. Flexural resistance of the test components can be determined by two independent methods throughout the elastic range of behavior. These

analysis methods, called the Direct Method and the Indirect Method, rely on different instrument subsets from the extensive instrumentation plan (800+ channels of data acquisition) for their calculation. The instruments are primarily made up of strain, load and displacement indication devices and are applied to strategic locations within the test frame and the bending components. Besides insuring an appropriate interpretation of results, the experiment data were used to validate a fully material and geometric non-linear finite element model. This model incorporates the as-built steel plate widths and thicknesses, and steel plate specific material properties based on the large suite of materials tests performed as a part of this project.

2.2 Component Test Matrix

The test frame was designed to be versatile. By reconfiguring the load and reaction locations, the test component location in G3 could be subjected to either constant moment (referred to herein as the bending component series of tests) or to a combination of high moment and high shear (referred to herein as the moment-shear interaction component series of tests). The bending component series included seven individual component specimen tests and are the primary subject of this dissertation. The moment-shear component series included individual tests conducted on four component specimens that are the subject of another report.

2.2.1 Bending Component Series

Each of the bending components, identified as B1 through B7, was designed to investigate an overlapping set of parameters by incorporating characteristics shared by other members of the test matrix. These shared characteristics were intended to produce

sufficient information to quantify the effects of compression flange slenderness, web slenderness and transverse web stiffening on the flexural capacity of horizontally curved steel I-girders.

Component B1 was designed doubly symmetric with a flange slenderness, b_f/t_f, of 23.3, a web slenderness, $2D_c/t_w$ or for doubly symmetric sections D/t_w, of 153.6 and transverse stiffener spacing, d_o, of 0.98D. These slenderness values slightly exceed the limits, 23 and 150 respectively, included in the AASHTO Guide Specifications for a stiffened non-compact girder. The B1 compression flange design was also used for components B2, B3 and B4. The B1 web design was also used for components B5, B6 and B7.

The doubly symmetric components B2 and B3 were designed with a thicker web plate than B1 lowering their web slenderness to 128.0. The differing characteristic between B2 and B3 is how their web plate was stiffened. While the web plate of component B2 had transverse stiffeners spaced again at approximately 0.98D, the web plate of component B3 was left unstiffened between cross-frame locations. This resulted in a d_o of 3.92D for component B3.

Component B4 had a designed compression flange slenderness of 23.3, but the section was made singly symmetric with a large tension flange to create a depth of web in compression of approximately 0.62D, which resulted in a web slenderness of 189.2.

The doubly symmetric component B5 was designed with a flange slenderness of 17.5, which is close to the compact flange limit of 17.0 specified in the AASHTO Guide Specifications.

Component B6 was also designed to be doubly symmetric with compact flanges. B6 was detailed with a flange slenderness of 13.6, which is well within the compact range of the AASHTO Guide Specifications.

The singly symmetric component B7 was designed with a slender compression flange of equal area to the tension flange. This flange combination generates a depth of web in compression that is very close to the mid-height of the girder maintaining the desired web slenderness of 153.6. This test component was designed to investigate the effects of a compression flange slenderness of 33.6, which is well in excess of the AASHTO Guide Specifications' limit of 23.

The target parameters of the bending component test series are compiled in Table 2-1.

Test Component	Compression Flange Slenderness $\frac{b_{fc}}{t_{fc}}$	Web Slenderness $\frac{2D_c}{t_w}$	Overall Depth mm (in.)	Panel Aspect Ratio	Notes
B1	23.3	153.6	1257 (49.5)	0.98	Top flange and web near non-compact limits
B2	23.3	128.0	1257 (49.5)	0.98	B1 with a stockier web
B3	23.3	128.0	1257 (49.5)	3.90	B2 with an unstiffened web
B4	23.3	189.2	1270 (50)	0.98	Singly symmetric
B5	17.5	153.6	1267 (49.875)	0.98	Top flange near compact limit
B6	13.6	153.6	1280 (50.375)	0.98	Very compact top flange
B7	33.6	153.6	1254 (49.375)	0.98	Slender top flange

Table 2-1: CSBRP Bending Specimen Target Parameter Test Matrix

2.2.2 Moment-Shear Interaction Component Series

Although the results of the moment-shear interaction component series tests are not included in this report, a brief description of these components is included in this section because the test frame was also designed to appropriately test these specimens.

The moment-shear interaction components were labeled MV1, MV1-S, MV2 and MV2-S. MV1 and MV1-S had flange and web slenderness combinations that duplicated those used for B1. MV2 and MV2-S had flange and web slenderness combinations that duplicated those used for B5. MV1 and MV2 had a transversely unstiffened web, d_o = 3.92D, while the webs of MV1-S and MV2-S had transverse stiffeners placed at a spacing of d_o = 0.98D.

2.3 Fabrication of Test Frame and Bending Components

All test series components and test frame components were fabricated with material and workmanship in accordance with the provisions and tolerances of the AASHTO Standard Specifications (15th Edition including the 1993 and 1994 Interims) and the American National Standards Institute (ANSI)/AASHTO/American Welding Society (AWS) D1.5 Bridge Welding Code (1988 Edition including 1989-1994 Interims). In addition, the design drawings specified that all girder and component specimen flanges should be cut curved and that heat adjustments could be made to obtain the desired final geometry with approval of the design engineer.

2.3.1 Materials

A variety of steels were used in the fabrication of the test frame girders, the cross-frames and diaphragms, and the different component test series.

2.3.1.1 Girders

Two steels were used to fabricate the horizontally curved girders of the test frame. G1 and G3 were fabricated from AASHTO M270M Grade 345 (M270 Grade 50) or ASTM A572M Grade 345 (A572 Grade 50) steel herein referred to as A572 steel. G2 was fabricated from plates of AASHTO M270M Grade 480W (M270 Grade 70W) or ASTM A852M (A852) steel herein referred to as A852 steel.

Both the flange and web plates were cut curved to produce the necessary horizontal and vertical curvature for each girder. Flange and web plates were attached using overmatched fillet welds produced with the submerged arc process.

Because of the quenching and tempering process required to produce the A852 steel limits plate lengths to approximately 15.4 m (50 ft), two butt welds were needed in each flange of G2. These full penetration groove welds were made at approximately 6.1 m (20 ft) measured along the girder centerline from either end of each flange.

2.3.1.2 Cross-Frames and Diaphragms

The K-type cross-frames and diaphragms used an ASTM A513 Grade 1026 structural steel tube for all horizontal and inclined legs. The tubes were attached to double gusset plates of A572 steel at each bolted connection location with a full penetration groove weld. To ease erection, the lower legs could be removed from the upper delta portion of the cross-frames and diaphragms (see Figure 2-2). All connections, except those on cross-frames N6L and N6R, were made with ASTM A325 high strength bolts. Because of the level of loading experienced by cross-frames N6L and N6R during testing, their connections were made using ASTM A490 high strength bolts.

2.3.1.3 Bending Components

All bending component and moment-shear interaction component flanges and webs were fabricated from A572 steel. The bending components, with the exception of specimen B7, were fabricated in the same manner as the girders of the test frame. The splice plates used to secure the inserted bending component into the test frame were drilled in place and were also made of A572 steel.

Bending component B7 was an addition to the original test matrix. This component test was added to most effectively use the downtime between the end of the first six bending component tests and the beginning of the moment-shear interaction series of tests. B7 was fabricated by using heat to restore, within tolerance, the tension (bottom) flange and web of bending component B1 and by replacing the compression (top) flange with a plate of almost equal area and increased slenderness.

2.3.2 As-Built Geometry

While the component fabrication was completed within the AWS and AASHTO tolerances, the as-built geometry slightly altered the target design slenderness of both the flanges and the web at the critical section (mid-length) of each member. In most cases, these minor changes in the slenderness ratio were the result of plate material that was slightly thicker than the nominally specified thickness due to permitted manufacturing tolerances. The bending component series as-built slenderness ratios are tabulated in Table 2-2.

Component	Compression Flange Slenderness $\frac{b_{fc}}{t_{fc}}$	Web Slenderness $\frac{2D_c}{t_w}$	Tension Flange Slenderness $\frac{b_{ft}}{t_{ft}}$
B1	22.8	147.0	22.9
B2	22.8	119.6	22.8
B3	22.7	119.5	22.9
B4	22.8	188.0	16.5
B5	17.0	143.6	17.1
B6	13.4	141.5	13.3
B7	32.5	144.2	23.2

Table 2-2: CSBRP Bending Specimen As-Built Parameter Test Matrix

2.4 Material Properties

Tension test specimens were cut from coupons taken from each steel plate used in the fabrication of the test frame and components. Coupons were also taken from the rolled sections that made up the lateral bracing and the tangential support frame, and from the structural steel tube sections from which the cross-frames were comprised. Three coupons were taken from each steel plate used for flange material and six coupons were taken from each steel plate used for web material. Static yield testing in accordance with the Structural Stability Research Council (SSRC) (see Galambos, 1988) provisions was conducted on most of the tension test specimens cut from each coupon. In general, tension tests were performed until two qualified results were obtained for each coupon location. A detailed set of results for these tests is available in Appendix A.

Due to the duplication of flange and web thicknesses used throughout the test matrix, several elements often could be cut from the same steel plate. The compression flanges of components B1, B2, B3 and B4 were all cut from Plate 21. The tension flanges of components B1, B2 and B3 were all cut from Plate 22. Both the compression and tension

flanges of components B5 and B6 were cut from Plates 23 and 24, respectively. The tension flange of component B4 was cut from Plate 25.

2.4.1 Plate Coupon Locations

Figures A-2 through A-14 show the location and orientation of the six coupons taken from the steel plates used for web material in both the test frame and bending components. The location and orientation for the three coupons taken from the steel plates used for flange material can be seen in Figures A-15 through A-27. The coupons taken from either end of the steel plate, designated as A and C on these figures, are located at mid-depth and oriented to be parallel to a tangent to the end of the horizontally curved flanges. The coupon at mid-length, designated B, is located near one side of the plate and is oriented to be parallel to the direction of rolling.

2.4.2 Tensile Strength Testing

The tensile tests were performed in accordance with the ASTM E8, *Standard Test Methods for Tension Testing of Metallic Materials* standard test method. In most cases, the E8 procedures were supplemented with the Structural Stability Research Council's (SSRC) *Technical Memorandum No. 7: Tension Testing* to generate consistent and uniform static yield strength levels. The E8 methods and procedures are designed to specifically determine yield strength, yield point elongation and tensile strength. In this document, the definitions of these terms are consistent with those definitions provided in the E8 Standard.

The static yield strength of individual plates was used in the analysis of the experimental data. The static yield strength and the ultimate yield strength results from individual plates were used to build true stress-true strain relationships suitable for use by

the analytical modeling effort. Appendix A contains a complete discussion of the tensile test results and their conversion to true stress-true strain.

2.4.3 Compressive Strength Testing

The compressive strength tests were performed in accordance with the ASTM E9, *Standard Test Methods of Compression Testing of Metallic Materials at Room Temperature* standard test method. These tests were limited to specimens taken from the steel plates that were used in the fabrication of the CSBRP bending component compression flanges. The purpose for this series of tests was to confirm that the behavior of the steels used was complementary in both tension and compression. A complete set of results for the compression tests is also included in Appendix A.

2.4.4 Elastic Modulus Testing

The elastic modulus testing was performed in accordance with the ASTM E111, *Standard Test Method for Young's Modulus, Tangent Modulus and Chord Modulus*, standard test method. Ten Young's modulus tests were conducted as a part of this program. Parameters included steel grade and plate thickness. The E111 Standard was used without modification to conduct the testing. Standard plate-type tension specimens, as described in Appendix A.1.2, were selected as the test specimens because the testing was performed in the tension stress-strain domain.

As a result of this testing, a Young's modulus of 204,000 MPa (29,600 ksi) was selected for use in both the experimental data analysis and in the finite element analysis of this project. Appendix A contains a discussion that details how this value of Young's modulus was selected.

2.5 Instrumentation Plan

A detailed and complete description of how the instrumentation plan was developed for these experiments and how these instruments were deployed is included in Linzell (1999). This plan consists of over 800 hard-wired instruments, subsets of which are interrogated by four separate data acquisition systems. Only the instruments that produced data that were used in this analysis and that are essential to this report are described in this section.

2.5.1 Test Frame Instrumentation

Each of the girders, cross-frames and lateral braces were instrumented at multiple sections during each of the bending component tests. Load cells monitored reactions at the girder ends as well as applied load at the hydraulic jack locations. Both of the independent channels of each load cell were recorded by separate data acquisition systems during testing to ensure redundancy of information. The load cells used to measure girder reactions had a 1,335,000 N (300 kip) capacity, while those used to monitor applied load had a 445,000 N (100 kip) capacity.

Strain gages were used to characterize sectional behavior at 10 locations throughout the test frame. On G1 and G2, strain gaged sections near each load point and at mid-span were monitored during each test. G3 sections near each load point and near cross-frames N4L and N4R were monitored during each bending component test. The location of each instrumented cross-section within the test frame is shown in Figure 2-5. This figure also indicates the instrument configuration at each location. A summary of instrument configurations and locations is contained in Table 2-3. The instrument configurations used are illustrated in Figures 2-5 through 2-12.

Configuration (Figure)	G3 and Bending Component Location Label	G2 Location Label	G1 Location Label	# Electrical Resistance Strain Gages	# Vibrating Wire Strain Gages
1 (2-5)	D, E			22	
2 (2-6)	A, J	A	A	15	
3 (2-7)	C, H			4	
V1 (2-8)	F			7	15
V2 (2-9)		B	B	7	8
V3 (2-10)	G			4	18
V5 (2-11)	B, I			11	11
V6 (2-12)		C	C	11	4

Table 2-3: Configuration and Location of Strain Gaged Sections

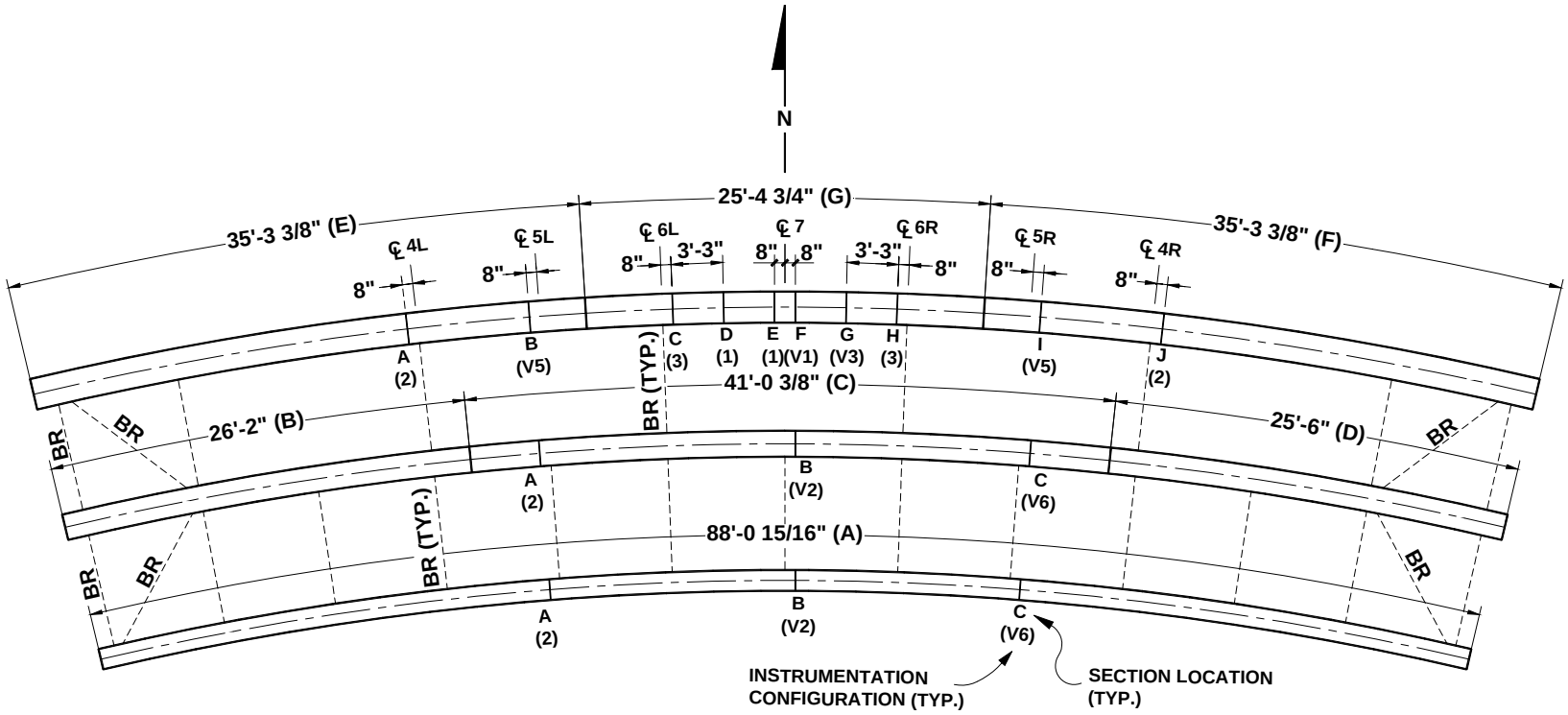

Figure 2-5: Location of Instrumented Cross-Sections

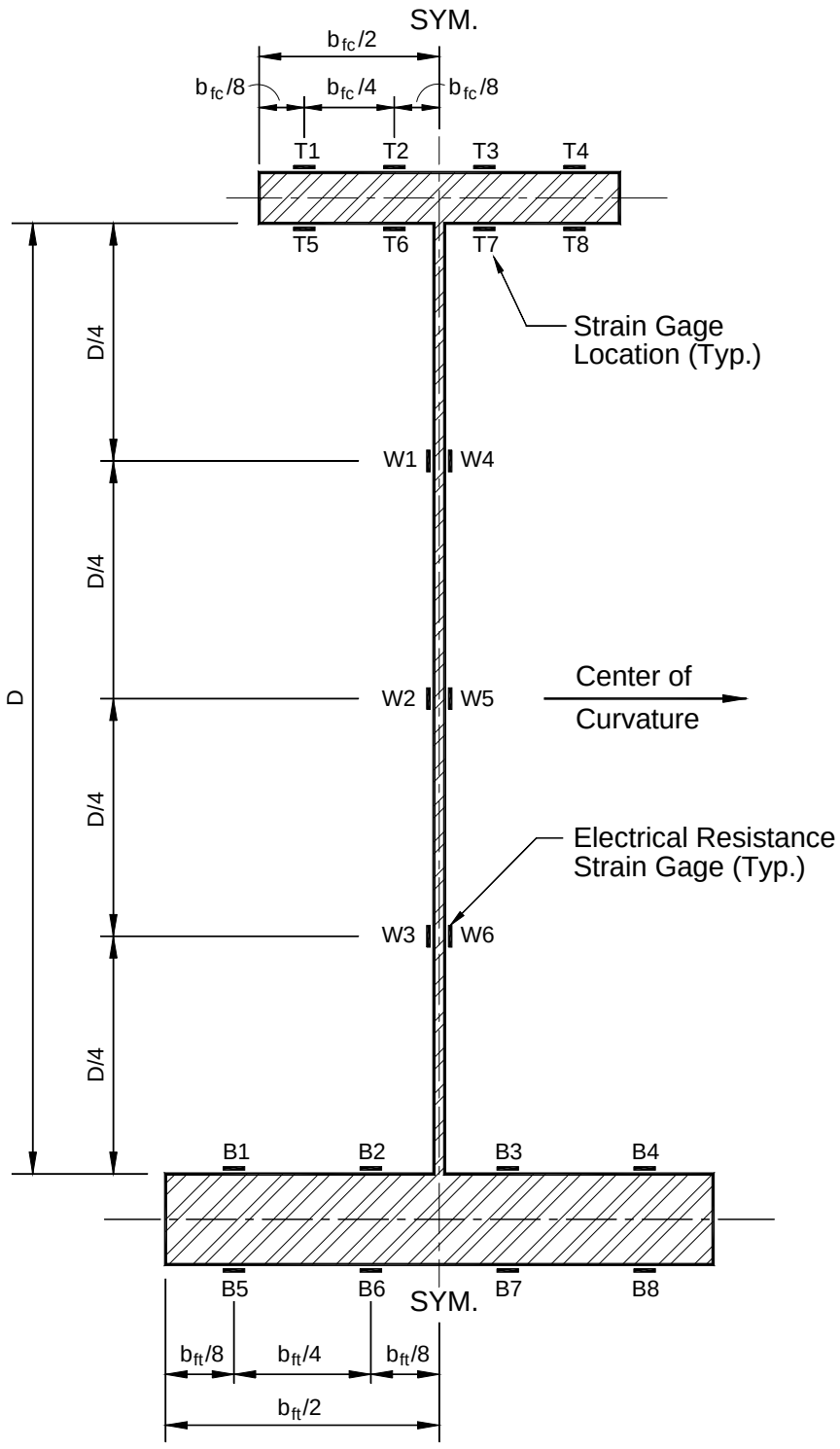

Figure 2-6: Instrumentation Configuration (1)

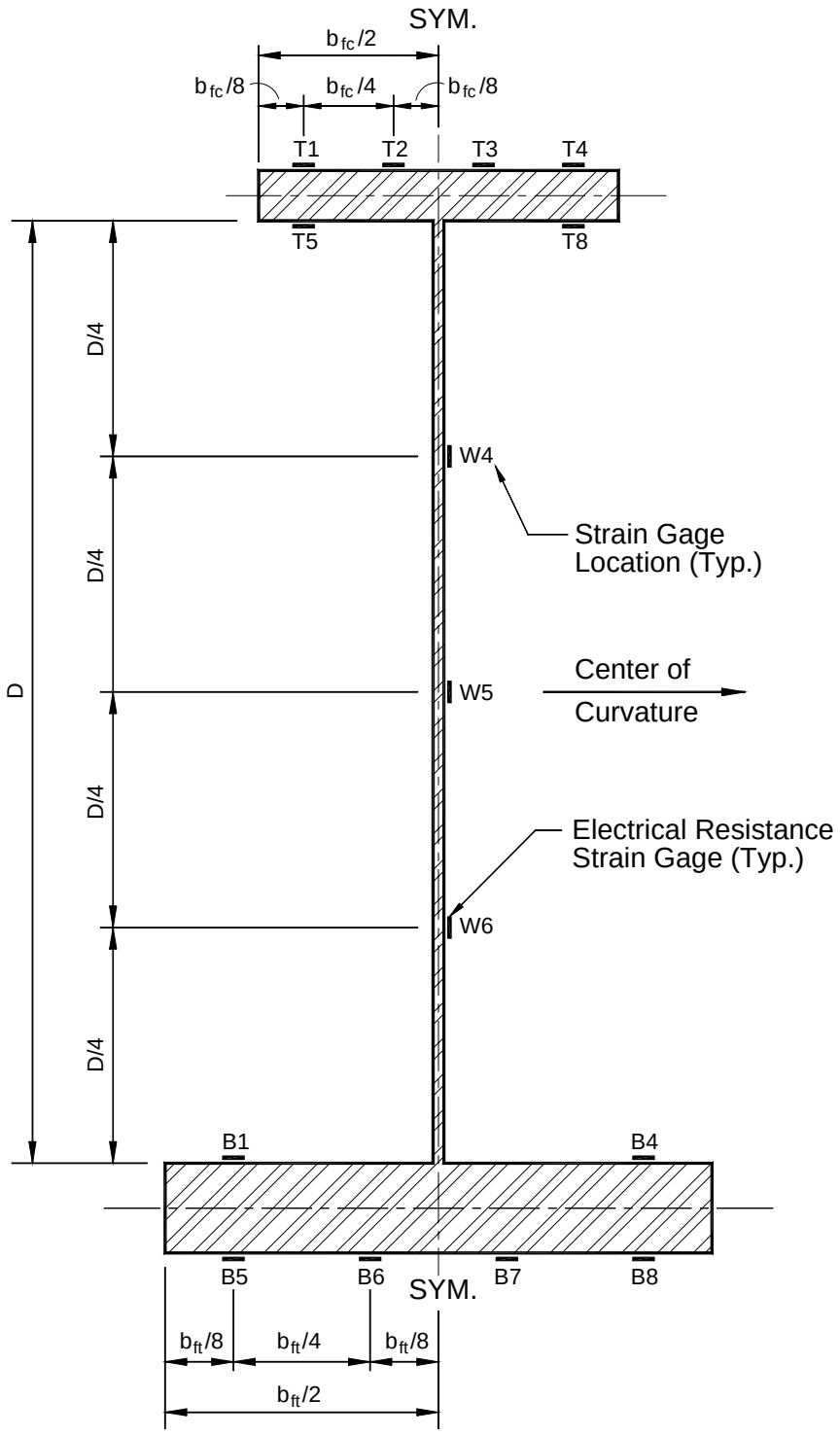

Figure 2-7: Instrumentation Configuration (2)

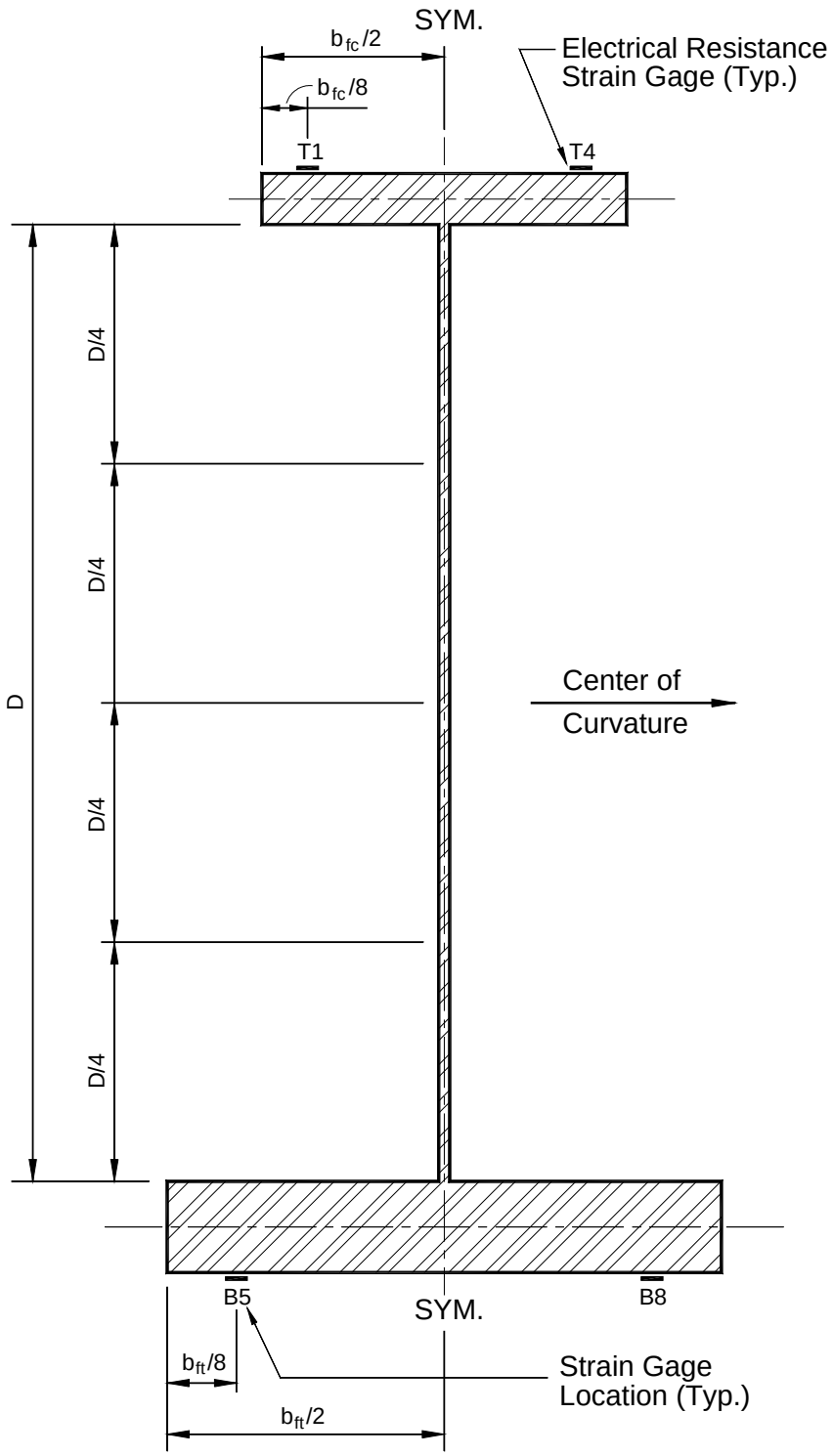

Figure 2-8: Instrumentation Configuration (3)

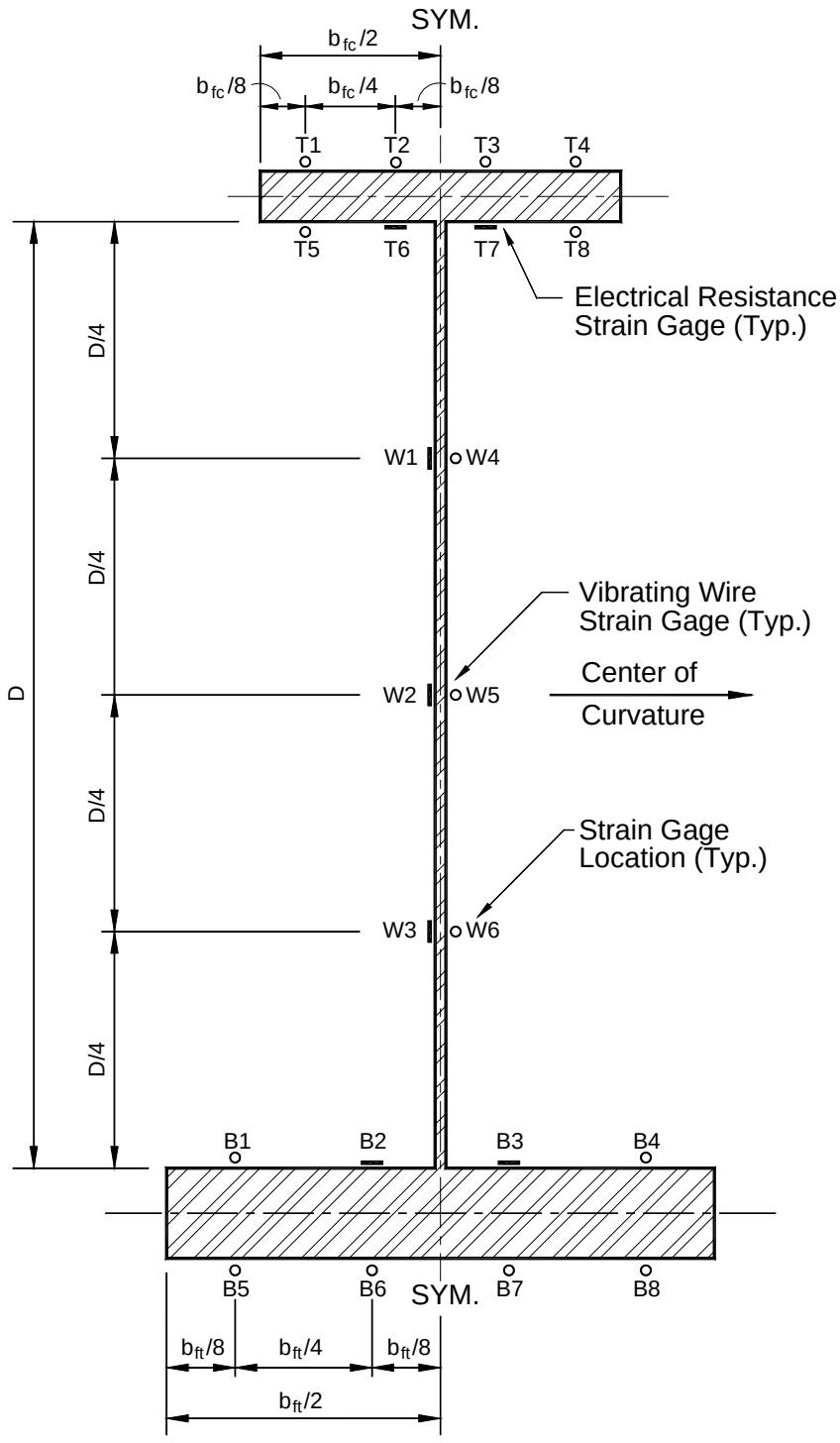

Figure 2-9: Instrumentation Configuration (V1)

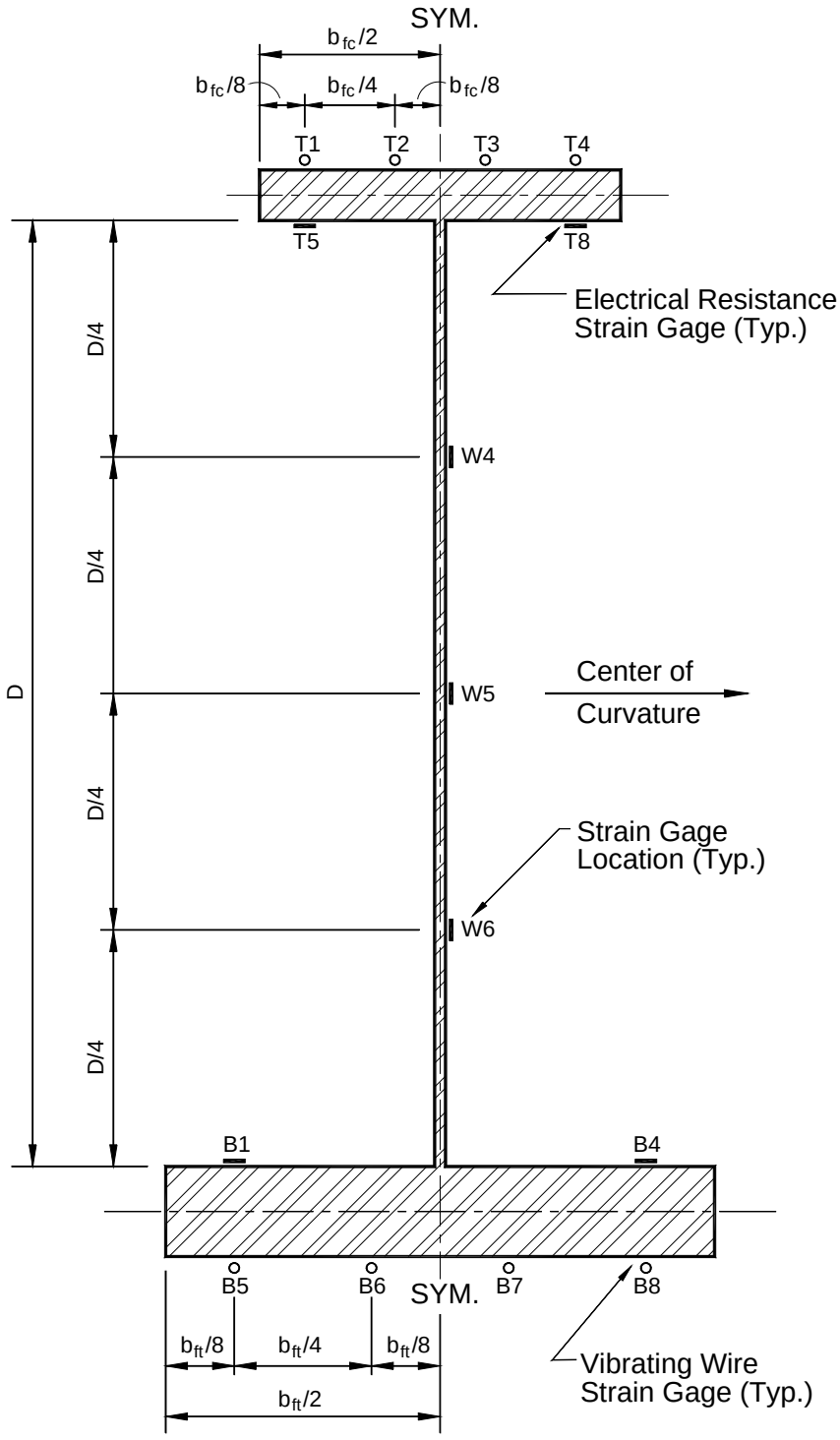

Figure 2-10: Instrumentation Configuration (V2)

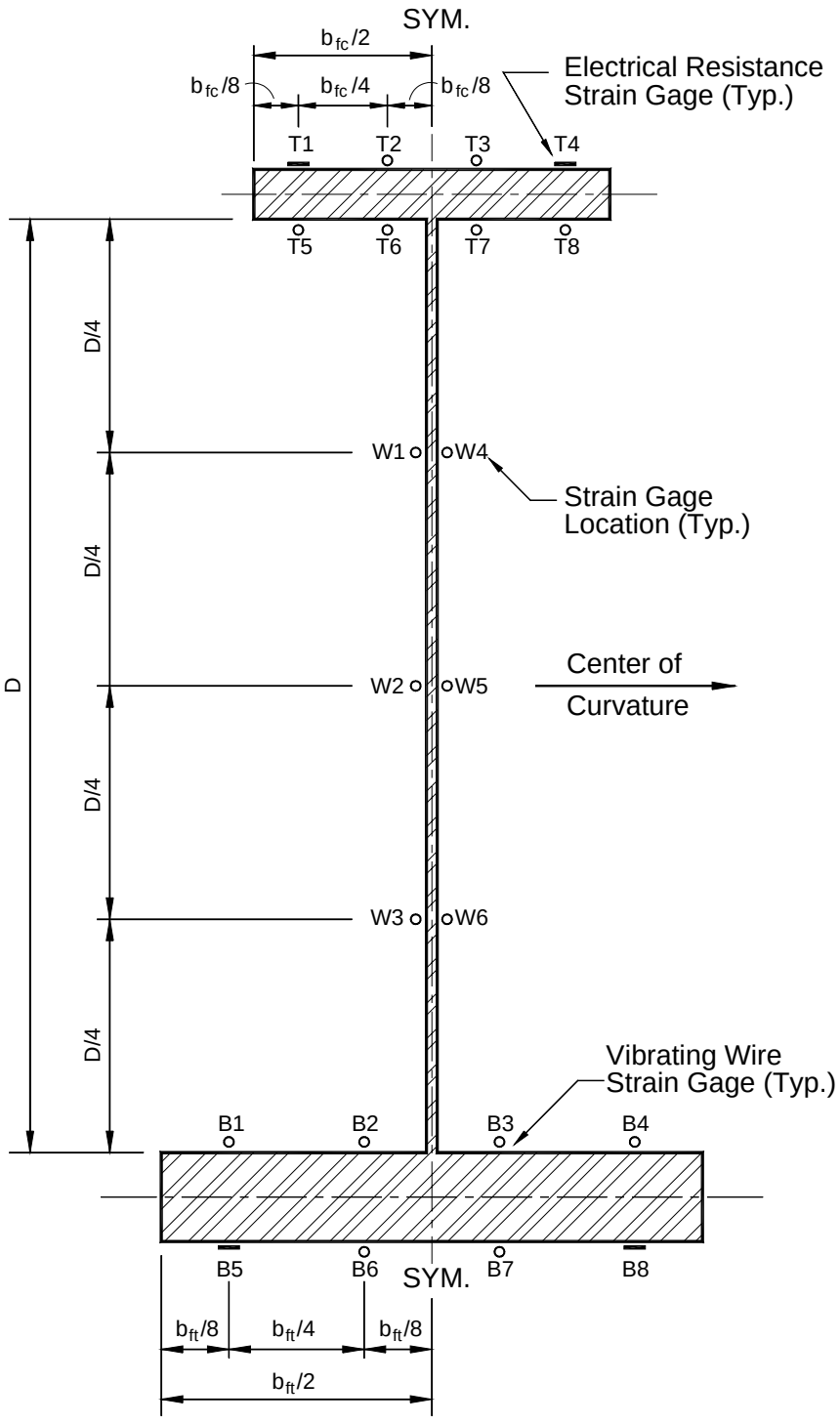

Figure 2-11: Instrumentation Configuration (V3)

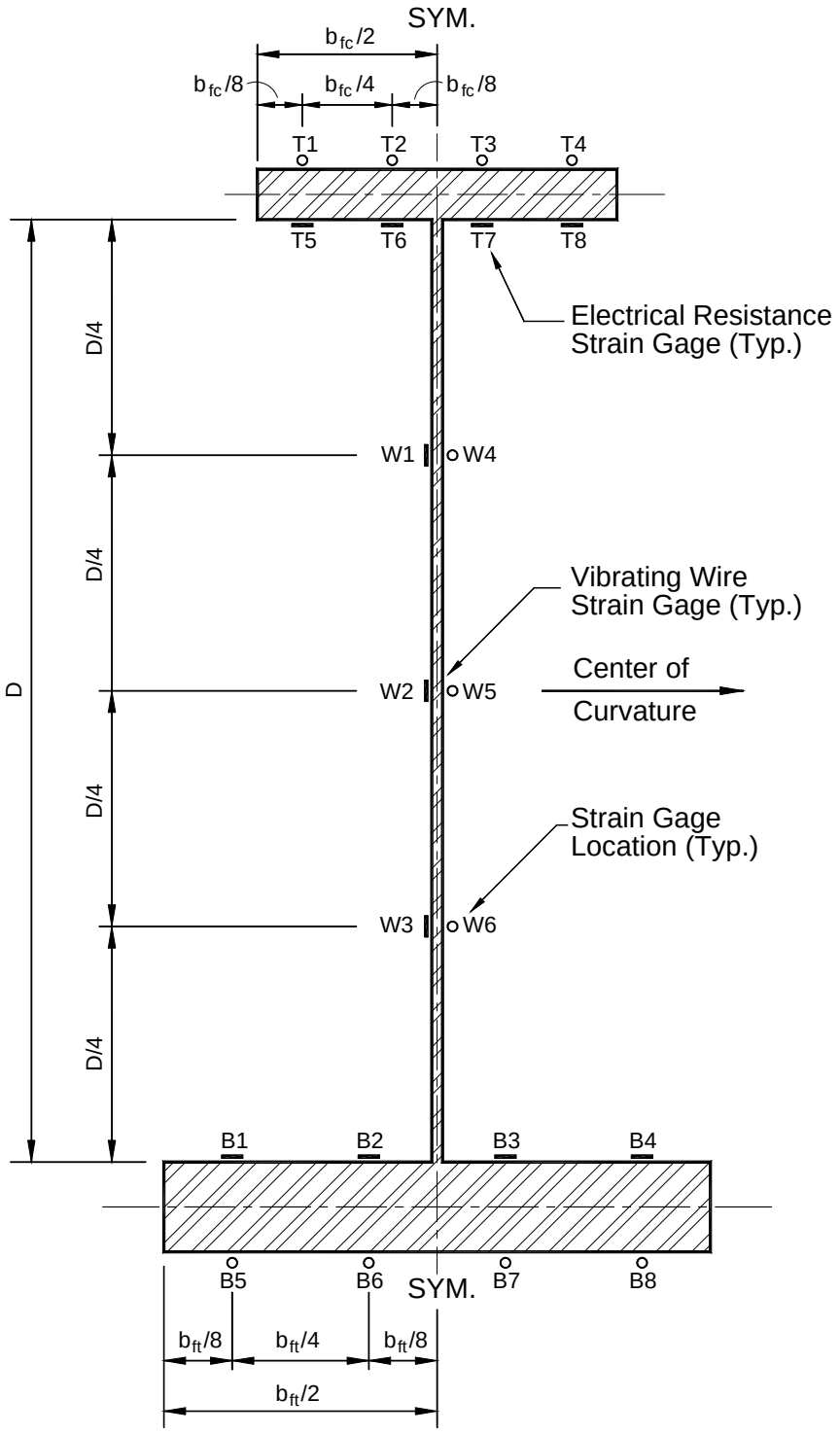

Figure 2-12: Instrumentation Configuration (V5)

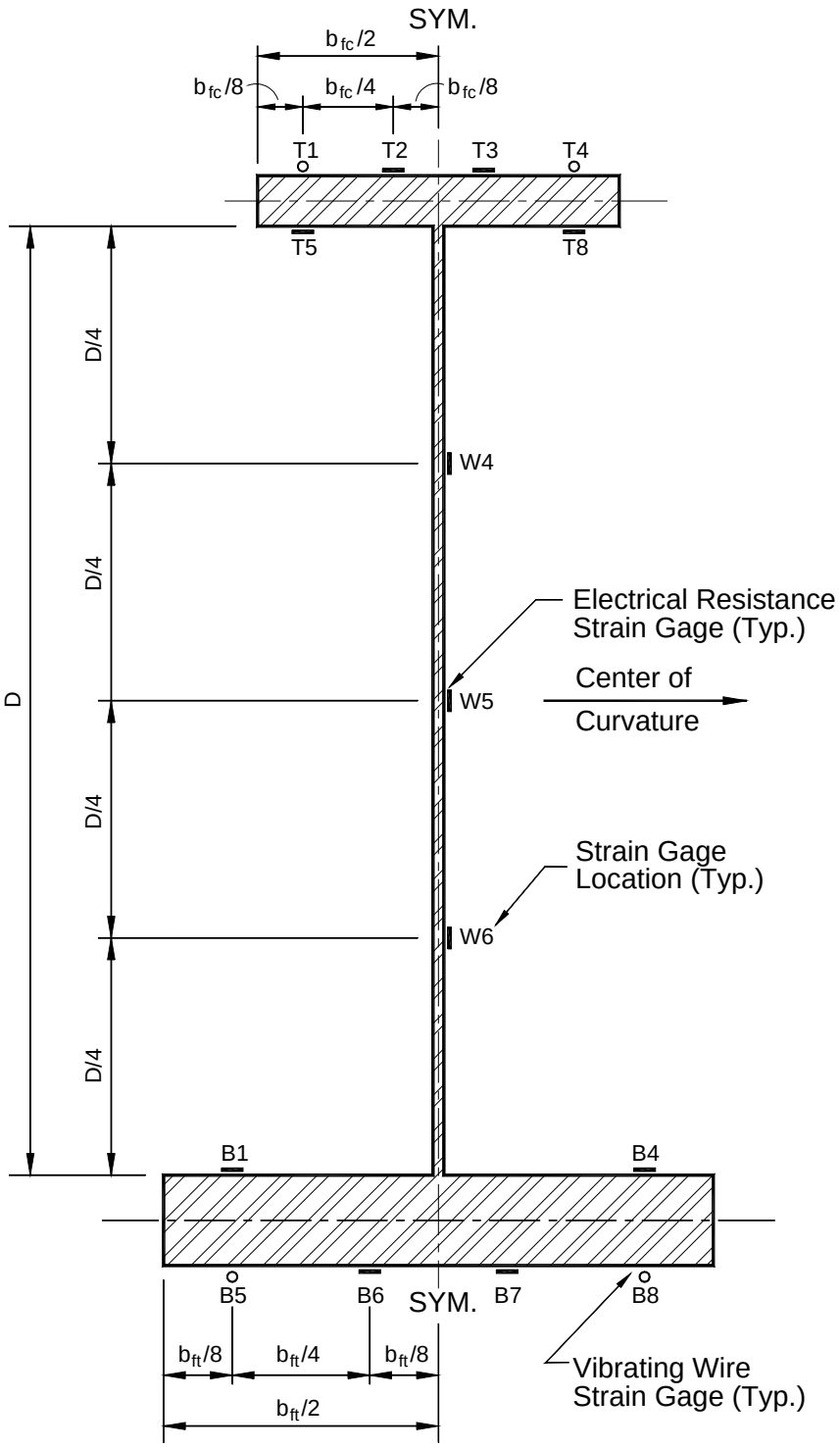

Figure 2-13: Instrumentation Configuration (V6)

2.5.2 Bending Component Instrumentation

Each bending component was instrumented at the six sections indicated in Figure 2-5. The sections labeled E and F are located 200 mm (8 in.) either side of mid-length of the component. These sections were used to determine the critical mid-span strains during each bending component test.

Section F used Instrumentation Configuration (V1) shown in Figure 2-9. The data produced by this instrumentation configuration captured the installation and dead-load effects experienced by each component prior to the applied load test. However, the instrumentation used at this section is primarily comprised of vibrating wire strain gages which have a limited reliable strain capacity, (<1800 μe) and are very sensitive to distortion. Therefore, as the steel flanges of the components approaches yield these instruments generally become inoperative.

Section E employed Instrument Configuration (1) shown in Figure 2-6. This configuration used only electrical resistance strain gages which have relatively large reliable strain capacities (>10,000 μe). However, this gage type tends to drift over extended periods of time. For this reason, the data needed to determine mid-span effects during the applied load portion of the component tests was acquired using the instrumentation at this section.

The Sections labeled C and H in Figure 2-5 employed Instrument Configuration (3) shown in Figure 2-8. These sections are located 200 mm (8 in.) towards mid-length of the component from the cross-frames N6L and N6R. The data acquired from these sections

during the applied load portion of the bending component tests was used to interpret the affect of the lateral bracing on the component.

2.6 Laboratory Equipment

2.6.1 Loading Apparatus

For the bending component testing, the curved steel girder test frame was loaded from above with six load frames at the locations indicated on Figure 2-1. These frames reacted off the floor of the structural laboratory and consisted of five major components, which are identified in Figure 2-14 and described below:

- The Cross Beam was comprised of two 2438 mm (8 ft) long MC310 x 67 (MC12 x 45) ASTM A572M Grade 345 (A572 Grade 50) channels bolted together around a series of spacers with 22 mm (7/8 in.) diameter ASTM A325 high strength bolts. The spacers were 75 mm (3 in.) lengths of schedule 40 pipe. The channels were set back-to-back with the spacers between them. The bolts passed through the web of one channel, then through the spacer and finally through the web of the other channel.
- The End Beams were duplicates of the Cross Beam with additional bolt holes in the webs near each end that allowed the attachment of the Brace Beams.

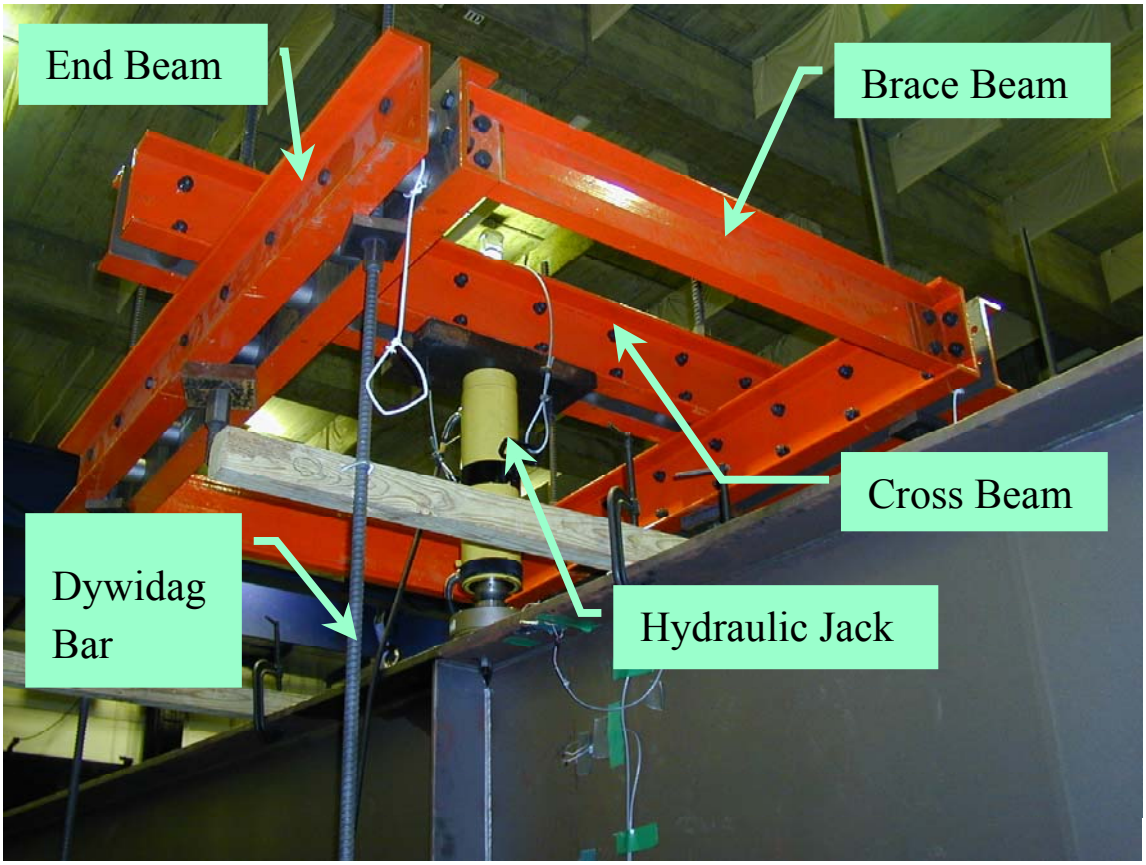

Figure 2-14: Typical Load Frame

- Approximately 1,372 mm (4 ft 6 in.) C250 x 22.8 (C10 x 15.3) ASTM A572M Grade 345 (A572 Grade 50) channels were used as braces and separators for the End Beams.
- Four 25 mm (1 in.) diameter Dywidag Grade 1030 (Grade 150) high strength thread-bars were used to attach each load assembly to the reaction floor.
- An Enerpac Model RR-10018 Heavy Duty Solid Plunger Double Acting Hydraulic Cylinder (jack) was used to load the test frame by reacting off the loading fixture. These jacks had an 890 kN (100 ton) capacity and a 457+ mm (18+ in.) stroke.

The load frames were secured to the reaction floor at tie down locations that were placed in a grid pattern at 914 mm (3 ft) centers. The four Dywidag bars of each load frame were connected to the floor tie downs at the corners of the 1829 mm (6 ft) north-south east-west square that was most centered on the load point. The bars extended from the floor to approximately 2438 mm (8 ft) above the top of the curved girder test frame.

One End Beam was connected to each of the northern and southern pair of Dywidag bars at approximately 610 mm (2 ft) above the top of the curved girder test frame. The bars passed through the spaced webs of the End Beams, which were held in place with anchor plates and nuts both above and below the beams. The End Beams were parallel, ran east-west and were 1829 mm (6 ft) apart.

The eastern and western ends of the End Beams were connected to a Brace Beam with 178 mm (7 in.) long L152 x 89 x 9.5 (L6 x 3½ x 3/8) angles. Two 22 mm (7/8 in.) diameter A325 bolts connected one leg of the angle to the web of the End Beam through standard holes. Two additional 22 mm (7/8 in.) diameter A325 bolts connected the other leg of the angle to the web of the Brace Beam through slotted holes.

The Cross Beam, with its weak axis in a vertical position, was then placed to span perpendicularly from one End Beam to the other over the load point on the curved girder test frame. The Cross Beam was connected to each of the End Beams with ±1219 mm (±4 ft) lengths of Dywidag thread-bars. At each of these connections, the Dywidag bar passed between the spaced webs of both the Cross Beam and the End Beam and was tensioned to securely hold the assembly together.

Before incorporation into the load frame assembly, the base of the hydraulic jack was attached to the center of a 305 mm x 610 mm x 51 mm (1 ft x 2 ft x 2 in.) thick steel

plate. The Jack was then attached to the Cross Beam at the load point location with ±1219 mm (±4 ft) lengths of Dywidag thread-bars. These bars passed between the spaced webs of the Cross Beam and through pre-drilled holes in the 51 mm (2 in.) plate and were tensioned to securely hold the assembly together. The Jack loaded the curved girder test frame through a machined ball and socket joint. The ball was attached to the hydraulic jack cylinder while the socket was attached to a load cell at the load point on the curved girder test frame.

All six hydraulic jacks were extended with a common pressure line. This line was fed by an Enerpac PEM-8418 Hi-Flow Hydraulic Pump capable of delivering up to 7.8 liters/minute (2 gallons/minute) at 68.9 MPa (10 ksi).

2.6.2 Instrumentation

The instrumentation plan was devised to provide redundancy in both the acquisition of data and analysis techniques. The plan was comprised of nearly 800 individual instruments, the vast majority of which were uni-axial electrical resistance strain gages.

2.6.2.1 Electrical Resistance Strain Gages

All electrical resistance strain gages used in this experimental program were manufactured by Measurements Group Incorporated and had an internal resistance of 120 ohms. Two types of electrical resistance strain gages were used: uni-axial or single-arm gages with a 6 mm (1/4 in.) gage length and rosettes with a 3 mm (1/8 in.) gage length.

Uni-axial gages or single-arm gages measure strain in one direction along the longitudinal axis of the gage. Rosette gages incorporate three uni-axial gages whose longitudinal axes coincide at a single point but are each separated by an angle of 50

gradients (45 degrees). This configuration allowed the three individual strain readings to be appropriately combined to determine the shear strain at that location.

Electrical resistance strain gages are very sensitive, have a large strain capacity and can be interrogated very quickly by a data acquisition system. However, they tend to drift over extended periods of time (days). Therefore, these gages were the primary source of data during the capacity testing of each bending component.

2.6.2.2 Vibrating Wire Strain Gages

Vibrating wire strain gages use changes in the natural frequency of vibration of a wire stretched between two points to measure strain. As the wire's length changes, the tension in the wire changes, which proportionally affects the wires natural frequency. The change in frequency can be mathematically equated to the change in length between the two points over which the wire is stretched. The gages used on this project were the Geokon models VK4100 that have a 51 mm (2 in.) gage length.

2.6.2.3 Load Cells

Load cells are essentially scales capable of measuring load along one axis. They use a circuit of multiple uni-axis strain gages, called a bridge, to determine load. All load cells used have an internal resistance of 350 ohms and have two electrical bridges that were independently monitored during testing by the MicroMeasurement 5000 (MM5000) and the Hewlett-Packard VXI (HP) data acquisition systems that are described in Sections 2.6.3.2 and 2.6.3.4, respectively.

StrainSert Model FL100U(C)-2DGKT Universal Flat Load Cells were used at each load point to determine the load applied to the test frame from the hydraulic rams. These

load cells have a capacity of 445 kN (100 kip) and are capable of measuring load to within 56 N (12.5 lbs).

StrainSert Model FL300U(C)-2DGKT Universal Flat Load Cells were used at each point of support to determine the vertical reaction of the test frame from all loads. These load cells have a capacity of 1,335 kN (300 kip) and are capable of measuring load to within 167 N (37.5 lbs).

2.6.3 Data Acquisition Systems

Four data acquisition devices were required to support the instrumentation plan. As previously stated, this plan included more than 800 instruments and required redundancy in many of the measurements. Of particular importance was the requirement to be able to interpret the data in near-real-time to direct the course of each experiment.

2.6.3.1 MicroMeasurements 4000

The MicroMeasurements 4000 (MM4000) has a 200-channel capacity and was used to monitor the 176 resistance strain gages on the cross-frames and lateral bracing in the south bay of the test frame between G1 and G2.

2.6.3.2 MicroMeasurements 5000

The MicroMeasurements 5000 (MM5000) data acquisition system has an 80-channel capacity. This system was used to monitor the rosette resistance gages on G3 as well as the load cells at the abutment and at the hydraulic actuator locations.

2.6.3.3 Geokon Micro-10

The Geokon Micro-10 system has an 80-channel capacity and was used in combination with five Model 8032 Multiplexers to monitor all 79 vibrating strain gages

used during each component test. This system was also used to monitor strains on the bending components as they were being installed.

2.6.3.4 Hewlett-Packard VXI

The Hewlett-Packard VXI (HP) data acquisition system has a 640-channel capacity. It was the workhorse of these experiments—monitoring a minimum of 576 instruments during each test. This system was used to monitor a majority of the electrical resistance strain gages and the entire set of load cells, potentiometers, tiltmeters, linearly variable displacement transducers (LVDTs) and instrumented studs used during the bending component experiments. The HP system is capable of manipulating and displaying the acquired data in near-real-time (about 90 seconds from recording initiation for these experiments).

Chapter 3. Analysis of Experimental Data

3.1 Execution of the Experiments

The test frame consisted of a three-girder bridge that was horizontally curved. Before any of the component testing began, the frame was erected with a prismatic outside girder (girder G3). This system was instrumented and elastically exercised over a period of months to prove the variety of instrumentation and data acquisition systems used.

The test frame was shored at the nine locations, shown in Figure 3-1, to begin the component testing. Load cells were utilized to monitor and to record the shoring reaction loads. Screw jacks were used to adjust the elevation of the shores—increasing or decreasing the shoring load—to obtain a desired reaction.

The shoring was used to eliminate as much of the dead load deflection from the structure as possible. The desired reactions were determined by constructing a finite element model shored at complimentary locations and by applying traction to simulate gravity. The results of the finite element analysis for the six girder abutment reactions and for the nine shoring reactions were used to establish a structural state that minimized the dead load effects within the test frame. This state will be referred to herein as the "no-load" condition.

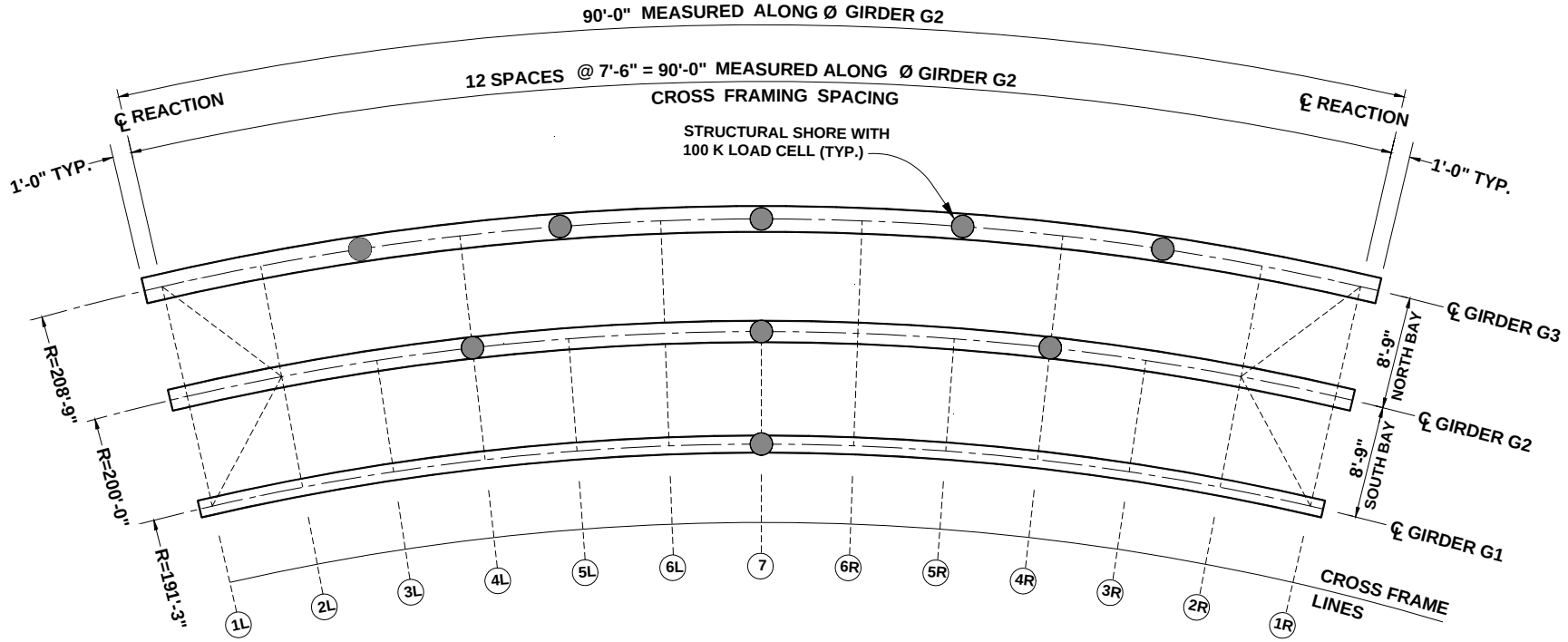

Figure 3-1: No-Load Condition Support Layout

Once the no-load condition was established, a bending component could be inserted into the outside girder (G3) of the test frame between the bolted field splices. After a bending component was bolted into G3, any outstanding instrumentation was applied, and all instruments were wired to one of the data acquisition systems. The shoring beneath the entire test frame and the component was then removed, and the dead load effects were captured using the data acquisition systems. This step, referred to as Shakedown-1 for each bending component test, was the first time the instrumentation supplied to the bending component was exercised over a significant range of strain. A complete set of data was acquired during Shakedown-1 in most of the bending component tests. However, individual pieces of instrumentation or the data acquisition systems occasionally did not perform as intended, and some data were corrupted or lost. These losses proved insignificant to the analysis of the results.

After the shoring was removed, frames were erected that supplied the load to two locations on the top flange of each of the three girders. These frames were tied to the reaction floor of the laboratory using four high-strength steel rods. Double action hydraulic actuators that were connected to the frames supplied the load to the top flanges through a ball and socket joint. The joint acted on a load cell attached to the top flange at each load point. The load frames are described in detail in Section 2.6.1.

If issues with the instrumentation or data acquisition systems arose during Shakedown-1, a series of loadings were applied to the entire test frame using the load frames. These proof tests were conducted repeatedly to exercise and prove the instrumentation and electronic equipment. These series of proof tests, referred to as

Shakedown-2, Shakedown-3 etc., were continued until all devices were working properly and as expected.

3.2 Data Analysis

The analysis in this report focuses primarily on the strain data acquired from two instrumented cross-sections. These cross-sections, labeled E and F in Figure 2-5, were located 203 mm (8 in.) from either side of the mid-span of each bending component. The offset from the actual mid-span location for each of these instrumented cross-sections was necessary due to the local influences of the mid-span transverse stiffener present on six of the seven bending components. However, the vertical bending, horizontal bending and torsion diagrams were all relatively constant throughout this range of the girder. This uniformity allowed a collective interpretation of the results.

Cross-section F was primarily instrumented with vibrating wire strain gages that had a long-term stability but a relatively small strain range. For this reason, the data collected at this section, during the usually multi-day process for the bending component installation, were used to determine the installation effects at mid-span. Cross-section E was instrumented completely with electrical resistance strain gages. Because these gages are highly accurate over large ranges of strain, their data are used to determine the conditions at mid-span throughout the applied-load portion of each experiment.

Analysis results included in this report for cross-sections other than E and F on the bending component are appropriately labeled.

Four force actions cause normal strain, ε, in an I-girder cross-section: bending about the strong axis, bending about the weak axis, warping torsion and axial load. Using the Beam theory, the normal strains that result from these force actions are appropriately

combined at any point on the I-girder cross-section (shown in Figure 3-2) using Equation 3-1.

$$\varepsilon = -\frac{M_x y}{EI_x} + \frac{M_y x}{EI_y} + \frac{BiW_n}{EC_w} + \frac{P_z}{EA} \qquad \text{Equation 3-1}$$

Where:

P_z = Axial force in the z-direction

E = Modulus of elasticity of steel

A = Cross-sectional area of the I-girder

M_x = Moment about the x-axis

y = Normal distance from the y-axis

I_x = Moment of inertia of the cross-section about the x-axis

M_y = Moment about the y-axis

x = Normal distance from the x-axis

I_y = Moment of inertia of the cross-section about the y-axis

C_w = Warping constant

Bi = Bimoment

W_n = Normalized unit warping

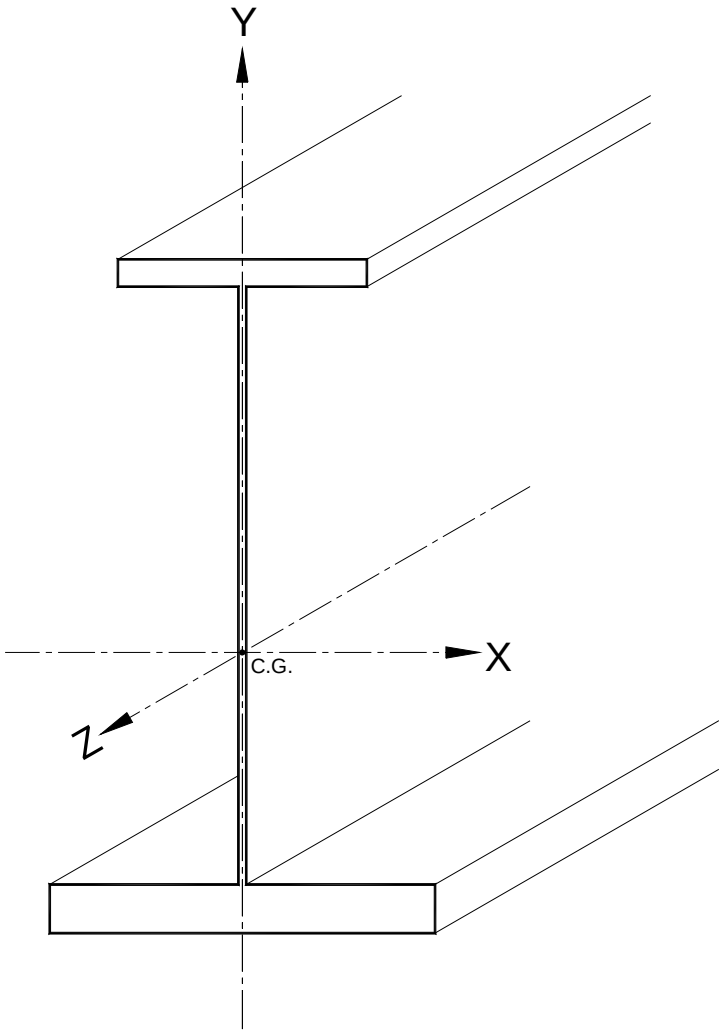

Figure 3-2: I-Girder Coordinate System

The aggregate normal strain distributions in the flanges can be separated using the thin-walled, open-section, Beam theory into each component of strain associated with a respective force action. The following equations utilize the magnitude of normal strain in the compression (top) flange tips as a unit quantity that can be scaled as indicated to determine the complementary strains in the tension (bottom) flange tips.

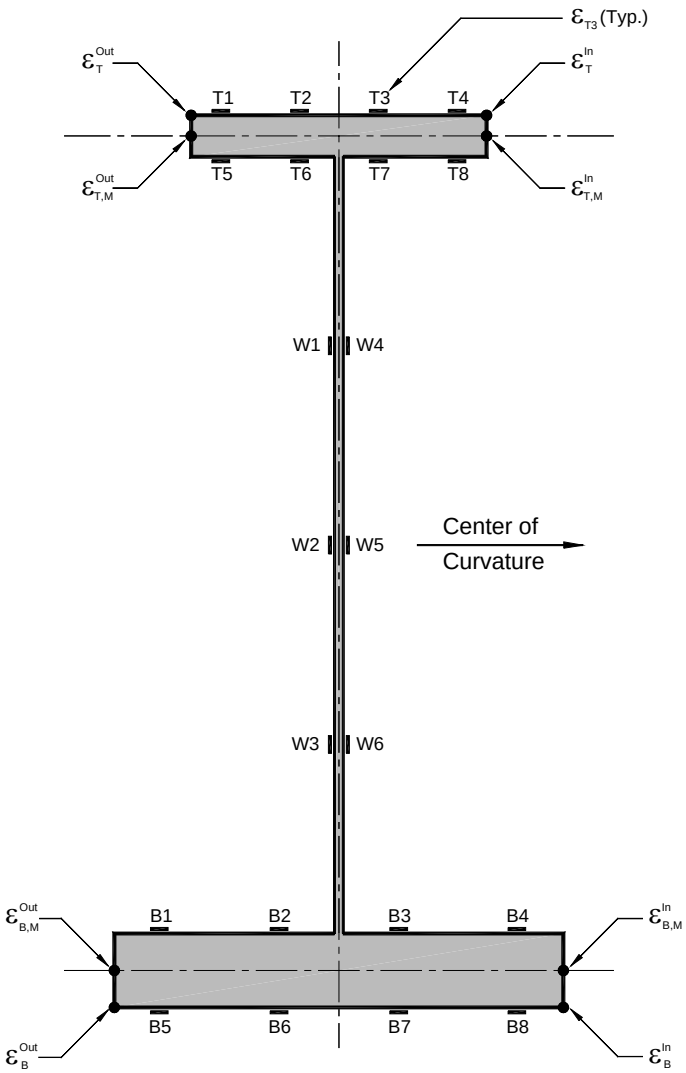

Figure 3-3: Identification of Strain Measurement and Resultant Locations

$$\varepsilon_{T,M}^{out.} = -\varepsilon_{z,M_x} + \varepsilon_{z,M_y} + \varepsilon_{z,M_z} - \varepsilon_{z,P_z} \qquad \text{Equation 3-2}$$

$$\varepsilon_{T,M}^{in.} = -\varepsilon_{z,M_x} - \varepsilon_{z,M_y} - \varepsilon_{z,M_z} - \varepsilon_{z,P_z} \qquad \text{Equation 3-3}$$

$$\varepsilon_{B,M}^{out.} = \alpha\varepsilon_{z,M_x} + \beta\varepsilon_{z,M_y} - \gamma\varepsilon_{z,M_z} - \varepsilon_{z,P_z} \qquad \text{Equation 3-4}$$

$$\varepsilon_{B,M}^{in.} = \alpha\varepsilon_{z,M_x} - \beta\varepsilon_{z,M_y} + \gamma\varepsilon_{z,M_z} - \varepsilon_{z,P_z} \qquad \text{Equation 3-5}$$

Where:

$$\alpha = \left[\frac{D - 2y_{NA} + t_{ft}}{D + 2y_{NA} + t_{fc}} \right] \qquad \text{Equation 3-6}$$

$$\beta = \left[\frac{b_{ft}}{b_{fc}} \right] \qquad \text{Equation 3-7}$$

$$\gamma = \left[\frac{D - 2y_{NA} - 2y_{SC} + t_{ft}}{D + 2y_{NA} + 2y_{SC} + t_{fc}} \right] \left[\frac{b_{ft}}{b_{fc}} \right] \qquad \text{Equation 3-8}$$

The location of these strain quantities on the cross-section of the girder is shown in Figure 3-3. The geometric characteristics are defined on Figure 3-4.

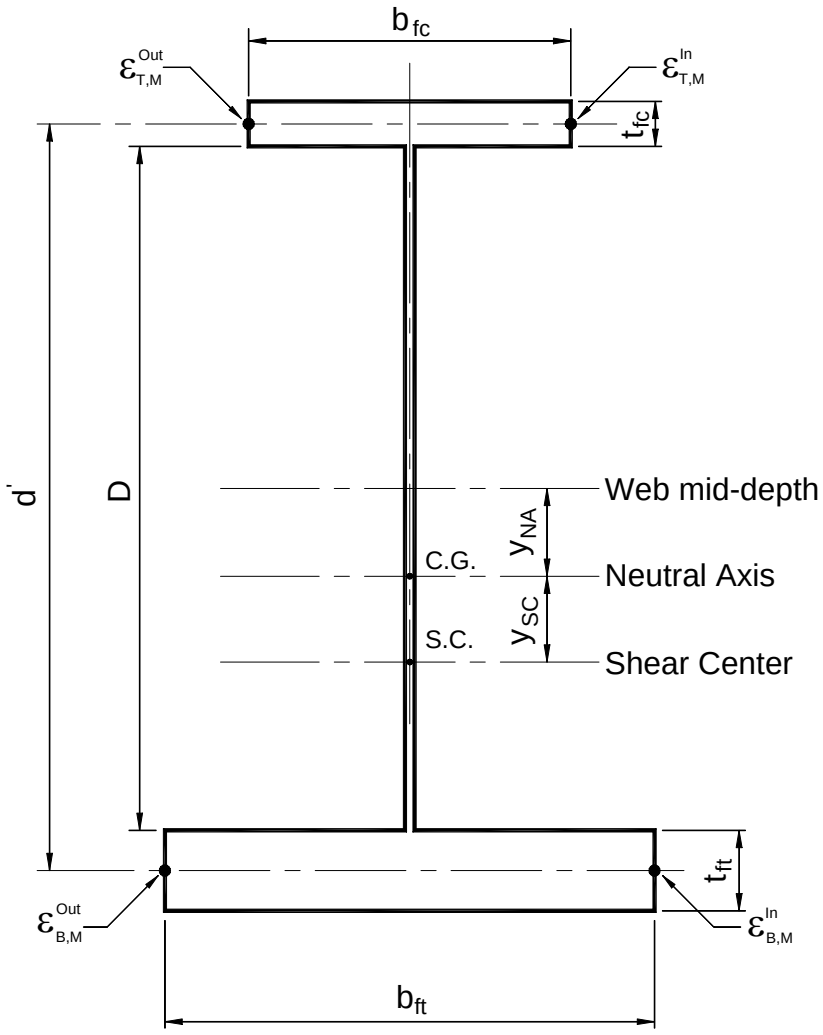

Figure 3-4: Cross-Sectional Parameters

In the tests of the cross-sections that are doubly symmetric, the scalars defined in Equations 3-6 through 3-8 are approximately equal to 1.0, which reduces Equations 3-4 and 3-5 to the following:

$$\varepsilon_{B,M}^{out.} = \varepsilon_{z,M_x} + \varepsilon_{z,M_y} - \varepsilon_{z,M_z} - \varepsilon_{z,P_z} \qquad \text{Equation 3-9}$$

$$\varepsilon_{B,M}^{in.} = \varepsilon_{z,M_x} - \varepsilon_{z,M_y} + \varepsilon_{z,M_z} - \varepsilon_{z,P_z} \qquad \text{Equation 3-10}$$

The resulting strain distribution from each described force action can be seen in Figure 3-5. Strong-axis bending produces a gradient of strain through the thickness of the flanges. At any location on the cross-section, the magnitude of strong axis bending strain is proportional to the normal distance from that location to the bending neutral axis shown in Figure 3-4. If this strain is determined for the extreme fiber tip of the compression flange using the first term in Equation 3-1, then this magnitude can be scaled by α (Equation 3-6) to determine the extreme fiber tip strain in the tension flange.

Weak-axis bending and torsional warping produce gradients of strain along the width of the flanges. For all I-girders, the magnitude of weak-axis bending strain is proportional to the normal distance from the location of interest to the y-axis defined in Figure 3-3, because this is an axis of symmetry for these section types. Weak-axis bending strain is determined by the second term in Equation 3-1. The extreme fiber compression flange tip strains are modified by β (Equation 3-7) to determine the extreme fiber tension flange tip strains.

The magnitude of flange tip torsional warping strain is proportional to the aggregate normal distances from the location of interest to both the y-axis and to the shear center of the section. The third term of Equation 3-1 is used to determine the normal strain due to warping. This term is presented using the Bimoment, *Bi*, so that it takes a familiar form.

The Bimoment represents the magnitude of lateral flange bending due to warping torsion in each flange multiplied by the distance between flange centroids. The torsional warping strain at the extreme fiber tip in the compression flange is scaled by γ (Equation 3-8) to obtain the extreme fiber tip strain in the tension flange.

The axial load produces a uniform strain throughout the cross-section. The magnitude of this strain is determined with the fourth term in Equation 3-1.

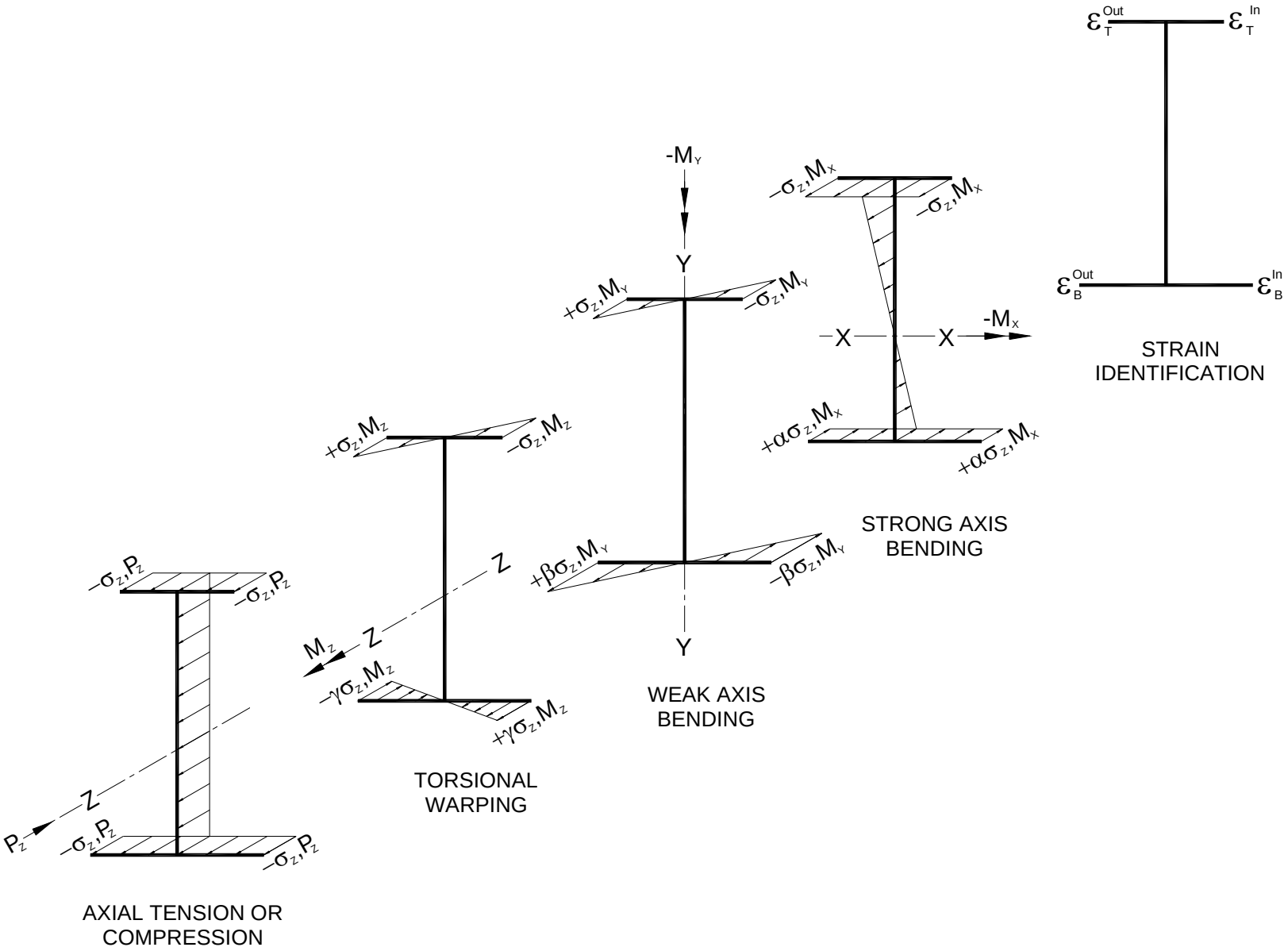

Figure 3-5: Components of Longitudinal Strain

3.3 Installation Strains

The installation of each of the bending components into the test frame locked forces into the system through the completion of each bolted field splice and the insertion of the cross-frames at locations N6L and N6R. The strain effects from this erection were monitored at two sections on the bending component with vibrating wire strain gages. The following process, used to acquire these strains, was designed to minimize the amount of longitudinal warping strain and primary-axis bending strain present in the bending component prior to being installed into the test frame.

1. Block bending component at approximately 1/3rd points while standing vertically.

2. Measure and record straight-line distance from inside of the flange tips at one end to inside of the flange tips at the other end.

3. Lay specimen on its side with blocking now provided at the ends and the 1/3rd points. Adjust blocking to recreate flange distance measurements.

4. Apply vibrating wire gages at all accessible locations. Read and record all applied gages three times. Individual gage readings should not be consecutive, but should be the result of a circuitous reading procedure.

5. Return component to vertical position blocked again at 1/3rd points.

6. Apply remaining vibrating wire gages. Read and record all gages, both those applied in this step and those applied previously, three times as stated above. Also, read and record all test frame instrumentation.

7. Bolt component into test frame. Read and record all operating instrumentation.

8. Bolt cross-frame N6L to the test frame and to the component. Read and record all operating instrumentation.

9. Bolt cross-frame N6R to the test frame and to the component. Read and record all operating instrumentation.

The acquisition of the vibrating wire strain gage data during the installation of bending component B1 was accomplished using a vibrating wire gage readout box and a single gage reader. The reader was manually placed over one gage at a time, and the readout box indication was recorded by hand. After reviewing the data, it became apparent that the strain readings were very sensitive to operator technique. This sensitivity was confirmed by having three individuals independently produce the vibrating wire gage data with the bending component and test frame in a steady-state condition. While some of the cross-referenced strain indications were consistent, large groups of the data included at least one divergent reading.

Therefore, to increase the consistency and value of the installation strain data, the process of manual readings was replaced with automatic strain data collection using an acquisition system. Each vibrating wire gage was hardwired to a data acquisition system as the gage was installed on the bending component. The installation strain data for bending components B2, B3, B4, B5, B6 and B7 were acquired with this acquisition system. Unfortunately, in spite of the best efforts of the laboratory staff, most of the recorded data from the installation of components B2 and B3 was corrupted.

An analysis of the installation strains collected for the components B4 through B7 instills high confidence in the data. Using the Beam theory analysis, detailed earlier in this Section, on independent subsets of the data produces the same group of equilibrated internal forces at the instrumented section. The results of the analysis on the installation strain data are summarized in Table 3-1 for these specimens.

Specimen	Normal strain (μe) from			
	M_x	M_y	M_z	P_z
B4	257	22	82	-31
B5	172	4	236	1
B6	157	-24	12	3
B7	74	199	122	-29

Table 3-1: Installation Strain Data Analysis Results for Specimens B4, B5, B6 and B7

The installation strain analysis for component B4 shows that the vast majority of strain is the result of strong-axis bending. The analysis also indicates that a small axial force, 6 MPa (0.9 ksi), is also present in the component. However, the presence of this force is not supported by other test frame data. This apparent axial force is most likely the result of distortion in the web plate, which has a slenderness of 188.0 due to the section geometry that is singly symmetric. A review of the web data collected during installation supports this interpretation. However, the review was not definitive because information for only one face of the web was available.

Figure 3-6 plots the B4 installation strain magnitudes onto their respective I-girder plate component. This figure is the first in a series used throughout this report to show the distribution of longitudinal strain along an I-girder cross-section. On these figures individual longitudinal strains are plotted at the location where they were recorded using the scales attached to each plate of the cross-section. Then, a line representing the linear

regression result of the family of data from any one surface is also plotted using the same scales. These linear regression lines essentially indicate the distribution of longitudinal strain along each plate and project a plate tip strain.

Flange strains are indicated with triangles. Triangles that point up show data from the top of the plate. Triangles that point down show data from the bottom of the plate. The shaded triangles indicate that the data is from the outside of the plate at the location of the extreme fiber for strong-axis bending. The open triangles indicate that the data is from the inside surface of the plate i.e. top of the bottom flange or bottom of the top flange.

Web strains on the inside of the web, the face closest to the center of curvature, are indicated with an open diamond. Web strains on the outside face of the web are indicated with a shaded square.

Returning to Figure 3-6, the regression line for the web data shown crosses the web at the approximate location of the bending neutral axis. However, its fit to the individual strain data is poor, which supports the hypothesis of web flexing as the cause of the apparent axial force. Also, while the data for the top and bottom of the compression (top) flange indicate similar trends, the tension (bottom) flange data reveal a slight localized bending on the outside of the plate by the intersection of the regression lines.

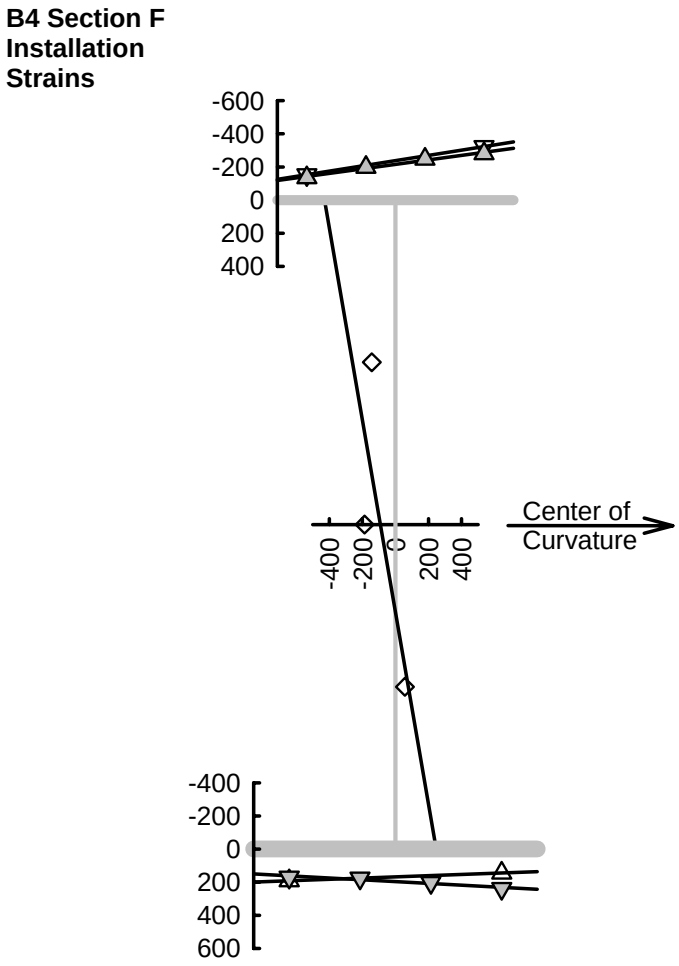

Figure 3-6: B4 Installation Strain Data

The installation strain analysis for doubly symmetric B5 reveals that a slight majority of the installation strain resulted from torsion in the component. This torsion was caused by the insertion of the cross-frames between B5 and G2. The remainder of the installation strains were caused by strong-axis bending due to the bolted field splices and to the dead load of the component suspended between supports.

Figure 3-7 shows the linear behavior of the B5 installation strains. The flange strain gradients, which trend oppositely in the constructed figure, indicate a large torsional warping component in the strain data.

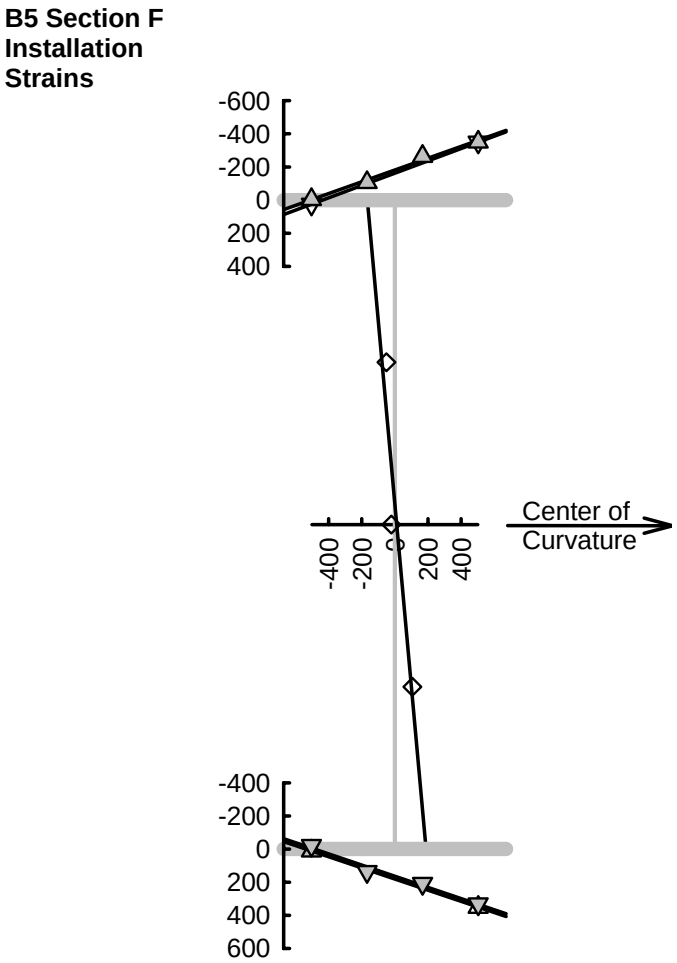

Figure 3-7: B5 Installation Strain Data

The installation strain analysis for doubly symmetric B6 shows that the insertion of the cross-frames was insignificant on this component. The strain from installation can be attributed almost entirely to the effect of the bolted field splices and to the vertical bending due to dead load. Figure 3-8 shows the near uniform strain across both flanges that supports the analysis.

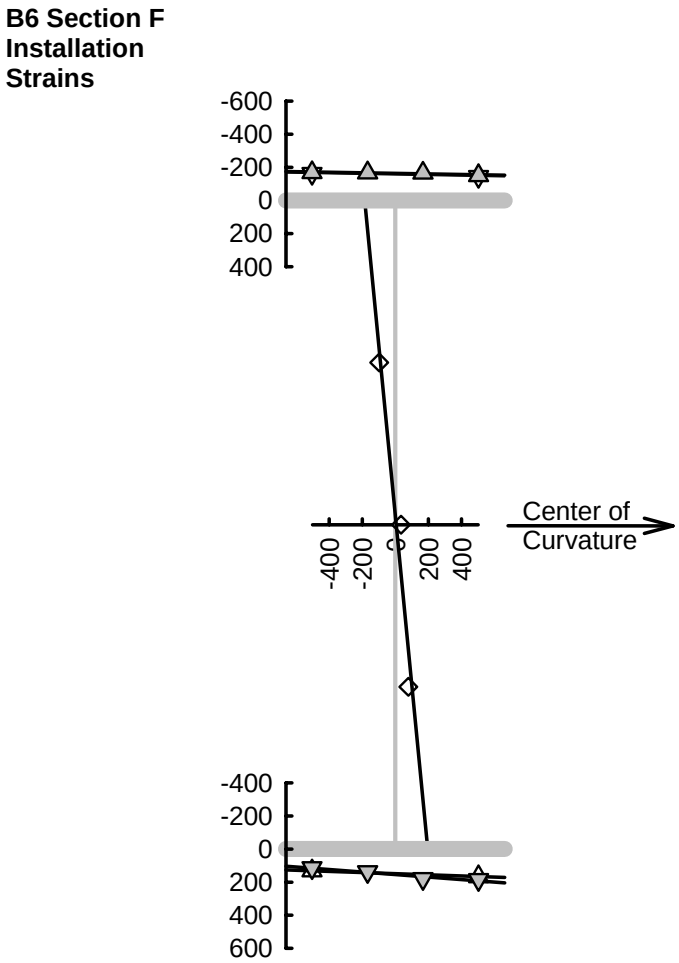

Figure 3-8: B6 Installation Strain Data

Similar to B4, bending component B7 is also singly symmetric. While the strain data that were acquired during installation are held in high confidence, the data analysis did not produce an ideal strain distribution and resulted in an apparent small axial stress acting on the cross-section, 6 MPa (0.9 ksi). However, this result is most likely due to the fabrication process used to create B7 that is described in Section 2.3.1.3.

Figure 3-9 shows the installation strains and associated regression lines for component B7. While the overall installation had little effect on the web and bottom (tension) flange, the top (compression) flange was influenced by the insertion of the cross-frames between B7 and G2. The figure indicates that the weak-axis bending and

warping components of normal strain are of similar magnitude because they negated each other in the tension flange and combined to produce a significant strain gradient in the compression flange. This graphic evidence supports the data analysis.

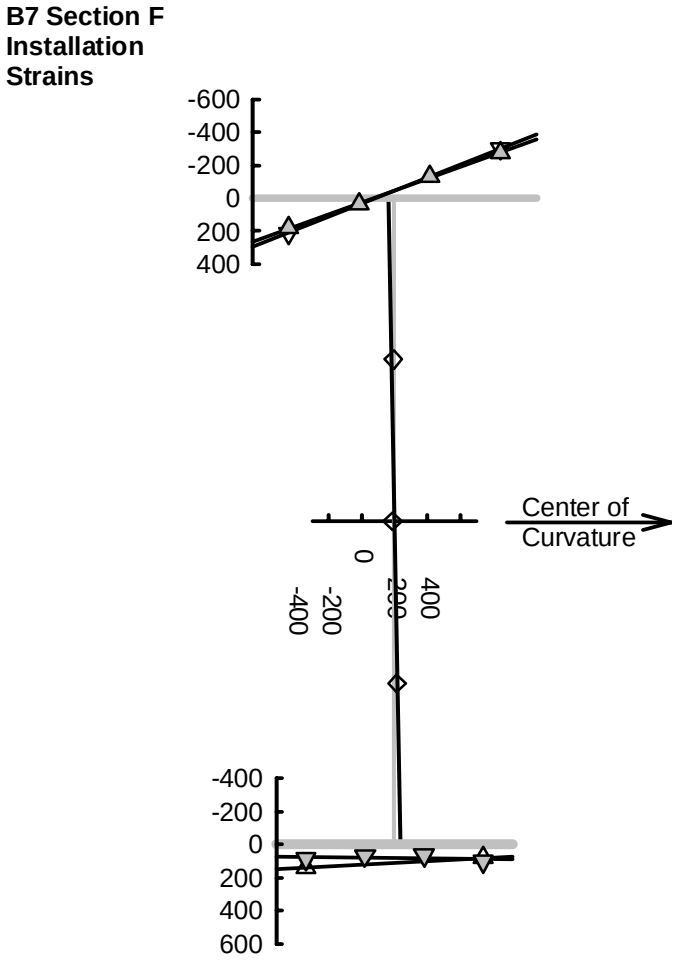

Figure 3-9: B7 Installation Strain Data

Because the installation strain data for B1 are considered suspect and the data for B2 and B3 were largely corrupted, an estimate of the installation strain levels for these components was made using the data from B5 and B6. The data from B4 were slightly affected by the single axis symmetric of the section; therefore, they were excluded from this estimate. The data from B7 were influenced by the fabrication process employed with this component and were also excluded from this estimate.

To create the model of the estimated installation strain levels for B1, B2 and B3, the strain data analyses for B5 and B6 were used to determine the moments about each axis that resulted from the installation process. These moments were averaged, and the averages were analyzed for their effects on sections B1, B2 and B3. The results of this operation are the sets of strain listed in Table 3-2 for components B1, B2 and B3. These strains are contrasted with the actual installation strain data for components B4 through B7 also in Table 3-2. These estimated installation strain levels were used to analyze the experimental data of B1, B2 and B3.

Strain Gage Location	Bending Specimen						
	B1*	B2*	B3*	B4	B5	B6	B7
	Installation Strain (μe)						
T1	-118	-110	-110	-136	-4	-168	183
T2	-182	-175	-174	-197	-106	-167	38
T3	-247	-240	-238	-247	-264	-166	-128
T4	-311	-304	-302	-280	-350	-150	-273
T5	-112	-104	-104	-153	25	-162	213
T8	-304	-298	-296	-322	-349	-144	-297
W4	-105	-102	-102	-143	-50	-97	-5
W5	-2	-2	-2	-186	-21	34	-11
W6	100	97	97	57	106	79	16
B1	85	78	78	191	11	132	141
B4	321	314	313	144	351	166	82
B5	92	85	84	170	-21	114	88
B6	170	163	162	176	137	138	71
B7	249	242	241	202	208	180	65
B8	327	321	319	239	332	185	102
*Strain levels estimated using B5 and B6 data.							

Table 3-2: Installation Strain Data Used in Bending Component Capacity Analysis

Figure 3-10 shows the regression lines that are the result of the estimated installation strain levels and the suspect installation strain data from B1. The estimated levels primarily indicate vertical bending and warping in the girder flanges and bound most of the suspect data.

Figure 3-11 shows the effects of the estimated installation strain levels on component B2.

Figure 3-12 shows the effects of the estimated installation strain levels on component B3 and the data that were determined reliable from the actual installation of B3. The actual data are once again adequately bound by the estimate, instilling confidence in the estimation procedure.

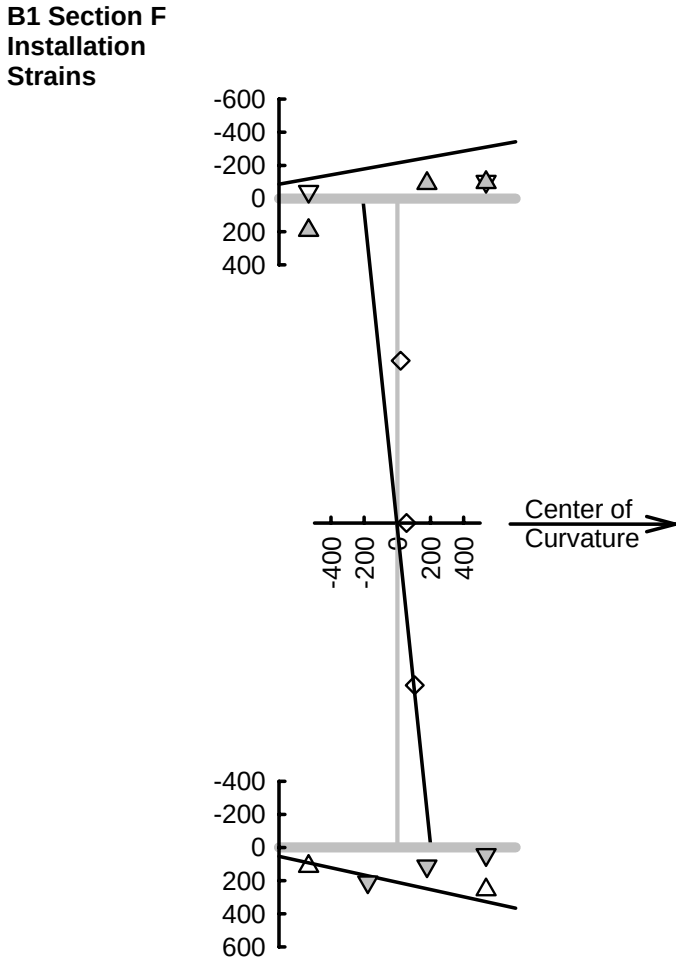

Figure 3-10: B1 Installation Strain Data with Regression Line Estimates

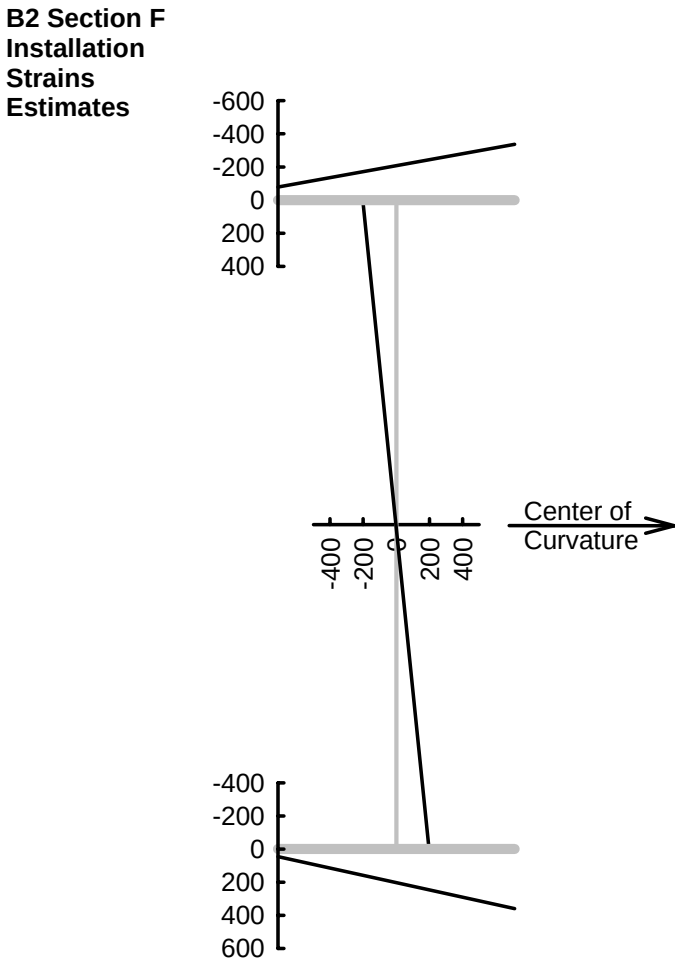

Figure 3-11: B2 Installation Strain Model From Regression Line Estimates

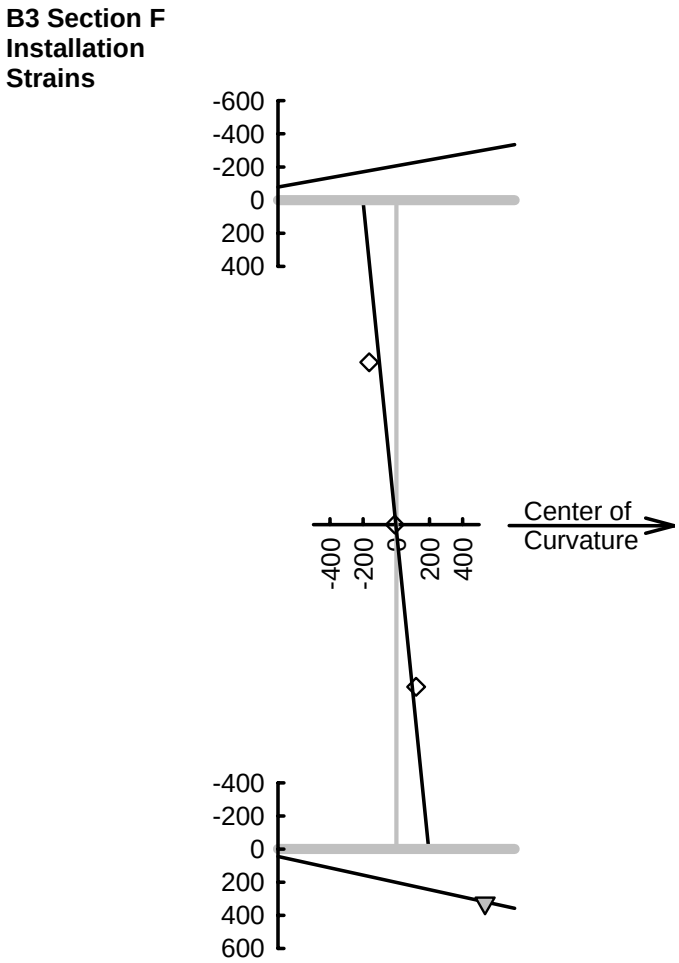

Figure 3-12: B3 Installation Strain Data With Regression Line Estimates

3.4 Bending Component B1 Test

The test frame containing bending component B1 was loaded in 28 steps to a maximum applied load of 1,354 kN (304.3 kip). As indicated in Table 3-3, the majority of these steps represent approximately 27 kN (6 kip) increments in applied load. Once the system became non-linear, both load increment and displacement increment were monitored in an effort to capture the peak resistance of each bending component.

The component behavior analyses in this report utilize the steel plate specific yield criteria established from material testing and reported in Appendix A. That is, each plate

of an I-girder cross-section has an associated yield strength determined through experimentation, which is used to interpret the behavior and performance of that plate.

Vertical bending moments at mid-span of the component are calculated by two methods in the elastic range; the direct method and the indirect method. The direct method converts the individual strain readings recorded at mid-span of the component to a moment using the Beam theory describe earlier in this Chapter.

The indirect method considers a free body of half the test frame between mid-span and one of the abutments. Using the applied loads and end reactions a mid-span vertical bending moment can be determined for the entire test frame. This moment can then be reduced to a component mid-span moment by employing the Beam theory to solve for the vertical bending moments in both G1 and G2, and then subtracting them from the total. While the indirect method is proven by and is redundant to the direct method in the elastic range, it is the sole method of determining the component mid-span moment in the inelastic range.

First yield in B1 occurred at the inside tip of the compression flange during load step 8 at a total applied load of 826 kN (185.6 kip). At the step 8 load level, the vertical bending moment resisted by B1 was determined to be 3,513 kN-m (2,591.0 k-ft) using the direct method of calculation and 3,516 kN-m (2,593.0 k-ft) using the indirect method of calculation. Table 3-4 contains a summary of the B1 mid-span stresses and the moments that are a result of the strain data analysis. This table shows that the ratio of vertical flange bending stress to lateral flange bending stress was between 0.46 and 0.47 throughout the elastic load range. Also, first yield occurred at a ratio of vertical bending moment to calculated vertical yield moment, M_x^{yield},of 0.69, and during the maximum

sustained applied load this ratio rose to 0.90. M_x^{yield} is calculated using the yield strength of the compression flange and is the strong-axis bending moment required to cause yielding at the extreme fiber of the compression flange without consideration for instability.

Figure 3-13 shows a comparison of the resisted vertical bending moment for each method of calculation, direct and indirect, throughout the elastic range of loading. The purpose of this figure is to establish the accuracy of the indirect method of calculation in determining the vertical bending moment being resisted by the component. The direct method relies on the principles of the Beam theory. Therefore, at load levels that cause the component to exceed its yield strength or distort significantly out of plane this method of determining the resisted vertical bending moment no longer applies. Accordingly the indirect method is relied upon in the non-linear region of component behavior.

Load Step	Total Applied Load	Mx (Total)	Mx (G1)	Mx (G2)	Mx (B1)		
					Indirect (a)	Direct (b)	(a)/(b)
	KN	kN-m	kN-m	kN-m	kN-m	kN-m	
B1 Elastic							
1	0.0	-1.0	0.4	-0.2	-1.1	-2.6	0.44
2	63.8	242.9	24.8	88.2	129.9	116.5	1.11
3	187.8	759.1	52.4	293.1	413.6	397.6	1.04
4	329.7	1379.3	84.2	538.3	756.8	735.8	1.03
5	459.8	1953.0	115.0	773.6	1064.4	1050.8	1.01
6	650.0	2798.1	158.1	1103.8	1536.3	1506.9	1.02
7	802.7	3481.2	187.7	1379.4	1914.2	1888.9	1.01
8	825.6	3582.1	190.8	1434.2	1957.1	1954.4	1.00
B1 Plastic							
9	844.5	3666.6	193.9	1468.9	2003.7	2004.9	1.00
10	878.1	3816.3	198.6	1537.0	2080.7	2116.2	0.98
11	900.0	3913.7	200.3	1582.9	2130.4	2201.0	0.97
12	923.8	4023.4	198.9	1633.8	2190.8		
13	957.0	4168.9	200.3	1703.2	2265.4		
14	982.6	4283.9	195.1	1764.2	2324.6		
15	1012.3	4415.9	193.7	1834.0	2388.2		
16	1035.5	4518.0	188.6	1894.7	2434.6		
17	1068.9	4668.2	192.1	1961.3	2514.8		
18	1094.2	4780.0	187.3	2018.8	2573.9		
19	1119.0	4893.7	185.4	2086.6	2621.6		
20	1139.7	4988.2	183.4	2145.2	2659.6		
21	1166.0	5106.3	177.1	2216.1	2713.1		
22	1197.5	5245.8	168.1	2308.7	2768.9		
23	1216.4	5314.1	155.2	2369.0	2789.9		
24	1248.3	5452.1	150.0	2457.9	2844.2		
25	1265.8	5528.1	140.1	2517.3	2870.6		
26	1296.8	5661.1	123.3	2631.9	2905.9		
27	1329.4	5803.4	96.9	2759.7	2946.9		
28	1353.5	5910.4	79.3	2850.9	2980.3		
29	1344.6	5860.0	8.2	3026.0	2825.8		

Table 3-3: B1 Applied Load Steps and Resulting Girder Moments

Load Case	Total Applied Load	Compression Flange, Inside Tip, Extreme Fiber Stress							Moments at Section					
		σ_z Total	σ_z from M_x (a)	σ_z From M_y	σ_z from M_z	σ_z from P_z	σ_z(lat.) (b)	(b)/(a)	M_x Direct	M_x Indirect (c)	M_y	Bi	$M_{lat.}$ Comp. Flange	(c)/M_x^{yield}
	kN	MPa	MPa	MPa	MPa	MPa	MPa		kN-m	kN-m	kN-m	kN-m^2	kN-m	
Elastic														
Install.		-69.97	-43.24	2.86	-29.06	-0.52	-26.20	0.61	536.8		-3.7	45.8	16.8	
DL		-109.90	-82.33	-2.06	-29.63	4.11	-31.68	0.38	1022.1		2.6	46.6	20.3	
Install.+DL		-179.87	-125.57	0.80	-58.69	3.59	-57.88	0.46	1559.0		-1.0	92.4	37.0	
(1)	0.0	-179.66	-125.36	0.86	-58.73	3.58	-57.87	0.46	1556.4	1557.8	-1.1	92.5	37.0	0.31
(2)	63.8	-193.78	-134.96	-0.10	-62.26	3.54	-62.36	0.46	1675.5	1688.9	0.1	98.0	39.9	0.33
(3)	187.8	-226.50	-157.60	-1.82	-70.68	3.59	-72.49	0.46	1956.5	1972.6	2.3	111.3	46.3	0.39
(4)	329.7	-265.90	-184.84	-3.84	-80.91	3.69	-84.75	0.46	2294.7	2315.8	4.9	127.4	54.2	0.46
(5)	459.8	-302.76	-210.21	-5.71	-90.64	3.79	-96.34	0.46	2609.8	2623.4	7.3	142.7	61.6	0.52
(6)	650.0	-356.74	-246.95	-8.99	-104.75	3.96	-113.74	0.46	3065.9	3095.3	11.5	164.9	72.7	0.61
(7)	802.7	-403.35	-277.72	-12.54	-117.10	4.00	-129.64	0.47	3447.8	3473.2	16.0	184.3	82.9	0.68
(8)	825.6	-411.82	-283.00	-13.47	-119.61	4.27	-133.09	0.47	3513.4	3516.1	17.2	188.3	85.1	0.69
Plastic														
(9)	844.5	-419.29	-287.06	-14.58	-121.79	4.15	-136.37	0.48	3563.9	3562.7	18.7	191.7	87.2	0.70
(10)	878.1	-441.20	-296.03	-19.25	-128.76	2.84	-148.01	0.50	3675.2	3639.7	24.6	202.7	94.6	0.72
.	.									.				.
.	.									.				.
.	.									.				.
(28)	1353.5									4539.2				0.90

Table 3-4: B1 Mid-Span Stresses and Moments

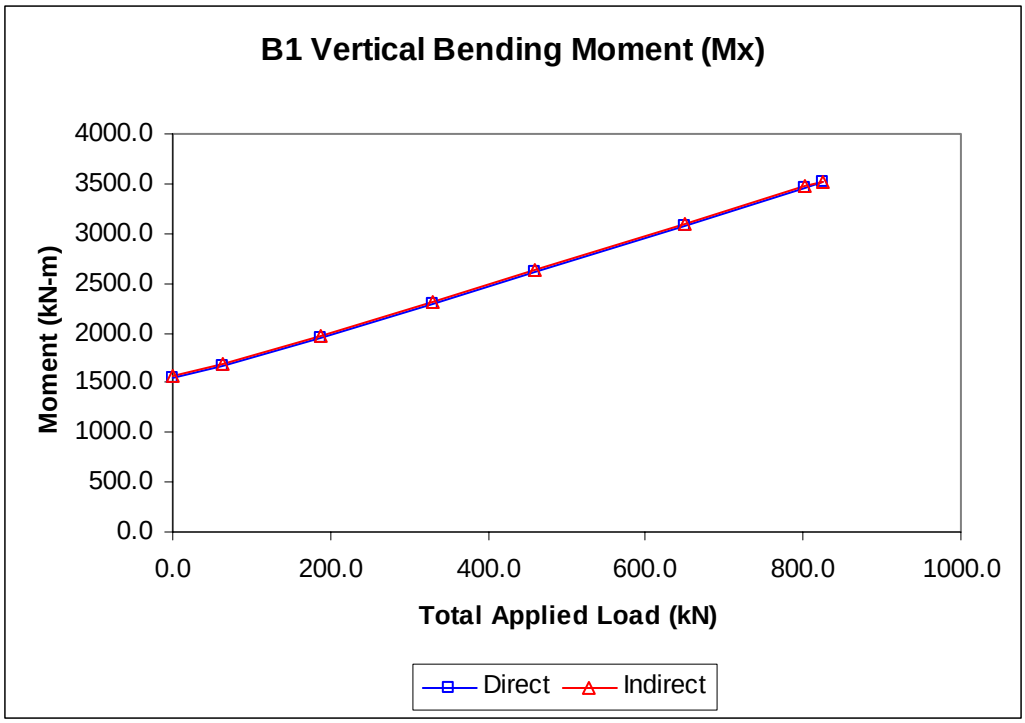

Figure 3-13: B1 Vertical Bending Moment

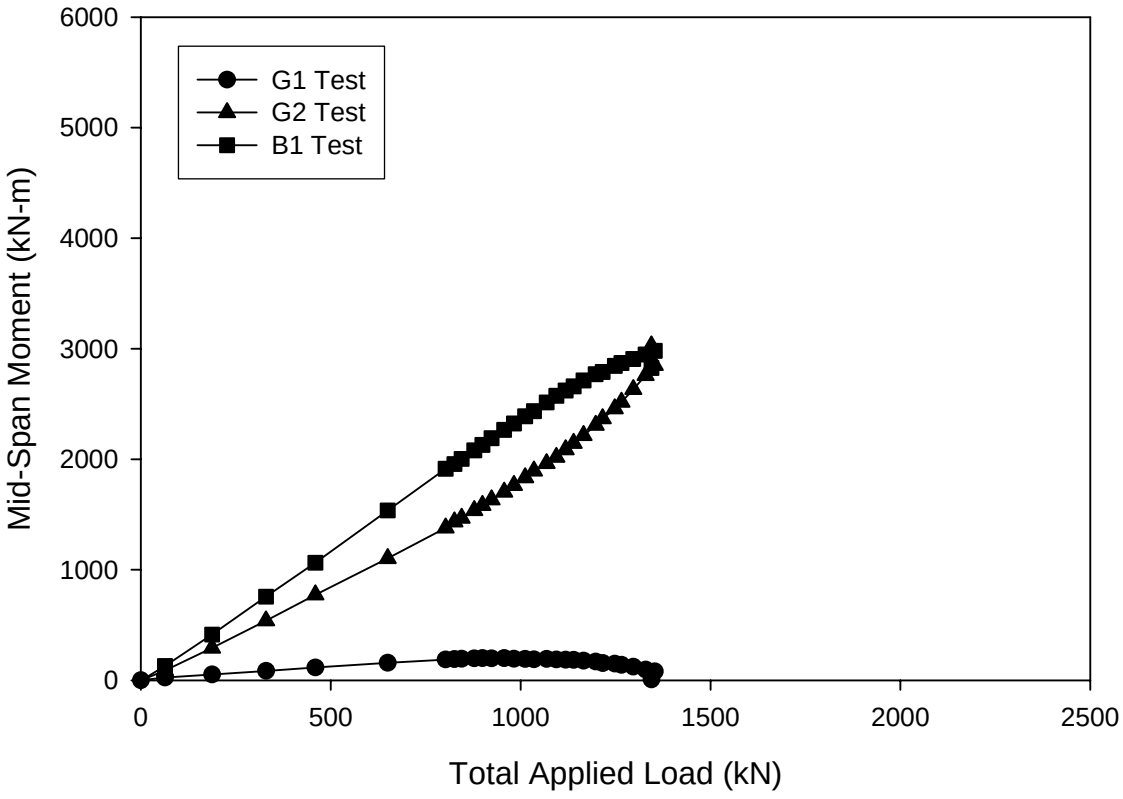

Figure 3-14: Test Frame Mid-Span Vertical Bending Moments, B1 Test

Figure 3-14 compares the mid-span vertical bending moments carried by B1, G2 and G1 due to the applied loading. The maximum sustained vertical bending moment in B1 was 4,539 kN-m (3,347.5 k-ft) and occurred at load step 28. Failure of B1 occurred during the displacement increase associated with load step 29. Failure is defined as the point at which a decrease in the component mid-span vertical bending resistance is associated with an increase in either the total load sustained by the test frame or the vertical displacement of the test frame. As the result of yielding and/or local compression flange buckling, the point of failure is generally coupled with dramatic load shedding from the component to G2. This is the condition illustrated by the last points (load step 29) of the B1 and G2 plots in Figure 3-14. At this load step, G2 is resisting more applied vertical bending moment than B1.

The effects of installation and dead load on the mid-span of B1 can be seen in Figure 3-15. The seemingly complementary strain gradients in the flanges indicate that the primary cause of longitudinal strain is strong-axis bending and warping. If a significant weak-axis bending moment was present its effect would increase the gradient of strain across the compression flange and decrease this gradient across the tension flange.

The mid-span longitudinal strain state at first yield in B1, load step 8, is shown in Figure 3-16. In addition to the longitudinal strains plotted on each plate as in previous figures, this figure and those in the subsequent sections also show the individual steel plate yield strain limits with dashed lines labeled ε_y.

Returning to Figure 3-16, despite the slight separation of the regression lines at the inside tip of the compression flange and at the top of the web, the section is essentially

behaving linearly elastically. This deduction is proven by the ratio of the direct to indirect calculation of resisted vertical moment, see Figure 3-13 and Table 3-4.

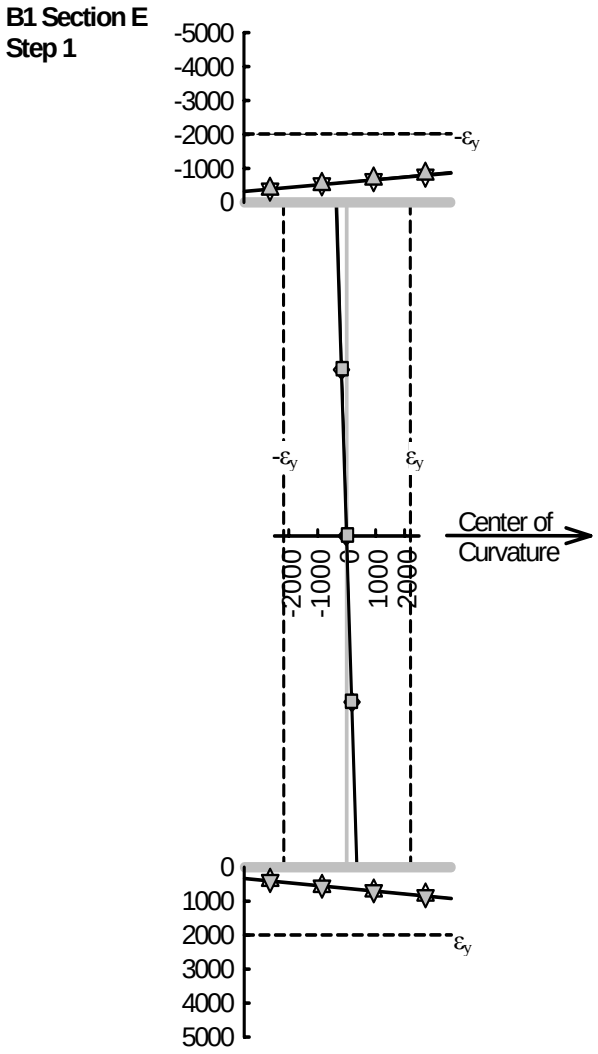

Figure 3-15: B1 Mid-Span Longitudinal Strain State Resulting From Installations and Dead Load (Step 1)

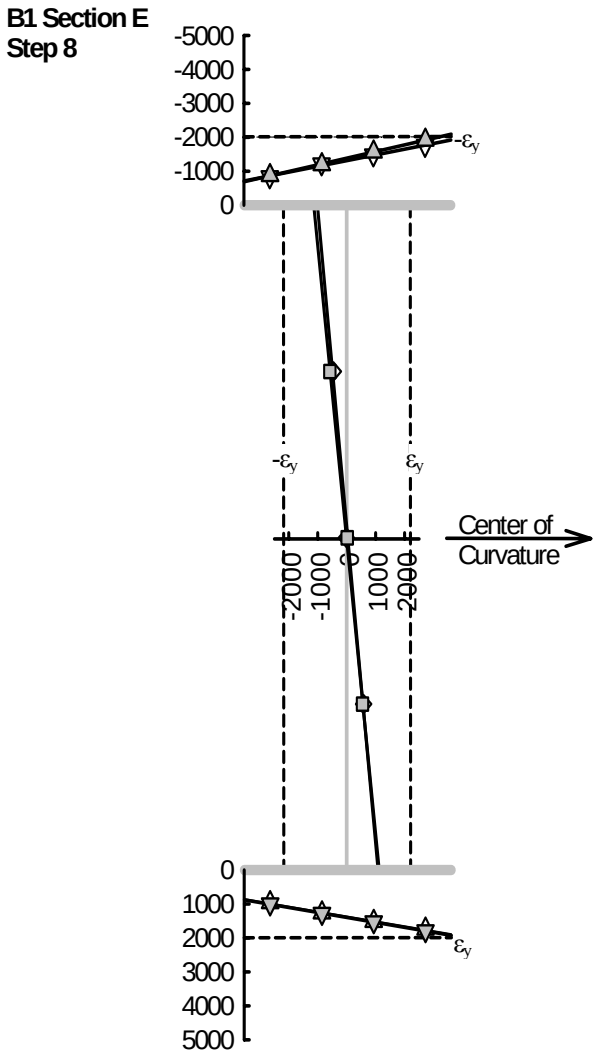

Figure 3-16: B1 Mid-Span Longitudinal Strain State During Step 8

The longitudinal strain state at the more critical cross-frame section for the B1 test at first yield (step 8) is shown in Figure 3-17. While this plot does not include the effects of installing the bending component on the cross-section, the most critical flange tip is more than 500 *με* away from its yield limit supporting the assertion that first yield in this component occurred at mid-span. At this cross-section, the flange strain gradients trend opposite to those for the mid-span cross-section because the lateral bending effect in the flange due to warping has gone through the expected inflection near the brace point.

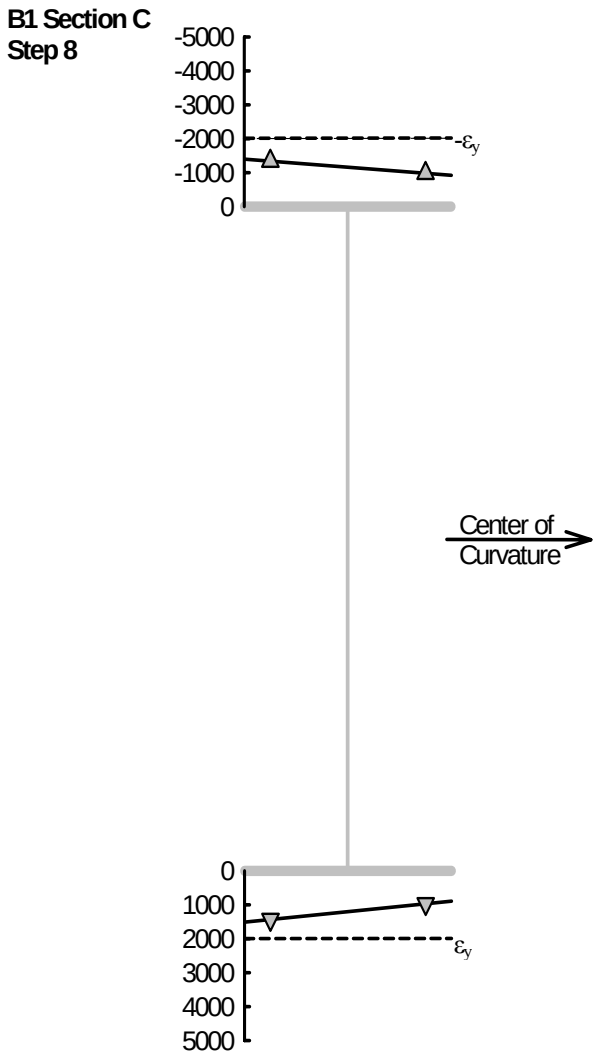

Figure 3-17: Longitudinal Strain State in B1 Near Cross-Frame N6L During Step 8 (Excluding Installation Effects)

Load step 11 for the mid-span of B1 is shown in Figure 3-18. At this load level, the inside compression flange tip is experiencing through thickness yielding. Also, first yield in the tension flange has been reached at the inside tip. The separation of the regression lines at the inside tip of the compression flange and at the top of the web indicates the presence of local plate bending or, perhaps, the onset of buckling.

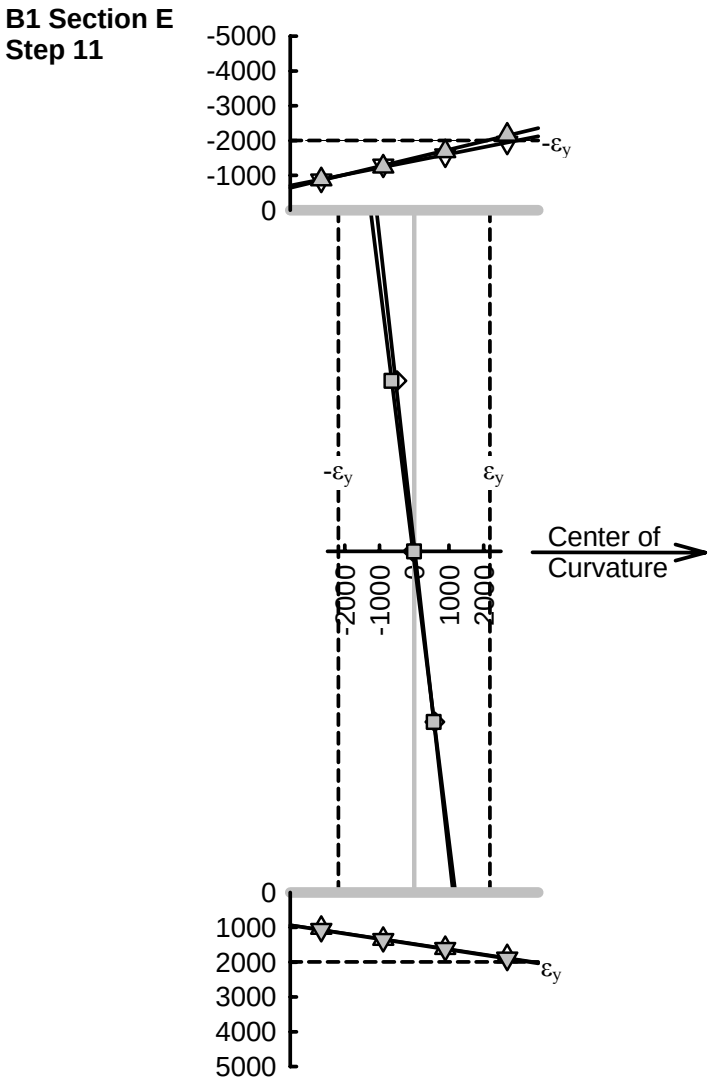

Figure 3-18: B1 Mid-Span Longitudinal Strain State During Step 11

Mid-span of B1 at load step 18 is shown in Figure 3-19. At this sustained load, approximately half of the compression flange and a quarter of the tension flange have exceeded their yield strengths. The local plate bending at the inside tip of the compression flange that was first observed at load step 8 has increased. However, the web strains are now indicating the distortions consistent with racking of the flanges. While the strain gradient across the tension flange has increased slightly through the progression of loading to this point, the gradient of strain across the compression flange

is nearly four times what it was across the tension flange at this load step. This amplification is the result of the increase lateral bending of the compression flange due to the P-delta effects of the horizontally curved flange.

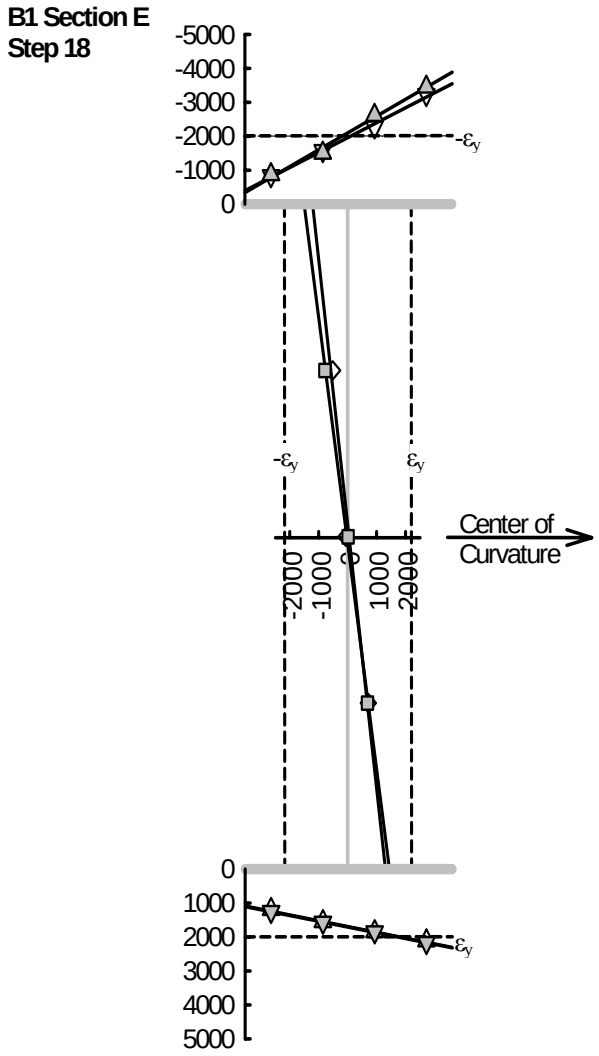

Figure 3-19: B1 Mid-Span Longitudinal Strain State During Step 18

The effects of the maximum sustained load during the B1 test are shown in Figure 3-20. The regression lines for the top flange data have been replaced with simple linear links. When the strain data across any surface of a plate becomes non-linear due to excessive yielding or buckling the regression line for that particular data set is replaced

with simple linear links. Shaded symbols are connected with a solid gray line while open symbols are connected with a dashed black line.

Returning to Figure 3-20, the maximum sustained load during the B1 test has caused through thickness yielding over approximately 5/8 of the compression flange and over half of the tension flange. The compression flange and web have buckled significantly as evidenced by the grossly disparate regression lines.

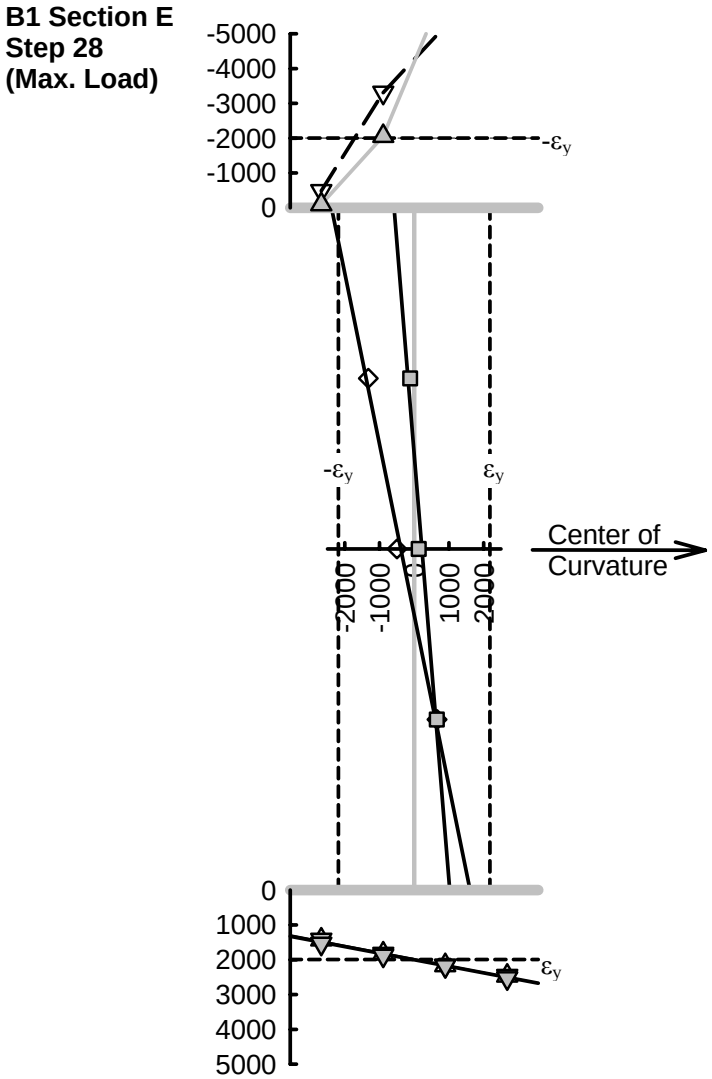

Figure 3-20: B1 Mid-Span Longitudinal Strain State During Step 28

Figure 3-21 shows the effects of the applied loads at step 29 on the mid-span longitudinal strains of G2. At this load step, G2 is resisting a majority of the applied moment, and B1 has failed. While the figure does not include any effects for installation of the B1 into the test frame, the applied load effects are far enough from the indicated yield limits to ensure elastic behavior. G2 and G1 as well as all cross-frame members were continuously monitored during each test to ensure they remained elastic as the bending component exceeded this limit.

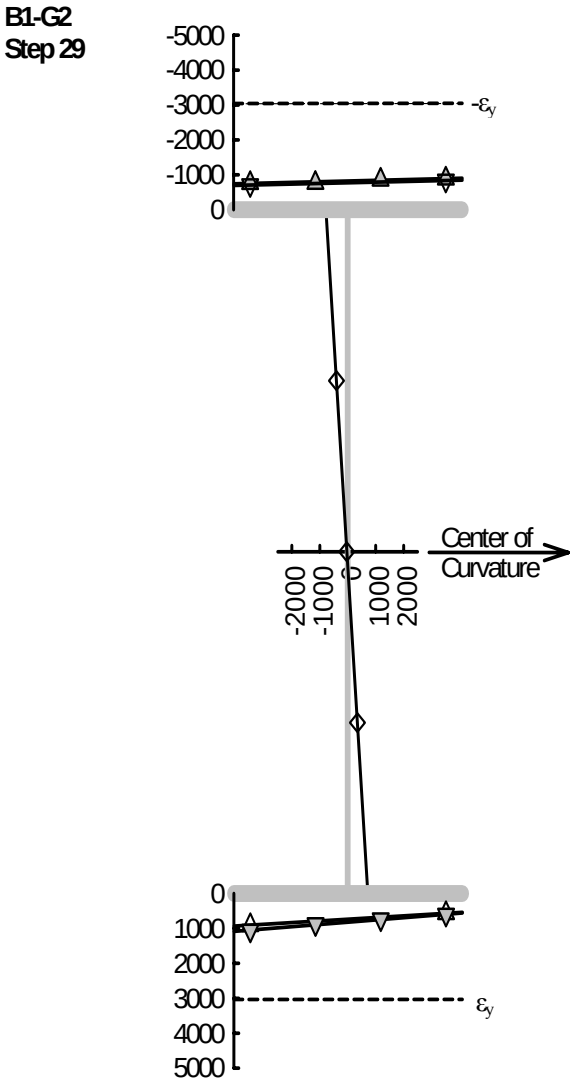

Figure 3-21: Most Critical G2 Mid-Span Longitudinal Strain State B1 Test (Step 29)

3.5 Bending Component B2 Test

The test frame that contains bending component B2 was loaded to a maximum of 1,434 kN (322.4 kip) in 33 steps. The applied load levels for each step and the associated vertical bending resistance for each girder element are listed in Table 3-5.

Table 3-6 contains the mid-span stresses and moments experienced by B2 throughout the elastic range of loading. When yield was first reached in the bending component at load step 10, the normalized vertical bending strength ratio was 0.67. Also, for the compression flange, the ratio of lateral bending stress to vertical bending stress ranged from 0.50 to 0.52 in this regime. A maximum vertical bending moment of 4,730 kN-m (3,487.9 k-ft) corresponding to a normalized ratio of 0.90 was sustained by B2 during step 33.

A comparison of the direct versus indirect methods of determining the vertical bending moment at mid-span of B2 is shown in Figure 3-22. The plot indicates good agreement between the two methods for determining the vertical bending resistance of B2. At first yield in B2, load step 10, the ratio of indirect to direct resistance is 0.98 (see Table 3-5).

Figure 3-23 shows the vertical bending moments at mid-span of each of the three girders of the test frame throughout the B2 test. The test progressed until G2 carried a greater percentage of the applied load than B2.

The installation and dead load effects on the longitudinal strain state at mid-span of B2 are shown on Figure 3-24. Recall that the installation strain data used in this analysis were derived from the B5 and B6 tests. The complementary gradients of strain in the flanges indicate that these effects are dominated by strong-axis bending and warping. The

web data are consistent and linear indicating a lack of plate flexing at this initial load level.

Load Step	Total Applied Load	Mx (Total)	Mx (G1)	Mx (G2)	Mx (B2)		
					Indirect (a)	Direct (b)	(a)/(b)
	kN	kN-m	kN-m	kN-m	kN-m	kN-m	
B2 Elastic							
1	0.0	-0.4	0.0	-0.4	0.0	0.6	-0.05
2	26.1	111.4	8.1	37.9	65.4	57.3	1.14
3	137.5	602.7	35.3	206.2	361.2	314.9	1.15
4	274.8	1204.6	70.6	451.6	682.4	643.2	1.06
5	404.7	1779.1	97.2	656.0	1025.9	957.4	1.07
6	535.5	2363.2	122.8	873.7	1366.7	1279.2	1.07
7	664.1	2937.2	150.4	1149.0	1637.7	1626.4	1.01
8	794.5	3510.4	160.8	1406.0	1943.6	2008.4	0.97
9	826.7	3651.9	165.4	1472.0	2014.6	1979.6	1.02
10	852.8	3767.4	169.6	1526.4	2071.3	2103.1	0.98
B2 Plastic							
11	874.0	3858.2	170.3	1572.9	2115.0	2179.5	0.97
12	907.8	4009.8	176.0	1630.2	2203.6	2251.5	0.98
13	938.5	4145.0	178.9	1690.5	2275.6	2353.1	0.97
14	963.7	4254.1	179.5	1740.9	2333.7		
15	983.0	4341.0	178.0	1789.5	2373.5		
16	1015.6	4485.6	180.7	1849.7	2455.2		
17	1040.9	4599.1	184.3	1905.5	2509.3		
18	1071.1	4732.4	186.2	1967.0	2579.2		
19	1090.9	4817.4	184.6	2015.1	2617.7		
20	1112.8	4909.6	177.1	2065.4	2667.1		
21	1143.3	5049.6	178.9	2129.7	2741.1		
22	1167.4	5153.9	178.3	2190.2	2785.4		
23	1199.9	5301.9	177.5	2255.0	2869.4		
24	1223.2	5405.1	173.6	2321.7	2909.8		
25	1251.6	5531.8	172.1	2388.2	2971.5		
26	1280.0	5660.0	168.5	2463.6	3028.0		
27	1306.5	5777.6	163.9	2528.3	3085.4		
28	1331.3	5884.8	154.4	2603.1	3127.3		
29	1358.1	6001.4	143.1	2683.5	3174.7		
30	1382.5	6110.3	131.5	2763.5	3215.3		
31	1410.8	6223.7	113.7	2855.9	3254.1		
32	1417.9	6256.3	94.8	2911.2	3250.3		
33	1434.1	6327.1	80.9	2981.5	3264.7		
34	1423.8	6277.7	50.9	3050.9	3176.0		
35	1392.4	6130.9	23.5	3042.5	3064.9		
36	1384.7	6095.6	-6.8	3115.1	2987.2		
37	1349.3	5935.6	-43.7	3099.7	2879.7		

Table 3-5: B2 Applied Load Steps and Resulting Girder Moments

Load Case	Total Applied Load	Compression Flange, Inside Tip, Extreme Fiber Stress							Moments at Section					
		σ_z Total	σ_z from M_x (a)	σ_z from M_y	σ_z from M_z	σ_z from P_z	σ_z(lat.) (b)	(b)/(a)	M_x Direct	M_x Indirect (c)	M_y	Bi	$M_{lat.}$ Comp. Flange	(c)/M_x^{yield}
	kN	MPa	MPa	MPa	MPa	MPa	MPa		kN-m	kN-m	kN-m	kN-m^2	kN-m	
Elastic														
Install.		-68.64	-41.81	2.88	-29.23	-0.48	-26.35	0.63	536.8		-3.7	45.8	16.7	
DL		-100.96	-72.29	-3.55	-27.98	2.86	-31.53	0.44	928.1		4.5	43.8	20.0	
Install.+DL		-169.60	-114.10	-0.67	-57.21	2.38	-57.88	0.51	1464.9		0.8	89.6	36.8	
(1)	0.0	-169.60	-114.14	-0.59	-57.31	2.44	-57.90	0.51	1465.5	1464.9	0.7	89.7	36.8	0.28
(2)	26.1	-176.09	-118.56	-1.09	-58.96	2.53	-60.05	0.51	1522.2	1530.3	1.4	92.3	38.2	0.29
(3)	137.5	-205.88	-138.63	-2.83	-66.84	2.42	-69.67	0.50	1779.8	1826.1	3.6	104.6	44.3	0.35
(4)	274.8	-243.54	-164.20	-4.79	-76.97	2.42	-81.76	0.50	2108.2	2147.3	6.1	120.5	52.0	0.41
(5)	404.7	-279.74	-188.67	-6.67	-86.84	2.43	-93.50	0.50	2422.3	2490.9	8.5	135.9	59.4	0.47
(6)	535.5	-317.23	-213.74	-8.85	-97.18	2.54	-106.03	0.50	2744.1	2831.6	11.2	152.1	67.4	0.54
(7)	664.1	-359.61	-240.78	-11.29	-110.14	2.61	-121.43	0.50	3091.3	3102.6	14.4	172.4	77.2	0.59
(8)	794.5	-407.85	-270.53	-15.61	-124.98	3.27	-140.59	0.52	3473.3	3408.5	19.8	195.6	89.3	0.65
(9)	826.7	-404.06	-268.29	-15.22	-124.09	3.53	-139.31	0.52	3444.5	3479.5	19.3	194.2	88.5	0.66
(10)	852.8	-419.90	-277.91	-16.95	-128.54	3.51	-145.49	0.52	3568.0	3536.2	21.6	201.2	92.5	0.67
Plastic														
(11)	874.0	-430.12	-283.86	-18.13	-131.62	3.49	-149.75	0.53	3644.4	3579.9	23.0	206.0	95.2	0.68
(12)	907.8	-441.56	-289.47	-20.05	-135.23	3.19	-155.27	0.54	3716.5	3668.6	25.5	211.7	98.7	0.70
.	.									.				.
.	.									.				.
.	.									.				.
(33)	1434.1									4729.6				0.90

Table 3-6: B2 Mid-Span Stresses and Moments

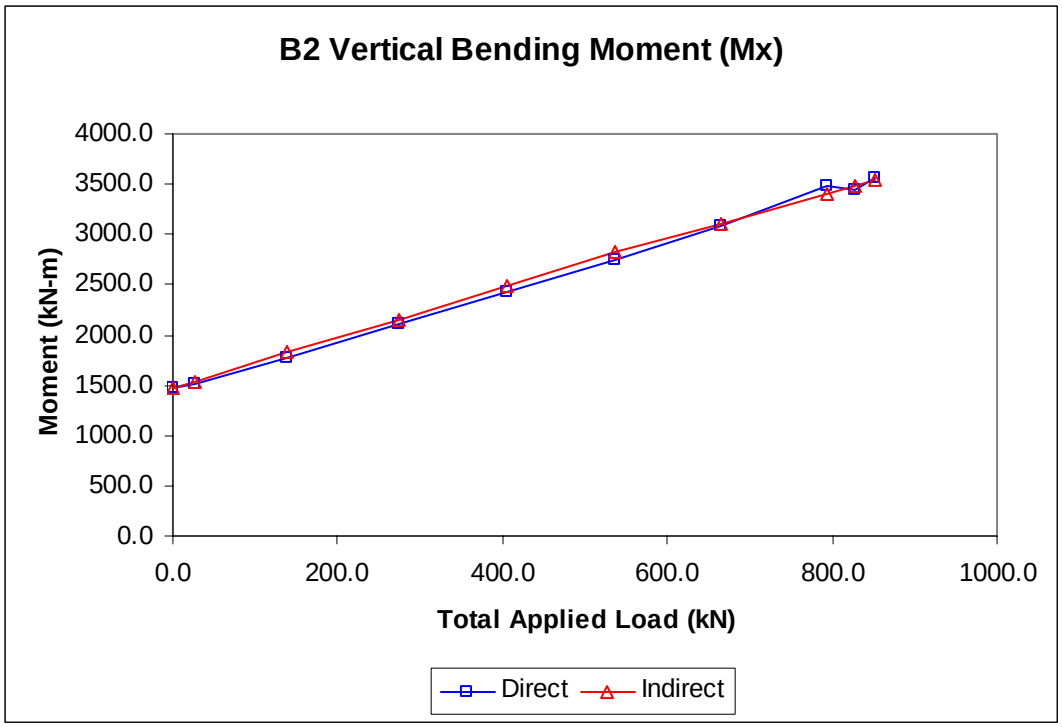

Figure 3-22: B2 Vertical Bending Moment in Elastic Range

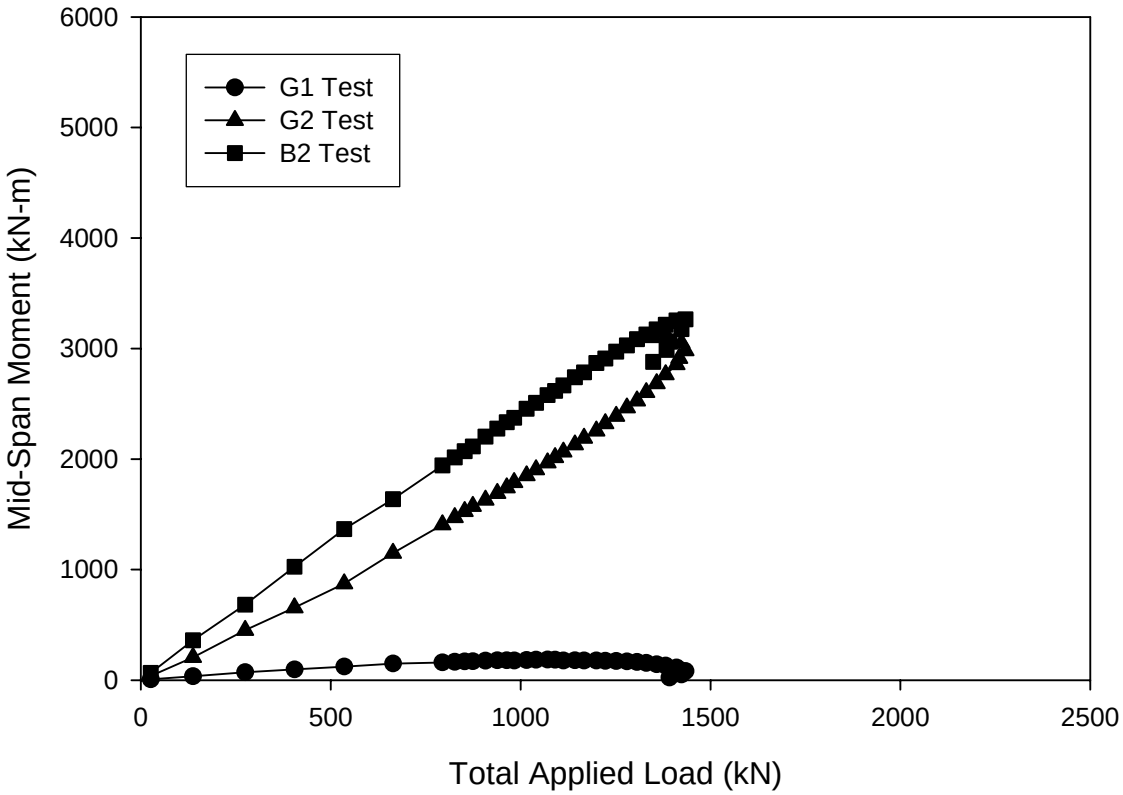

Figure 3-23: Test Frame Mid-Span Vertical Bending Moments, B2 Test

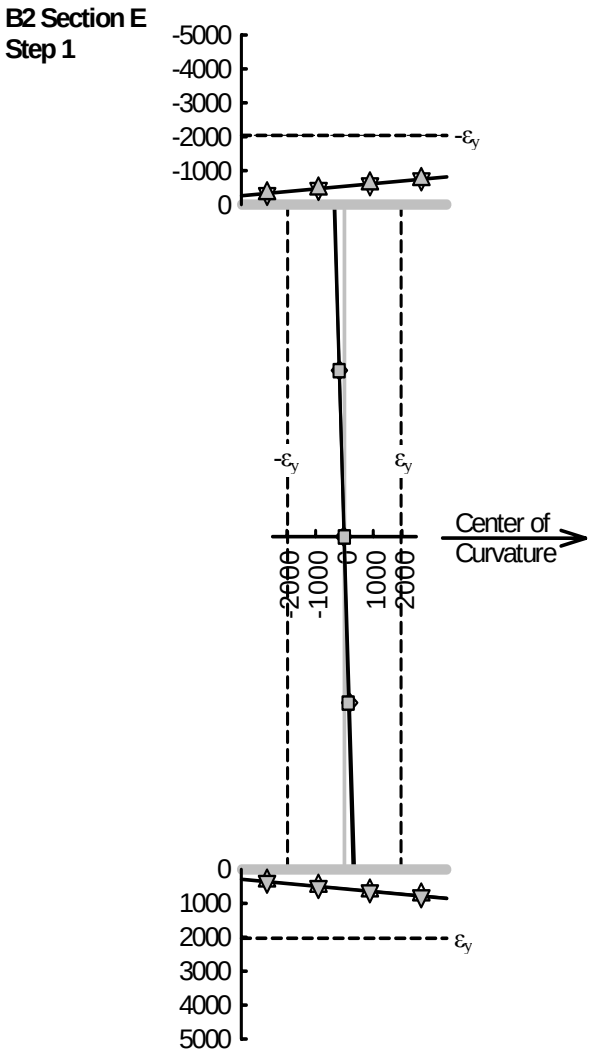

Figure 3-24: B2 Mid-Span Longitudinal Strain State Resulting From Installation and Dead Load (Step 1)

First yield in the B2 test occurred at the inside compression flange tip at mid-span of the component during load step 10. The longitudinal strain state of the mid-span cross-section at step 10 can be seen in Figure 3-25. The slightly flatter strain gradient in the tension (bottom) flange compared with the compression (top) flange indicates that there is a significant weak-axis bending effect at mid-span of B2 at this load level. The regression lines fit the data well, which is representative of linear-elastic behavior.

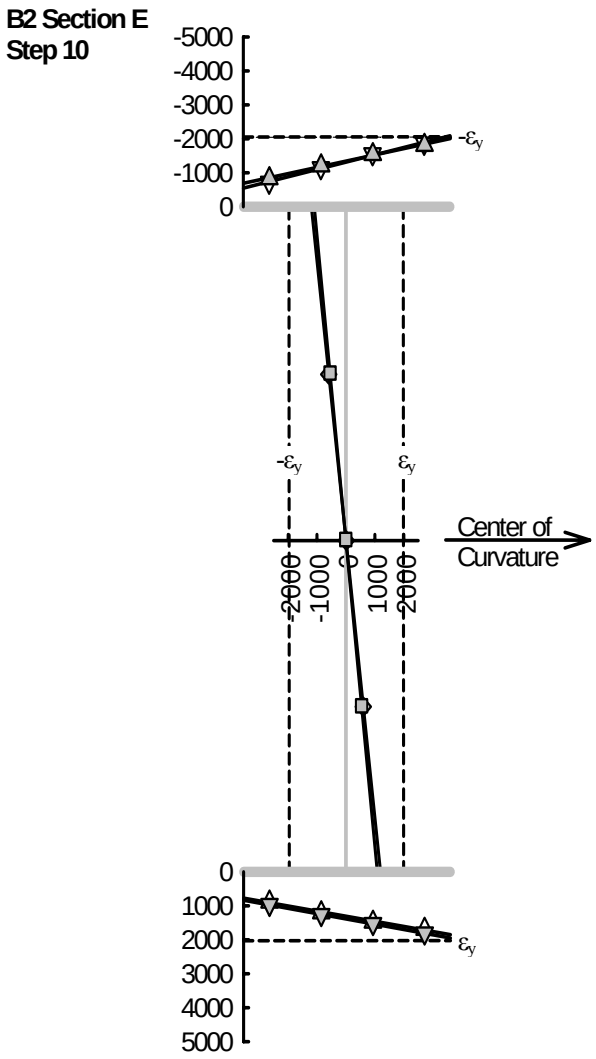

Figure 3-25: B2 Mid-Span Longitudinal Strain State During Step 10

The most critical braced section of B2 at step 10, the instrumented section adjacent to cross-frame N6L, is shown in Figure 3-26. Although the effects of installation are not included in this figure, the outside tension flange tip is still more than 500 *με* from its yield limit. This result supports the conclusion that first yield occurred at mid-span of B2 during this test.

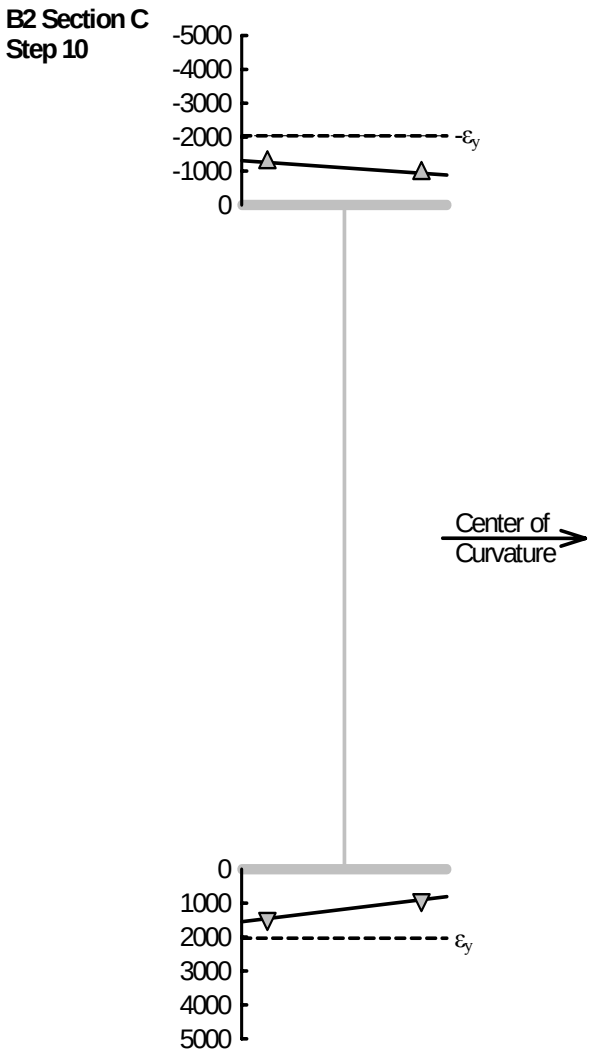

Figure 3-26: Longitudinal Strain State in B2 Near Cross-Frame N6L During Step 10 (Excluding Installation Effects)

Figure 3-27 depicts the longitudinal strain state at mid-span of B2 when the tension flange also reaches its yield limit. At this point, the inside tip of the compression flange is experiencing through-thickness yielding and the regression lines of the compression flange are starting to slightly separate. This separation indicates that the local plate bending or buckling has initiated.

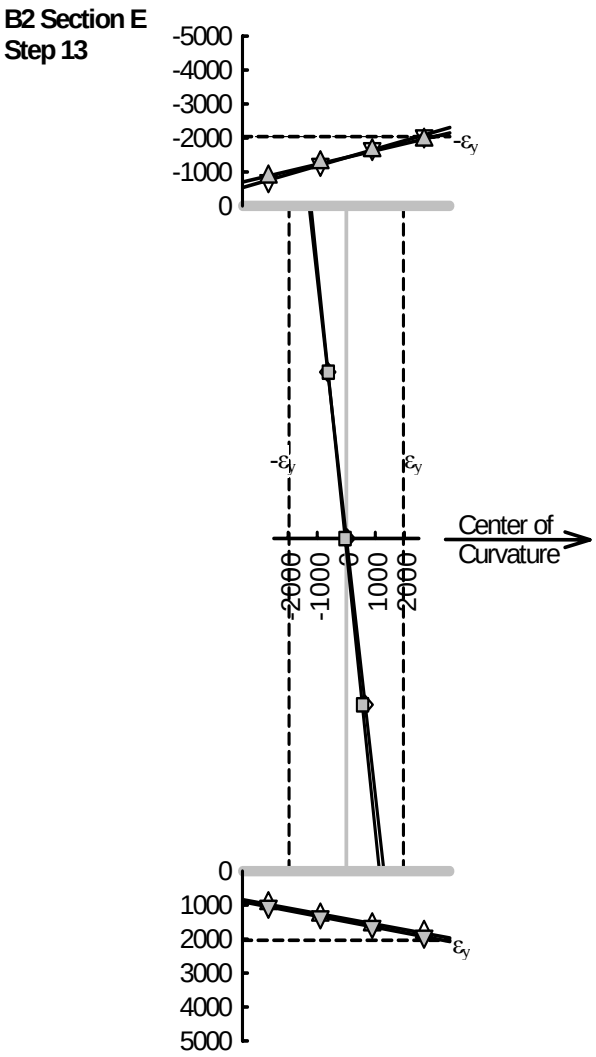

Figure 3-27: B2 Mid-Span Longitudinal Strain State During Step 13

At step 22 of the B2 test, the outside tip of the tension flange at cross-frame N6L and the outside tips of both flanges of the cross-section at cross-frame N6R have reached their yield limits as can be seen in Figures 3-28 and 3-29 respectively. At load step 27, the cross-sections adjacent to N6L and N6R were experiencing yielding in all outside flange tips.

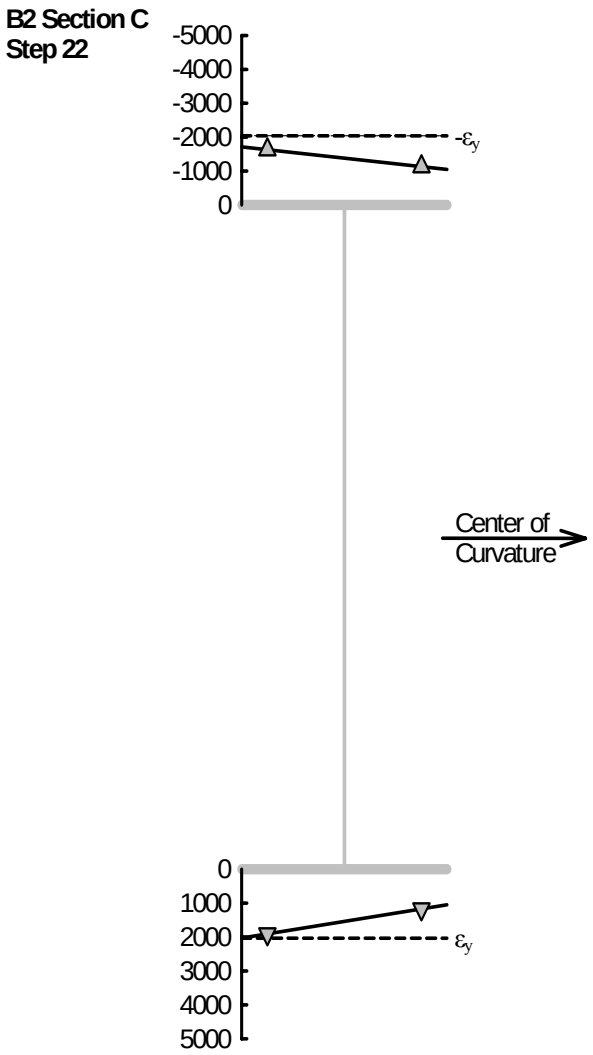

Figure 3-28: Longitudinal Strain State in B2 Near Cross-Frame N6L During Step 22 (Excluding Installation Effects)

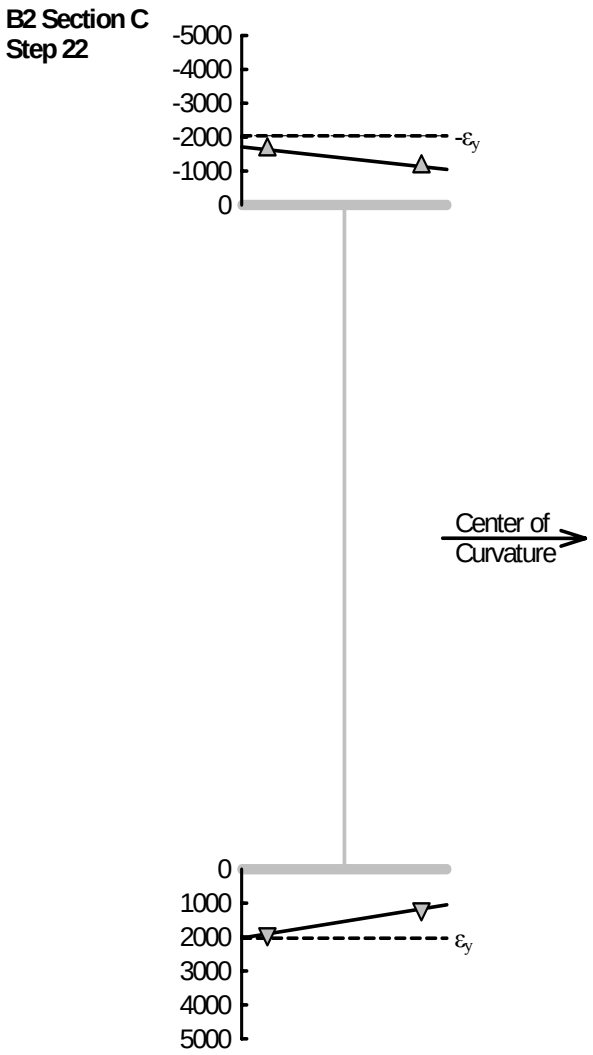

Figure 3-29: Longitudinal Strain State in B2 Near Cross-Frame N6R During Step 22 (Excluding Installation Effects)

The longitudinal strain state of mid-span B2 during the maximum sustained moment of the test, step 33, is illustrated in Figure 3-30. The figure shows that approximately 5/8 of the compression flange and ½ of the tension flange had yielded at this load level. The separations of the compression flange and web data regression lines indicate local bending and buckling of these plates.

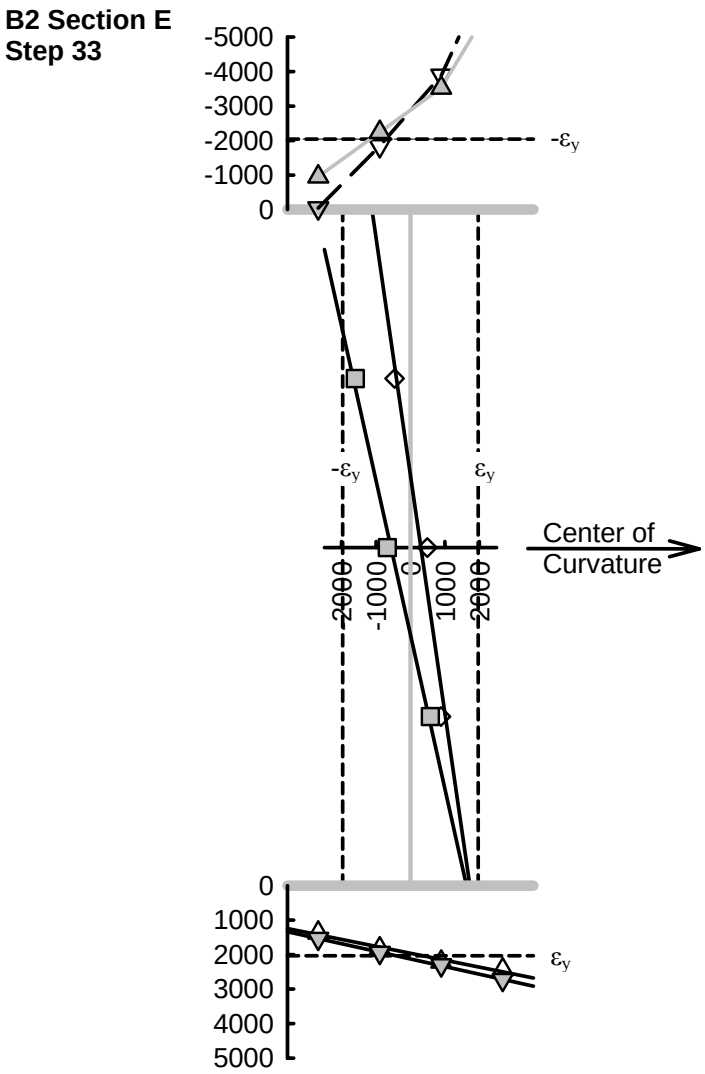

Figure 3-30: B2 Mid-Span Longitudinal Strain State During Step 33

Figure 3-31 illustrates the strain state of the mid-span of G2 at the maximum load that this girder sustained during the B2 test. The data reveal linear elastic behavior well below the yield limit in all three plates of the cross-section.

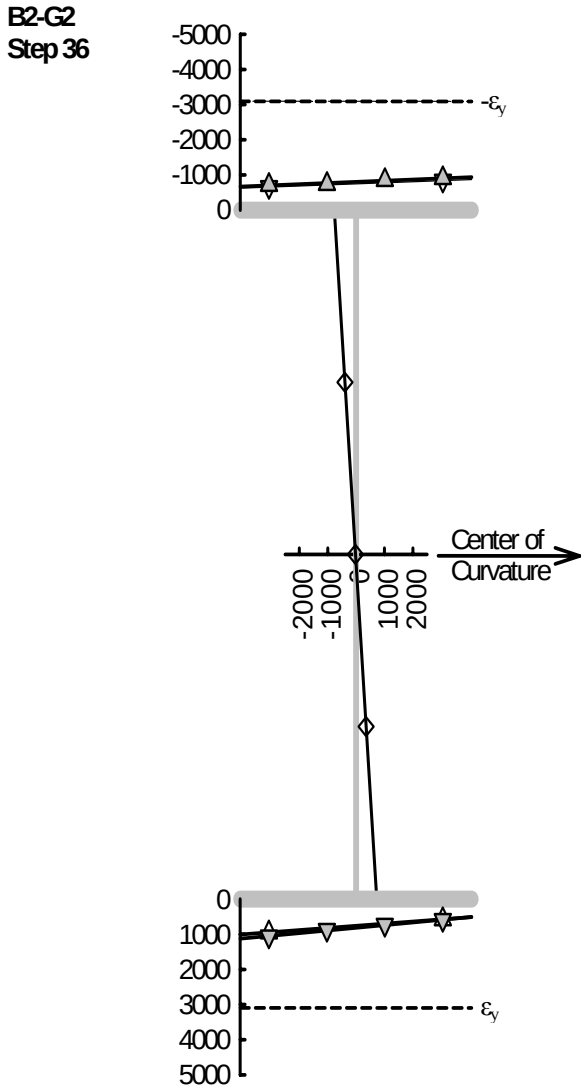

Figure 3-31: Most Critical G2 Mid-Span Longitudinal Strain State During B2 Test (Step 36)

3.6 Bending Component B3 Test

The test frame containing component B3 was loaded in 45 steps to a maximum applied load of 1,504 kN (338.1 kip). From step 8 to step 31, these load step increments represent approximately 27 kN (6 kip) increases in applied load. From step 31 to the end of the test, the experiment was conducted in displacement control. The maximum applied vertical bending moment sustained by B3, 3,375 kN-m (2,489.2 k-ft), occurred during

load step 44. Table 3-7 and Table 3-8 contain these results along with other selected information regarding the B3 test.

Load Step	Total Applied Load	Mx (Total)	Mx (G1)	Mx (G2)	Mx (B3)		
					Indirect (a)	Direct (b)	(a)/(b)
	kN	kN-m	kN-m	kN-m	kN-m	kN-m	
B3 Elastic							
1	0	-0.7	-0.1	0.4	-1	0.2	-5.4
2	56.4	240.9	14.2	81.7	144.9	126.9	1.14
3	148.9	651.2	40.4	231.4	379.4	338.4	1.12
4	276.5	1219.2	70.3	451.8	697.1	644.6	1.08
5	406.5	1793.6	96.9	674.8	1021.9	962.6	1.06
6	536	2362.5	119.6	901	1341.8	1283.3	1.05
7	664.9	2931.3	141.9	1135.5	1654	1604.4	1.03
8	802.3	3545.4	172.2	1373.7	1999.5	1936.9	1.03
9	826	3650.1	178.8	1419.1	2052.2	1998.5	1.03
10	852.7	3766.8	178	1469.1	2119.8	2075.8	1.02
B3 Plastic							
11	872.2	3850	180.7	1511.3	2158.1	2137.9	1.01
12	906.6	4005.6	189.6	1569.7	2246.3	2229.9	1.01
13	934.8	4129.4	193.6	1625.9	2309.9		
14	960.4	4239.7	193.1	1686.1	2360.5		
15	984.3	4347.6	190	1737.8	2419.8		
16	1012.9	4474	194.3	1792.5	2487.2		
17	1033.9	4566	189.2	1841	2535.8		
18	1060.8	4684.5	193	1900.7	2590.8		
19	1092.1	4823.4	193	1966.1	2664.2		
20	1116.5	4930.9	189.2	2017.1	2724.6		
21	1141.4	5039.1	188.8	2080	2770.4		
22	1169.6	5167.8	193.7	2138.3	2835.8		

Table 3-7: B3 Applied Load Steps and Resulting Girder Moments (Part I)

Load Step	Total Applied Load	Mx (Total)	Mx (G1)	Mx (G2)	Mx (B3)		
					Indirect (a)	Direct (b)	(a)/(b)
	kN	kN-m	kN-m	kN-m	kN-m	kN-m	
23	1195.5	5281.5	185.2	2205.5	2890.8		
24	1223.4	5407.3	185.1	2279.2	2943		
25	1249.4	5524.3	181	2340.4	3002.9		
26	1273.7	5633.7	176	2403.7	3054		
27	1299.6	5748.6	171.8	2471.3	3105.6		
28	1326.3	5868.3	160.5	2549.1	3158.6		
29	1347.9	5962.8	146.5	2629	3187.2		
30	1371.9	6068.6	153.1	2678.9	3236.6		
31	1401.8	6201.2	140.9	2777.5	3282.9		
32	1417.9	6271.6	128.9	2830.3	3312.4		
33	1434.6	6345.2	111.6	2896.9	3336.7		
34	1445.2	6395.5	103.8	2940.9	3350.8		
35	1452.6	6426.7	94.6	2966.8	3365.2		
36	1454.9	6436.9	85.4	2996.4	3355.2		
37	1457.8	6450.3	79	3009.6	3361.7		
38	1406.5	6203.7	44.1	2950.2	3209.4		
39	1452.6	6426.4	71.2	3023.6	3331.5		
40	1455.5	6440.7	68.7	3034.7	3337.3		
41	1459.9	6459.8	65.2	3046.5	3348		
42	1458.6	6457.1	62.8	3055.7	3338.6		
43	1460.4	6463.9	59.4	3062.5	3342		
44	1499.7	6620	68.7	3175.9	3375.4		
45	1503.8	6634.5	21.9	3329.1	3283.5		
46	1479.9	6533.4	-154.5	3671.2	3016.7		

Table 3-8: B3 Applied Load Steps and Resulting Girder Moments (Part II)

Load Case	Total Applied Load	Compression Flange, Inside Tip, Extreme Fiber Stress							Moments at Section					
		σ_z Total	σ_z from M_x (a)	σ_z from M_y	σ_z from M_z	σ_z from P_z	σ_z(lat.) (b)	(b)/(a)	M_x Direct	M_x Indirect (c)	M_y	Bi	$M_{lat.}$ Comp. Flange	(c)/M_x^{yield}
	kN	MPa	MPa	MPa	MPa	MPa	MPa		kN-m	kN-m	kN-m	kN-m^2	kN-m	
Elastic														
Install.		-68.26	-41.64	2.86	-29.00	-0.48	-26.14	0.63	536.8		-3.7	45.8	16.7	
DL		-102.30	-71.53	-4.12	-27.85	1.21	-31.98	0.45	922.2		5.3	43.9	20.4	
Install.+DL		-170.56	-113.17	-1.26	-56.85	0.73	-58.12	0.51	1459.1		1.6	89.7	37.0	
(1)	0.0	-170.52	-113.18	-1.25	-56.84	0.76	-58.10	0.51	1459.2	1458.1	6.9	89.7	37.0	0.28
(2)	56.4	-185.29	-123.01	-2.42	-60.76	0.91	-63.19	0.51	1585.9	1604.0	8.5	95.9	40.3	0.30
(3)	148.9	-209.34	-139.41	-4.03	-67.00	1.11	-71.04	0.51	1797.4	1838.5	15.4	105.7	45.3	0.35
(4)	276.5	-244.41	-163.17	-6.42	-76.20	1.38	-82.62	0.51	2103.7	2156.2	23.9	120.2	52.6	0.41
(5)	406.5	-280.65	-187.83	-8.71	-85.81	1.71	-94.53	0.50	2421.7	2481.0	39.3	135.4	60.2	0.47
(6)	536.0	-317.54	-212.71	-11.28	-95.70	2.15	-106.99	0.50	2742.4	2800.9	63.3	151.0	68.2	0.53
(7)	664.9	-354.77	-237.61	-14.09	-105.71	2.65	-119.81	0.50	3063.4	3113.0	102.6	166.8	76.3	0.59
(8)	802.3	-394.28	-263.40	-17.49	-116.34	2.95	-133.83	0.51	3396.0	3458.6	165.9	183.6	85.3	0.66
(9)	826.0	-401.90	-268.18	-18.16	-118.65	3.10	-136.82	0.51	3457.6	3511.2	268.5	187.2	87.2	0.67
(10)	852.7	-411.88	-274.18	-19.21	-121.65	3.15	-140.85	0.51	3534.9	3578.9	434.3	191.9	89.7	0.68
Plastic														
(11)	872.2	-421.46	-278.99	-20.69	-124.98	3.19	-145.67	0.52	3596.9	3617.1	702.8	204.5	92.8	0.69
(12)	906.6	-435.84	-286.13	-23.11	-129.62	3.02	-152.73	0.53	3689.0	3705.3	1137.1	89.7	97.3	0.70
.										.				.
.										.				.
.										.				.
(44)	1499.7									4834.4				0.92

Table 3-9: B3 Mid-Span Stresses and Moments

Table 3-9 contains the B3 test mid-span stresses and moments. First yield occurred at the inside tip of the component compression flange during step 10. At this load level, B3 was resisting a vertical bending moment of 3,535 kN-m (2,606.8 k-ft), which represents approximately 68% of the vertical yield moment for this component. This normalized ratio was raised to 0.92 at step 44 when B3 was resisting a maximum of 4,834 kN-m (3,565.2 k-ft). The ratio of lateral flange bending stress to vertical flange bending stress ranged between 0.50 and 0.51 throughout the elastic regime of this test.

A comparison of the indirect and direct methods of determining the vertical moment resistance of the B3 component is presented in Figure 3-32. The individual results are included in Table 3-7. At first yield, step 10, these results differ by 2%.

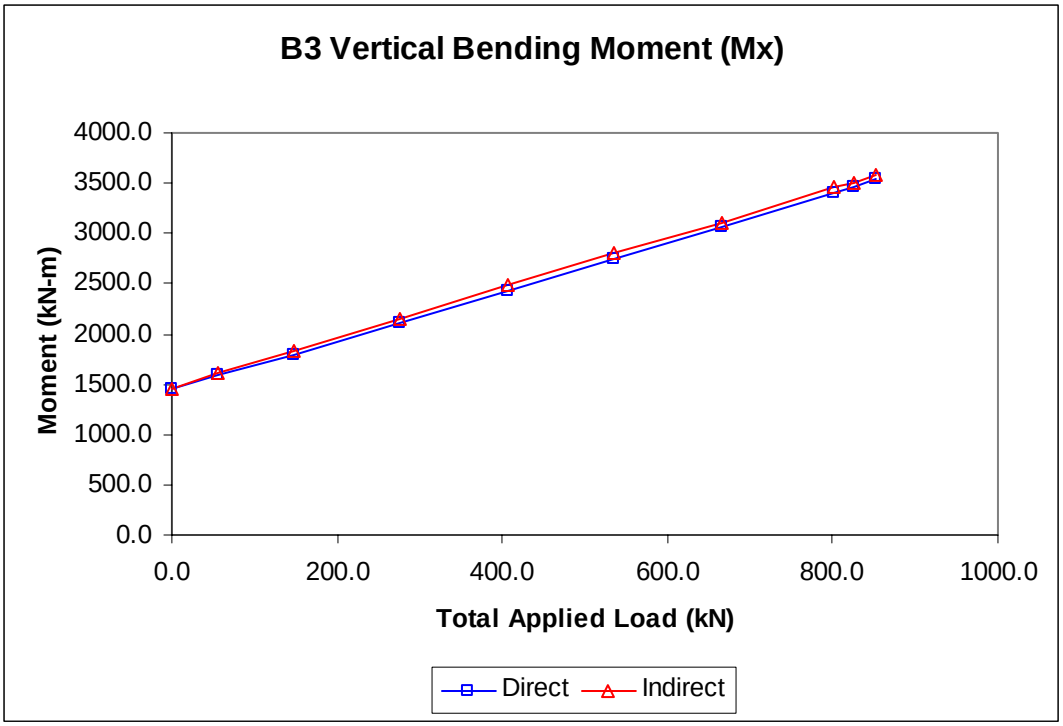

Figure 3-32: B3 Vertical Bending Moment

Figure 3-33 illustrates the mid-span vertical bending moments of G1, G2 and B3 as a function of the total applied load for this component test. The test progressed until G2

resisted a majority of the applied mid-span moment. However, this condition was not assured until load step 46, because at load step 45 the applied vertical bending moments carried by G2 and B3 were very similar 3,329 kN-m vs. 3,284 kN-m (2,455.1 k-ft vs. 2,421.5 k-ft).

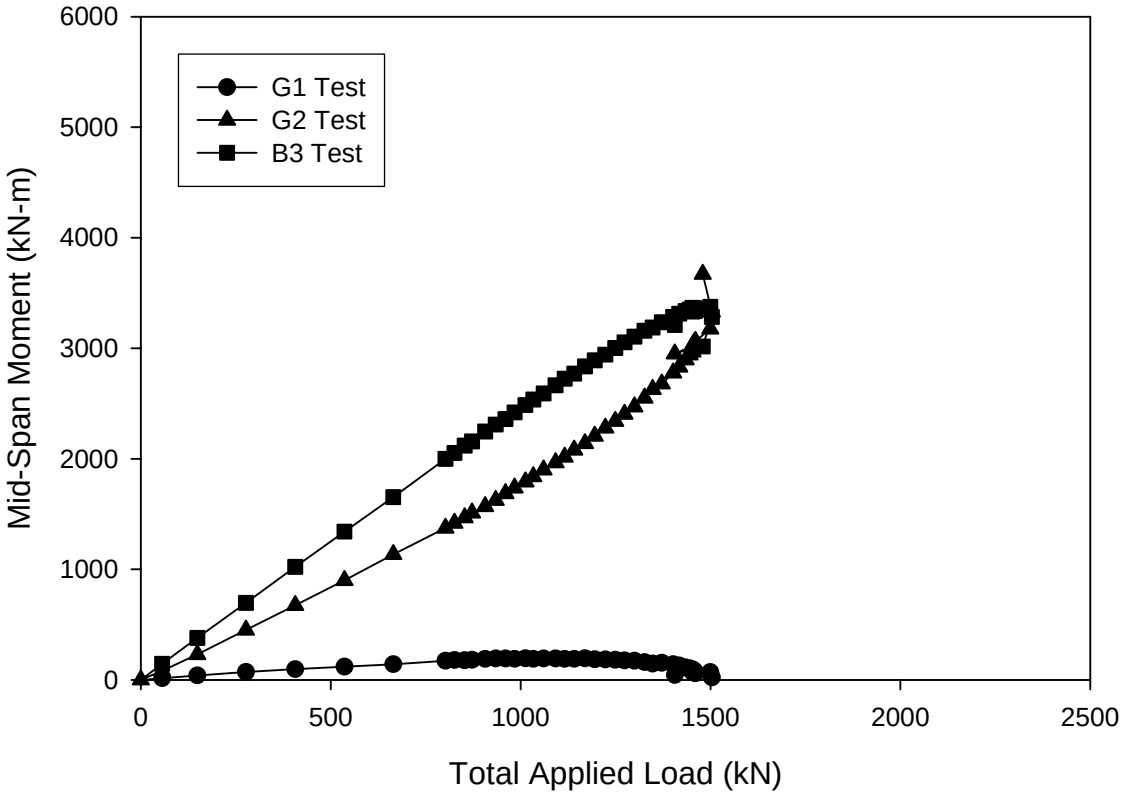

Figure 3-33: Test Frame Mid-Span Vertical Bending Moments, B3 Test

The effects of dead load and installation on the longitudinal strain state at mid-span of B3 are shown in Figure 3-34. The overlapping regression lines indicate linear-elastic behavior and the absence of local plate distortion at this cross-section under these small loads. Figure 3-35 shows the state of B3 mid-span longitudinal strain at the load level required to produce first yield in the cross-section. At this load level, step 10, the separating regression lines of the web in compression as well as the crossing and

separating regression lines across the compression flange are evidence of local plate bending in the cross-section.

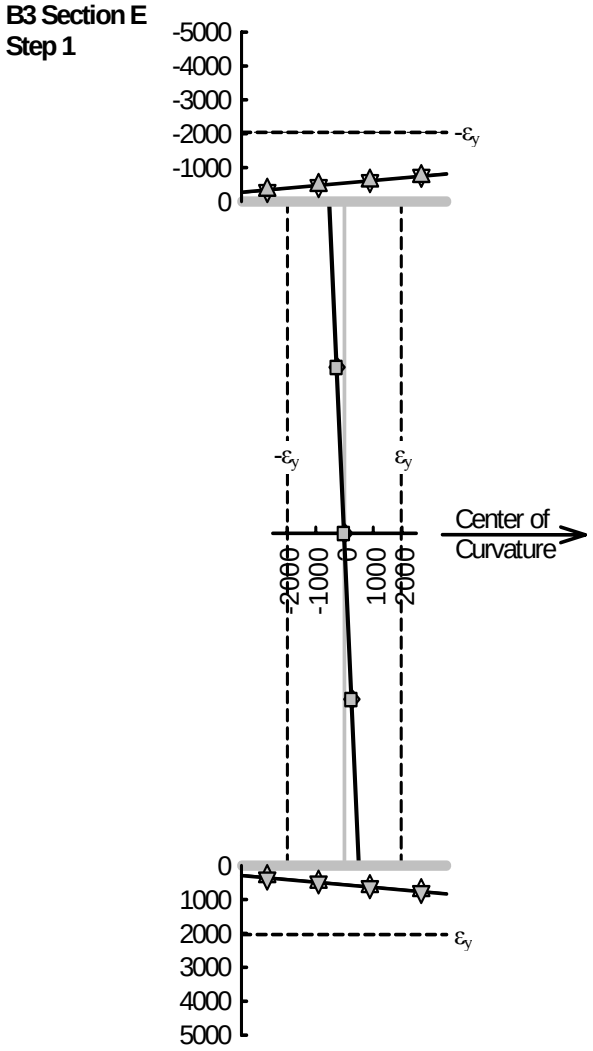

Figure 3-34: B3 Mid-Span Longitudinal Strain State Resulting From Installation and Dead Load (Step 1)

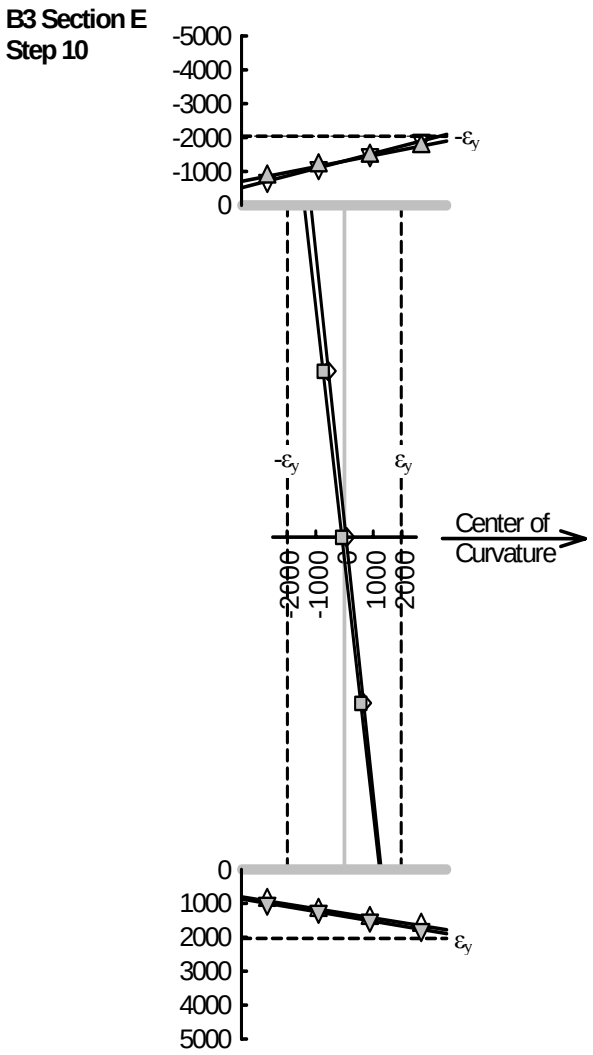

Figure 3-35: B3 Mid-Span Longitudinal Strain State During Step 10

Figures 3-36 and 3-37 show the very similar longitudinal strain states at cross-frames N6L and N6R, respectively, produced during step 10. In fact, both braced sections behaved almost identically throughout both the elastic and inelastic portions of the B3 test.

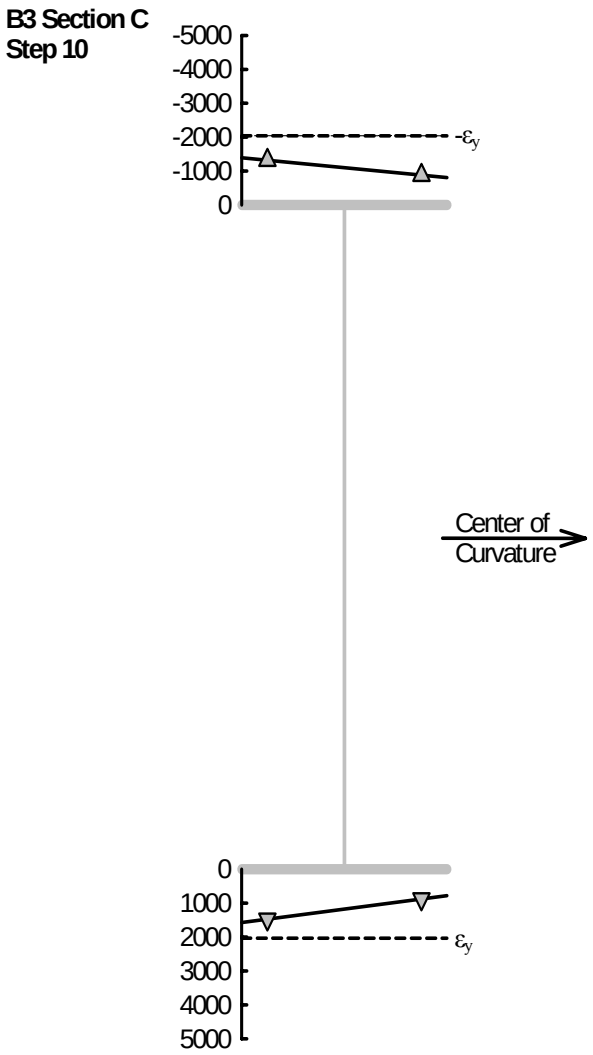

Figure 3-36: Longitudinal Strain State in B3 Near Cross-Frame N6L During Step 10 (Excluding Installation Effects)

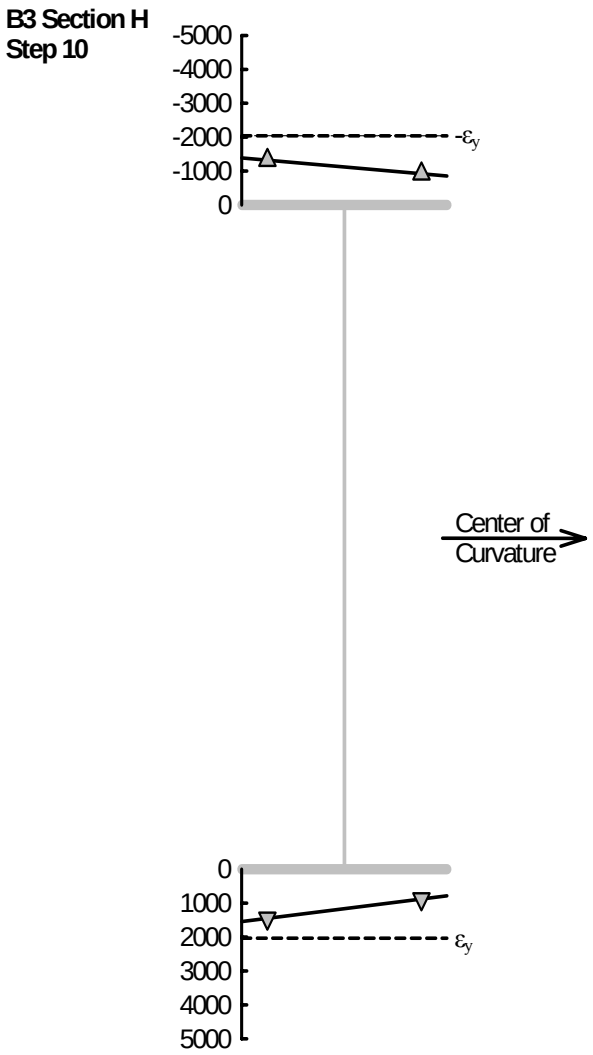

Figure 3-37: Longitudinal Strain State in B3 Near Cross-Frame N6R During Step 10 (Excluding Installation Effects)

The yield limit of the steel in the tension flange of B3 at mid-span was first reached during step 14. As seen in Figure 3-38, at this load level there is evidence of through thickness yielding at the inside tip of the compression flange and of an increase in the local plate bending in this flange and along the depth of the web in compression.

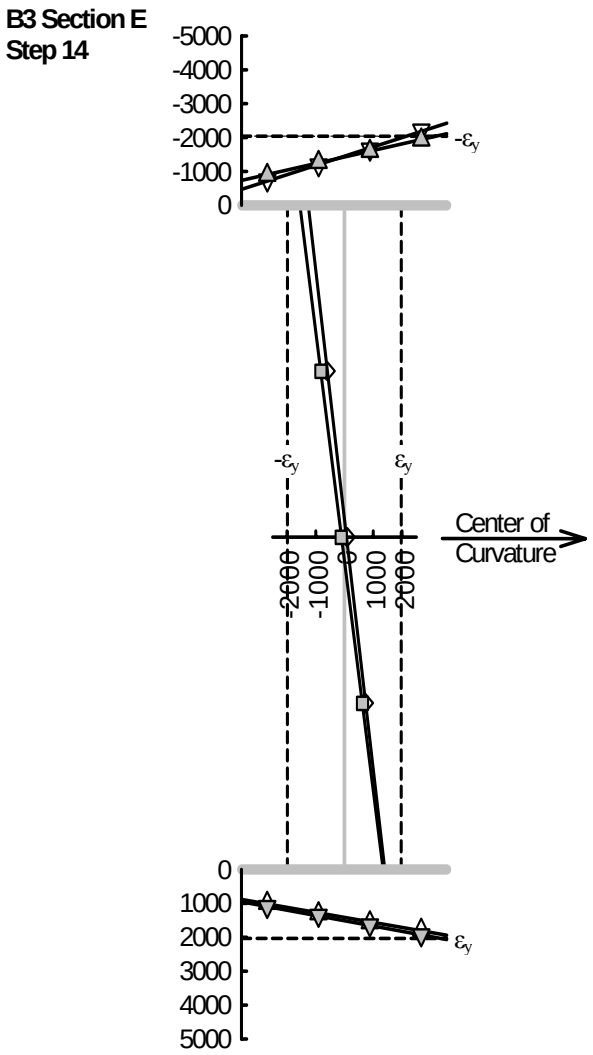

Figure 3-38: B3 Mid-Span Longitudinal Strain State During Step 14

Figures 3-39 and 3-40 show the longitudinal strain state at cross-sections N6L and N6R, respectively, during step 21. At this load level, the outside tip of tension flange at both locations has just reached its yield limit. The outside tip of the compression flange at N6R reaches yield during step 22, and the outside tip of the compression flange at N6L reaches yield at step 23. The longitudinal strain states at these locations at the respective load steps can be seen in Figures 3-41 and 3-42.

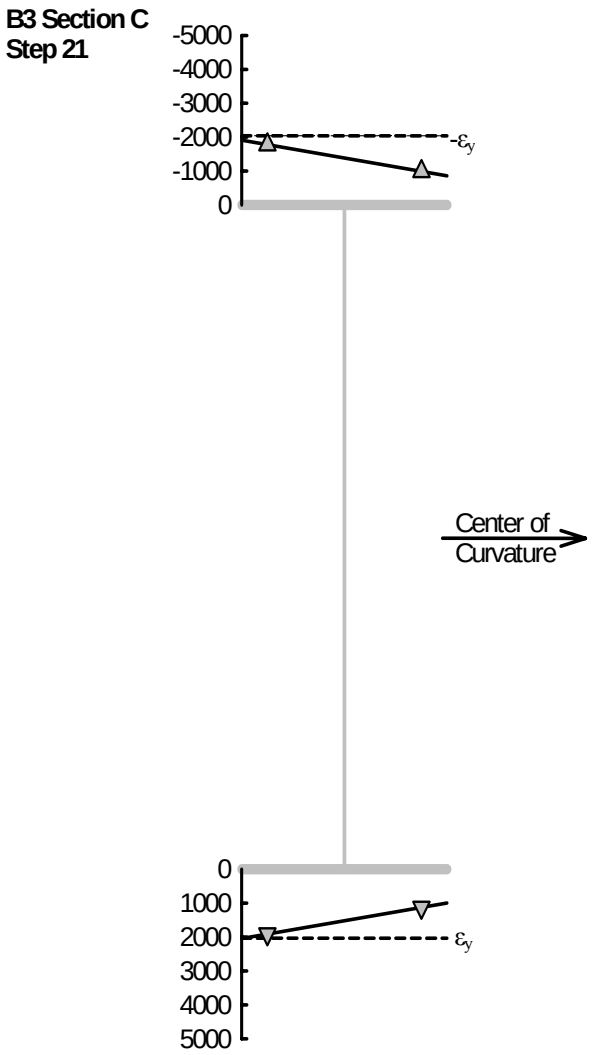

Figure 3-39: Longitudinal Strain State in B3 Near Cross-Frame N6L During Step 21 (Excluding Installation Effects)

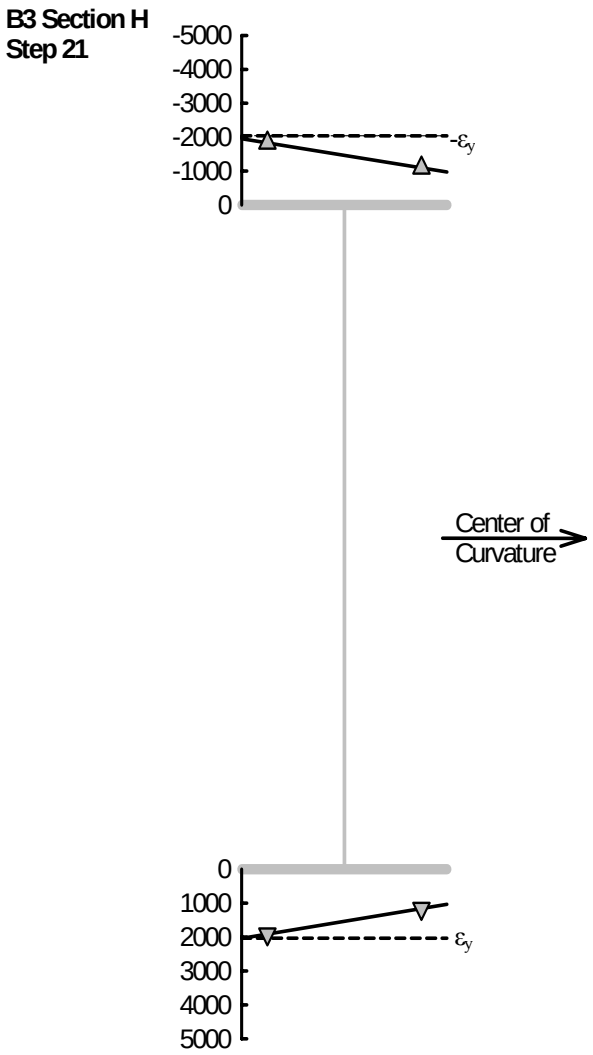

Figure 3-40: Longitudinal Strain State in B3 Near Cross-Frame N6R During Step 21 (Excluding Installation Effects)

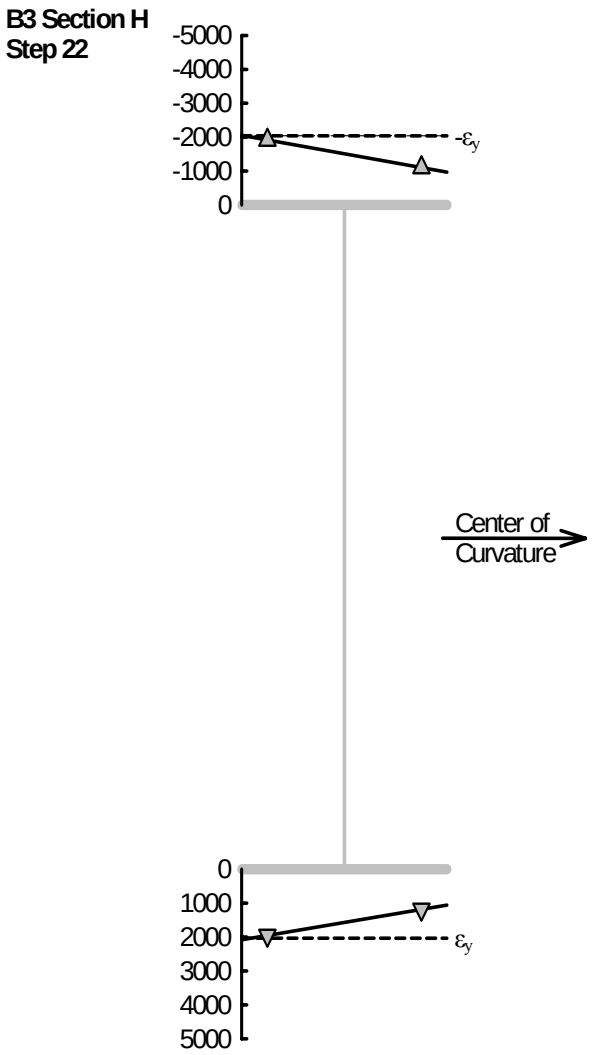

Figure 3-41: Longitudinal Strain State in B3 Near Cross-Frame N6R During Step 22 (Excluding Installation Effects)

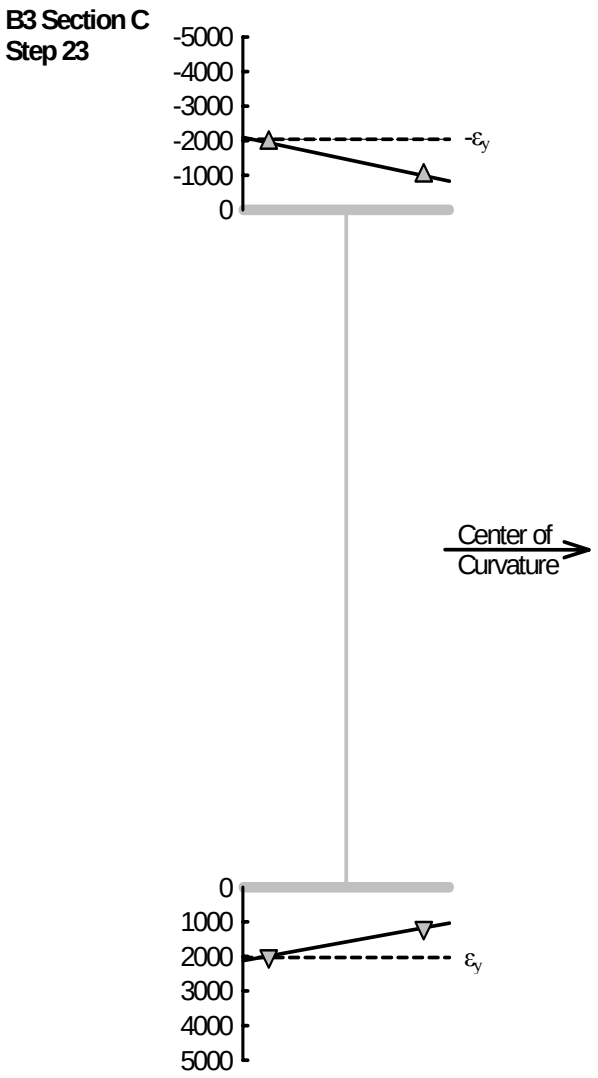

Figure 3-42: Longitudinal Strain State in B3 Near Cross-Frame N6L During Step 23 (Excluding Installation Effects)

The test frame's response briefly became weaker after step 31. The longitudinal strain state at that load step is shown in Figure 3-43. The compression flange data indicate significant buckling across the plate and through-thickness yielding on the inside half of the plate. The web data also indicate significant plate bending at the cross-section. While the tension flange data at this location show yielding across half of the plate, little evidence of significant local plate bending is displayed.

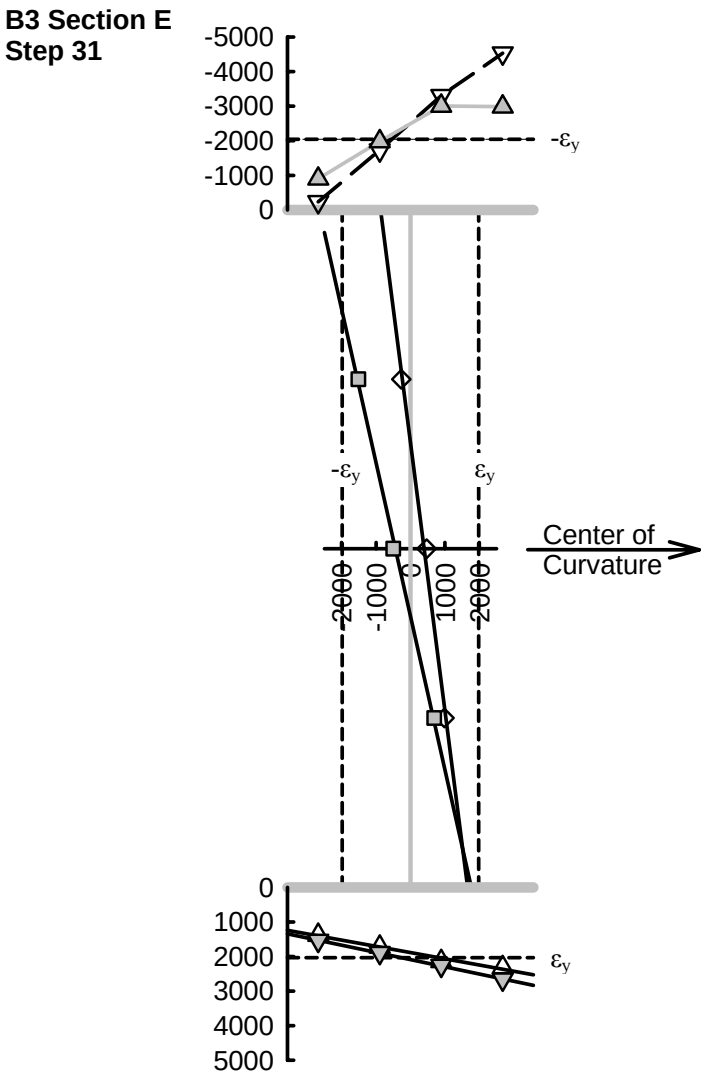

Figure 3-43: B3 Mid-Span Longitudinal Strain State During Step 31

In a post-buckled state, the stiffness of B3 remained stable until an applied load of 1,500 kN (337.2 kips) was reached during step 44. The longitudinal strain state of the B3 mid-span section at this step is shown in Figure 3-44. This load level corresponds to the maximum resisted vertical bending moment by B3 of 4,834 kN-m (3,565.2 k-ft). The frame remained stable enough to sustain an additional load increment, step 45, at a total applied load of 1,504 kN (338.1 kip), despite the failure of B3.

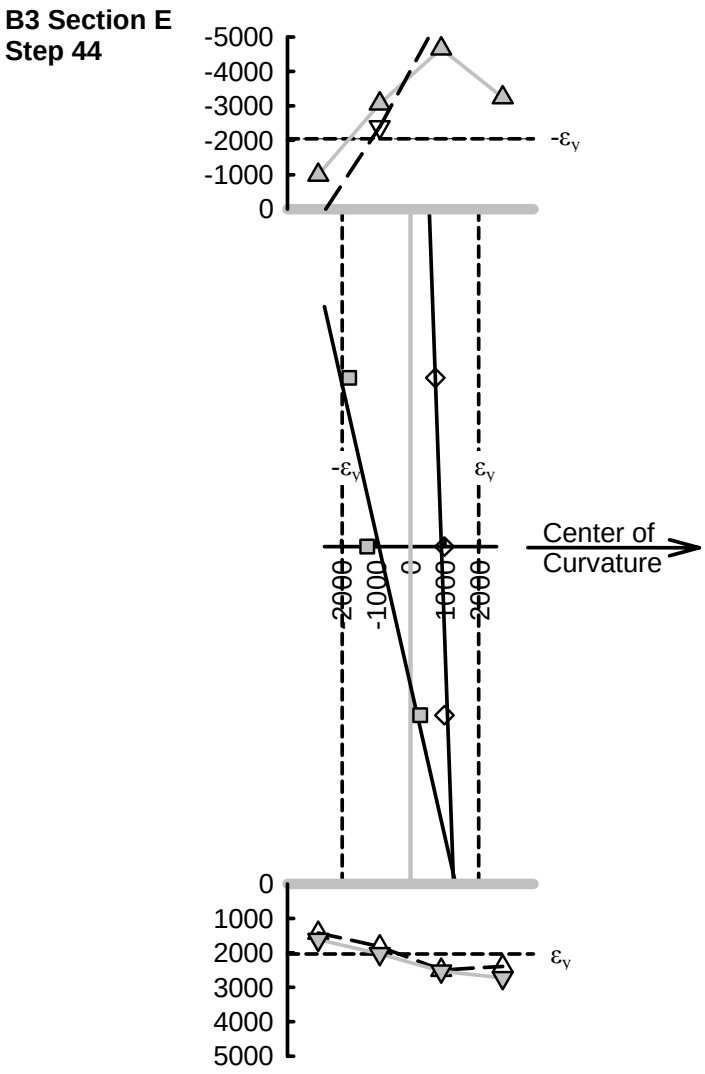

Figure 3-44: B3 Mid-Span Longitudinal Strain State During Step 44

Figure 3-45 depicts the longitudinal strain state of the mid-span of G2 while it experienced the greatest demand of the B3 test, step 46. While the data plotted do not include the effects of installation of the B3 component, all measurements are far enough away from their respective yield limits to ensure that this girder remained elastic throughout the test.

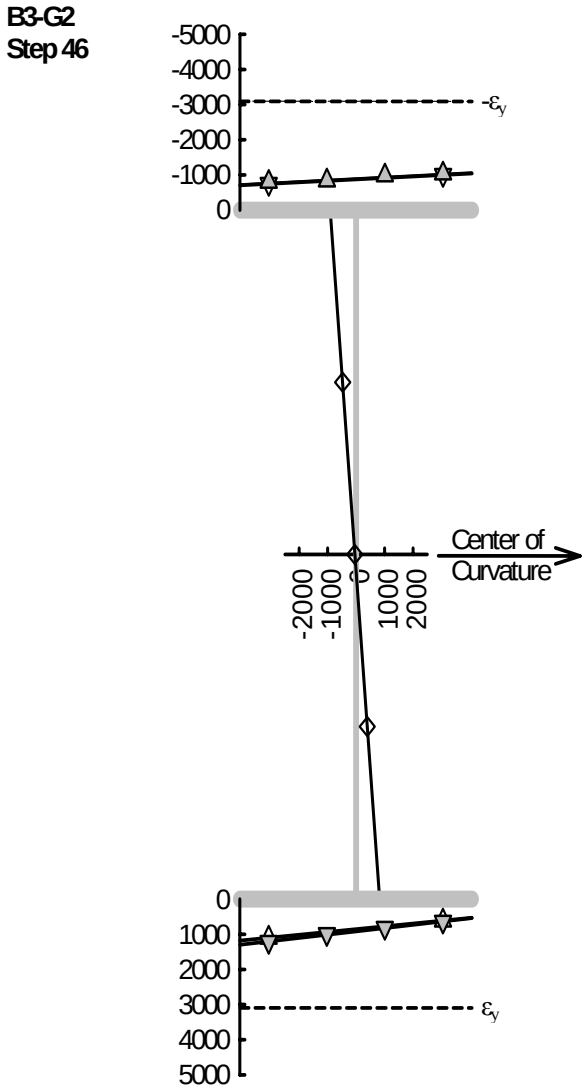

Figure 3-45: Most Critical G2 Mid-Span Longitudinal Strain State During B3 Test

3.7 Bending Component B4 Test

The test frame, including the singly symmetric B4 component, was loaded to a maximum applied load level of 1,354 kN (304.5 kip) during step 29 of this test. This load level corresponded to an applied vertical bending moment of 3,223 kN-m (2,376.9 k-ft) at mid-span of the component. The individual applied load levels and the effects of each step on the test frame girders are summarized in Table 3-10.

Load Step	Total Applied Load	Mx (Total)	Mx (G1)	Mx (G2)	Mx (B4)		
					Indirect (a)	Direct (b)	(a)/(b)
	kN	kN-m	kN-m	kN-m	kN-m	kN-m	
B4 Elastic							
1	0.0	-2.2	0.1	0.5	-2.8	-0.2	16.78
2	45.8	196.4	16.9	61.3	118.2	106.5	1.11
3	143.9	623.6	42.8	195.4	385.4	344.1	1.12
4	268.5	1174.1	76.5	363.4	734.3	653.4	1.12
5	405.7	1774.9	121.7	606.5	1046.7	997.4	1.05
6	535.1	2345.6	157.4	801.6	1386.6	1327.2	1.04
7	672.5	2954.5	201.4	1037.3	1715.8	1676.1	1.02
8	802.7	3530.6	228.3	1262.4	2039.9	2060.3	0.99
B4 Plastic							
9	826.5	3635.2	232.9	1303.8	2098.5	2136.2	0.98
10	855.8	3765.3	241.9	1357.2	2166.3	2222.6	0.97
11	879.5	3871.0	242.3	1398.8	2229.9	2302.1	0.97
12	908.3	3998.4	251.2	1452.8	2294.3		
13	934.6	4116.5	254.8	1501.2	2360.5		
14	959.9	4227.8	259.7	1551.1	2417.0		
15	985.9	4342.1	261.5	1598.7	2481.9		
16	1012.6	4462.3	270.8	1650.6	2541.0		
17	1040.6	4587.1	271.6	1702.8	2612.7		
18	1065.7	4698.4	274.9	1753.1	2670.3		
19	1093.5	4820.2	277.7	1811.4	2731.0		
20	1117.6	4931.3	278.9	1860.8	2791.7		
21	1142.1	5041.6	276.1	1916.3	2849.2		
22	1169.2	5166.3	277.0	1976.7	2912.7		
23	1193.6	5271.9	272.3	2037.2	2962.5		
24	1219.9	5390.8	268.5	2106.1	3016.2		
25	1246.3	5511.7	264.0	2176.6	3071.1		
26	1269.4	5616.4	252.1	2246.0	3118.2		
27	1295.1	5732.6	245.7	2323.0	3163.9		
28	1319.8	5841.8	239.6	2402.1	3200.1		
29	1354.5	5995.8	224.1	2548.6	3223.0		
30	1295.0	5719.8	122.6	2707.6	2889.6		
31	1267.4	5596.4	-65.7	3049.3	2612.8		

Table 3-10: B4 Applied Load Steps and Resulting Girder Moments

The ratio of indirect to direct method for determining the mid-span moment of B4 was 0.99 for load step 8, which is the load level that produced first yield in B4. This ratio is illustrated throughout the entire range of elastic behavior of this test in Figure 3-46.

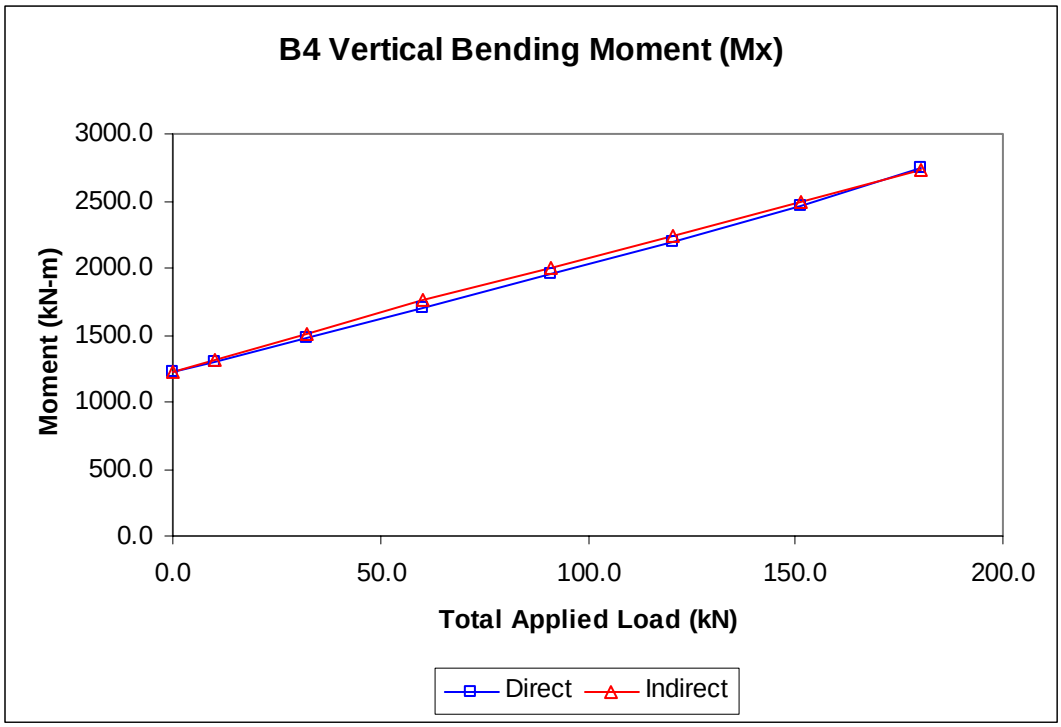

Figure 3-46: B4 Vertical Bending Moment

Table 3-11 contains the B4 mid-span stresses and moments for the entire elastic regime of loading. The table also includes selected information at the maximum resisted vertical bending moment in the component. The ratio of lateral flange bending stress to vertical flange bending stress in the compression flange of this component ranged from 0.43 to 0.49 in the elastic load range. At first yield in B4, the ratio of mid-span vertical bending moment to yield moment was 0.69. This ratio increased to 0.90 at the maximum sustained load level.

Load Case	Total Applied Load	Compression Flange, Inside Tip, Extreme Fiber Stress							Moments at Section					
		σ_z Total	σ_z from M_x (a)	σ_z from M_y	σ_z from M_z	σ_z from P_z	σ_z(lat.) (b)	(b)/(a)	M_x Direct	M_x Indirect (c)	M_y	Bi	$M_{lat.}$ Comp. Flange	(c)/M_x^{yield}
	kN	MPa	MPa	MPa	MPa	MPa	MPa		kN-m	kN-m	kN-m	kN-m^2	kN-m	
Elastic														
Install.		-67.45	-52.46	-4.55	-16.82	6.38	-21.37	0.41	696.0		11.3	51.8	13.6	
DL		-104.75	-72.41	-3.00	-29.58	0.24	-32.57	0.45	960.7		7.5	91.1	20.7	
Install.+DL		-172.20	-124.88	-7.55	-46.39	6.62	-53.94	0.43	1656.7		18.8	142.9	34.3	
(1)	0.0	-172.34	-124.86	-7.58	-46.48	6.58	-54.06	0.43	1656.5	1653.9	18.8	143.1	34.3	0.31
(2)	0.0	-184.23	-132.90	-8.17	-49.72	6.57	-57.90	0.44	1763.2	1774.9	20.3	153.1	36.8	0.33
(3)	0.4	-210.62	-150.81	-9.44	-56.90	6.52	-66.33	0.44	2000.7	2042.1	23.5	175.2	42.1	0.38
(4)	0.4	-245.02	-174.13	-10.82	-66.58	6.51	-77.40	0.44	2310.1	2390.9	26.9	205.0	49.2	0.44
(5)	0.4	-283.33	-200.06	-12.20	-77.56	6.49	-89.76	0.45	2654.1	2703.3	30.3	238.8	57.0	0.50
(6)	0.4	-320.36	-224.92	-13.68	-88.28	6.52	-101.96	0.45	2983.9	3043.3	34.0	271.8	64.8	0.56
(7)	0.4	-360.63	-251.22	-15.53	-100.20	6.31	-115.73	0.46	3332.8	3372.5	38.6	308.5	73.5	0.62
(8)	0.4	-411.08	-280.18	-18.53	-117.66	5.28	-136.18	0.49	3717.0	3696.6	46.1	362.3	86.5	0.68
Plastic														
(9)	0.4	-421.11	-285.90	-19.20	-121.14	5.12	-140.34	0.49	3792.9	3755.2	47.7	373.0	89.2	0.69
(10)	0.5	-433.11	-292.41	-20.02	-125.48	4.80	-145.50	0.50	3879.3	3823.0	49.8	386.4	92.5	0.71
.	.									.				.
.	.									.				.
.	.									.				.
(29)	0.0									4879.7				0.90

Table 3-11: B4 Mid-Span Stresses and Moments

The mid-span vertical bending moments for each of the girders of the test frame during the B4 test are shown in Figure 3-47. The plots in this figure illustrate the data included for G1, G2 and B4 (indirect method) in Table 3-10. While the maximum sustained load occurred at step 29, the test was continued until step 31. At this point, G2 was resisting a majority of the applied vertical bending moment. The last point in each plot of the figure describes this condition.

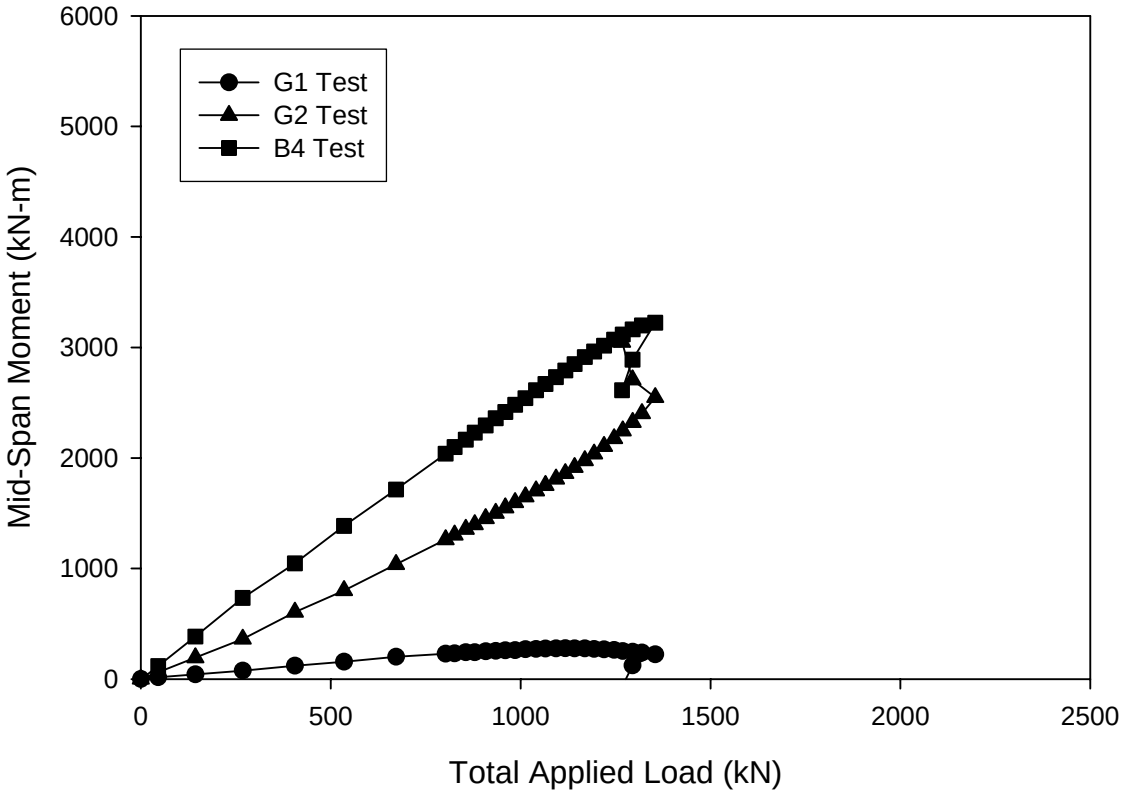

Figure 3-47: Test Frame Mid-Span Vertical Bending Moments, B4 Test

Figure 3-48 shows the longitudinal strain state of the B4 mid-span resulting from the installation of the component and from the dead load effects of the test frame. In general, the data indicate linear-elastic behavior of the section. The magnitude and gradient of

strain in each of the plates of this cross-section are consistent with the expected singly symmetric behavior.

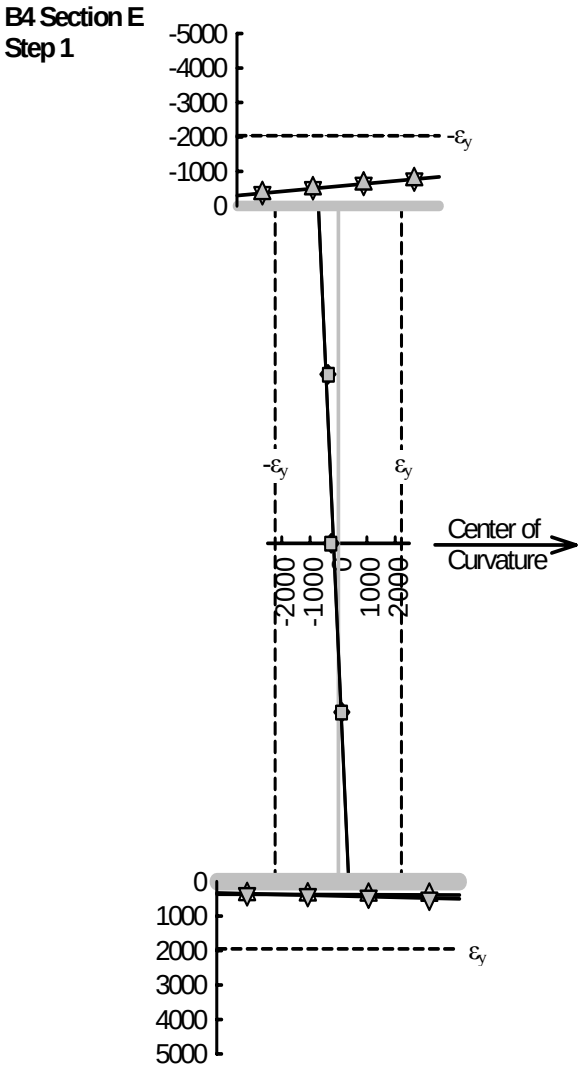

Figure 3-48: B4 Mid-Span Longitudinal Strain State Resulting From Installation and Dead Load (Step 1)

Figure 3-49 illustrates the first yield strain state at mid-span of B4 that occurred at step 8 of the test. At this load level, the web data indicate significant local elastic plate bending that is the result of the elevated web slenderness, 188.0. The cross-sections at N6L and N6R during step 8 are shown in Figures 3-50 and 3-51 respectively. These plots do not include the effects that the installation had on the cross-sections. However, the

data are far enough from the indicated yield limit to support the conclusion that first yield occurred at mid-span.

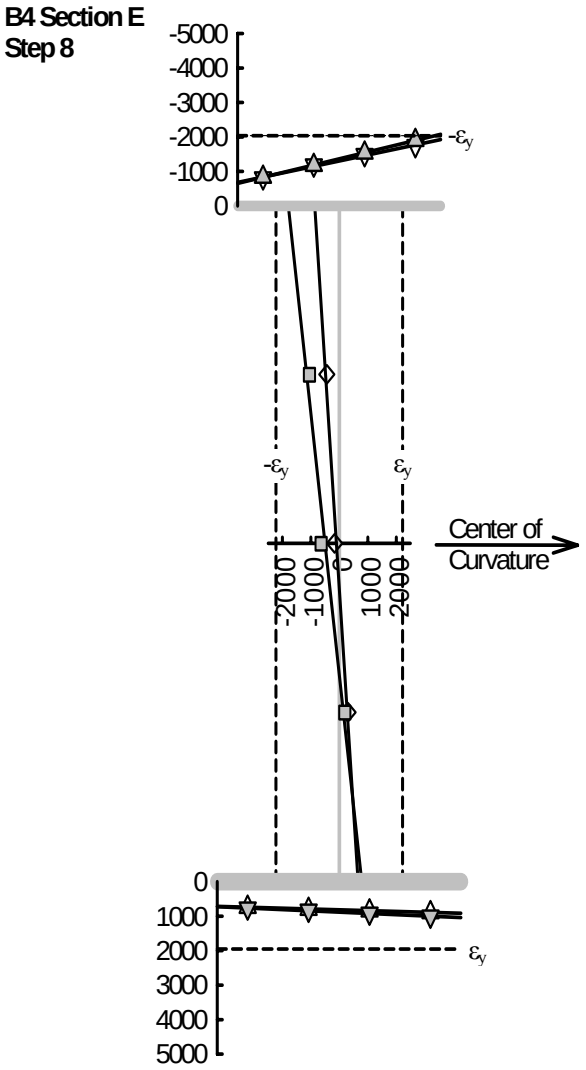

Figure 3-49: B4 Mid-Span Longitudinal Strain State During Step 8

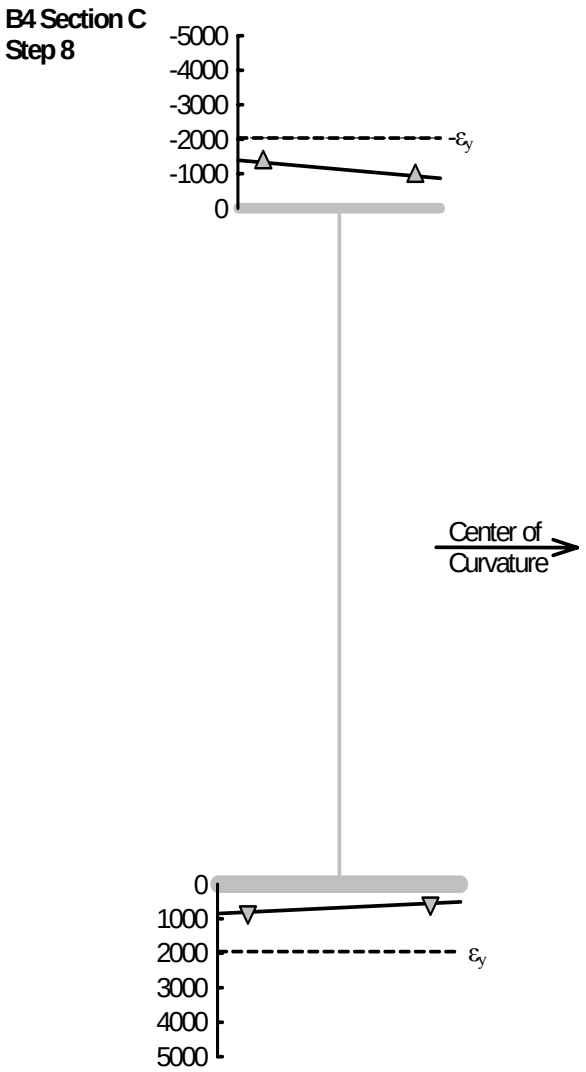

Figure 3-50: Longitudinal Strain State in B4 Near Cross-Frame N6L During Step 8 (Excluding Installation Effects)

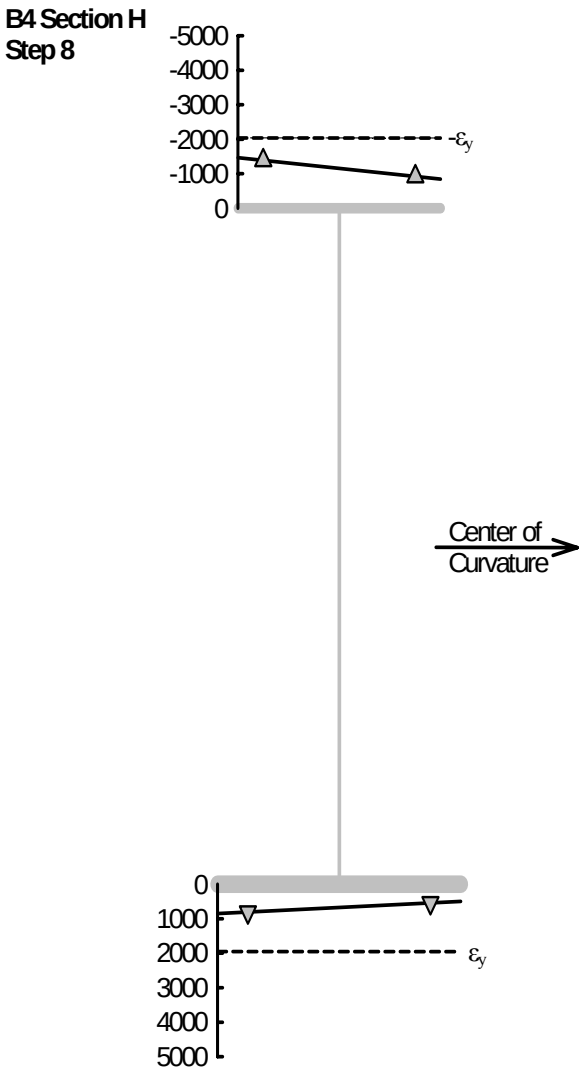

Figure 3-51: Longitudinal Strain State in B4 Near Cross-Frame N6R During Step 8 (Excluding Installation Effects)

The outside tip of the top flange at N6L (Figure 3-52) and at N6R (Figure 3-53) reached their yield limit at steps 18 and 19 respectively. However, the tension (bottom) flange of B4 never came close to the yield limit at anytime during the test.

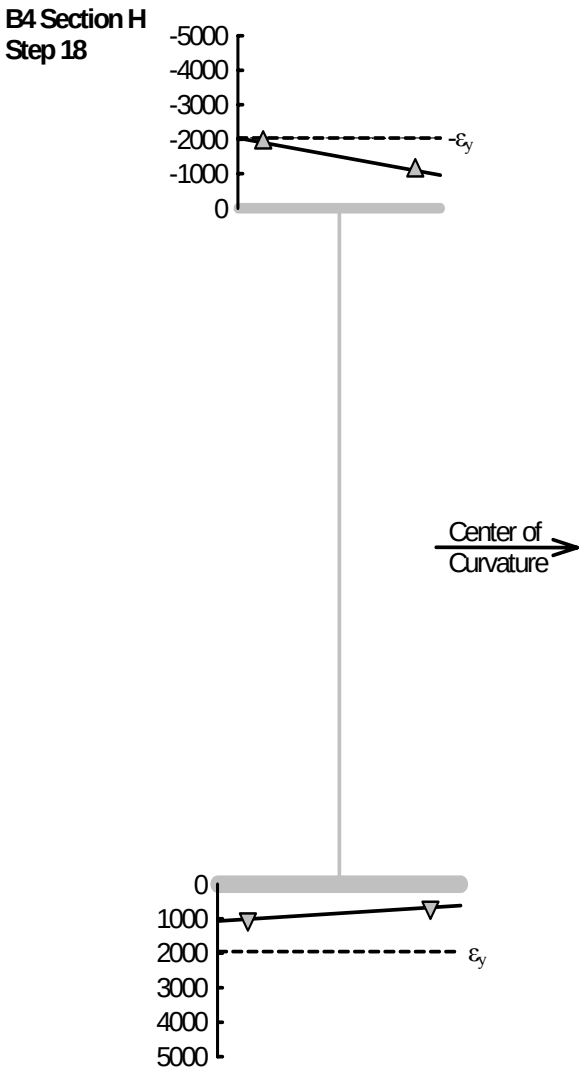

Figure 3-52: Longitudinal Strain State in B4 Near Cross-Frame N6R During Step 18 (Excluding Installation Effects)

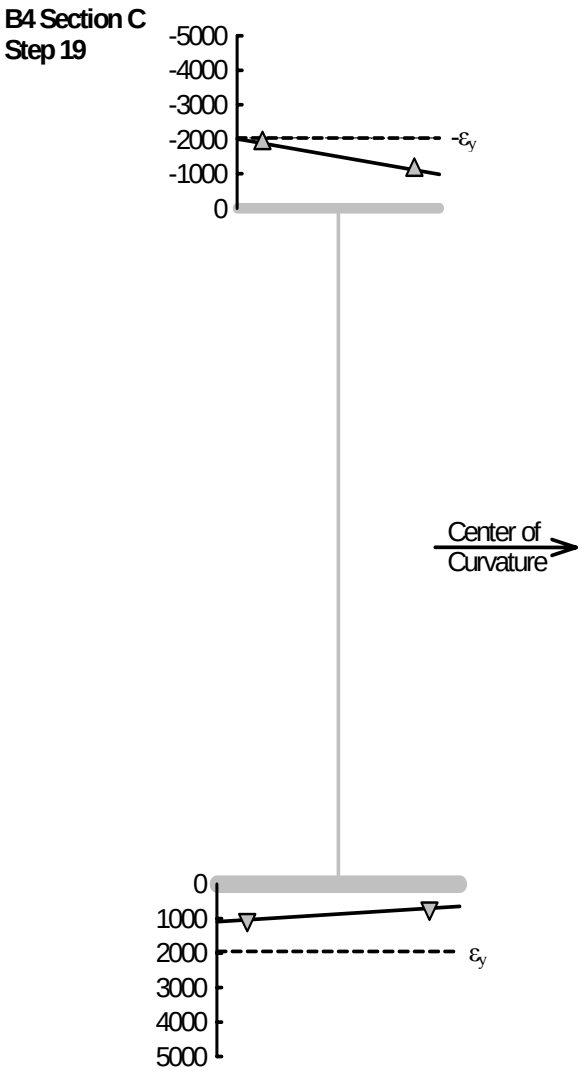

Figure 3-53: Longitudinal Strain State in B4 Near Cross-Frame N6L During Step 19 (Excluding Installation Effects)

The maximum sustained applied load during the B4 test produced the longitudinal strain state shown in Figure 3-54 at mid-span of the component. The associated vertical bending moment being resisted by the section at this load step was 4,880 kN-m (3,598.6 k-ft). The figure indicates significant buckling and yielding in the compression flange. The data also project yielding within the compression depth of the web in conjunction with significant web distortion. The state of longitudinal strain in the tension flange is linear and consistent at this load level.

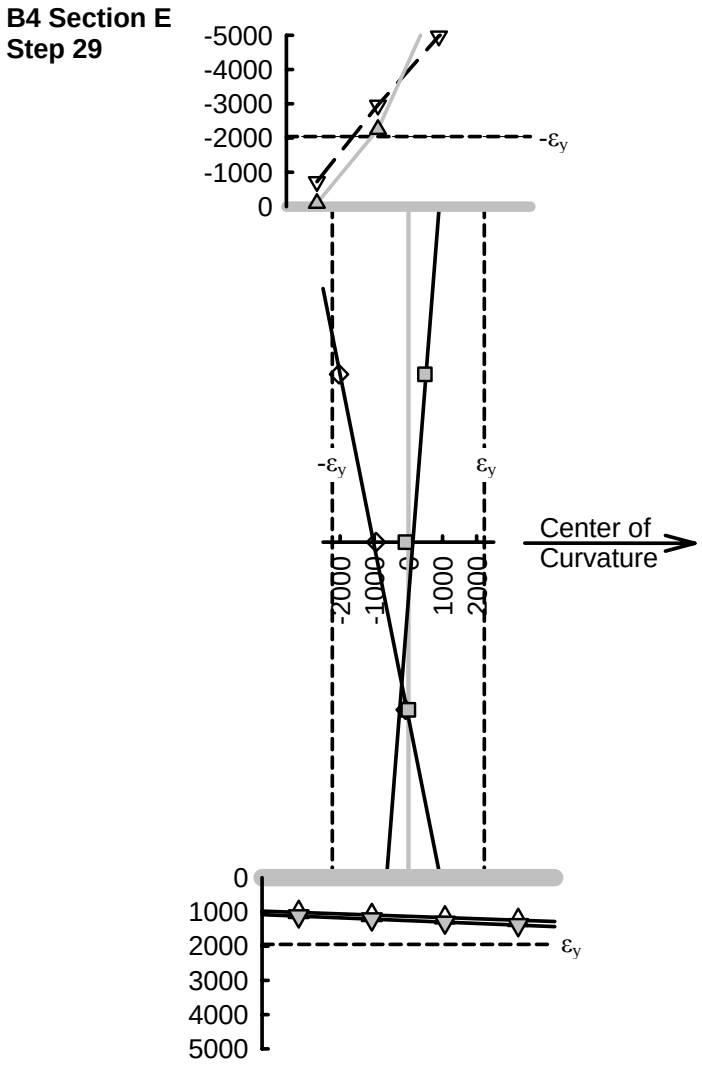

Figure 3-54: B4 Mid-Span Longitudinal Strain State During Step 29

Figure 3-55 demonstrates that G2 remained elastic throughout the loading regime. The strain data plotted are significantly below the respective yield limits shown. Also, the regression lines do not indicate any degree of local plate bending.

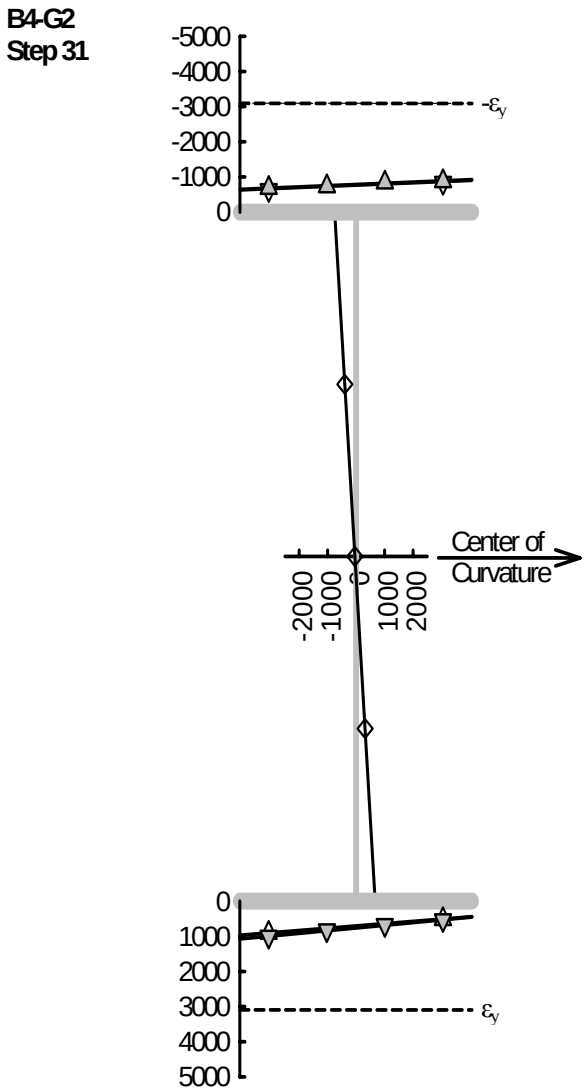

Figure 3-55: Most Critical G2 Mid-Span Longitudinal Strain State During B4 Test

3.8 Bending Component B5 Test

The test frame containing component B5 was loaded in 46 steps to a maximum of 1,833 kN (412.2 kip). However, the maximum moment resisted by B5 occurred at step 38 at an applied load level of 1,732 kN (389.5 kips). A summary of applied loading information for this component test is presented in Table 3-12 and Table 3-13.

Load Step	Total Applied Load	Mx (Total)	Mx (G1)	Mx (G2)	Mx (B5)		
					Indirect (a)	Direct (b)	(a)/(b)
	kN	kN-m	kN-m	kN-m	kN-m	kN-m	
B5 Elastic							
1	0	0.9	-0.1	0.4	0.6	0.7	0.92
2	57.7	271.9	20	85	166.9	135.3	1.23
3	151.9	668.4	49.8	215.5	403.1	351.1	1.15
4	274.2	1203.1	75.5	419.3	708.4	658	1.08
5	406.2	1786.2	107.7	641	1037.5	990.7	1.05
6	534.9	2358.8	137.6	862.5	1358.6	1328.1	1.02
7	670.1	2957.5	162.7	1105.1	1689.6	1697	1
8	798.8	3525.8	185.6	1338.7	2001.5	2052.7	0.98
9	917.2	4037.7	198.8	1568.9	2269.9	2393.8	0.95
B5 Plastic							
10	1066.4	4703	226.4	1833.9	2642.7	2792.8	0.95
11	1101.5	4857.8	232.6	1888.6	2736.6	2884.5	0.95
12	1130.6	4982	237.7	1949.7	2794.5		
13	1159.3	5110.7	245.4	2008.9	2856.5		
14	1184.5	5222.5	245.8	2055.6	2921.2		
15	1208.1	5327.7	248.1	2113.1	2966.5		
16	1243.2	5481.9	251.5	2185.2	3045.2		
17	1268.9	5596.4	251.5	2225.7	3119.2		
18	1290	5690.5	248.4	2280.1	3162		
19	1314.3	5797.9	251.2	2338.6	3208.1		
20	1346.2	5936.4	249.7	2406.1	3280.6		
21	1365.6	6019.3	240.3	2469.7	3309.3		
22	1396.7	6157.6	240.8	2532.7	3384.1		
23	1425.4	6285.1	237.1	2602.1	3445.9		
24	1449.7	6393.4	231.8	2680.7	3480.9		

Table 3-12: B5 Applied Load Steps and Resulting Girder Moments (Part I)

Load Step	Total Applied Load	Mx (Total)	Mx (G1)	Mx (G2)	Mx (B5)		
					Indirect (a)	Direct (b)	(a)/(b)
	kN	kN-m	kN-m	kN-m	kN-m	kN-m	
25	1483.2	6540.3	225.4	2768.1	3546.8		
26	1493.5	6587	200.1	2841.3	3545.6		
27	1529.6	6745.4	203.2	2908.2	3634		
28	1554.6	6854.8	189.6	3008.5	3656.7		
29	1587.6	6999.9	173.4	3091.3	3735.2		
30	1616.8	7128.8	169.2	3193.7	3765.8		
31	1642.8	7246.3	135.6	3276.6	3834.1		
32	1662.9	7336.1	127.4	3392.6	3816		
33	1696.1	7479.2	103.8	3526.9	3848.5		
34	1703.8	7517.8	68.1	3585.2	3864.5		
35	1654.5	7298	8.9	3549.7	3739.4		
36	1680.5	7416.8	20.8	3605.9	3790.1		
37	1708	7537.5	35.5	3662.7	3839.3		
38	1732.7	7646	31.7	3745	3869.3		
39	1733.2	7647.3	-0.6	3794.6	3853.2		
40	1749.9	7719.9	-19.3	3877	3862.2		
41	1768.5	7803.9	-35.1	3987.7	3851.3		
42	1782.1	7861	-71	4110.1	3821.9		
43	1799.1	7937.9	-108.2	4210.7	3835.4		
44	1814.2	8006	-166.2	4391.5	3780.7		
45	1826.8	8061.5	-214.9	4531.1	3745.3		
46	1833.3	8092.1	-265.9	4664.7	3693.3		
47	1819.8	8030.6	-347.6	4809.1	3569.1		
48	1809.1	7983.8	-428	4990.4	3421.3		
49	1804.1	7961.9	-506.2	5122.2	3345.9		

Table 3-13: B5 Applied Load Steps and Resulting Girder Moments (Part II)

Load Case	Total Applied Load	Compression Flange, Inside Tip, Extreme Fiber Stress							Moments at Section					
		σ_z Total	σ_z from M_x (a)	σ_z from M_y	σ_z from M_z	σ_z from P_z	σ_z(lat.) (b)	(b)/(a)	M_x Direct	M_x Indirect (c)	M_y	Bi	$M_{lat.}$ Comp. Flange	(c)/M_x^{yield}
	kN	MPa	MPa	MPa	MPa	MPa	MPa		kN-m	kN-m	kN-m	kN-m^2	kN-m	
Elastic														
Install.		-84.28	-35.14	-0.91	-48.08	-0.15	-49.00	1.39	511.9		1.3	86.2	35.4	
DL		-89.63	-61.57	-5.19	-22.35	-0.52	-27.54	0.45	896.9		7.5	40.1	19.9	
Install.+DL		-173.91	-96.71	-6.10	-70.44	-0.66	-76.54	0.79	1408.8		8.8	126.3	55.3	
(1)	0.0	-173.96	-96.75	-6.18	-70.44	-0.59	-76.62	0.79	1409.5	1409.4	8.9	126.3	55.3	0.24
(2)	57.7	-187.78	-106.00	-7.17	-73.86	-0.75	-81.04	0.76	1544.1	1575.7	10.4	132.4	58.5	0.27
(3)	151.9	-209.70	-120.81	-8.78	-79.33	-0.78	-88.11	0.73	1759.8	1811.9	12.7	142.2	63.6	0.31
(4)	274.2	-240.77	-141.88	-10.89	-87.16	-0.84	-98.05	0.69	2066.8	2117.1	15.8	156.3	70.8	0.37
(5)	406.2	-274.40	-164.72	-13.13	-95.77	-0.77	-108.91	0.66	2399.5	2446.2	19.0	171.7	78.6	0.43
(6)	534.9	-307.69	-187.88	-14.89	-105.03	0.10	-119.92	0.64	2736.9	2767.4	21.5	188.3	86.6	0.48
(7)	670.1	-343.90	-213.20	-16.55	-115.84	1.69	-132.39	0.62	3105.8	3098.4	23.9	207.7	95.6	0.54
(8)	798.8	-378.93	-237.62	-18.09	-126.47	3.25	-144.56	0.61	3461.4	3410.3	26.2	226.8	104.4	0.59
(9)	917.2	-411.94	-261.03	-19.25	-136.61	4.94	-155.85	0.60	3802.6	3678.7	27.8	245.0	112.5	0.64
Plastic														
(10)	1066.4	-453.46	-288.43	-22.42	-148.95	6.34	-171.37	0.59	4201.6	4051.5	32.4	267.1	123.7	0.70
(11)	1101.5	-462.69	-294.72	-23.13	-151.67	6.84	-174.80	0.59	4293.3	4145.4	33.5	272.0	126.2	0.72
.	.									.				.
.	.									.				.
.	.									.				.
(38)	1732.7									5278.1				0.92

Table 3-14: B5 Mid-Span Stresses and Moments

Table 3-14 primarily shows the elastic range B5 mid-span stresses and moments. First yield in the component was projected to have occurred during load step 9 at a load level of 917.2 kN (206.2 kip). At this step, the total resisted mid-span vertical bending moment in B5 was 3,679 kN-m (2,712.9 k-ft). This amount, when normalized by the vertical bending yield moment, results in a performance ratio of 0.64. At the maximum vertical bending moment resisted by B5 during step 38, 5,278 kN-m (3,892.4 k-ft) this normalized ratio increased to 0.92.

A comparison of the direct and indirect methods to determine the resisted vertical moment in B5 is shown in Figure 3-56. While this comparison shows good agreement throughout most of the elastic regime of loading, the methods have diverged approximately 5% at the point that inelasticity is introduced into the system.

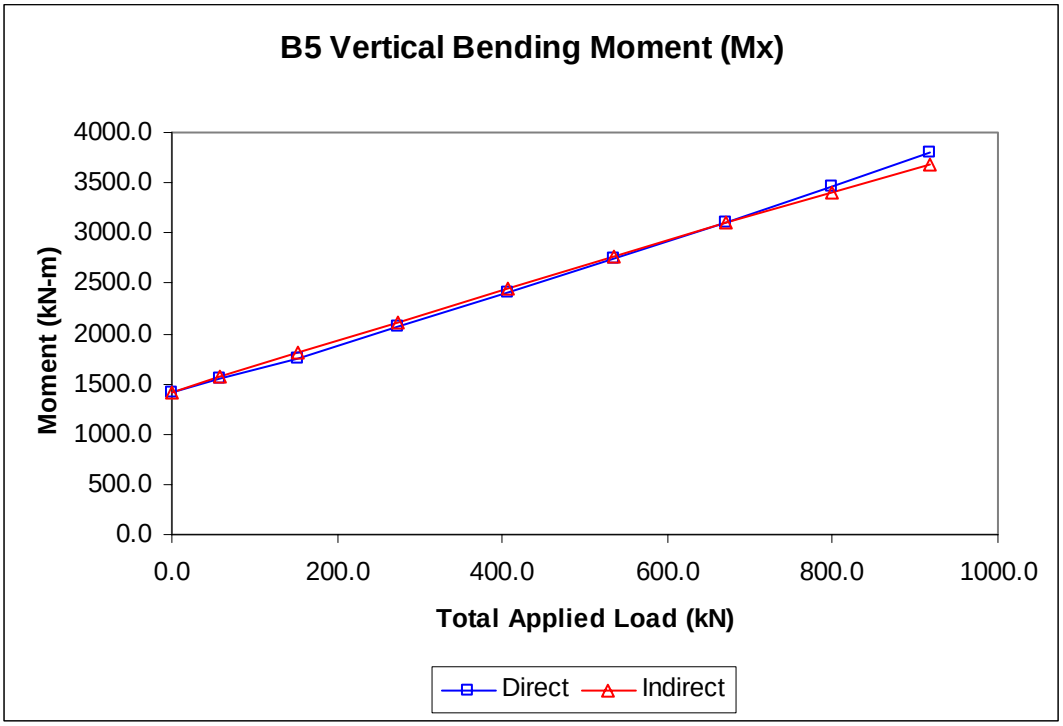

Figure 3-56: B5 Vertical Bending Moment

The mid-span vertical bending moments of the test frame that result from the applied loading are shown in Figure 3-57 for the B5 test. The B5 test record shows a small plateau of post-peak stability prior to ultimate failure of the section and a dramatic shedding of load to the test frame, in particular for G2.

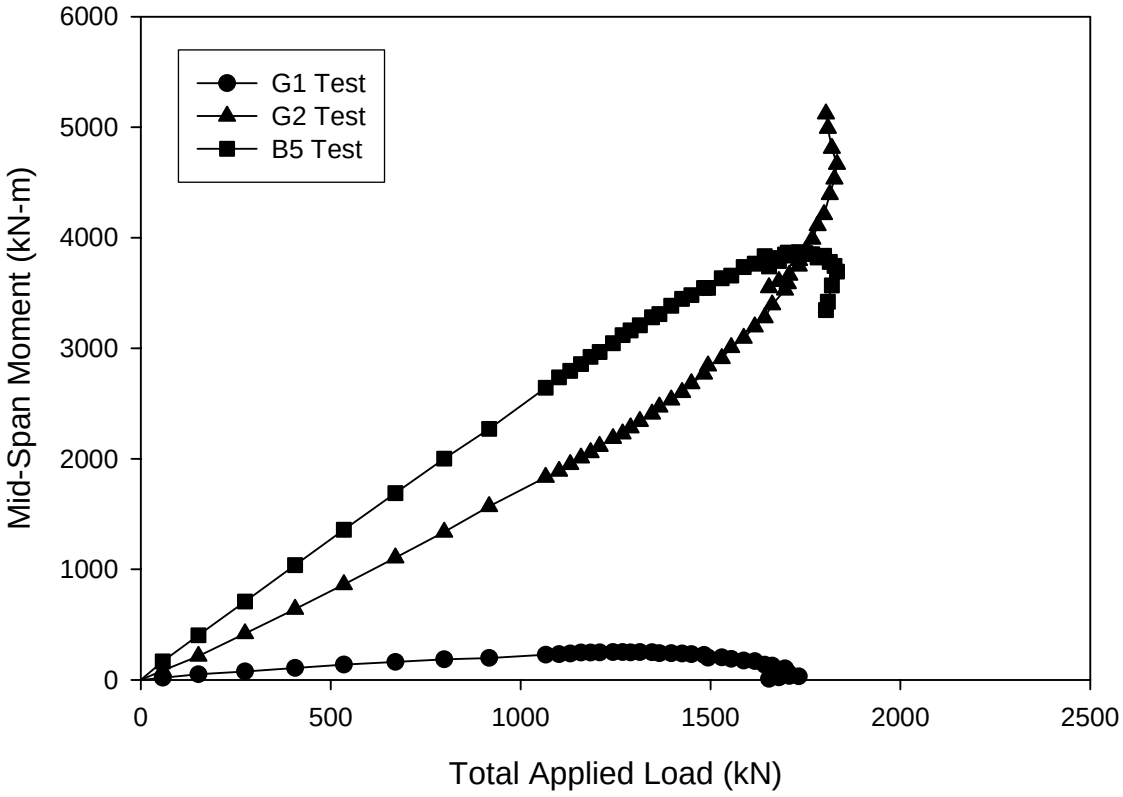

Figure 3-57: Test Frame Mid-Span Vertical Bending Moments, B5 Test

The effects of installation and dead load on the mid-span longitudinal strain state of B5 are shown in Figure 3-58. The complementary strain gradients across the flanges indicate the presence of a significant torsional warping strain. The separation of the regression lines across the tension flange is evidence of some local vertical plate bending.

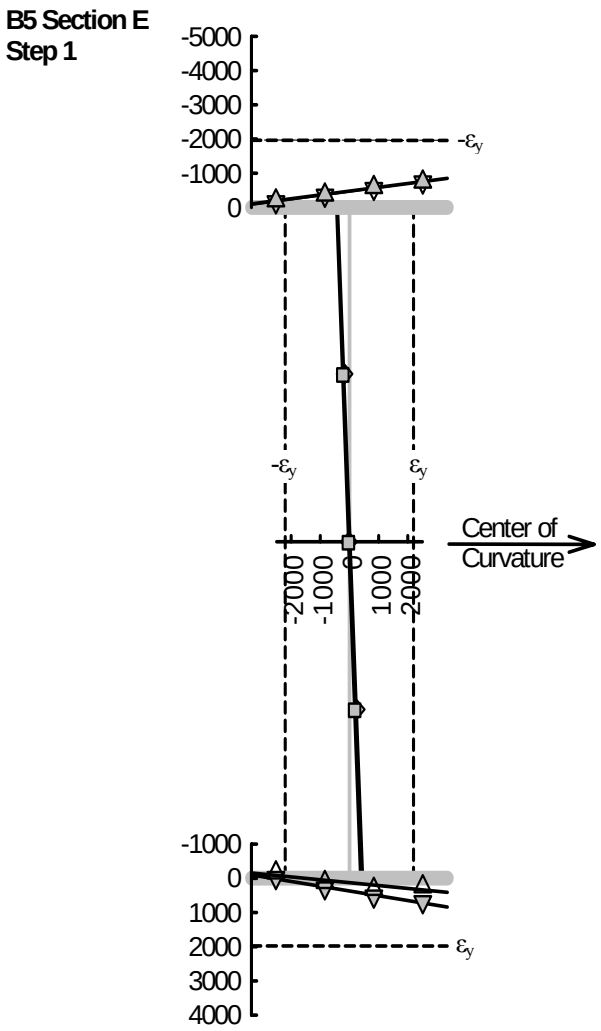

Figure 3-58: B5 Mid-Span Longitudinal Strain State Resulting From Installation and Dead Load (Step 1)

At the first projected yield in the B5 test, shown in Figure 3-59, the compression flange of the mid-span section has minimal distortion. However, the web plate data indicate a uniform flexing that causes tension on the inside face and compression on the outside face of the web. Also, the distortion in the tension flange that resulted from the installation and dead load effects has not progressed at this load level.

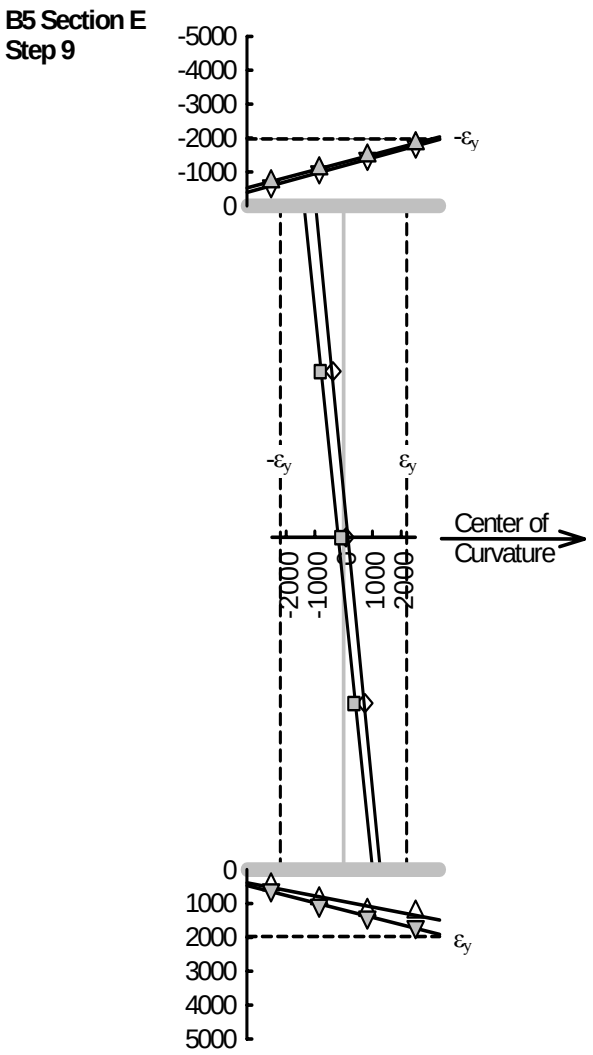

Figure 3-59: B5 Mid-Span Longitudinal Strain State During Step 9

The cross-section at N6L, shown in Figure 3-60, was the braced-section during step 9 that was the most critical. While the strain data plotted do not include the effects of installation on the cross-section, the magnitudes fall significantly short of the yield limits indicated. The tension flange at this section does reach its indicated yield limit at step 16 (see Figure 3-61).

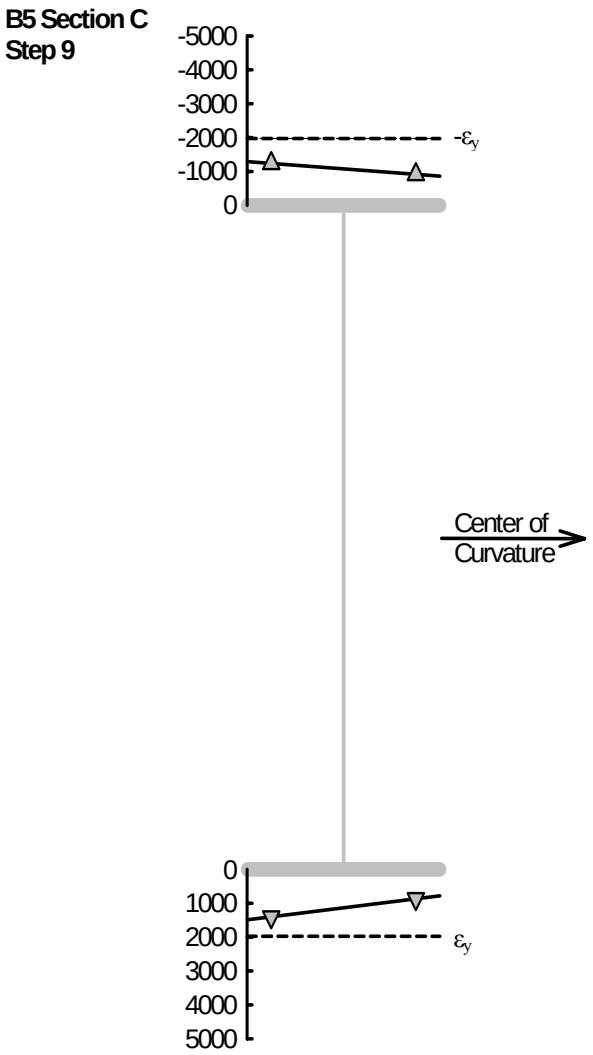

Figure 3-60: Longitudinal Strain State in B5 Near Cross-Frame N6L During Step 9 (Excluding Installation Effects)

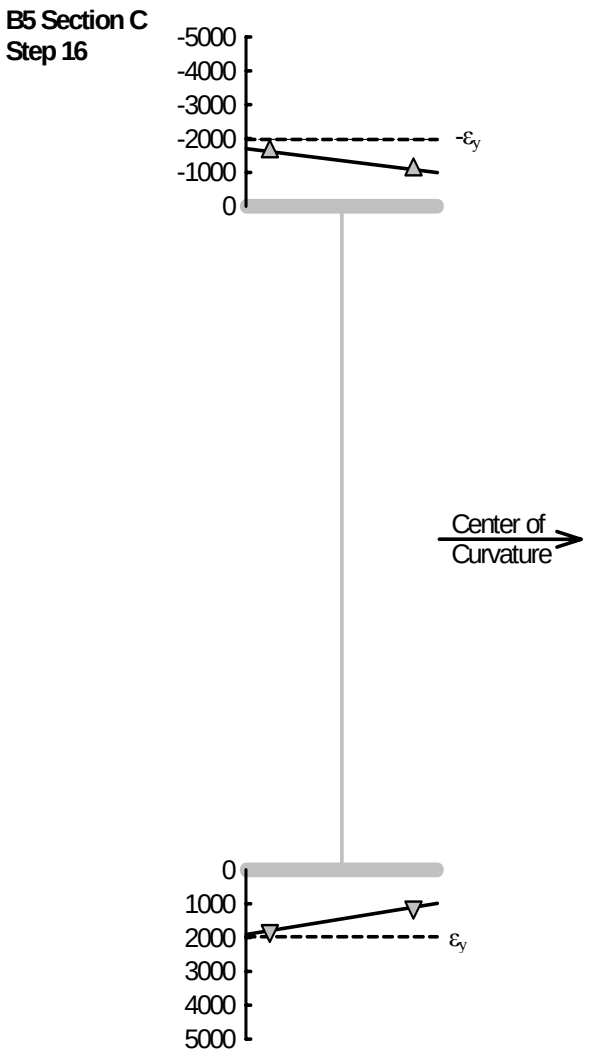

Figure 3-61: Longitudinal Strain State in B5 Near Cross-Frame N6L During Step 16 (Excluding Installation Effects)

The effects on the longitudinal strain state at mid-span of B5 during the maximum sustained moment of the test, step 38, are shown in Figure 3-62. At this load step, most of the compression flange has yielded and distorted significantly. Also, a large portion of the depth of web in compression has yielded the outside face of the plate. The inside face of the web plate in this region has been prevented from yielding by the tensile strains caused by the local buckling of the plate. The tension flange has also reached its yield

limit over approximately the inside half of the plate. However, the regression lines for each surface of data do not indicate an increase in the local level of lateral distortion.

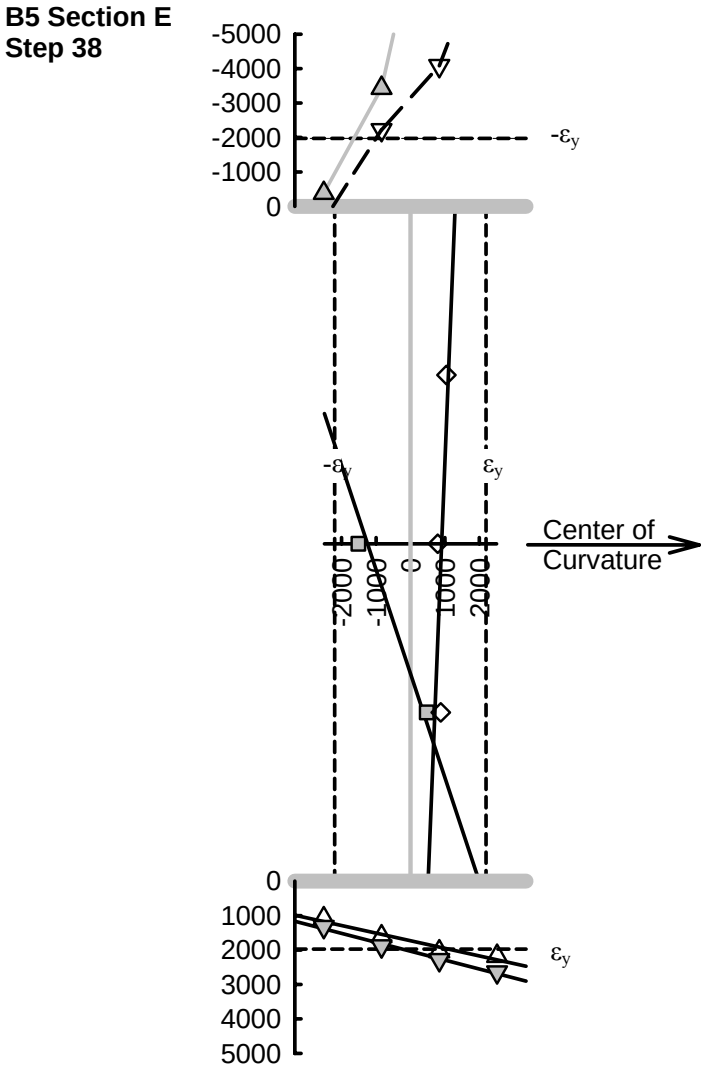

Figure 3-62: B5 Mid-Span Longitudinal Strain State During Step 38

Figure 3-63 shows the longitudinal strain state at mid-span of G2 during the maximum vertical bending moment that it experienced during the B5 test, step 49. This figure confirms that G2 remained well within the elastic region throughout this component test.

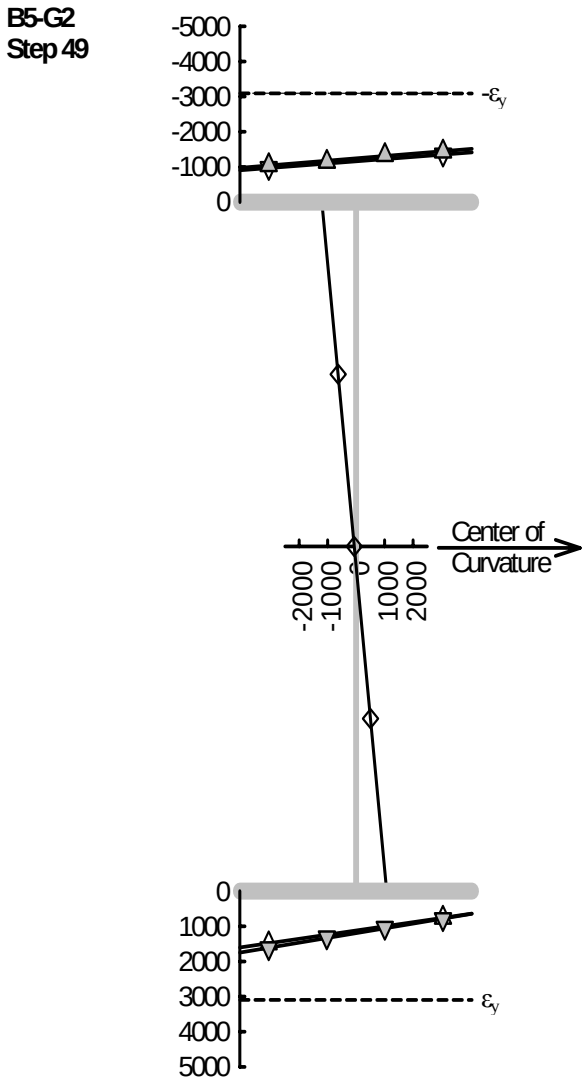

Figure 3-63: Most Critical G2 Mid-Span Longitudinal Strain State During B5 Test

3.9 Bending Component B6 Test

Table 3-15 and Table 3-16 contain the applied load levels associated with each step of the B6 component test. The mid-span girder vertical bending moments that resulted from the applied loading for G1, G2 and B6 are also in Table 3-15 and Table 3-16. First yield in B6 was projected to occur during step 13 with a sustained load level of 1,354 kN (304.5 kip). At this step, the resisted vertical bending moment due to the applied loading

in B6 was 3,442 kN-m (2,538.3 k-ft). The maximum vertical bending moment resisted by B6 was 4,886 kN-m (3,603.4 k-ft) and occurred during step 38.

Load Step	Total Applied Load	Mx (Total)	Mx (G1)	Mx (G2)	Mx (B6)		
					Indirect (a)	Direct (b)	(a)/(b)
	kN	kN-m	kN-m	kN-m	kN-m	kN-m	
B6 Elastic							
1	0.1	-0.5	0.1	0.6	-1.2	0.2	-6.83
2	51.9	216.6	17.1	69.3	130.3	122.3	1.06
3	136.1	594.3	46.4	180.8	367.1	326.3	1.12
4	271.8	1188.5	88.4	384.8	715.3	671	1.07
5	404	1771.4	130	583.3	1058.1	1004.6	1.05
6	535.3	2355.6	169.5	793.1	1393	1355.7	1.03
7	670.7	2953.2	208.4	1003.7	1741.1	1724	1.01
8	804.9	3541	244.3	1223.7	2073	2095.1	0.99
9	937.6	4133.2	278.8	1436.1	2418.4	2462.6	0.98
10	1068.8	4707.4	306.1	1659.5	2741.8	2839.7	0.97
11	1197.9	5278	334.4	1878.6	3065	3210.8	0.95
12	1331.1	5858.3	359.7	2097.5	3401.1	3592.7	0.95
13	1354.2	5960.4	365.4	2153.1	3441.9	3665.2	0.94
B6 Plastic							
14	1378.4	6065.3	371	2192.8	3501.4	3732.6	0.94
15	1405.5	6187.1	369.8	2236.8	3580.5	3814.7	0.94
16	1432.1	6306.1	389.1	2279.2	3637.7		
17	1486.3	6544.5	403.1	2365.7	3775.7		
18	1517.2	6681.2	405.3	2429.8	3846.1		
19	1541.8	6788.5	405.8	2464	3918.6		
20	1566.3	6898.1	412.6	2522.7	3962.9		
21	1594.4	7024.3	414.5	2567.4	4042.4		

Table 3-15: B6 Applied Load Steps and Resulting Girder Moments (Part I)

Load Step	Total Applied Load	Mx (Total)	Mx (G1)	Mx (G2)	Mx (B6)		
					Indirect (a)	Direct (b)	(a)/(b)
	kN	kN-m	kN-m	kN-m	kN-m	kN-m	
22	1625	7157.1	418.7	2627.1	4111.4		
23	1646.8	7251.5	414	2674.8	4162.7		
24	1673	7367.8	415	2731.9	4220.8		
25	1707.7	7520.7	419.5	2794.4	4306.8		
26	1726.3	7603.1	416.3	2853.3	4333.5		
27	1765.4	7771.8	421.4	2937.3	4413.1		
28	1772.9	7807.3	403.4	2982.2	4421.7		
29	1812	7981	409.1	3048.8	4523.1		
30	1839.6	8102	405.1	3119.7	4577.2		
31	1871	8243.4	397.7	3217.1	4628.6		
32	1903.2	8385.5	394.4	3306.7	4684.4		
33	1922.7	8472.3	372.8	3378.5	4721		
34	1949.1	8590.6	365.4	3455.7	4769.5		
35	1981.1	8736.4	343	3588.3	4805.1		
36	2007.6	8856.8	319.6	3693	4844.2		
37	2033.9	8973.3	295.5	3807.8	4870		
38	2071.6	9140.3	248.2	4006	4886.2		
39	2095.4	9252.8	183.9	4195.9	4873		
40	2113.2	9332.8	138.9	4335.8	4858.1		
41	2138.3	9446.9	46.6	4626.2	4774.1		
42	2165.1	9572.4	-85.9	4981.9	4676.4		
43	2171.4	9598.2	-208.7	5282	4525		

Table 3-16: B6 Applied Load Steps and Resulting Girder Moments (Part II)

Selected stresses and moments, primarily from the elastic regime of loading, are listed in Table 3-17 for the mid-span cross-section of B6. These data indicate that at first yield in the component, the ratio of compression flange lateral bending stress to vertical bending stress was 0.37. Also, the largest sustained vertical bending moment in the elastic range was 4,955 kn-m (3,654.3 k-ft). This amount, when normalized by the theoretical vertical bending yield moment, yields a performance ratio of 0.73. This ratio

increases to 0.94 at the maximum moment resisted by B6, 6,400 kN-m (4,719.4 k-ft), which occurred during step 38 of this test.

The direct and indirect methods of determining the resisted vertical bending moment at mid-span of B6 during the elastic loading regime of this component test are contrasted in Figure 3-64. The methods again begin to diverge at about the 890 kN (200 kip) total applied load level. This separation represents approximately 6% at the load step during which first yield is projected to have occurred.

Load Case	Total Applied Load	Compression Flange, Inside Tip, Extreme Fiber Stress							Moments at Section					
		σ_z Total	σ_z from M_x (a)	σ_z from M_y	σ_z from M_z	σ_z from P_z	σ_z(lat.) (b)	(b)/(a)	M_x Direct	M_x Indirect (c)	M_y	Bi	$M_{lat.}$ Comp. Flange	(c)/M_x^{yield}
	kN	MPa	MPa	MPa	MPa	MPa	MPa		kN-m	kN-m	kN-m	kN-m^2	kN-m	
Elastic														
Install.		-30.18	-31.98	4.84	-2.38	-0.66	2.46	-0.08	561.9		-8.6	5.3	2.2	
DL		-74.77	-54.15	-2.14	-18.12	-0.36	-20.25	0.37	951.5		3.8	39.9	-17.9	
Install.+DL		-104.95	-86.13	2.70	-20.50	-1.02	-17.79	0.21	1513.3		-4.8	45.2	-15.7	
(1)	0.1	-104.82	-86.14	2.73	-20.49	-0.93	-17.75	0.21	1513.5	1512.2	-4.8	45.2	-15.7	0.22
(2)	51.9	-114.86	-93.09	1.99	-22.83	-0.93	-20.84	0.22	1635.7	1643.6	-3.5	50.3	-18.4	0.24
(3)	136.1	-131.63	-104.70	0.92	-26.74	-1.11	-25.82	0.25	1839.6	1880.4	-1.6	58.9	-22.8	0.28
(4)	271.8	-159.04	-124.31	-0.44	-33.22	-1.07	-33.66	0.27	2184.3	2228.6	0.8	73.2	-29.8	0.33
(5)	404.0	-185.53	-143.30	-1.63	-39.65	-0.95	-41.28	0.29	2517.9	2571.4	2.9	87.4	-36.5	0.38
(6)	535.3	-212.55	-163.29	-2.41	-46.77	-0.08	-49.18	0.30	2869.1	2906.3	4.3	103.1	-43.5	0.43
(7)	670.7	-240.61	-184.24	-3.09	-54.54	1.27	-57.63	0.31	3237.3	3254.4	5.5	120.2	-51.0	0.48
(8)	804.9	-269.15	-205.36	-4.12	-62.32	2.66	-66.44	0.32	3608.4	3586.4	7.3	137.4	-58.8	0.53
(9)	937.6	-297.49	-226.28	-5.43	-69.90	4.12	-75.33	0.33	3975.9	3931.7	9.6	154.1	-66.6	0.58
(10)	1068.8	-326.92	-247.74	-7.56	-77.35	5.73	-84.91	0.34	4353.0	4255.2	13.4	170.5	-75.1	0.62
(11)	1197.9	-356.30	-268.86	-10.14	-84.62	7.33	-94.76	0.35	4724.1	4578.4	18.0	186.5	-83.8	0.67
(12)	1331.1	-387.18	-290.60	-13.58	-92.02	9.02	-105.60	0.36	5106.1	4914.4	24.0	202.8	-93.4	0.72
(13)	1354.2	-393.05	-294.72	-14.48	-93.35	9.49	-107.83	0.37	5178.5	4955.3	25.6	205.8	-95.4	0.73
Plastic														
(14)	1378.4	-398.68	-298.56	-15.30	-94.65	9.83	-109.95	0.37	5246.0	5014.7	27.1	208.6	-97.3	0.74
(15)	1405.5	-405.70	-303.23	-16.44	-96.35	10.32	-112.79	0.37	5328.0	5093.8	29.1	212.4	-99.8	0.75
.	.									.				.
.	.									.				.
.	.									.				.
(38)	2071.6									6399.5				0.94

Table 3-17: B6 Mid-Span Stresses and Moments

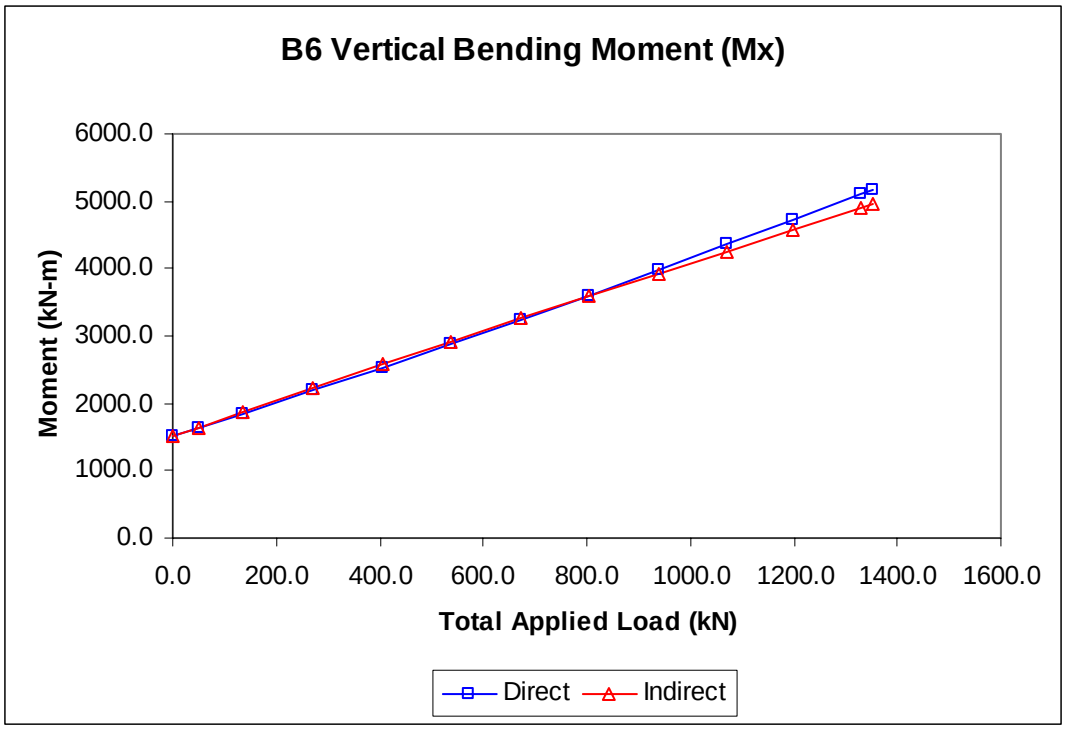

Figure 3-64: B6 Vertical Bending Moment

The mid-span vertical bending moments in G1, G2 and B6, which are due to the applied loading throughout the entire regime of the B6 test, are plotted in Figure 3-65. The peak resisted vertical bending moment in B6 occurred during load step 38. The section initially remained viable post-peak as the test frame continued to take load up until load step 43 when the test was halted. At this load level, 2,172 kN (488.2 kip), B6 was carrying significantly less of the applied moment than girder G2.

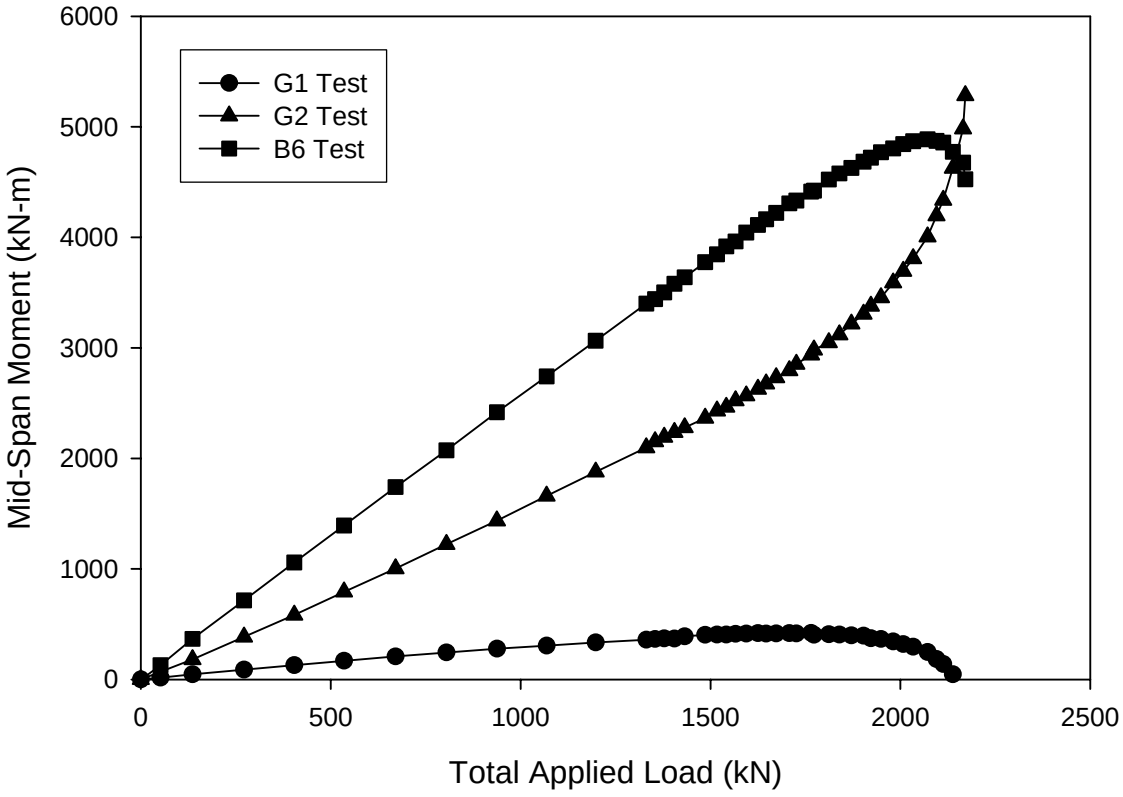

Figure 3-65: Test Frame Mid-Span Vertical Bending Moments, B6 Test

The dead load and installation effects on the mid-span longitudinal strain state are shown in Figure 3-66. This plot primarily indicates that vertical bending was the dominate force effect that resulted from these loadings. The data describe linear elastic behavior in all plates of the section.

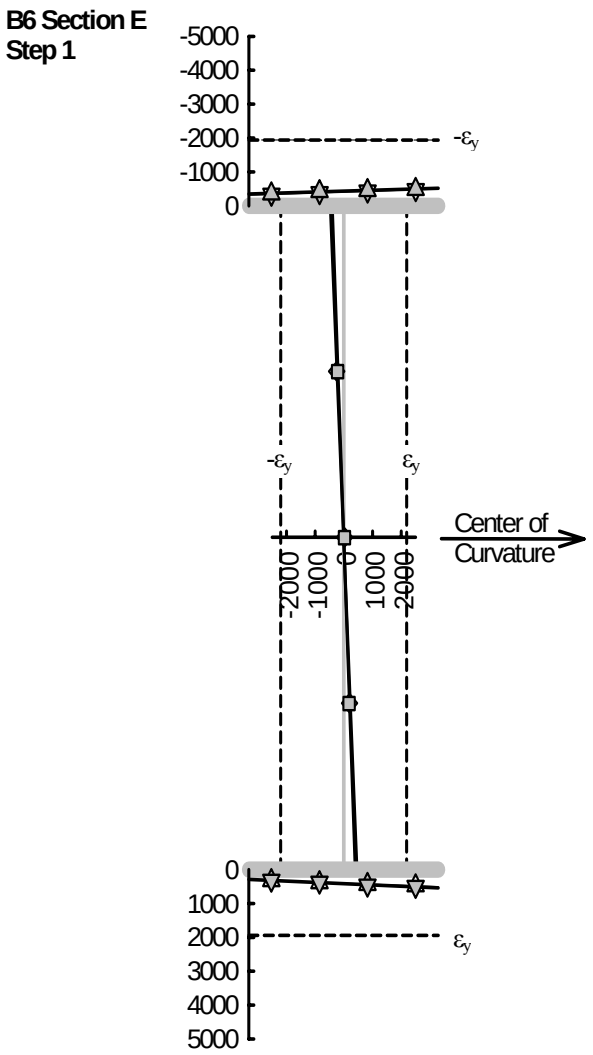

Figure 3-66: B6 Mid-Span Longitudinal Strain State Resulting From Installation and Dead Load (Step 1)

Figure 3-67 presents the mid-span longitudinal strain state of B6 at load step 13. This load step is projected to have caused first yield in the cross-section on the inside tip of the compression flange. However, first yield in the component most likely occurred at the brace point cross-sections. The data from the cross-sections near the cross-frames N6L and N6R, shown in Figures 3-68 and 3-69 respectively, also projected strain levels in the outside tips of the tension flange. These levels also exceed the yield strain limits at this

same load step. These data do not include any effects for installation of the component; therefore, they most likely reached their yield limits earlier in the loading regime.

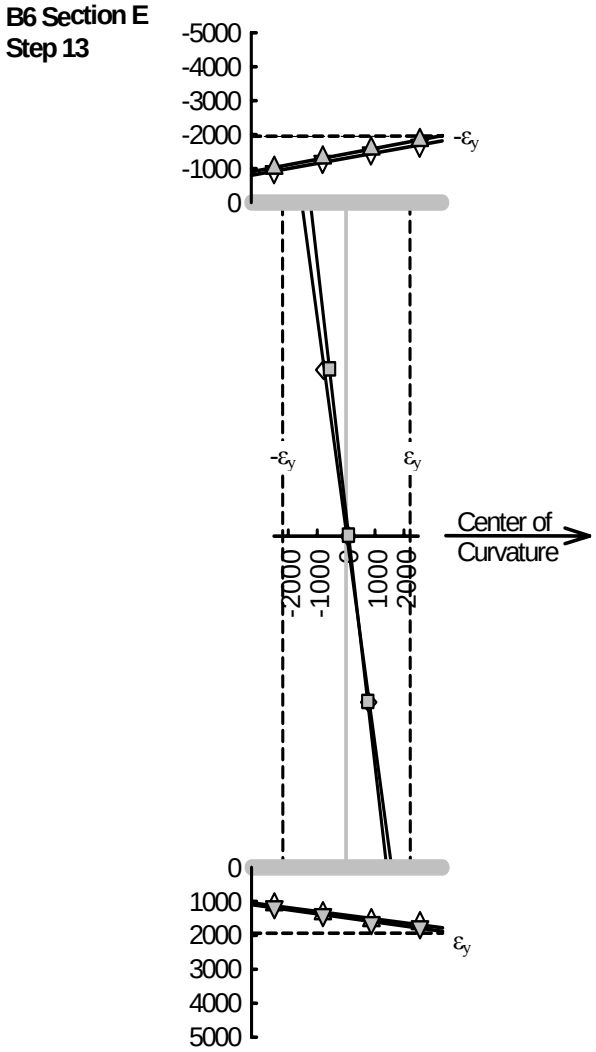

Figure 3-67: B6 Mid-Span Longitudinal Strain State During Step 13

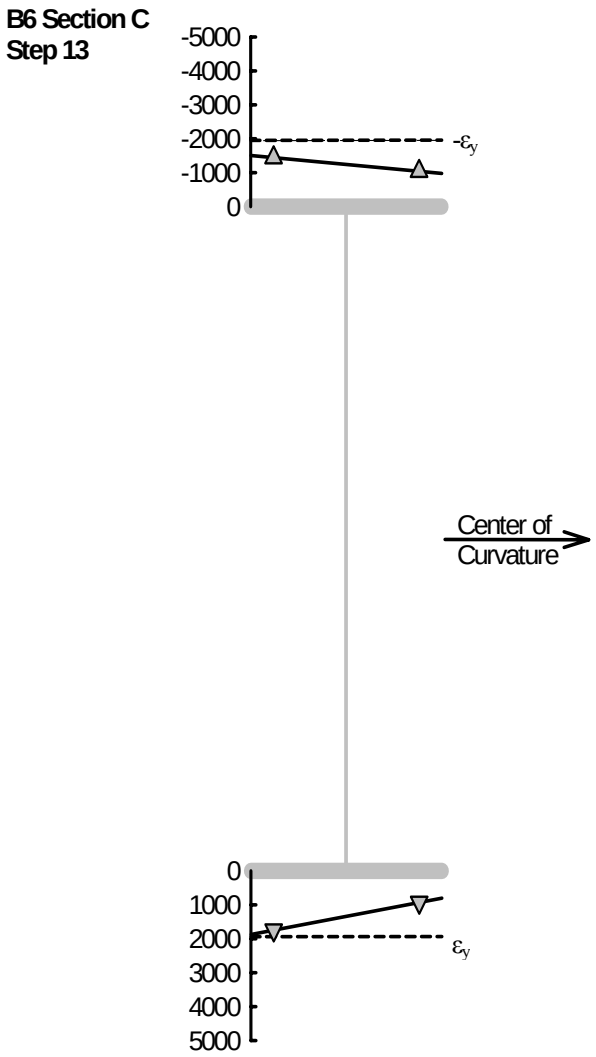

Figure 3-68: Longitudinal Strain State in B6 Near Cross-Frame N6L During Step 13 (Excluding Installation Effects)

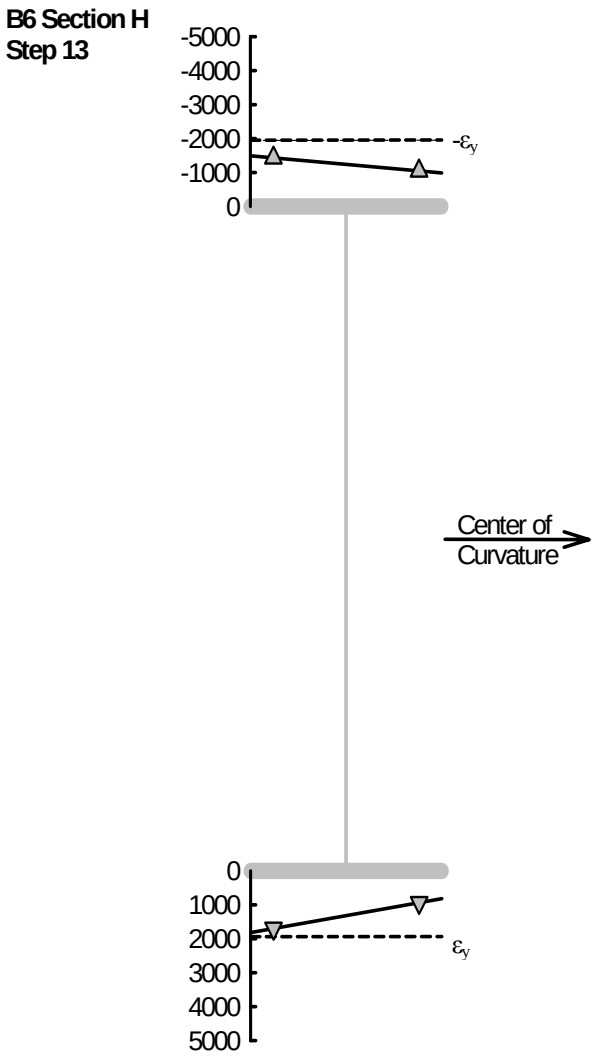

Figure 3-69: Longitudinal Strain State in B6 Near Cross-Frame N6R During Step 13 (Excluding Installation Effects)

Approximately half of each flange of B6 has exceeded its yield limit by load step 28, shown in Figure 3-70. At this load level, the plotted data indicate that the compression flange has buckled while the tension flange displays no evidence of local bending. Also, very little out of plane effect exists in the web data on the figure.

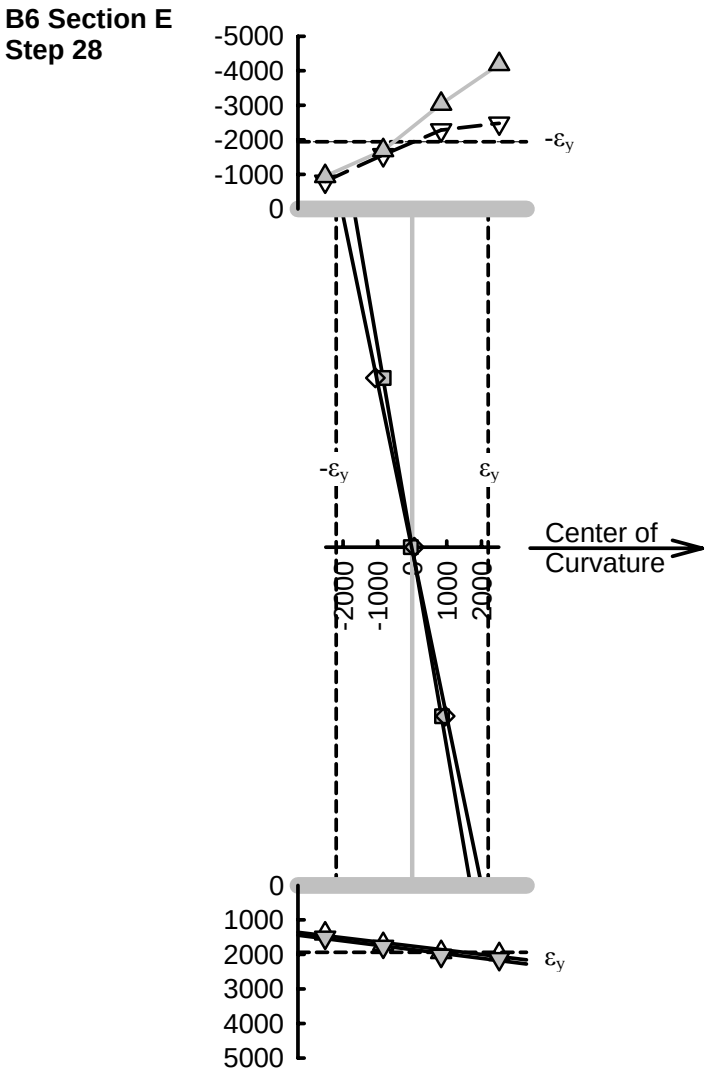

Figure 3-70: B6 Mid-Span Longitudinal Strain State During Step 28

Figure 3-71 shows the mid-span longitudinal strain state during the maximum sustained vertical bending moment in the component during the B6 test. The compression flange data indicate gross yielding and buckling across most of the plate. The top of the web has also picked up much of the buckling evident in the compression flange and has yielded along its outside face. The tension flange data again indicate yielding across most of the plate, but there is no evidence of local bending.

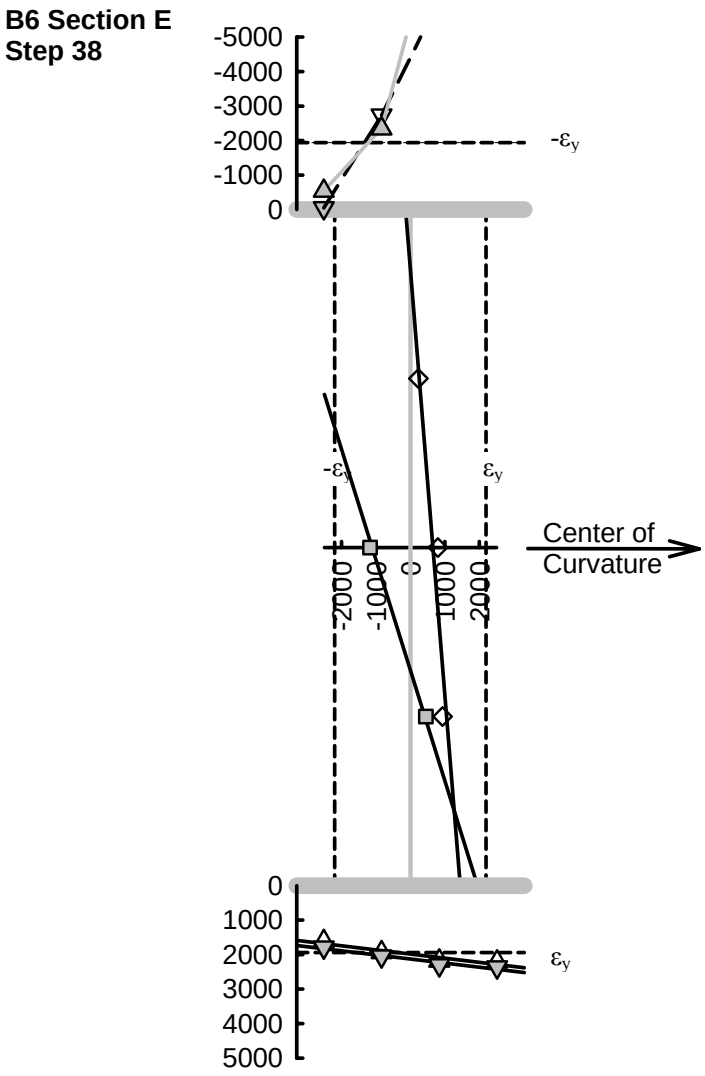

Figure 3-71: B6 Mid-Span Longitudinal Strain State During Step 38

Figure 3-72 illustrates the linear elastic state of the mid-span of G2 at its critical load of the B6 component test.

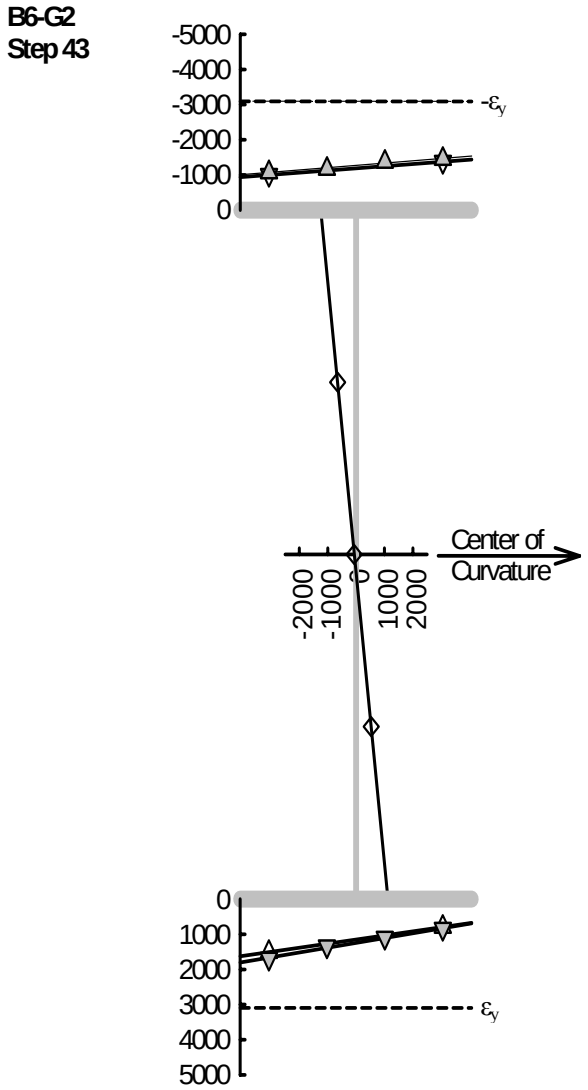

Figure 3-72: Most Critical G2 Mid-Span Longitudinal Strain State During B6 Test

3.10 Bending Component B7 Test

The maximum sustained vertical bending moment due to the applied loading at mid-span of B7 was 2,501 kN-m (1,844.5 k-ft). This moment occurred very early in this component test during step 13. First yield in the component was projected at load step 8. The test frame continued to take load until the test was halted at step 38 with a total applied load of 1,317 kN (296.1 kip). The resulting vertical bending moment in G2 was

4,635 kN-m (3,418.5 k-ft). Table 3-18 contains a selected set of data from this test.

Load Step	Total Applied Load	Mx (Total)	Mx (G1)	Mx (G2)	Mx (B7)		
					Indirect (a)	Direct (b)	(a)/(b)
	kN	kN-m	kN-m	kN-m	kN-m	kN-m	
B7 Elastic							
1	0.0	-0.7	0.2	0.0	-0.8	-0.1	7.34
2	55.1	254.6	13.9	78.3	162.4	126.3	1.29
3	139.2	609.0	33.6	209.6	365.7	316.0	1.16
4	275.2	1210.8	59.7	432.3	718.7	650.7	1.10
5	403.7	1779.3	81.8	678.5	1019.0	973.2	1.05
6	532.4	2359.3	98.0	930.8	1330.5	1280.2	1.04
7	672.1	2966.5	104.3	1240.2	1622.1	1596.4	1.02
8	808.5	3565.9	105.8	1540.4	1919.7	1908.7	1.01
B7 Plastic							
9	939.3	4143.0	109.0	1837.0	2197.0	2193.2	1.00
10	991.1	4370.7	107.1	1954.8	2308.8	2537.6	0.91
11	1041.8	4595.7	97.8	2078.2	2419.7		
12	1071.1	4724.6	95.3	2167.5	2461.8		
13	1095.5	4830.5	81.0	2248.4	2501.1		
14	1123.6	4956.3	42.1	2415.0	2499.2		
15	1109.2	4892.7	12.0	2416.8	2463.9		
16	1114.4	4912.2	-8.4	2510.0	2410.6		
17	1122.8	4950.9	-41.2	2588.3	2403.8		
18	1123.6	4956.4	-65.7	2617.5	2404.6		
19	1138.3	5020.3	-92.2	2734.0	2378.5		
20	1149.3	5070.9	-123.9	2829.5	2365.2		
21	1157.5	5105.9	-158.6	2930.5	2334.0		
22	1171.4	5169.8	-188.8	3031.4	2327.2		
23	1179.5	5206.6	-213.0	3067.5	2352.0		
24	1195.7	5277.5	-232.5	3194.9	2315.1		
25	1200.3	5298.8	-280.3	3293.3	2285.9		
26	1216.2	5371.3	-311.3	3408.8	2273.8		
27	1224.1	5406.5	-346.9	3522.2	2231.2		
28	1232.7	5446.2	-385.4	3606.4	2225.1		
29	1243.0	5492.4	-418.9	3733.4	2177.9		
30	1255.0	5548.1	-452.7	3812.2	2188.6		
31	1262.3	5581.6	-487.1	3926.2	2142.5		
32	1270.2	5614.6	-520.9	4010.3	2125.2		
33	1273.7	5630.5	-567.2	4134.6	2063.0		
34	1285.7	5685.9	-605.2	4228.2	2062.9		
35	1292.2	5713.9	-638.2	4325.7	2026.3		
36	1301.4	5755.8	-669.4	4444.7	1980.5		
37	1306.3	5777.4	-704.1	4540.9	1940.5		
38	1317.2	5828.0	-741.2	4635.5	1933.7		

Table 3-18: B7 Applied Load Steps and Resulting Girder Moments

Figure 3-73 contrasts the direct and indirect methods of determining the resisted vertical bending moment at mid-span of B6 during the elastic loading regime of this component test. The methods again show good agreement throughout the elastic range. At a total applied load of 808.5 kN (182.8 k), the point at which first yield is projected to have been reached in B7, the results of these analysis methods are less than one percent different.

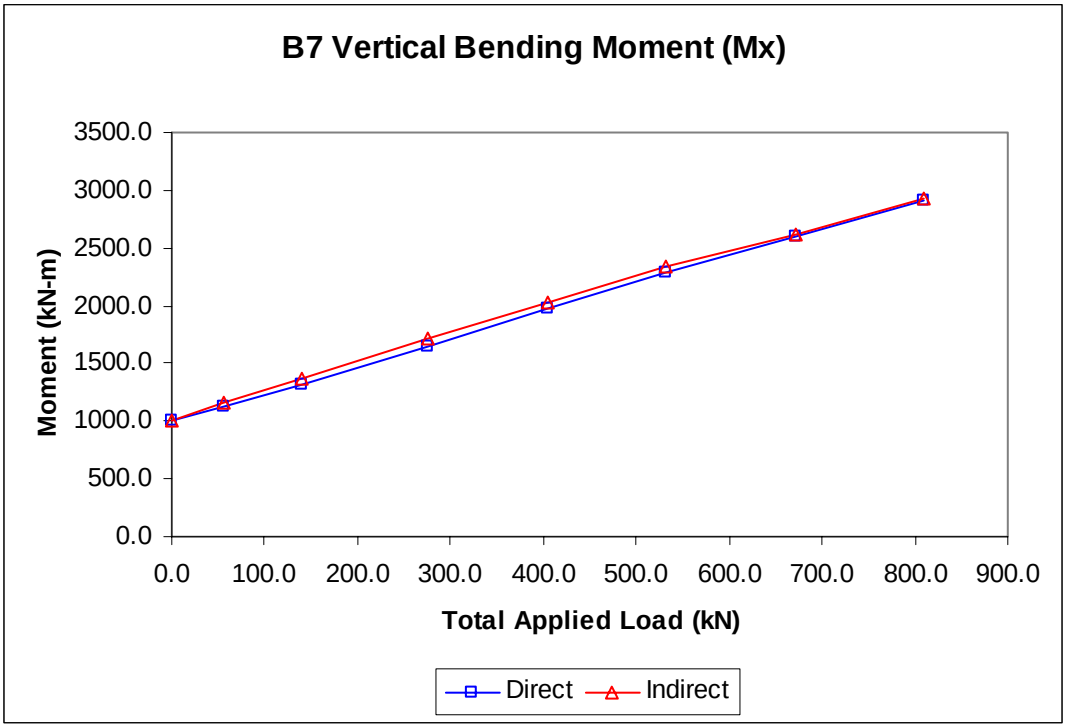

Figure 3-73: B7 Vertical Bending Moment

The mid-span vertical bending moments in G1, G2 and B7, which are due to the applied loading throughout the entire load regime of the B7 test, are plotted in Figure 3-74. The peak resisted vertical bending moment in B7 occurred very early in the test during load step 13. The section remained viable post-peak as the test frame continued to take load up until load step 38 when the test was halted. At this load level, 1,317 kN (296.1 kip), B7 was carrying significantly less of the applied moment than girder G2.

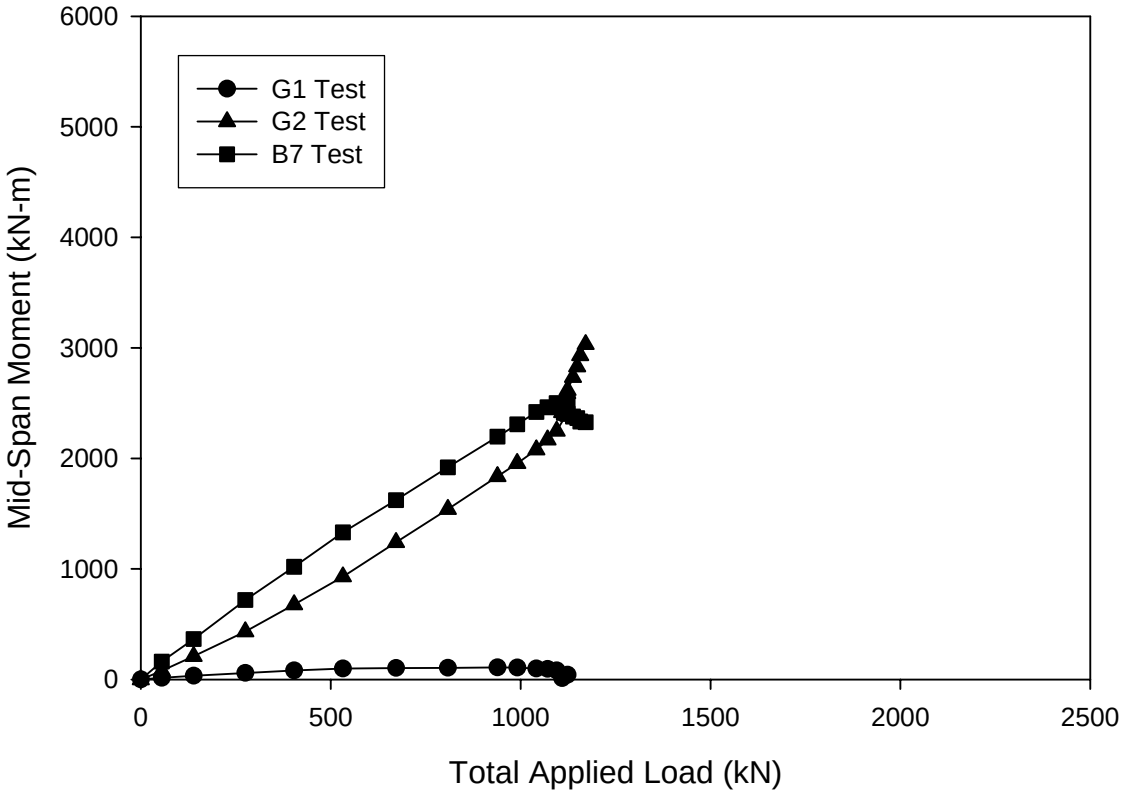

Figure 3-74: Test Frame Mid-Span Vertical Bending Moments, B7 Test

The mid-span B7 stresses and moments are presented in Table 3-19. At first yield in the component, the ratio of lateral flange bending stress to vertical bending stress was 0.68. The maximum elastic regime vertical bending moment carried by B7 was 2,922 kN-m (2,154.8 k-ft). A ratio of 0.61 resulted when the maximum elastic vertical bending moment was normalized by the vertical yield moment. At the maximum vertical bending moment sustained by B7, 3,503 kN-m (2,583.6 k-ft), this ratio increased to 0.73.

Load Case	Total Applied Load	Compression Flange, Inside Tip, Extreme Fiber Stress							Moments at Section					
		σ_z Total	σ_z from M_x (a)	σ_z from M_y	σ_z from M_z	σ_z from P_z	σ_z(lat.) (b)	(b)/(a)	M_x Direct	M_x Indirect (c)	M_y	Bi	$M_{lat.}$ Comp. Flange	(c)/M_x^{yield}
	kN	MPa	MPa	MPa	MPa	MPa	MPa		kN-m	kN-m	kN-m	kN-m^2	kN-m	
Elastic														
Install.		-74.84	-15.07	-40.71	-24.99	5.93	-65.71	4.36	190.4		53.1	40.2	-51.2	
DL		-90.04	-64.26	-4.34	-21.58	0.14	-25.92	0.40	811.8		5.7	34.7	-20.2	
Install.+DL		-164.88	-79.33	-45.06	-46.57	6.07	-91.63	1.16	1002.2		58.8	74.9	-71.4	
(1)	0.0	-164.98	-79.32	-45.08	-46.62	6.04	-91.70	1.16	1002.1	1001.4	58.8	75.0	-71.5	0.21
(2)	55.1	-179.39	-89.33	-46.26	-49.73	5.93	-95.99	1.07	1128.5	1164.6	60.4	80.0	-74.8	0.24
(3)	139.2	-201.17	-104.34	-48.23	-54.59	5.99	-102.83	0.99	1318.2	1367.9	63.0	87.9	-80.1	0.29
(4)	275.2	-240.62	-130.83	-51.61	-63.12	4.94	-114.72	0.88	1652.9	1720.9	67.4	101.6	-89.4	0.36
(5)	403.7	-277.82	-156.36	-54.29	-71.29	4.12	-125.58	0.80	1975.4	2021.2	70.9	114.7	-97.9	0.42
(6)	532.4	-312.13	-180.66	-56.04	-78.75	3.32	-134.79	0.75	2282.4	2332.7	73.1	126.7	-105.1	0.49
(7)	672.1	-350.94	-205.69	-60.05	-87.81	2.61	-147.86	0.72	2598.6	2624.3	78.4	141.3	-115.2	0.55
(8)	808.5	-385.98	-230.41	-62.49	-95.26	2.18	-157.75	0.68	2910.9	2921.9	81.6	153.3	-122.9	0.61
Plastic														
(9)	939.3	-413.32	-252.92	-62.89	-100.42	2.91	-163.30	0.65	3195.4	3199.2	82.1	161.6	-127.3	0.67
(10)	991.1	-531.03	-280.19	-105.04	-130.65	-15.15	-235.69	0.84	3539.9	3311.0	137.1	210.3	-183.7	0.69
.	.									.				.
.	.									.				.
(13)	1095.5									3503.3				0.73

Table 3-19: B7 Mid-Span Stresses and Moments

The longitudinal strain state at the mid-span of B7 resulting from the installation and dead load effects is shown in Figure 3-75. All data indicate a linear elastic response from the steel plates of the cross-section. The warping strain has pushed the outside tip of the compression flange into tension at this low load level.

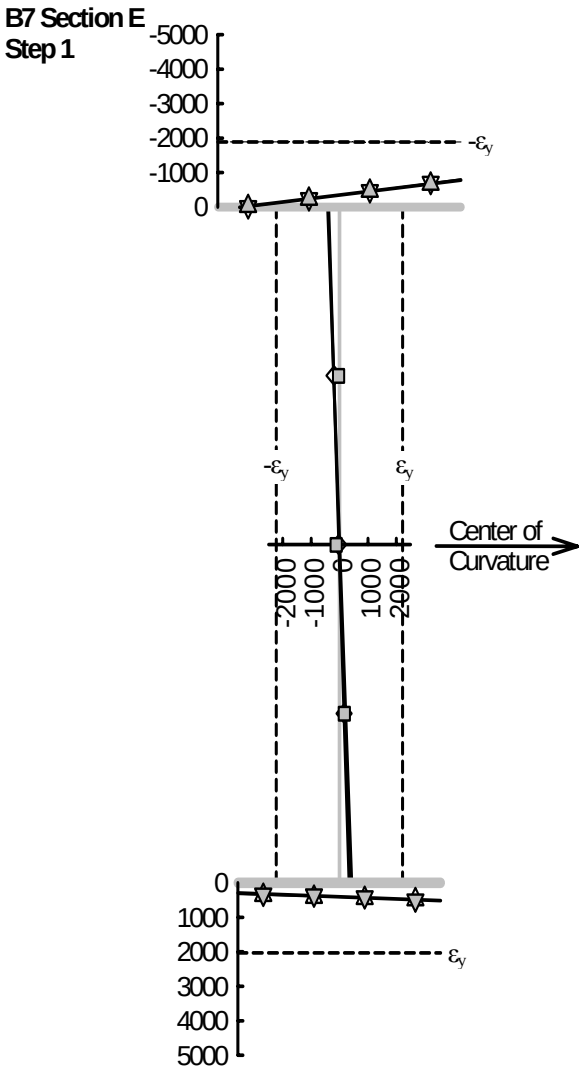

Figure 3-75: B7 Mid-Span Longitudinal Strain State Resulting From Installation and Dead Load (Step 1)

The projected first yield in the component occurs at mid-span during step 8, shown in Figure 3-76. At this load level, the compression depth of the web is already showing significant out-of-plane bending effects. The strain data for the inside tip of the

compression flange also contains evidence of local bending, which is illustrated by the separating regression lines.

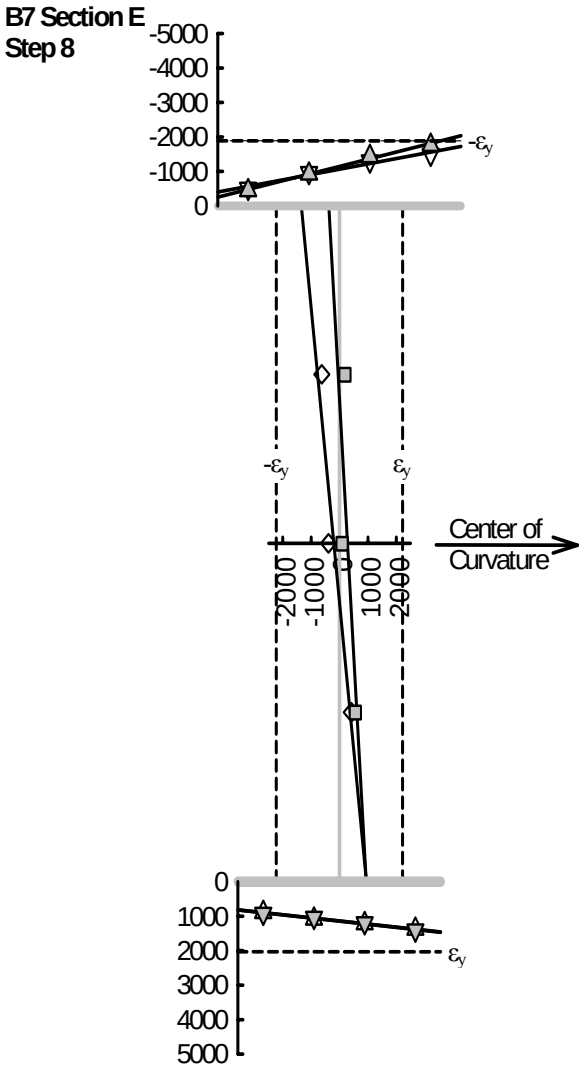

Figure 3-76: B7 Mid-Span Longitudinal Strain State During Step 8

Figures 3-77 and 3-78 support the assertion that first yield occurred at mid-span in the B7 component during step 8. The data in these figures do not include any effect for installation of B into the test frame. However, the strain levels plotted fall significantly from the indicated yield limits.

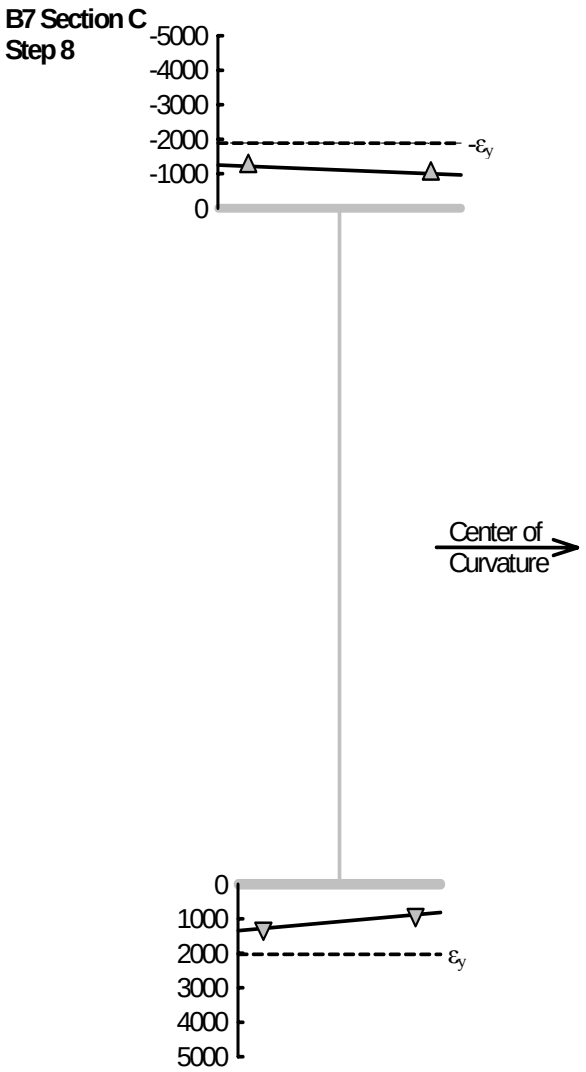

Figure 3-77: Longitudinal Strain State in B7 Near Cross-Frame N6L During Step 8 (Excluding Installation Effects)

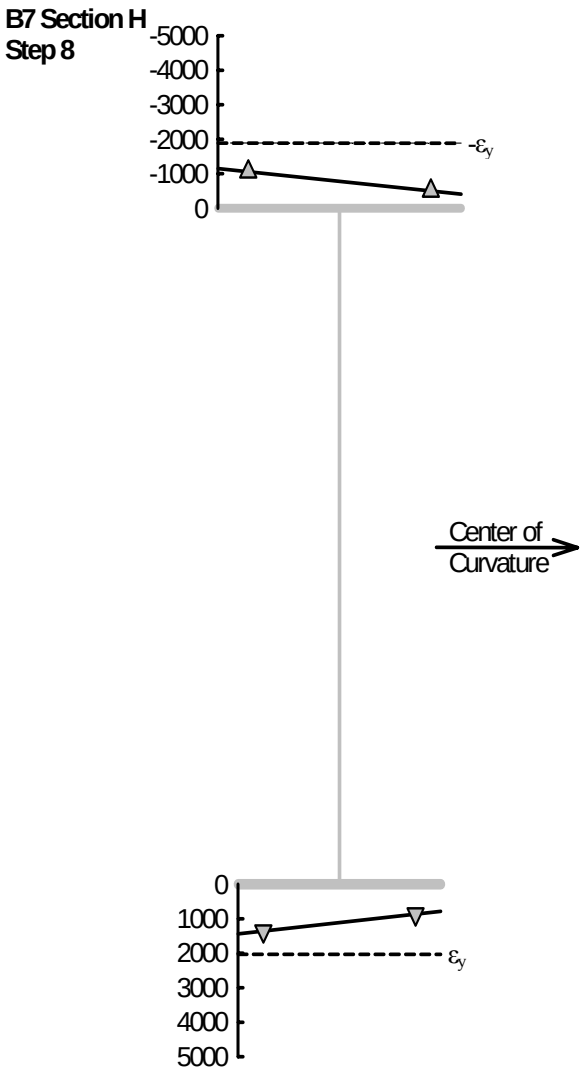

Figure 3-78: Longitudinal Strain State in B7 Near Cross-Frame N6R During Step 8 (Excluding Installation Effects)

The B7 mid-span longitudinal strain state at step 10 is shown in Figure 3-79. At this load step, the first evidence of local buckling appears in the compression flange data. The compression depth of the web data shows increased levels of local bending as the web tries to restrain the now buckled compression flange.

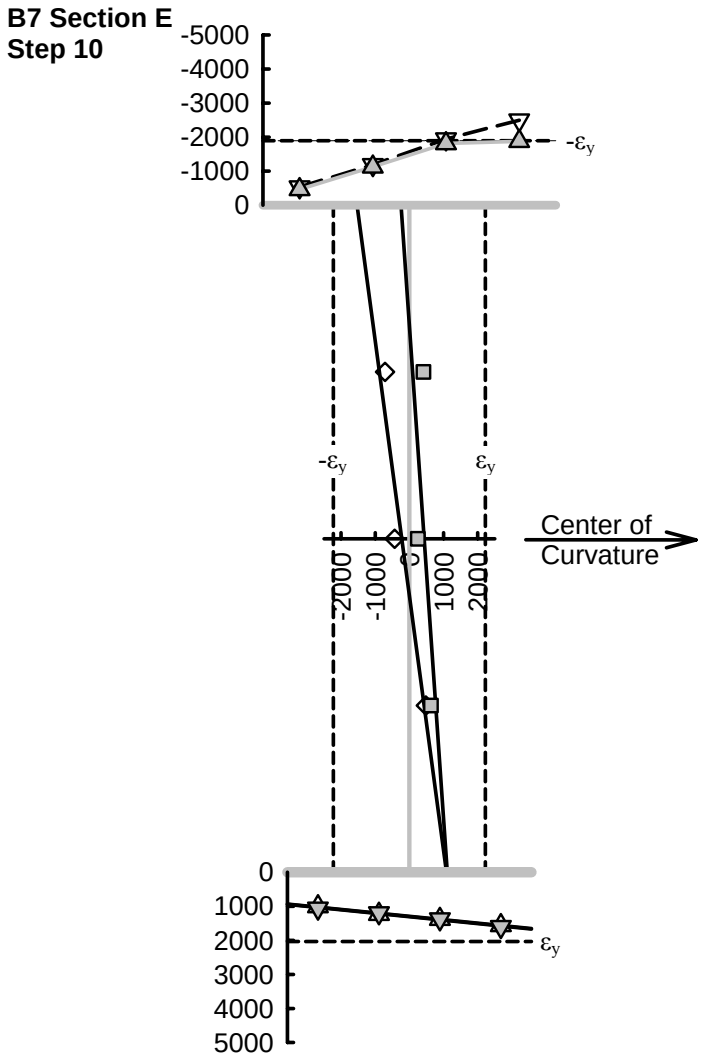

Figure 3-79: B7 Mid-Span Longitudinal Strain State During Step 10

The maximum sustained vertical bending moment by mid-span B7 occurred during load step 13. The longitudinal strain state at that cross-section during step 13 is shown in Figure 3-80. The strain data indicate that the inside half of the compression flange has surpassed its yield limit and is buckled. The web data contain evidence of local bending that could also be the result of buckling. Finally, the tension flange is still linearly elastic at this load step.

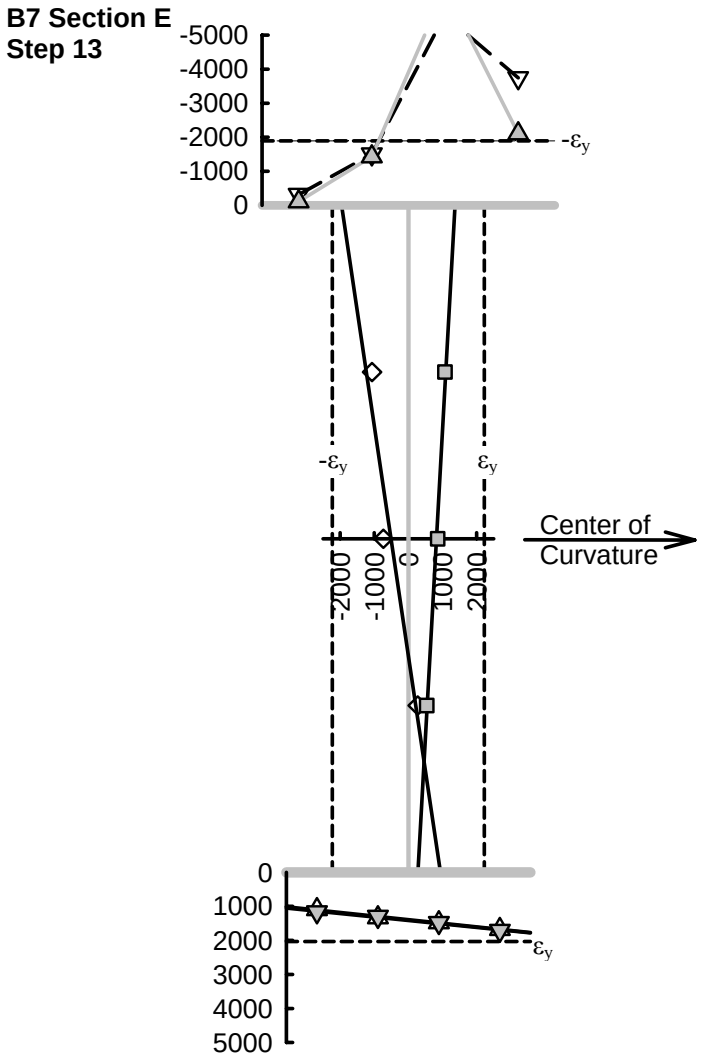

Figure 3-80: B7 Mid-Span Longitudinal Strain State During Step 13

While the maximum vertical bending moment sustained by B7 occurred at step 13, the test progressed through step 38 when the test frame was resisting a maximum applied load of 1,317 kN (296.1 kip). Figure 3-81 indicates that G2 remained linearly-elastic through step 38.

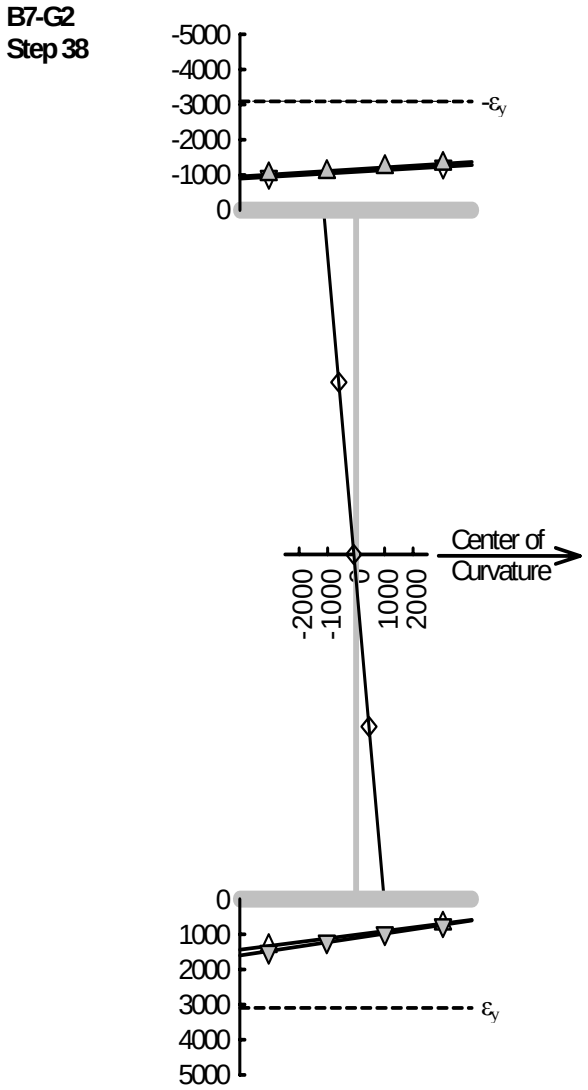

Figure 3-81: Most Critical G2 Mid-Span Longitudinal Strain State During B7 Test

3.11 Boundary Conditions

The test frame was loaded from above. The hydraulic actuators reacted off floating frames that were anchored to the laboratory floor using high-strength steel rods. This loading system is described in detail in Section 2.6.1. Radially aligned abutments at each end supported the test frame. Each end of the three girders that made up the test frame sat on a compound polytetrafluoroethylene (PTFE) sliding surface bearing.

The bearings that supported either end of G1 and G3 were free to rotate and slide in any direction. The bearings that supported both ends of G2 were free to rotate in any direction and were guided to slide in a direction along the tangent to the radius of curvature at the point of support. While approximately 6 mm (1/4 in.) of play existed in the guided direction, these bearing were essentially fixed radially.

An attempt to monitor horizontal loads transmitted through the bearings was made using two sets of instrumented studs. However, beyond providing evidence that supported the coefficient of friction, determined for the bearings with a proof load test, the data from the instrumented studs were inconclusive.

3.12 Effect of Installation Strains on Capacity

The effect of including the strains captured as a result of the installation process on the moment at first yield and the maximum resisted moment for each component can be seen in the data contained in Table 3-20. Recall that while the installation strains applied to B1, B2 and B3 were derived from the data acquired during the installation of B5 and B6, the regression line models used reasonably captured any uncorrupted data from those components. Also recall that the installation of B7 was accomplished relatively free of installation effects because the splice plates for the compression flange were drilled in place for this component.

Component	Total Applied Load kN	w/Installation Effects		w/o Installation Effects	
		Moment Resisted M kN-m	Normalized Moment M/M_x^{yield}	Moment Resisted M kN-m	Normalized Moment M/M_x^{yield}
At First Yield					
B1	825.5	3516.1	0.69	2979.3	0.58
B2	852.7	3536.2	0.67	2999.3	0.57
B3	852.7	3578.9	0.68	3042.1	0.58
B4	802.9	3696.6	0.68	3000.6	0.55
B5	917.2	3678.7	0.64	3166.8	0.55
B6	1354.4	4955.2	0.73	4393.4	0.65
B7	808.6	2921.9	0.61	2731.5	0.57
At Maximum Moment					
B1	1353.5	4539.2	0.90	4002.4	0.79
B2	1434.0	4729.6	0.90	4192.8	0.80
B3	1499.9	4834.4	0.92	4297.6	0.82
B4	1354.4	4879.7	0.90	4183.7	0.77
B5	1732.5	5278.1	0.92	4766.2	0.83
B6	2071.4	6399.5	0.94	5837.7	0.86
B7	1095.5	3503.4	0.73	3313.0	0.69

Table 3-20: Summary of Experimental Results

With the exception of B7, the data indicate that the effect of including installation strains on the capacity calculations were in effect uniform accounting for approximately 10% of the moment capacity at either first yield or ultimate strength. The reduced effect of installation on B7 was expected due to the manner in which this component was installed as noted above.

3.13 Effect of Compression Flange Slenderness

The effect of compression flange slenderness on the moment at first yield and the maximum moment resisted are illustrated in Figure 3-82 (also see Table 3-20). Both sets of data trend as expected with compression flange slenderness having a smaller effect on the moment at first yield than on maximum moment.

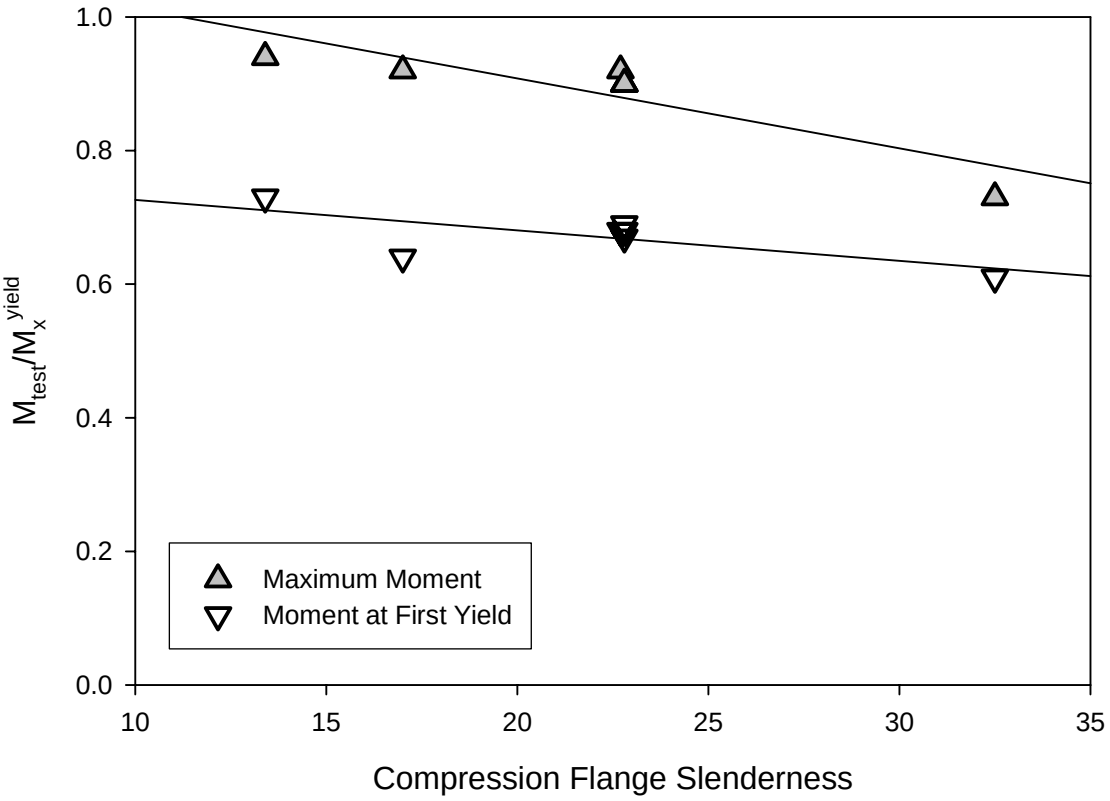

Figure 3-82: Effect of Compression Flange Slenderness

However, with the exception of B7, which has a very slender compression flange, the normalized maximum moments seemed relatively unaffected by compression flange slenderness. Results for all specimens excluding B7 fell within a 4% range (0.90 to 0.94). Also, with B7 removed from the data set, the trends shown in Figure 3-83 for both moment at first yield and ultimate moment are very similar. These similarities are most likely due to the fact that the failure mode in all cases was a lateral mechanism at mid-span of the component. This mechanism was initially made by a local flange buckle on the inside half of the compression flange and yielding on the outside half.

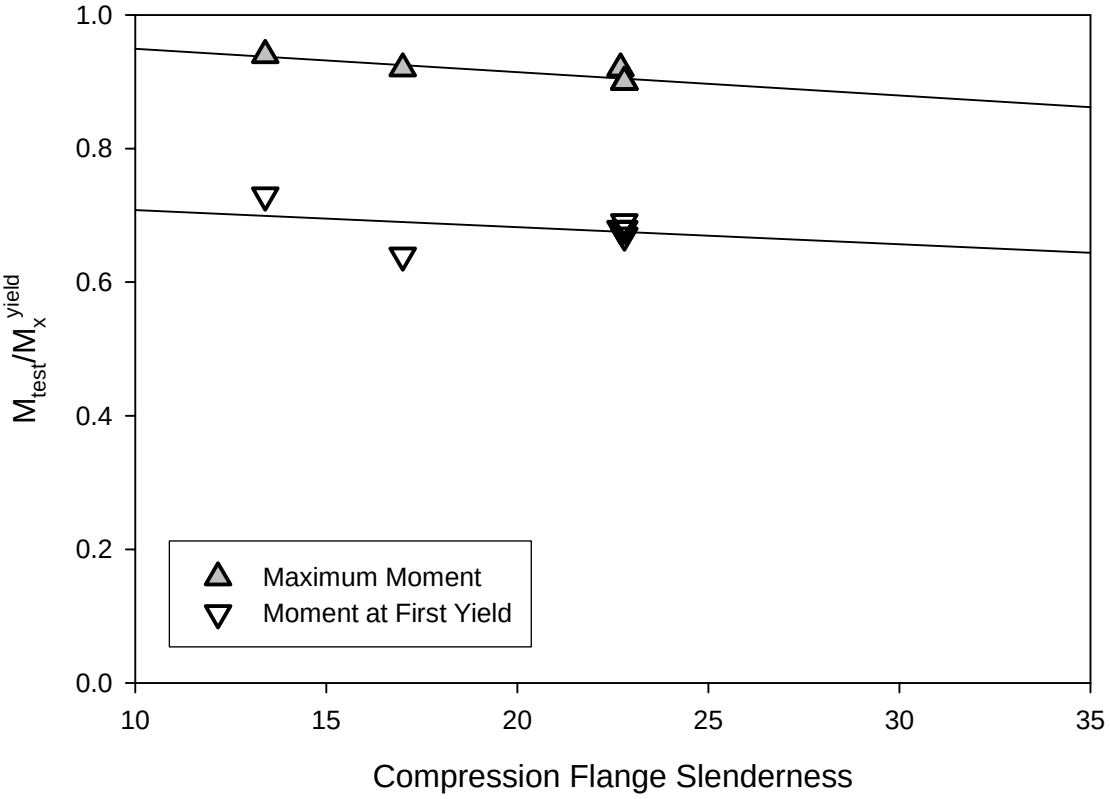

Figure 3-83: Effect of Compression Flange Slenderness (w/o B7)

While compression flange slenderness had little effect on either the moment at first yield or the maximum moment sustained, it did have an effect on the post-peak capacity of these sections. Components B5 and B6 had compact flanges and exhibited a post-peak capacity reduction of less than 0.5%. The remaining components, all with non-compact or slender compression flanges, exhibited post-peak capacity reductions of 3% to 10%. Also unlike the remaining components, B5 and B6 never exhibited a dramatic unloading prior to the ending of these tests.

3.14 Effect of Web Slenderness on Capacity

Web slenderness did not effect moment at first yield or ultimate moment for these sections. However, the slender web of B4 had significantly more buckling as evidenced by the strain measurements than did the non-compact webs of the remaining components.

3.15 Effect of Transverse Stiffener Spacing

The presence of transverse stiffeners had no effect on vertical bending capacity. The performance ratios of B2 and B3, components with a stiffened and unstiffened web of identical slenderness, were essentially the same for all conditions. However, the absence of stiffeners on B3 elevated the level of cross-sectional distortion in both the flange and web when compared to the behavior of B2 at similar load levels.

Chapter 4. Analytical Results

4.1 Finite Element Model

The finite element software — ABAQUS, Version 6.4 (ABAQUS, 2003) — was used to conduct the linear-elastic and fully non-linear (geometric and material) analytical studies that were conducted during this research. Girder flanges and webs were modeled using the general-purpose conventional shell element S4R. The cross frame members and the lateral bracing were modeled with B32 beam elements. Figure 4-1 shows a typical undeformed finite element model used in this investigation.

Mesh density was chosen based on the recommendation reported in White et al. (2001). Figure 4-2 shows the typical mesh densities used to model the individual members of these investigations. Bending component flanges were modeled with 10 elements across their width. Bending component webs were modeled with 20 elements along their depth. An element aspect ratio of approximately one was maintained along the length of the girder. In general, G1, G2 and G3 had coarser mesh densities. G1 and G2 utilized four elements across a flange and five elements along the depth of a web. G3 used six elements across a flange and 10 elements along the depth of the web. However, mesh densities were increased on all three girder models on elements local to the cross-frame connections.

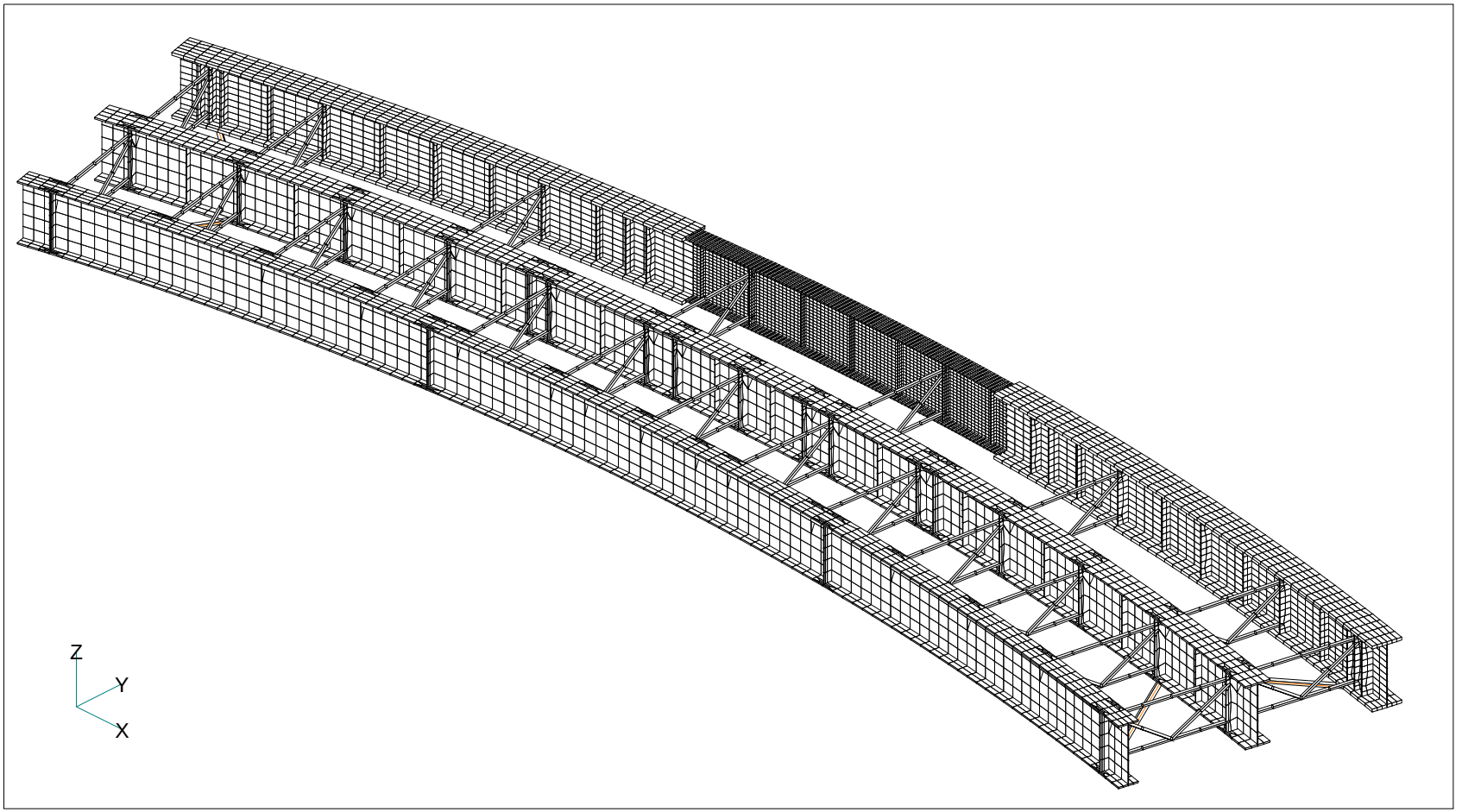

Figure 4-1: Typical Finite Element Model Used in this Study

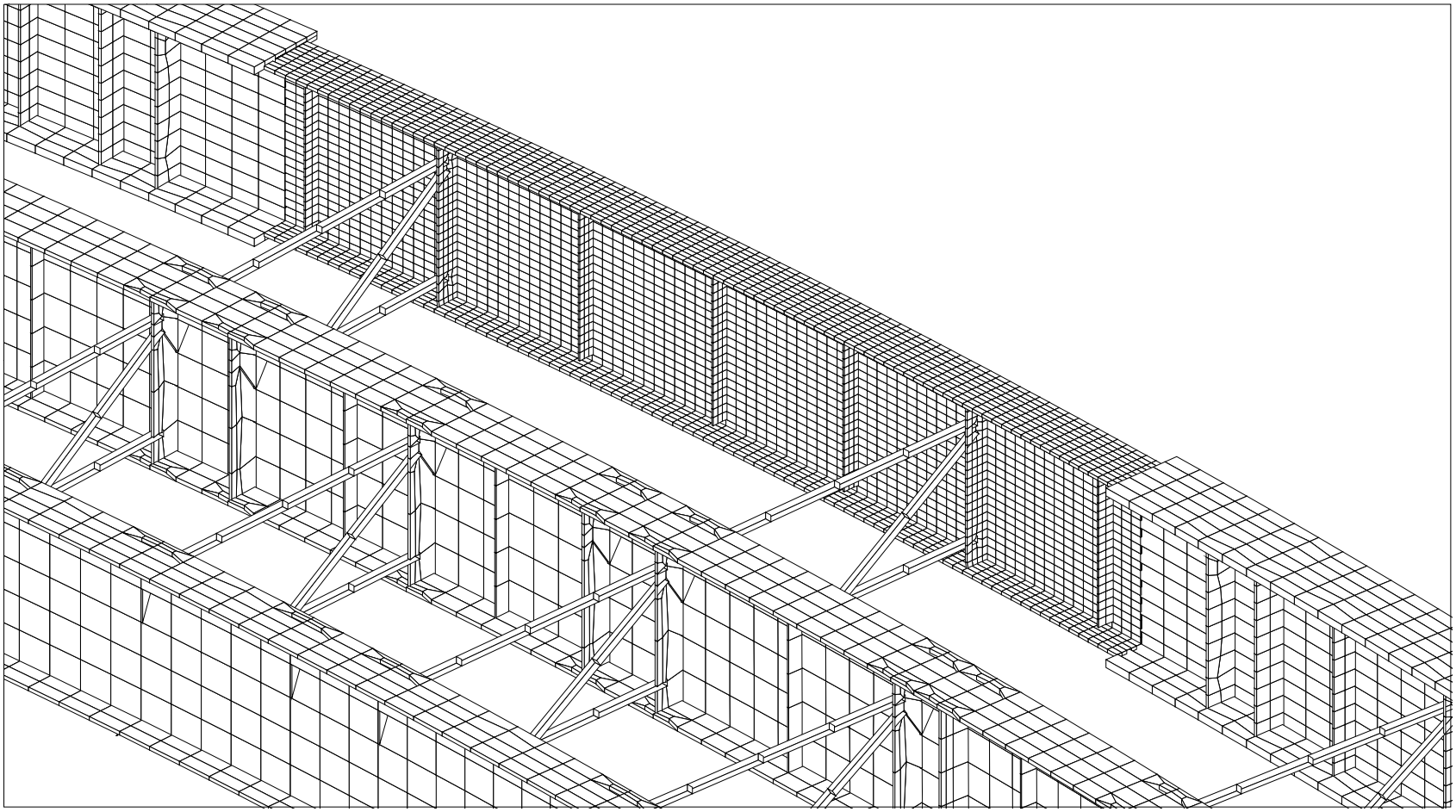

Figure 4-2: Typical Bending Component Finite Element Mesh Density

4.1.1 Stress-Strain Relationship

Engineering stress-strain relationships were constructed for each of the steel plates used in the fabrication of the bending components. After considering the property test data produced as a part of the CSBRP, a generic stress-strain relationship was developed that was easily tailored to represent the behavior of individual steel plates. An example of the generic seven part linear construction is shown in Figure 4-3. The following process is used to modify this construction to represent individual steel plate properties:

1. Average the static yield strength (σ_{sy}), the offset yield strength ($\sigma_{0.2\%}$), the strain at the onset of strain hardening (ε_{st}), the strain hardening modulus (E_{st}), the tensile strength (σ_u) and the strain at the tensile strength (ε_u) for all tension test results produced by specimens from a particular steel plate. Table 4-1 cross-references each bending component element to the steel plate from which it was cut. Table 4-2 contains a summary of the average material properties used to construct the stress-strain relationships used by the finite element models for the bending components.

Bending Component	Compression Flange Plate Number	Web Plate Number	Tension Flange Plate Number
B1	21	8	22
B2	21	9	22
B3	21	10	22
B4	21	11	25
B5	23	12	23
B6	24	13	24
B7	30	8	22

Table 4-1: Cross-reference of Steel Plate Number and Bending Component Element

Steel Plate Number	$\sigma_{0.2\%}$ MPa	σ_{sy} MPa	ε_{st} %	E_{st} GPa	ε_u %	σ_u MPa
8	460.1	445.4	1.978	3.110	16.38	592.2
9	405.5	393.6	1.941	3.195	16.11	530.3
10	407.8	396.3	2.171	3.149	16.87	540.6
11	457.8	445.2	2.182	2.901	16.51	584.6
12	455.6	439.6	2.089	3.050	15.17	585.6
13	454.8	439.7	2.044	2.995	16.72	584.6
21	425.1	408.5	1.472	4.170	15.88	582.6
22	417.4	406.9	1.711	3.775	16.18	575.2
23	405.2	395.0	1.632	4.111	16.11	570.4
24	401.1	388.1	1.704	3.695	16.68	558.5
25	404.4	390.5	1.753	3.984	16.60	564.7
30	390.2	378.3	1.291	3.422	12.36	530.5

Table 4-2: Average Steel Plate Properties for Selected Steel Plates

2. Use the averaged results, a Young's modulus (E) of 204 GPa (29,600 ksi) and the functional relationships in Table 4-3 to construct a specific engineering stress-strain curve for each steel plate.

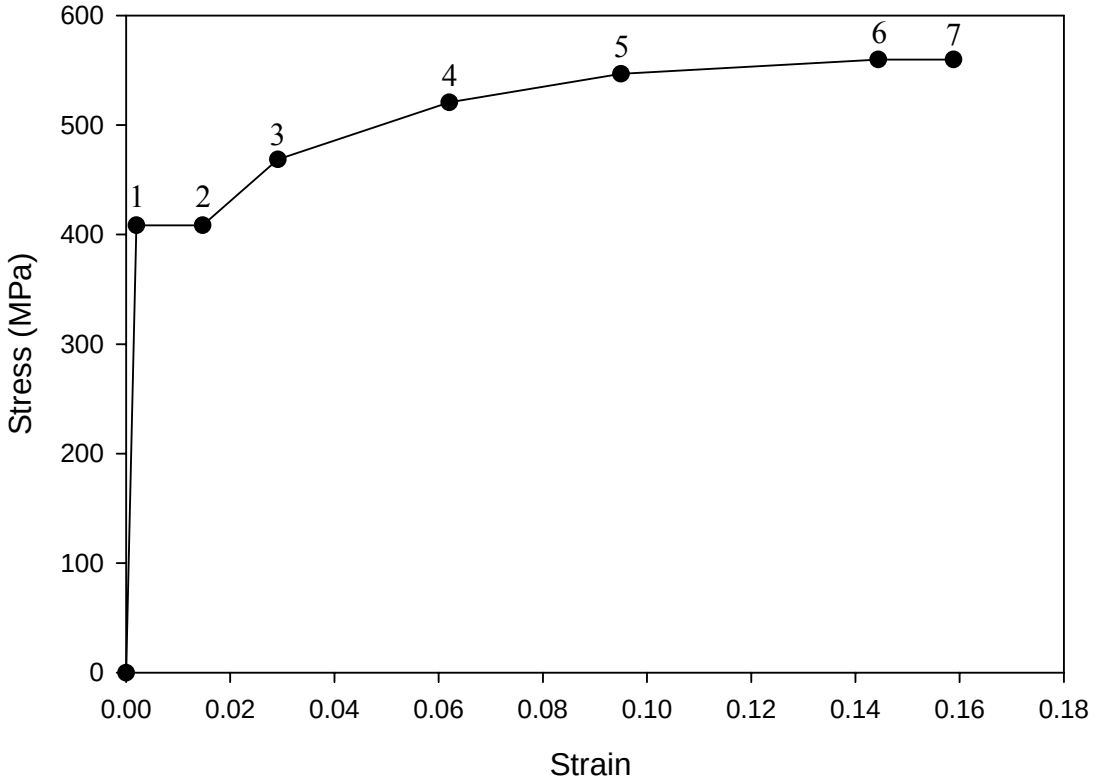

Figure 4-3: Typical Engineering Stress-Strain Relationship Used by FE Model

Point	Strain	Stress (MPa)
1	$\frac{\sigma_{sy}}{E}$	σ_{sy}
2	ε_{st}	σ_{sy}
3	$\frac{(\varepsilon_u - \varepsilon_{st})}{10} + \varepsilon_{st}$	$\frac{E_{st}(\varepsilon_u - \varepsilon_{st})}{10} + \sigma_{sy}$
4	$\frac{2(\varepsilon_6 - \varepsilon_3)}{7} + \varepsilon_3$	$\frac{4(\sigma_6 - \sigma_3)}{7} + \sigma_3$
5	$\frac{2(\varepsilon_6 - \varepsilon_3)}{7} + \varepsilon_4$	$\frac{2(\sigma_6 - \sigma_3)}{7} + \sigma_4$
6	$\varepsilon_u - \frac{(\varepsilon_u - \varepsilon_{st})}{10}$	$\left(\frac{\sigma_{sy}}{\sigma_{0.2\%}}\right)\sigma_u - \frac{100(\varepsilon_u - \varepsilon_{st})}{E_{st}}$
7	ε_u	$\left(\frac{\sigma_{sy}}{\sigma_{0.2\%}}\right)\sigma_u$

Table 4-1: Equations Used to Establish Typical Stress-Strain Relationships for the FE Model

The Young's modulus that was used to determine the yield strain for Point 1 of the curve, $\varepsilon_{eng,1}$, of the finite-element model's stress-strain relationship was 204 GPa (29,600 ksi). As reported in Appendix A, the Young's modulus tests that were preformed determined an average modulus of 204.7 GPa (29,700 ksi) for the steels used in these experiments. This result has an associated standard deviation of 0.6 GPa (87 ksi) which is very small. The Young's modulus for these steels was also determined during the tension and compression testing. These results are 201.5 GPa (29,200 ksi) and 204.5 GPa (29,700 ksi) respectively. The Young's modulus that was determined from tension and compression testing is slightly lower and has a much larger standard deviation than the modulus determined using the more accurate Young's modulus test. After all of these results were reviewed, a Young's modulus of 204 GPa (29,600 ksi) was chosen for use in all analytical efforts throughout this report.

The tension testing that was conducted as a part of this study was done in accordance with the ASTM E8 standard except that it was modified by the Structural Stability Research Council's (SSRC) Technical Memorandum No. 7 to produce static yield strengths. The SSRC procedure eliminates any effect that strain-rate may have on the demonstrated yield strength of the material. In general, strain-rate affected the yield strengths of the plate steels used in this study by elevating their values by approximately 2%. This result was determined by comparing the static yield strength values to the offset yield strength values for individual tests.

Analyses of the tension test data did not support the determination of any functional relationship between strain-rate and its effect on yield strength. Therefore, demonstrated tensile strengths, σ_u, were also scaled by the ratio of associated static to offset yield

strength in an attempt to eliminate the strain-rate effect from the stress-strain model. This adjustment is detailed in the calculation for the engineering strain at Point 7, $\varepsilon_{eng,7}$, in Table 4-1.

The relationships for Points 1, 2 and 7 on the engineering stress-strain model are taken directly from the summary record of the tension tests. Points 3 and 6 also utilize information from the summary record; however, the strain step that was indicated was selected to best capture the general shape of the family of A572 tension test records. The stress and strain relationships for Points 4 and 5 were also selected to best capture the general shape of the tension test records and to rely on coordinate calculations from elsewhere in the model.

The engineering stress-strain curves were converted to true stress-stain curves for use by the finite element program using the following relationships that are derived in Appendix A:

$$\varepsilon_{true} = \ln(1 + \varepsilon_{eng}) \qquad \text{Equation 4-1}$$

$$\sigma_{true} = \sigma_{eng}(1 + \varepsilon_{eng}) \qquad \text{Equation 4-2}$$

A comparison between an engineering stress-strain model and its true stress-strain conversion is shown in Figure 4-4.

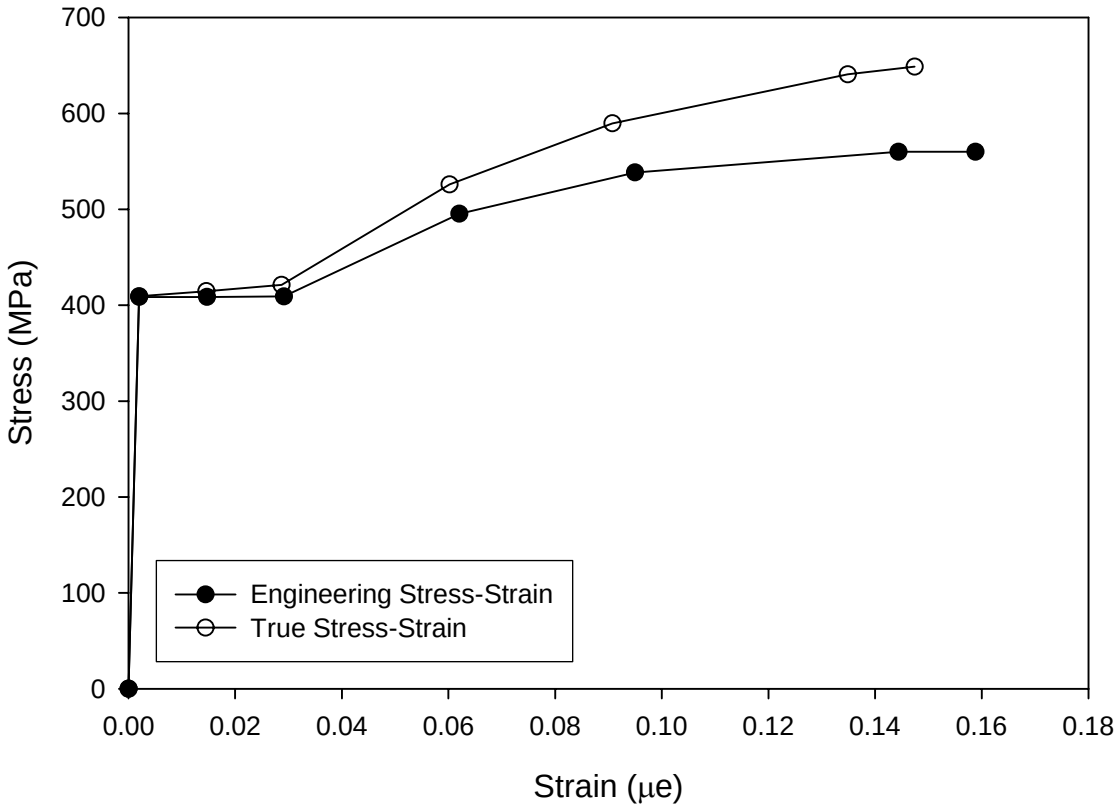

Figure 4-4: Engineering Versus True Stress-Strain

Figure 4-5 shows the family of tension and compression test results for material testing that were performed on samples taken from Plate 21 (see Appendix A for a description of this plate) in addition to the constructed material model. These results are shown on a field of engineering stress and strain. The test results differ slightly, with lower strengths displayed by the tension test results and higher strengths by the compression test results, due to the specimen necking or barreling that is inherent to each respective test method.

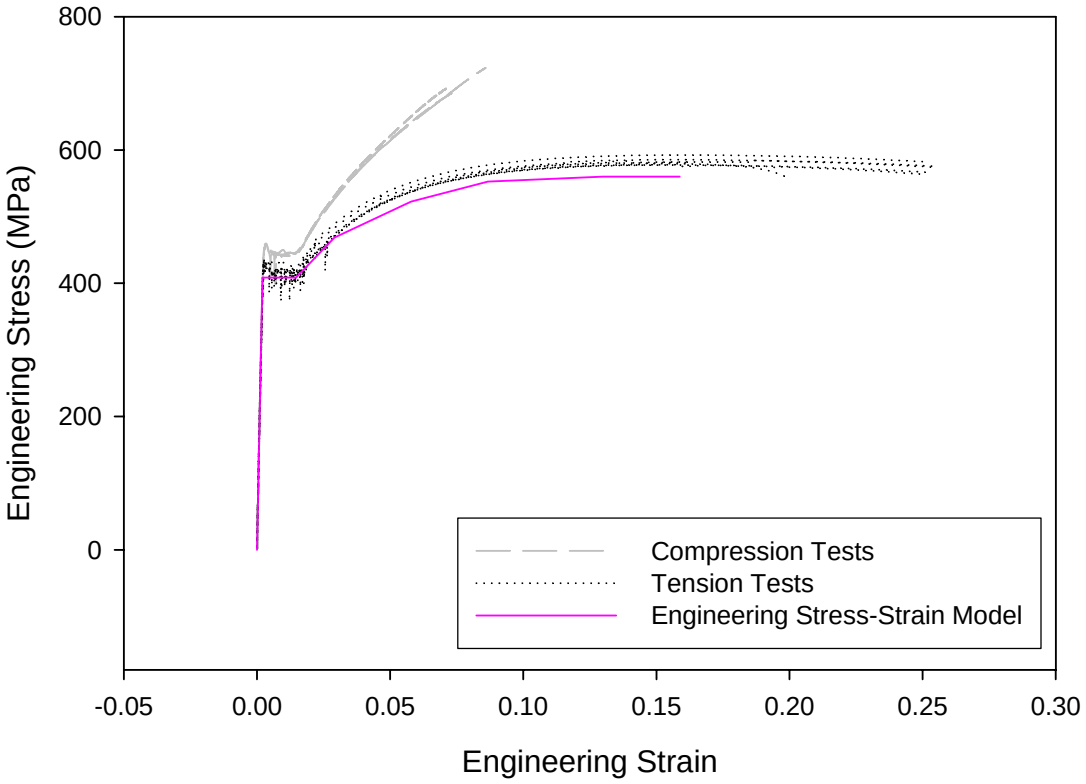

Figure 4-5: Plate 21 Compression and Tension Test Results Compared with the FE Material Model in Engineering Stress-Strain

However, when the tension and compression test results are converted from engineering stress-strain to true stress-strain the differences in behavior become insignificant. Figure 4-6 shows the same family of Plate 21 results after conversion to true stress-strain. Once converted, the tension and compression test results essentially overlay each other, as shown in Figure 4-6. This figure supports the widely accepted material behavior model for steel with respect to tensile and compressive stress. Therefore, with the agreement between tension and compression test results established, a separate material model is not needed to account for the stress-strain behavior of these

steels in the compression domain. All material properties used in any associated analytical efforts will be drawn from the tension test results.

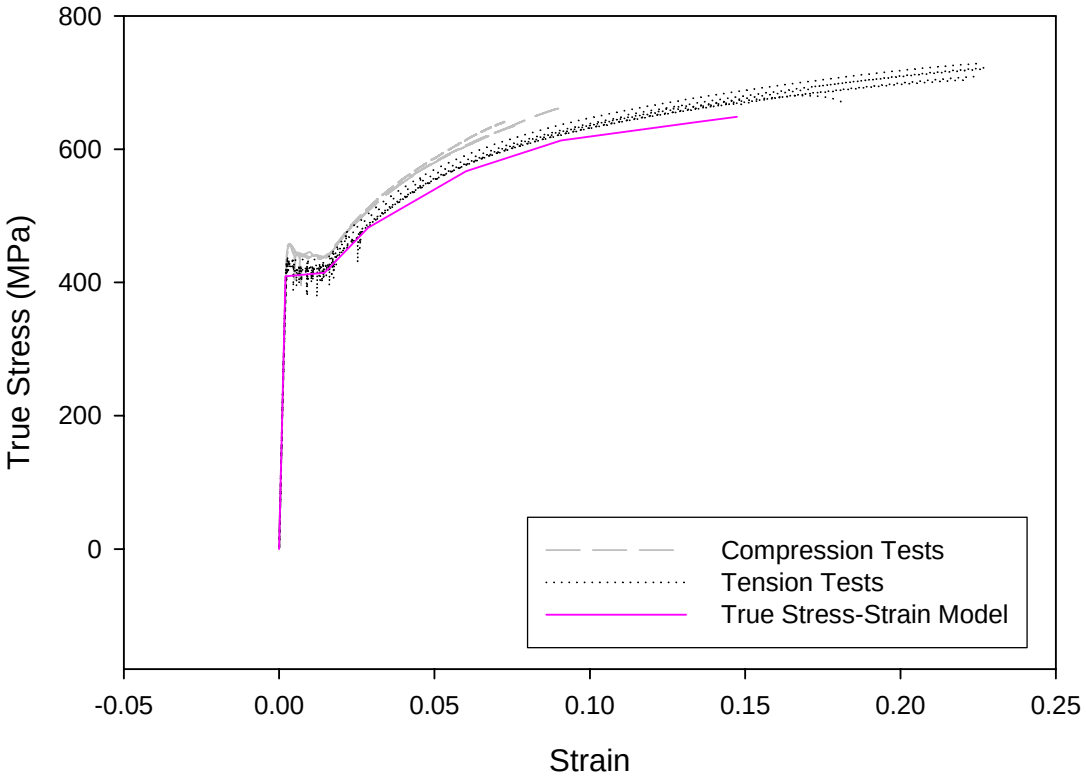

Figure 4-6: Plate 21 Compression and Tension Test Results Compared with the FE Material Model in True Stress-Strain

4.1.2 As-Built Geometry

Prior to testing, the flanges and web of each bending component were measured at regular intervals for width or depth, and thickness. Six sets of measurements were taken along each component between cross-frame locations 6L and 6R. The numbers reported in Table 4-2 are the averages for the center four sets of those measurements. A decision was made to use these measurements for the analytical model because this middle section was the location of failure in all of the experiments.

Bending Component	Compression Flange		Web		Tension Flange	
	b_f (mm)	t_f (mm)	D (mm)	t_w (mm)	b_f (mm)	t_f (mm)
B1	443.7	19.5	1210.7	8.2	444.5	19.4
B2	442.9	19.4	1211.9	10.1	442.9	19.4
B3	442.9	19.5	1213.4	10.2	444.5	19.4
B4	442.9	19.4	1212.4	8.1	533.4	32.4
B5	419.1	24.7	1215.2	8.5	419.9	24.6
B6	414.4	30.9	1213.6	8.6	413.9	31.0
B7	533.4	16.4	1215.2	8.4	444.5	19.2

Table 4-2: Bending Specimen As-Built Plate Dimensions

The thickness measurements were made with an ultrasonic device. The device employed had a 12.7mm (½ in.) diameter transducer. Three individual thickness measurements were taken at each measurement location. During each successive measurement, the transducer partially covered the area used in the previous measurement. The device had an integrated platen that was regularly used to recheck the calibration.

The width and depth measurements were made using a steel tape that was scaled in U.S. Customary units.

All pieces of the test frame had their dimensions measured and recorded in the same manner that was used for the bending components. These measurements have been summarized by Linzell (1999).

4.1.3 Installation Strains

The installation strains that were recorded during the erection of each bending component and that were used in the analysis of the experimental data (discussed in Chapter 3) were not utilized to refine the predictions of the analytical model. Although these strains do exist and were captured for the mid-span section of each component, not

enough information was obtained to determine their distribution along the length of each component to appropriately model their effects.

4.1.4 Modeling of Residual Stresses

The fabrication process to construct I-girders from steel plates requires both flame cutting and welding. In the areas adjacent to the application of these processes, sufficient thermal stresses are created to plastically deform the steel plate. The steel is affected by the heat, and as it cools its elastic recovery is constrained by cooler portions of the plate. The elastic recovery and constraint compete until an equilibrium of internal stress is achieved. This remaining internal stress profile is referred to as residual stress because it is a consequence of either the cutting or welding process.

Several researchers have attempted to measure residual stresses. The sectioning method, which is employed most often, requires careful monitoring of changes in the strain profile throughout a cross-section of a plate as a portion or section of that plate is removed. These studies along with many analytical efforts have resulted in the publication of several residual stress models for I-girders fabricated from steel plates. For this investigation, residual stress predictions are made using the recommendations of the European Convention for Constructional Steelwork (ECCS, 1976).

The ECCS method includes residual stress models for flanges and webs that were subjected to both flame cutting and welding. Each plate modeled is divided into zones of tension and compression. The heat affected zones from flame cutting or welding are modeled as small regions of uniform high tensile stress. The remainder of the plate is considered to be at a constant compressive stress level of necessary scale to equilibrate the aggregate tensile stresses.

The ECCS procedure specifies the equivalent rectangular tension block width, c_f, adjacent to a flame cut plate edge as:

$$c_f = \frac{1100\sqrt{t}}{F_y} \qquad \text{Equation 4-3}$$

where:

t = plate thickness (mm)

F_y = plate yield strength (MPa)

For single pass welds, the ECCS procedure specifies an equivalent rectangular tension block width, c_w, for each plate joined at that weld of:

$$c_w = \frac{12000\,p(A_w)}{F_y(\sum t)} \qquad \text{Equation 4-4}$$

where:

p = efficiency factor (0.9 for the submerged arc welding process)

A_w = cross-sectional area of weld metal (mm^2)

F_y = plate yield strength (MPa)

Σt = sum of plate thicknesses meeting at the weld (mm)

The web-to-flange fillet welds were placed simultaneously at the top and bottom of one side of the web during the fabrication of the bending components. This method of fabrication resulted in the web-to-flange fillet welds being placed on opposite faces of the web at different times. In the flange plate, both of the consecutive welds both slightly lowered the residual tensile stresses caused at each flange tip by the flame cutting process. Also, this two–step welding procedure lowered the level of residual stress at the weld location because the heat input from the second weld relieved the tensile stresses

created by the first weld. According to the ECCS method, the resulting equivalent stress block for the two welds placed consecutively and spaced *d* mm apart is given by:

$$c_2 = c + 0.5d \qquad \text{Equation 4-5}$$

where:

c = equivalent tension block width of a single pass or weld (mm)

$d \leq 2c$

In the web plate, the residual stresses of the flame cut edge are partially relieved by both the first and second welds. In addition, the residual stresses from the first weld are partially relieved by the heat input of the second weld. To account for this combination of effects, the ECCS method suggests that the combined tension block width created by welding and flame cutting, c_{fw}, is approximated by the following relationship:

$$c_{fw}^4 = c_f^4 + c_w^4 \qquad \text{Equation 4-6}$$

where:

c_f = equivalent tension block width created by flame cutting (mm)

c_w = equivalent tension block width due to welding (mm)

The ECCS method also includes a predictor for the final tension block width produced by multi-pass welds or superimposed welds of equal size.

$$c_n = cn^{1/4} \qquad \text{Equation 4-7}$$

where:

c = equivalent tension block width of a single pass or weld (mm)

n = number of weld passes or superimposed welds of equal size

The residual stress profiles that resulted from flame cutting and welding were determined for each flange and web of the bending components using equations 4-3

through 4-6. The equivalent widths of the rectangular tension block do not match the element size of the finite element model. Therefore, net element stresses were also determined to apply to each of the 10 elements across the width of a flange and to each of the 20 elements along the depth of a web. The results of these calculations for each compression flange, web and tension flange of the bending components are compiled in Tables 4-3 through 4-5.

Component	Tension at Each Flange Tip			Tension at Welds			Compression
	Resultant	Width	Net per Element	Resultant	Width	Net per Element	
	(MPa)	(mm)	(MPa)	(MPa)	(mm)	(MPa)	(MPa)
B1	374.2	11.9	56.7	408.5	34.4	121.7	-59.5
B2	363.9	11.9	56.7	408.5	33.4	119.3	-57.8
B3	364	11.9	56.8	408.5	33.4	119	-57.7
B4	362.7	11.9	55.5	408.5	34.5	124.3	-59
B5	350.6	13.8	76.9	395	30.9	106.4	-60.1
B6	346.1	15.8	96.1	388.1	26.7	85.8	-59.6
B7	338.5	11.8	37.2	378.3	40.7	114.4	-49.8

Table 4-3: Compression Flange Plate Residual Stresses

Component	Tension at Top of Web			Tension at Bottom of Web			Compression
	Resultant	Width	Net per Element	Resultant	Width	Net per Element	
	(MPa)	(mm)	(MPa)	(MPa)	(mm)	(MPa)	(MPa)
B1	445.4	31.9	221.3	445.4	31.9	221.3	-24.8
B2	393.6	34.5	212.4	393.6	34.5	212.4	-23.8
B3	396.3	34.2	211.9	396.3	34.3	212.6	-23.7
B4	445.2	32	223.6	445.2	23	154.8	-21.2
B5	439.6	27.7	188.2	439.6	27.8	189	-21.1
B6	439.7	24	162.1	439.7	23.9	161.4	-18.1
B7	445.4	35.2	246.2	445.4	32.1	222.2	-26.1

Table 4-4: Web Plate Residual Stresses

Component	Tension at Each Flange Tip			Tension at Welds			Compression
	Resultant	Width	Net per Element	Resultant	Width	Net per Element	
	(MPa)	(mm)	(MPa)	(MPa)	(mm)	(MPa)	(MPa)
B1	397.5	11.2	56	431.9	32.8	121.9	-59.3
B2	398.4	11.2	57.3	431.9	31.9	118	-58.5
B3	398.5	11.2	57.2	431.9	31.9	117.5	-58.2
B4	370.7	16	79.2	390.5	25.7	59.1	-46.1
B5	364.1	13.8	78.8	395	30.5	104.4	-61
B6	361.5	15.8	100.1	388.1	26.6	83	-61.1
B7	397.3	11.1	55.1	431.9	33	123	-59.4

Table 4-5: Tension Flange Plate Residual Stresses

Typical residual stress profiles for a flange and web are shown in Figures 4-5 and 4-6. These figures illustrate profiles that represent both the resultant residual stresses determined using the ECCS method for flame cutting and welding and the net residual stresses determined to apply to individual elements that make up each flange or web of the analytical model.

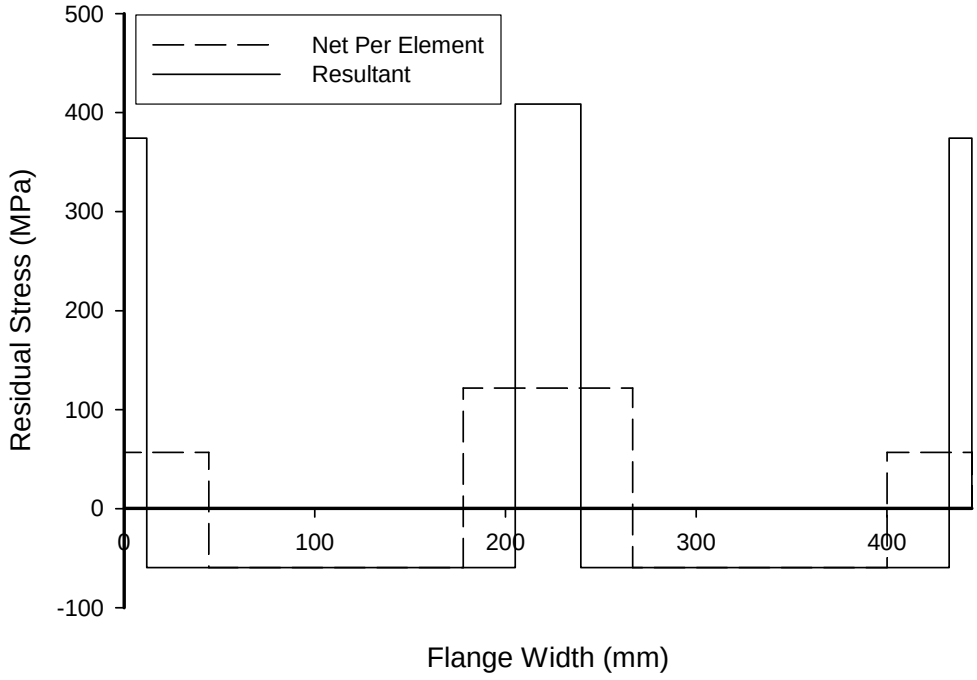

Figure 4-7: Example Flange Plate Residual Stress Profile

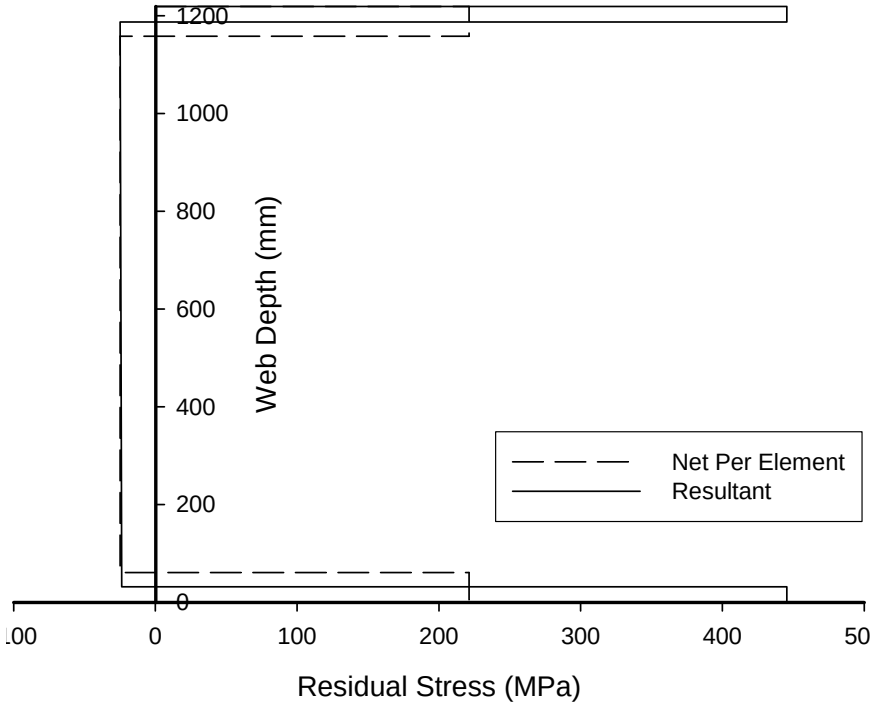

Figure 4-8: Example Web Plate Residual Stress Profile

4.1.5 Modeling of Boundary Conditions

Reactions were modeled using a gap element that prevented vertical deflection but allowed lift-off. These elements incorporate a frictional resistance to horizontal translation that was set at the experimentally determined frictional coefficient for the actual bearings. Reactions under G1 and G3 were free to translate in any horizontal direction while the G2 reactions allowed only tangential translation as they were fixed radially. All reactions allowed rotation about the point of support.

The loads were applied to the top flange of all three girders as a point load at the appropriate node. Early results were scrutinized to insure that this method of applying load did not cause any local instability.

A tangential support frame was attached to the west end of the experimental test frame as a safety precaution. This frame was mounted to the floor of the structural laboratory and was attached to the test frame with a large cotter pin. The pin passed through one side of a double gusset plate that was attached to the tangential support frame, then through an oversized slot in the G2 web and finally through the other side of the tangential support frame's double gusset. This structure was intended to prevent the test frame from a global translation off of the bearings. This structure was not modeled in the finite element analyses since the strain readings recorded during each test indicated that it was never engaged.

4.1.6 Predictions

A diligent effort was made to account for the variation in thickness and width of the steel plates used in the fabrication of the test frame and bending components. However, with the exception of B7, the finite element models predicted less component mid-span

moment due to self-weight than what was measured during the tests. These results are not uncommon, especially on a large structure in which the weight of weld metal, bolts, nuts, washers, instrumentation etc. cannot be dismissed as insignificant. Also, the gusset plates, connections and stiffening on each of the cross-frames are not adequately incorporated in the finite element models for the software to predict a representative weight. Regardless, the self-weight moment predictions were within 5% of the measured values for all components except for B1 and B2.

The prediction for B1 dramatically departed from the measured value by a reduction of 17%. A review of the experimental test log and other test documentation, as well as a careful review of the finite element model provide no explanations as to why this difference is so great. However, this difference did not adversely affect the flexural capacity analysis for B1 that is presented in Section 4.1.6.1.

The predicted self-weight moment for B2 was 7% less than that deduced from the measured strains. This difference is acceptable and had no effect on the flexural capacity analysis of this component (similar to B1).

The predicted self-weight moment for B7 was greater than that generated from the strain measurements by 5%. This difference is not alarming, and is only of interest because it is an over prediction that is contrary to the displayed and expected trend. It is however an indication that all force-actions were not properly accounted for prior to the applied loading portion of this test.

Also, with B6 as the only exception, the finite element models predicted a greater maximum applied load than what was measured during the experiments. This additional applied load accounted for the differences in self-weight and installation effects between

the predictions and the experimental data in most of the analyses. That is, the finite element model predicted vertical moment capacities considered the influences of residual stress but were primarily the result of self-weight and applied load. The experimental data contains measurements of strain associated with self-weight, installation and applied load. Regardless of what combination of loads caused the maximum mid-span moment, the measured and predicted flexural resistance of the bending components were virtually the same for all bending components with the exception of B7.

4.1.6.1 B1 Finite Element Model Results

The finite element model of the B1 component test predicted a maximum sustainable applied load of 1532.3 kN. This load equated to a mid-span moment of 3726.3 kN-m. When combined with the self-weight effects the predicted maximum mid-span moment resisted by B1 was 4573.9 kN-m which is comparable to the measured maximum mid-span resisted moment of 4539.2 kN-m. These results are summarized in Table 4-6.

B1		Test (a)	FE (b)	Ratio (b)/(a)
Max. Applied Load	(kN)	1353.5	1532.3	1.13
Mid-Span Moment				
Self-Weight	(kN-m)	1022.2	847.6	0.83
Installation	(kN-m)	536.8		
Max. Applied Load	(kN-m)	2980.2	3726.3	1.25
Flexural Resistance	(kN-m)	4539.2	4573.9	1.01

Table 4-6: B1 Test and Finite Element Model Results

Figure 4-9 shows the effect of the applied loads on the G1, G2 and B1 mid-span moments from both the experimental test and the finite element model. The predictions match the physical results very well indicating that the load is being distributed as expected within the load frame.

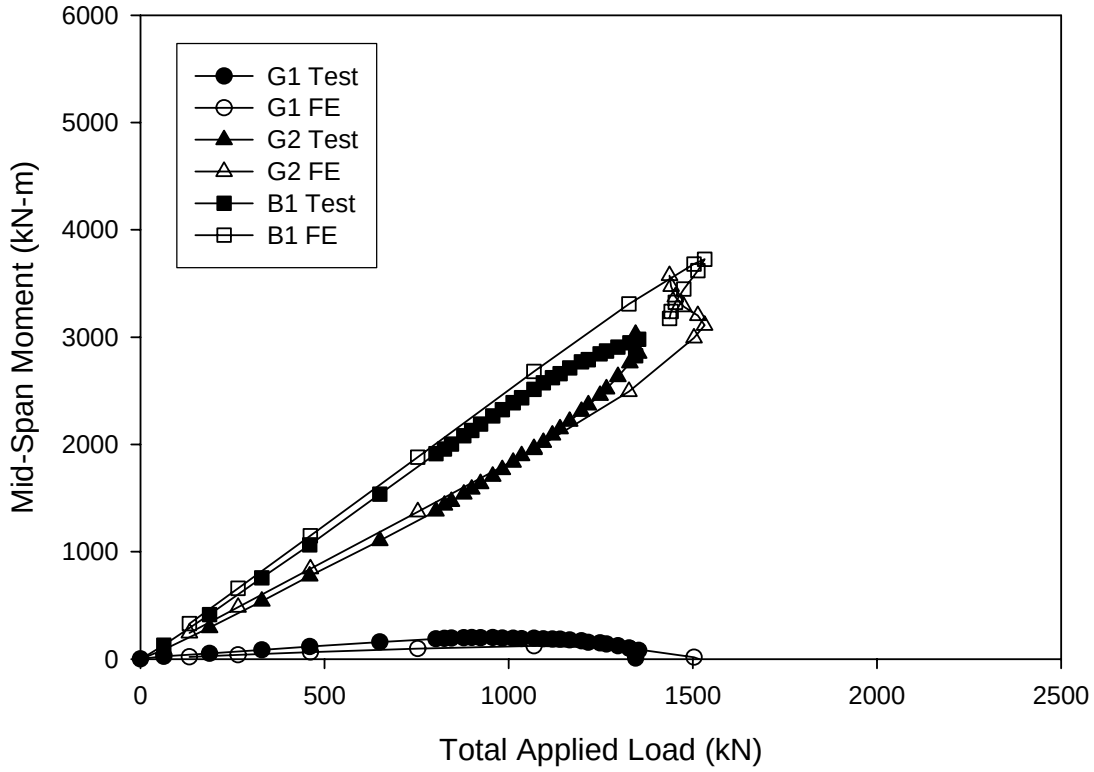

Figure 4-9: B1 Test Mid-Span Moments and Finite Element Predictions

Figure 4-10 shows the B1 mid-span moment from the applied loads normalized with respect to the strong-axis yield moment, M_x^{yield}, as a function of deflection for both the finite element model and the experimental data. The test results fall short of the predicted capacity and contain some pre-peak non-linearity. However, the shapes of the curves are very similar. The exhibited and predicted flexural resistance capacities are within 1% once the differences in self-weight and the effects of the recorded installation strains are added to the test results.

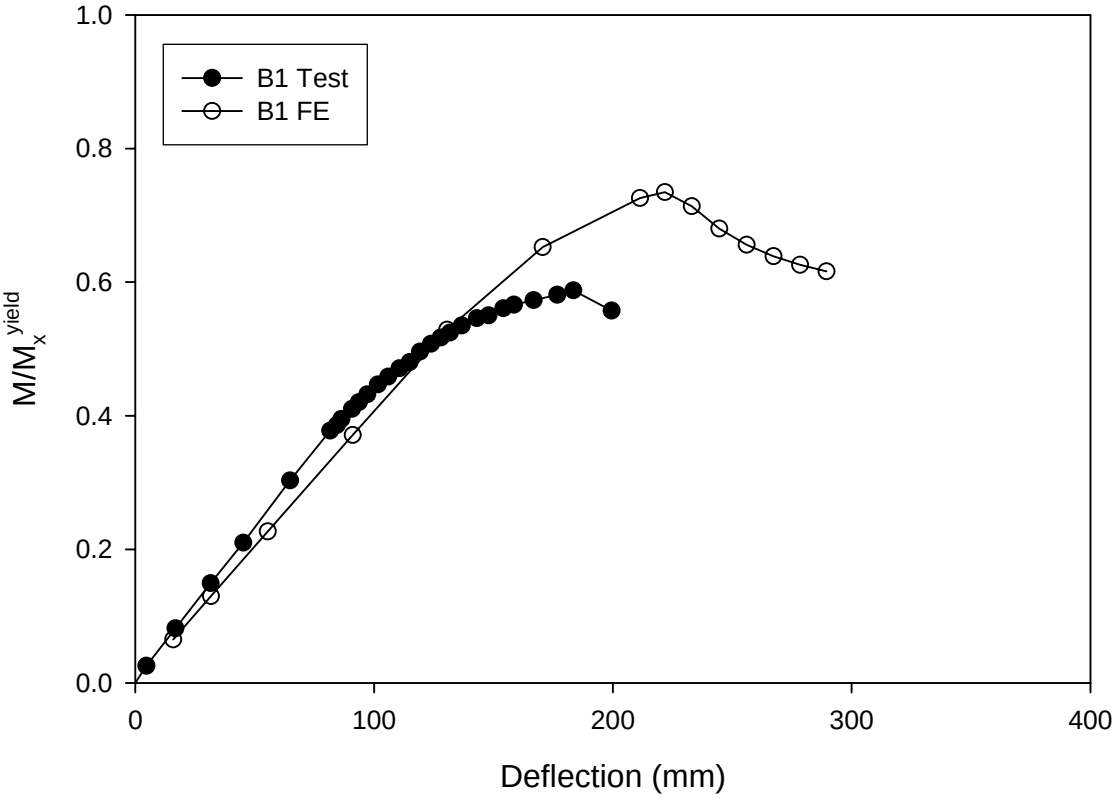

Figure 4-10: B1 Mid-Span Moment vs. Deflection

4.1.6.2 B2 Finite Element Model Results

A summary of the B2 experimental and finite element results is included in Table 4-7. The finite element model of the B2 component test predicted a maximum sustainable applied load of 1596.8 kN. This load equated to a mid-span moment of 3910.8 kN-m. When combined with the self-weight effects the predicted maximum mid-span moment resisted by B2 was 4774.5 kN-m. This amount is comparable to the measured maximum mid-span resisted moment of 4729.6 kN-m.

B2		Test (a)	FE (b)	Ratio (b)/(a)
Max. Applied Load	(kN)	1432.3	1596.8	1.11
Mid-Span Moment				
Self-Weight	(kN-m)	928.0	863.6	0.93
Installation	(kN-m)	536.8		
Max. Applied Load	(kN-m)	3264.7	3910.8	1.20
Flexural Resistance	(kN-m)	4729.6	4774.5	1.01

Table 4-7: B2 Test and Finite Element Model Results

Figure 4-11 shows the effect that the applied loads had on the mid-span moments of G1, G2 and B2 from both the experimental test and the finite element model. The predictions match the physical results very well indicating that the load is being distributed as expected within the load frame.

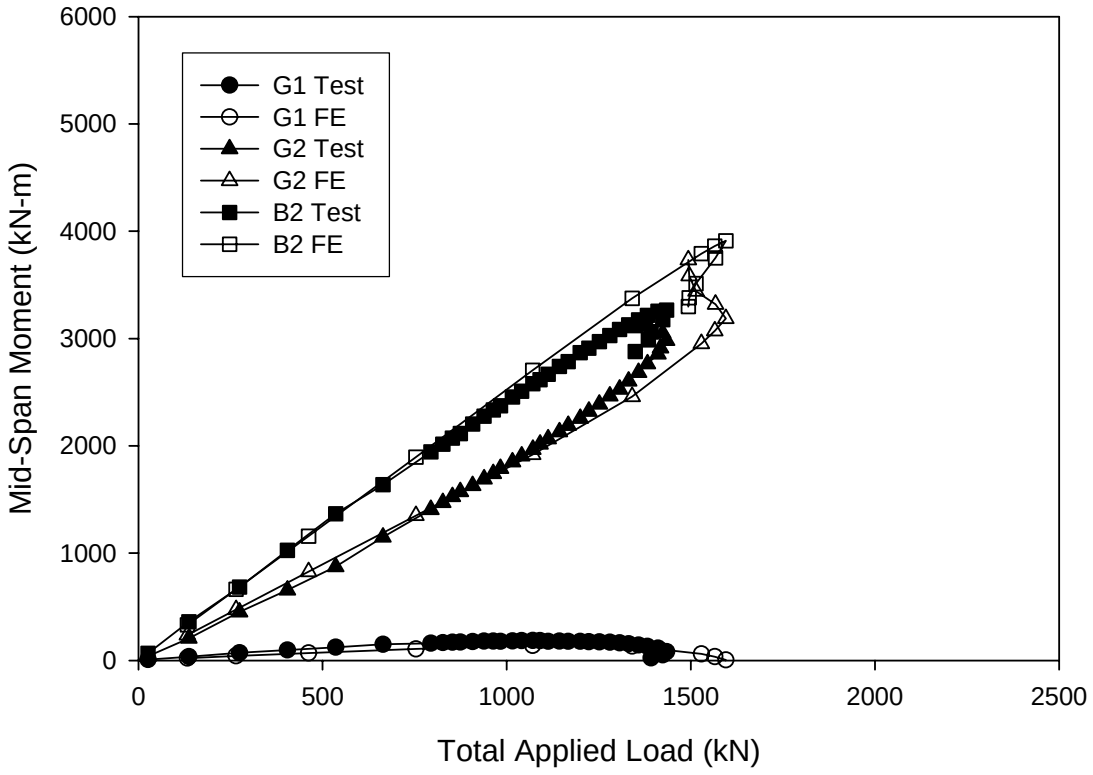

Figure 4-11: B2 Test Mid-Span Moments and Finite Element Predictions

Figure 4-12 shows the normalized B2 mid-span moment from the applied loads as a function of deflection for both the finite element model and the experimental data. The test results fall short of the predicted capacity and contain a greater degree of pre-peak non-linearity. However, the shapes of the curves are very similar. The exhibited and predicted flexural resistance capacities are within 1% once the difference in self-weight and the recorded installation strains are added to the test results.

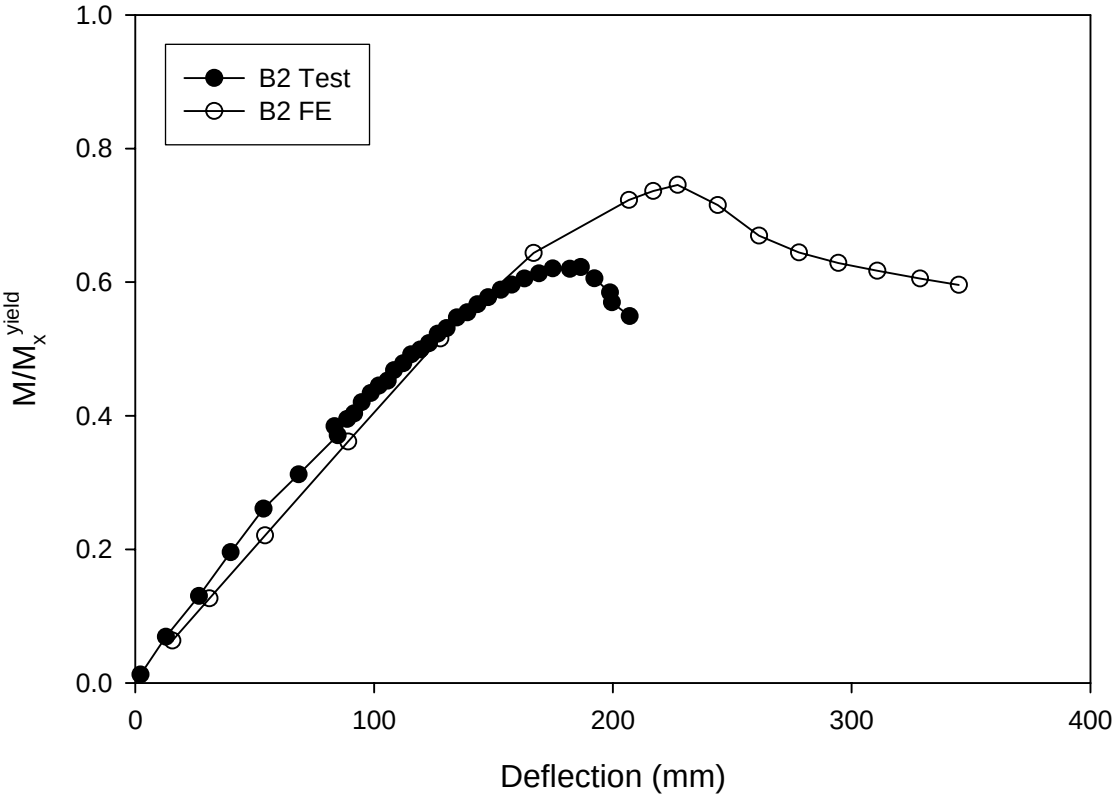

Figure 4-12: B2 Mid-Span Moment vs. Deflection

4.1.6.3 B3 Finite Element Model Results

The B3 finite element model predicted a maximum sustainable applied load of 1598.2 kN which resulted in a mid-span moment of 3904.6 kN-m. When combined with the self-weight effects the predicted maximum mid-span moment resisted by B3 was 4778.0 kN-m. This moment is comparable to the measured maximum mid-span resisted moment of 4834.4 kN-m. Table 4-8 contains a summary of the B3 experimental and finite element results.

B3		Test (a)	FE (b)	Ratio (b)/(a)
Max. Applied Load	(kN)	1499.9	1593.2	1.06
Mid-Span Moment				
Self-Weight	(kN-m)	922.2	873.4	0.95
Installation	(kN-m)	536.8	0.0	
Max. Applied Load	(kN-m)	3375.4	3903.3	1.16
Flexural Resistance	(kN-m)	4834.4	4776.7	0.99

Table 4-8: B3 Test and Finite Element Model Results

Figure 4-13 shows the effect that the applied loads had on the mid-span moments of the test frame girders from both the B3 experimental test and the finite element model. The figure indicates that the finite element model is accurately predicting the distribution of load within the test frame and that the pre-peak behavior prediction agrees well with the experiment.

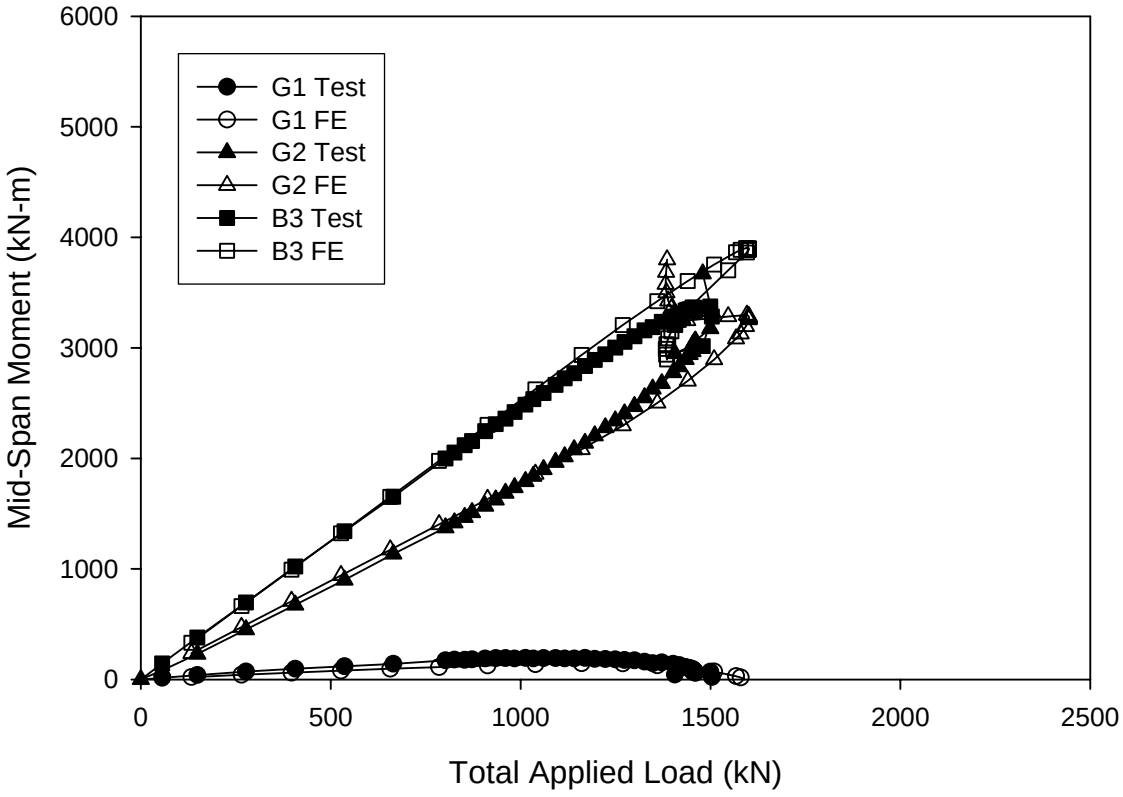

Figure 4-13: B3 Test Mid-Span Moments and Finite Element Predictions

Figure 4-14 shows the normalized B3 mid-span moment from the applied loads as a function of deflection for both the finite element model and the experimental data. The experimental results indicate that the component was initially stiffer than the predicted behavior. The test results cross the prediction curve prior to the predicted maximum capacity and return to the prediction curve again in the post-peak field of behavior. However, the analytical results predict a severe post-peak capacity drop that was not captured during the physical test. After adjusting for the difference in self-weight and the recorded installation effects, the results are within 1% of the predicted flexural capacity.

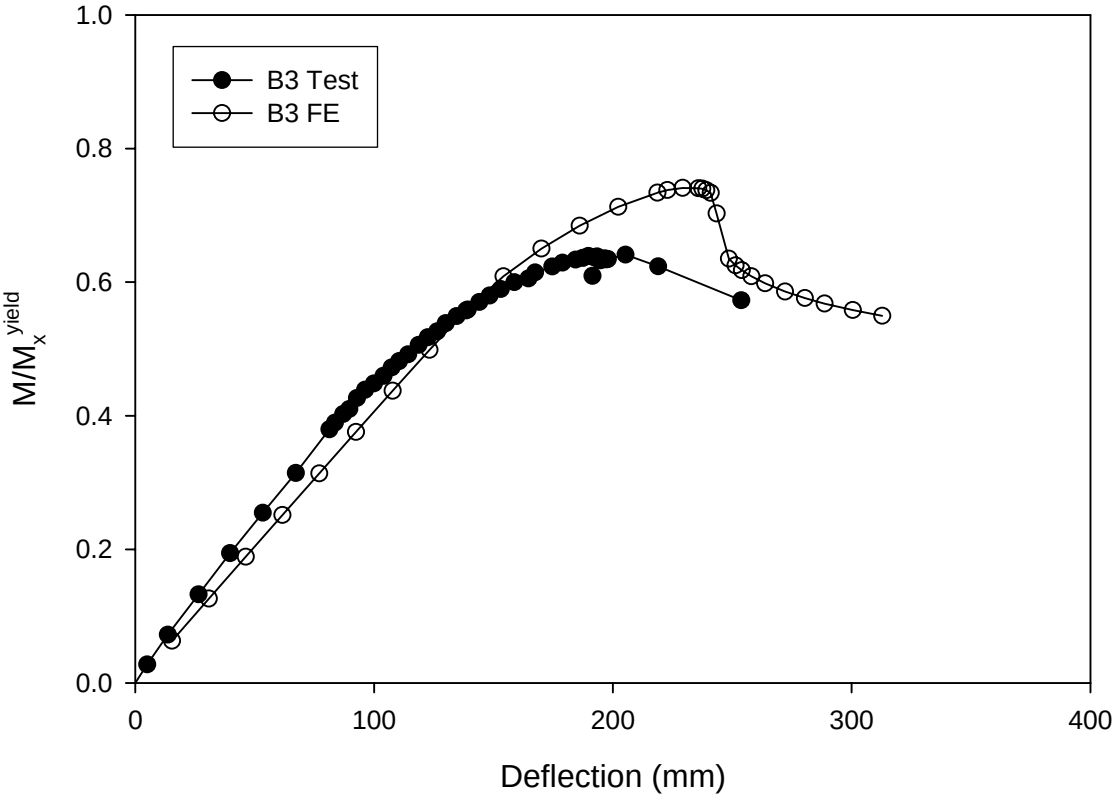

Figure 4-14: B3 Mid-Span Moment vs. Deflection

4.1.6.4 B4 Finite Element Model Results

A summary of the B4 experimental and finite element results is included in Table 4-9. A maximum sustainable applied load of 1475.4 kN was predicted by the finite element model for the B4 component test. This load equated to a mid-span moment of 3790.7 kN-m. When combined with the self-weight effects the predicted maximum mid-span moment resisted by B4 was 4718.3 kN-m is comparable to the measured maximum mid-span resisted moment of 4879.7 kN-m.

B4		Test (a)	FE (b)	Ratio (b)/(a)
Max. Applied Load	(kN)	1354.4	1475.4	1.09
Mid-Span Moment				
Self-Weight	(kN-m)	960.7	927.6	0.97
Installation	(kN-m)	696.0	0.0	
Max. Applied Load	(kN-m)	3223.1	3790.7	1.18
Flexural Resistance	(kN-m)	4879.7	4718.3	0.97

Table 4-9: B4 Test and Finite Element Model Results

Figure 4-15 shows the effect that the applied loads had on the mid-span moments of G1, G2 and B2 from both the experimental test and the finite element model. The predictions match the physical results very well prior to the failure of B4, indicating that the model is accurately accounting for the actual physical behavior.

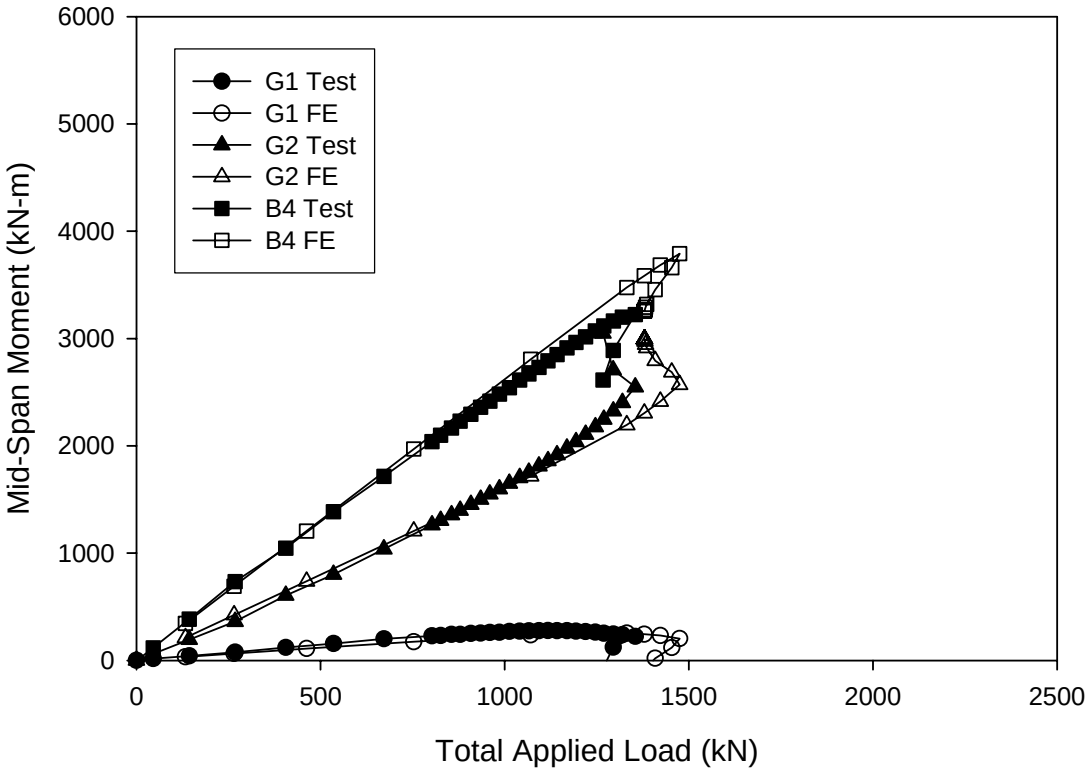

Figure 4-15: B4 Test Mid-Span Moments and Finite Element Predictions

Figure 4-16 shows the normalized B4 mid-span moment from the applied loads as a function of deflection for both the finite element model and the experimental data. The test results fall short of the predicted capacity and contain some pre-peak non-linearity. However, the shape of the curves is very similar, and when the test results include the difference in self-weight and the recorded installation effects the exhibited and predicted flexural resistance capacities are within 3%.

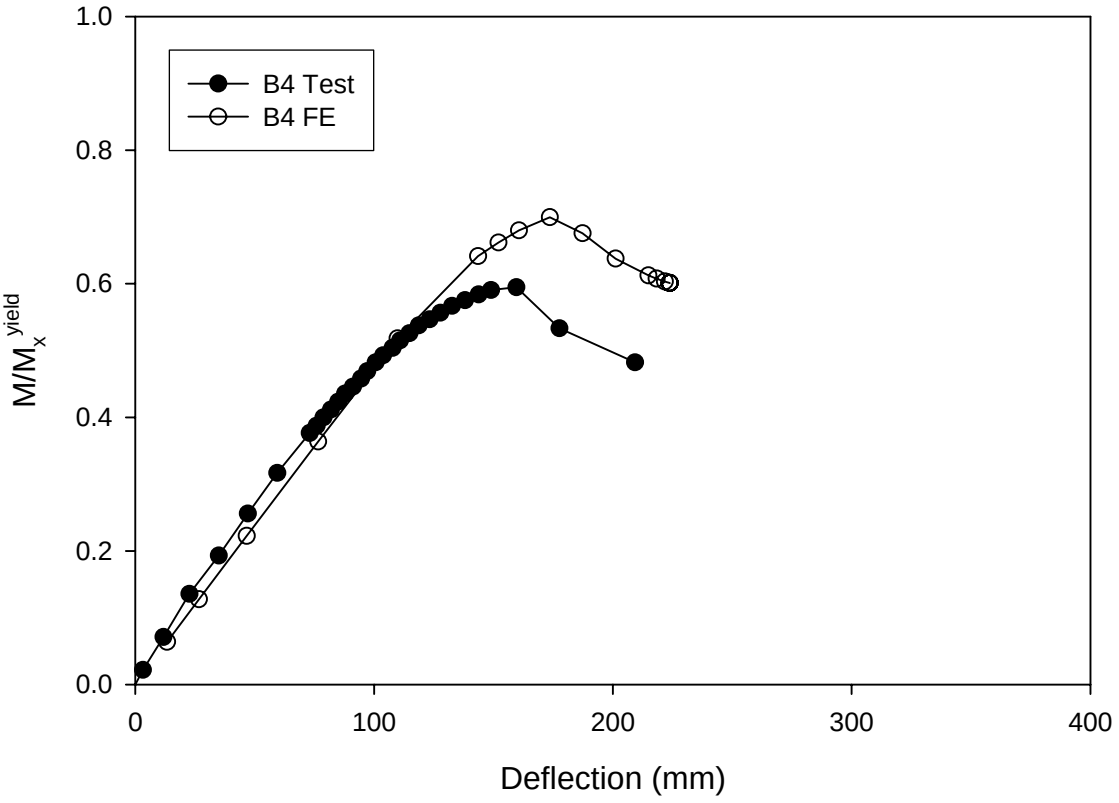

Figure 4-16: B4 Mid-Span Moment vs. Deflection

4.1.6.5 B5 Finite Element Model Results

The finite element model of the B5 test predicted a maximum sustainable applied load of 1742.7 kN, which produced a moment of 4361.3 kN-m at mid-span of the

component. When combined with the self-weight effects the predicted maximum mid-span moment resisted by B5 was 5255.2 kN-m. This result is essentially the same as the measured maximum mid-span resisted moment of 5278.1 kN-m. A summary of the B4 experimental and finite element results is included in Table 4-10.

B5		Test (a)	FE (b)	Ratio (b)/(a)
Max. Applied Load	(kN)	1732.5	1742.7	1.01
Mid-Span Moment				
Self-Weight	(kN-m)	896.9	893.9	1.00
Installation	(kN-m)	511.9	0.0	
Max. Applied Load	(kN-m)	3869.3	4361.3	1.13
Flexural Resistance	(kN-m)	5278.1	5255.2	1.00

Table 4-10: B5 Test and Finite Element Model Results

Figure 4-17 shows the effect that the applied loads had on the mid-span moments of G1, G2 and B2 from both the experimental test and the finite element model. The predictions match the physical results very well early in the loading regime and maintain the same characteristic shape throughout the figure.

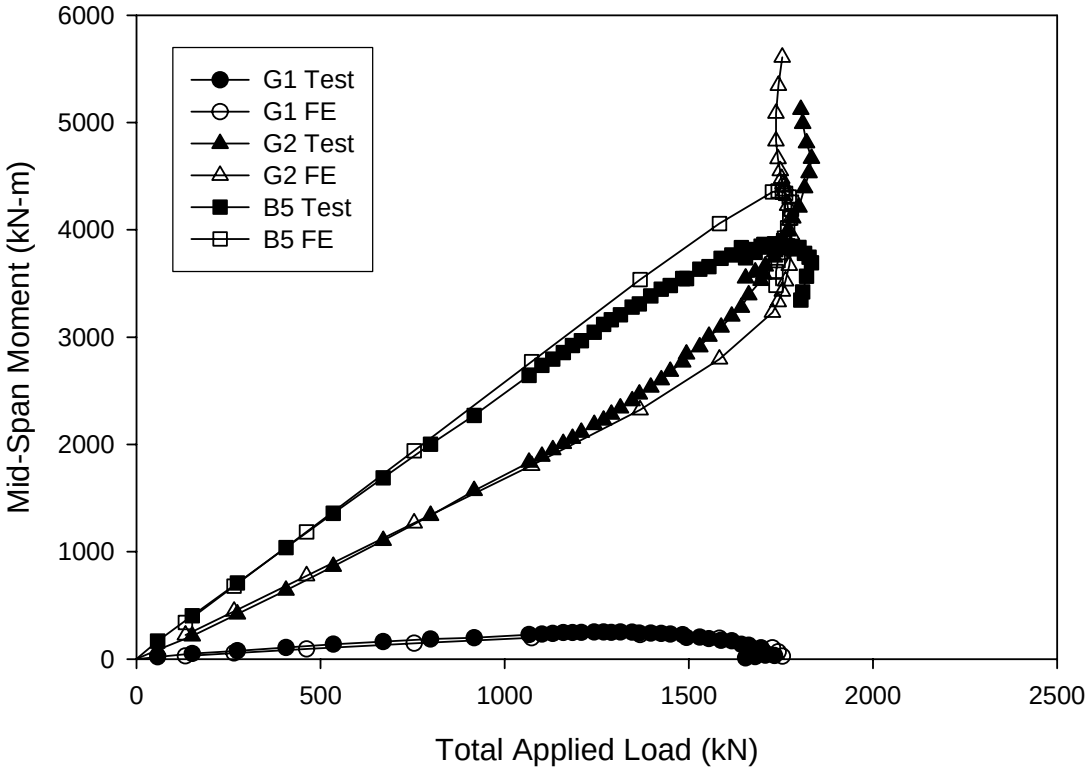

Figure 4-17: B5 Test Mid-Span Moments and Finite Element Predictions

Figure 4-18 shows the normalized B1 mid-span moment from the applied loads as a function of deflection for both the finite element model and the experimental data. The test results fall short of the predicted capacity and contain additional pre-peak non-linearity. However, the shapes of the curves are very similar. When the test results are include the difference in self-weight and the recorded installation effects, the exhibited and predicted flexural resistance capacities are nearly identical.

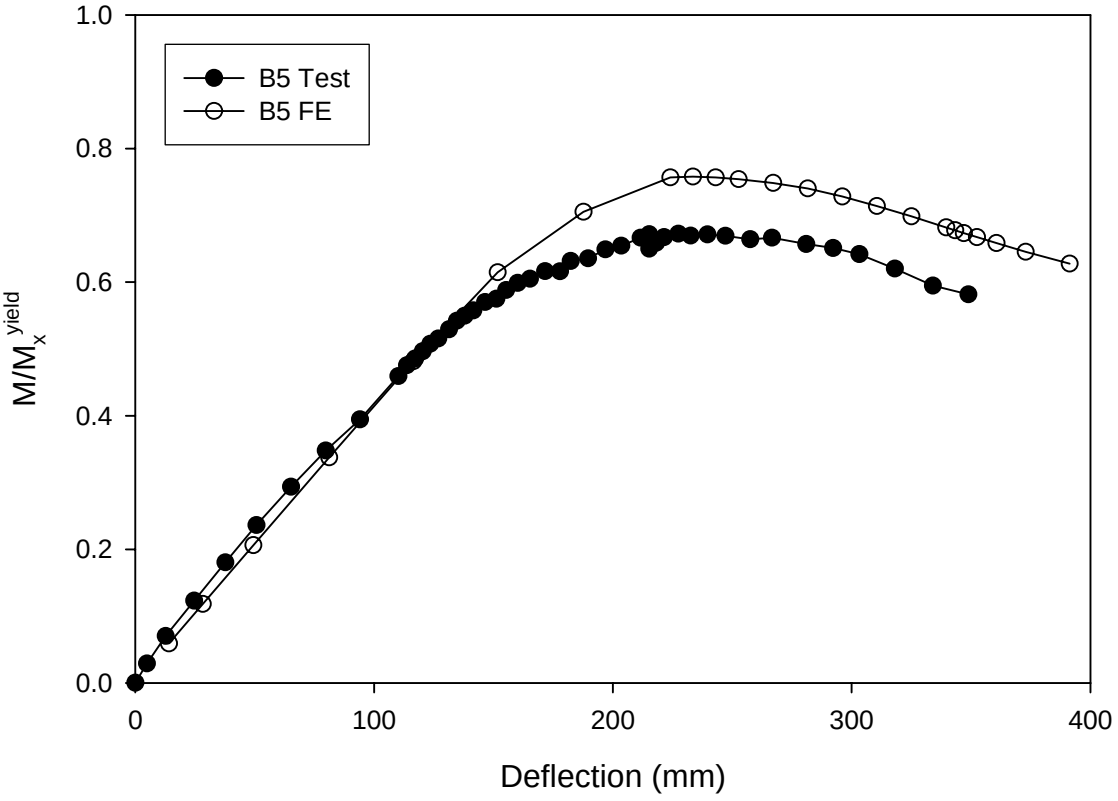

Figure 4-18: B5 Mid-Span Moment vs. Deflection

4.1.6.6 B6 Finite Element Model Results

A summary of the B6 experimental and finite element results is included in Table 4-11. The finite element model of the B6 component test predicted a maximum sustainable applied load of 2038.5 kN. This load equated to a mid-span moment of 5319.3 kN-m. When combined with the self-weight effects the predicted maximum mid-span moment resisted by B6 was 6257.8 kN-m. This result is comparable to the measured maximum mid-span resisted moment of 6399.5 kN-m.

B6		Test (a)	FE (b)	Ratio (b)/(a)
Max. Applied Load	(kN)	2071.4	2038.5	0.98
Mid-Span Moment				
Self-Weight	(kN-m)	951.5	938.5	0.99
Installation	(kN-m)	561.8	0.0	
Max. Applied Load	(kN-m)	4886.2	5319.3	1.09
Flexural Resistance	(kN-m)	6399.5	6257.8	0.98

Table 4-11: B6 Test and Finite Element Model Results

The effect that the applied loads had on the mid-span moments of the test frame girders during the B6 test from both the experimental data and the finite element model results are shown in Figure 4-19. The predicted post-peak drop in capacity for B6 is slightly more dramatic than the measured behavior. However, the predictions match the physical results very well for the mid-span test frame cross-section.

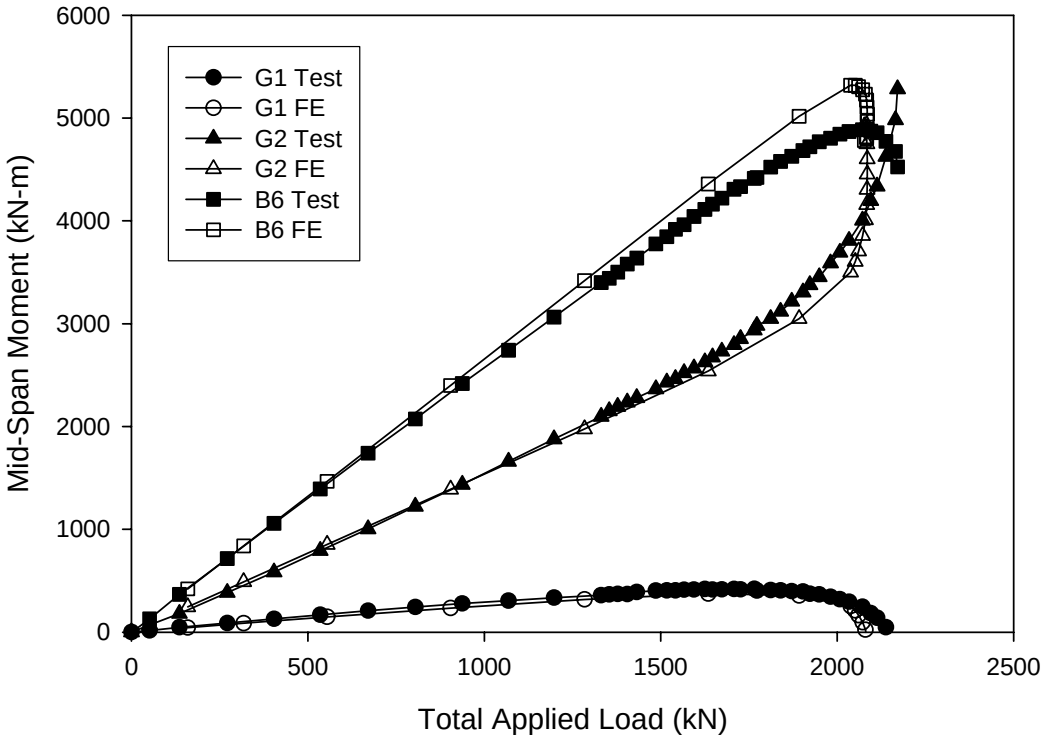

Figure 4-19: B6 Test Mid-Span Moments and Finite Element Predictions

Figure 4-40 shows the normalized B6 mid-span moment from the applied loads as a function of deflection for both the finite element model and the experimental data. The test results again fall short of the predicted capacity. However, the prediction curve matches the measured behavior through the elastic range and maintains a very similar shape pre- and post-peak. When the B6 test results are amended for the difference in self-weight and the recorded installation effects, the exhibited and predicted flexural resistance capacities are within 2%.

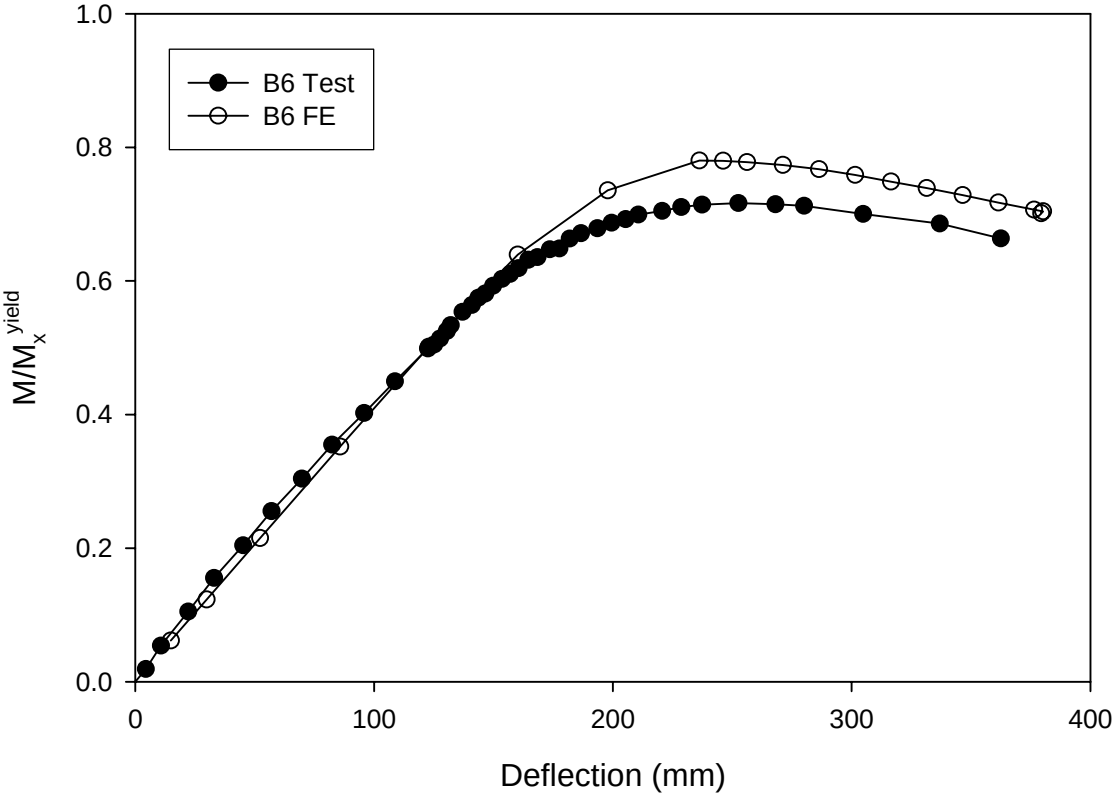

Figure 4-40: B6 Mid-Span Moment vs. Deflection

4.1.6.7 B7 Finite Element Model Results

Table 4-12 contains a summary of the B7 experimental and finite element results. The B7 finite element model predicted a maximum sustainable applied load of 1269.9 kN. This load equated to a mid-span moment of 3138.1 kN-m. When combined with the self-weight effects the predicted maximum mid-span moment resisted by B7 was 3993.3 kN-m. This result is a significant over-strength, compared with the measured maximum mid-span resisted moment of 3503.4 kN-m.

B7		Test (a)	FE (b)	Ratio (b)/(a)
Max. Applied Load	(kN)	1095.5	1269.9	1.16
Mid-Span Moment				
Self-Weight	(kN-m)	811.8	855.2	1.05
Installation	(kN-m)	190.4	0.0	
Max. Applied Load	(kN-m)	2501.1	3138.1	1.25
Flexural Resistance	(kN-m)	3503.4	3993.3	1.14

Table 4-12: B7 Test and Finite Element Model Results

The effect that the applied loads had on the mid-span moments of G1, G2 and B7 from both the experimental test and the finite element model are shown in Figure 4-41. The predictions match the physical results very well early in the loading regime indicating that the finite element model adequately forecasts the elastic behavior of the test frame.

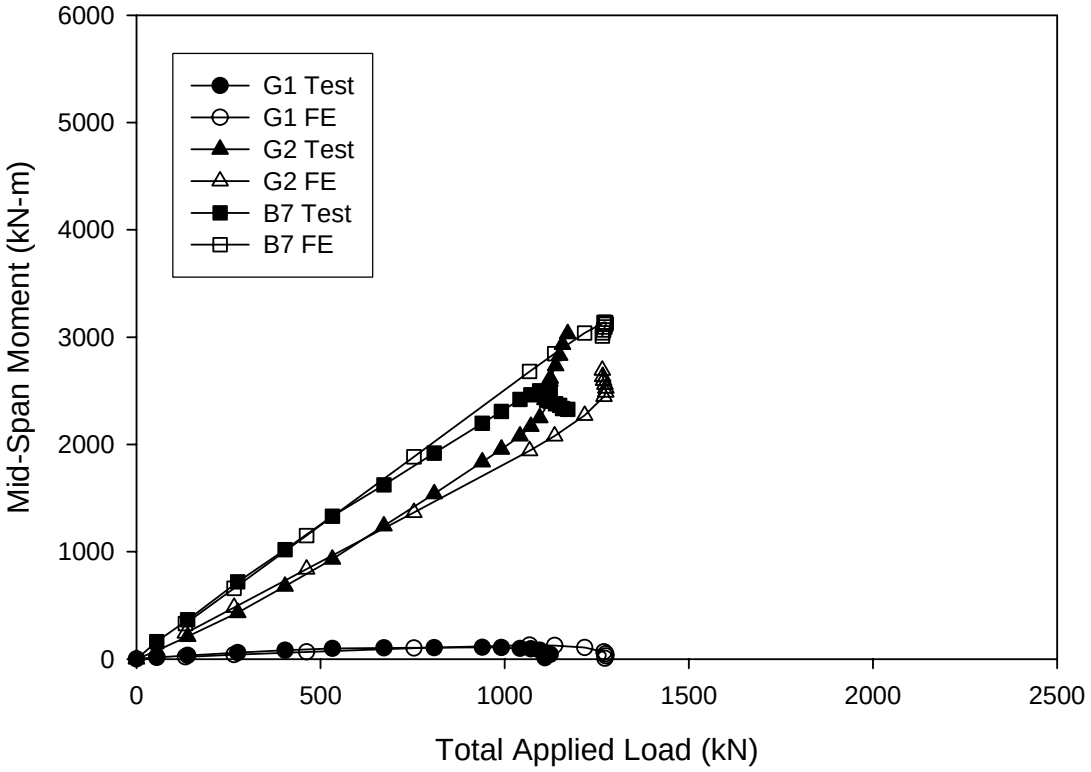

Figure 4-41: B7 Test Mid-Span Moments and Finite Element Predictions

Figure 4-42 shows the normalized B7 mid-span moment from the applied loads as a function of deflection for both the finite element model and the experimental data. Although the overall shape of the prediction and experimental curves remains similar throughout the figure, the experimental data indicate a significant early stiffness difference and, later, a failure of the section well short of the predicted peak. These differences are most likely due to the nature in which B7 was fabricated and the inability to quantify these differences and incorporate them into the model. This resulted in fully analyzed test results for flexural resistance that include the difference in self-weight and recorded installation effects that are nearly 14% less than predicted.

In addition to the fabrication issues that affected the performance of B7, it is difficult for any general purpose finite element program to predict the onset of local buckling for slender plates such as the top flange of this specimen. These slender sections are sensitive to geometric imperfections that were not a part of this analytical study. White et al. (2001) modeled B7 with and without estimates for geometric imperfections. Their results without the geometric imperfection estimates were very similar to those in this study. Their results including the geometric imperfection estimates matched the physical test results much more closely; the results are within 4%. Because this study employs modeling very similar to that used by White et al. (2001), a similar correction in behavior is expected with the incorporation of geometric imperfections into the B7 model.

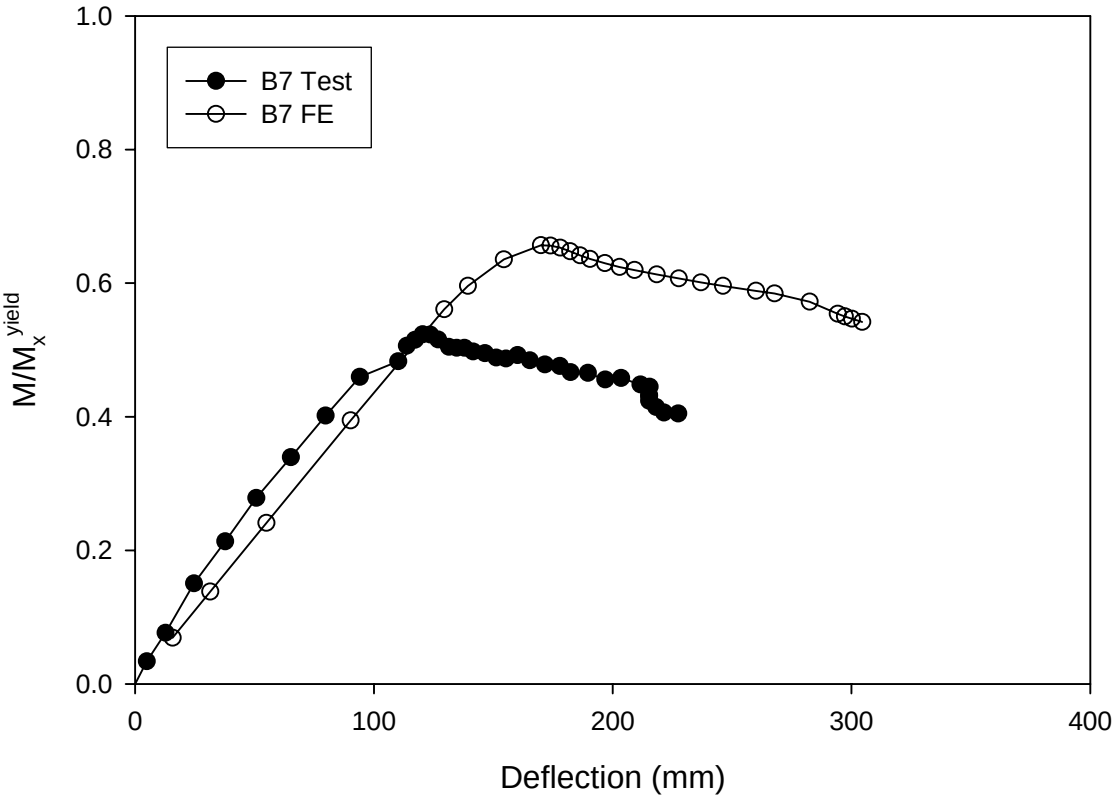

Figure 4-42: B7 Mid-Span Moment vs. Deflection

4.2 AASHTO Guide Specification Predictions

Bending capacities for each of the bending components can be determined using the provisions of the Guide Specifications. These provisions, which are summarized in Appendix B.1, utilized the vertical bending stress, f_b, and the lateral flange bending stress, f_l, results of a 1st order analysis to determine a maximum strong-axis flexural resistance. The 1st order analysis used in this report was generated with the same finite element model that was used for the fully non-linear analysis. However, the model was limited to linear-elastic behavior.

Table 4-13 includes the vertical bending capacities, M_n, as determined by the Guide Specifications (example calculations to demonstrate how these numbers were generated are included in Sections 4.1.1 and 4.1.2), and a summary of the experimental results for these sections, M_x^{test}, as reported in Chapter 3. A performance ratio that is produced by normalizing the capacity of the Guide Specifications by the experimental results is listed in the far right column of Table 4-13. A statistical summary of the normalized performance ratios is shown in the box just under the far right column.

The average performance ratio was 0.71, or roughly 29% conservative. However, this average was associated with a rather large standard deviation of 0.15 or 21% of the mean, indicating a very poor consistency of prediction. The range of results extended from 9% conservative to 43% conservative.

Component	M_n From Guide Specifications (kN-m)	f_l/f_b From 1st Order Analysis	M_x^{test} (kN-m)	M_n/M_x^{test}
B1	2702	0.32	4339	0.62
B2	2778	0.33	4730	0.59
B3	2748	0.36	4834	0.57
B4	2900	0.31	4880	0.59
B5	4790	0.32	5278	0.91
B6	5649	0.31	6400	0.88
B7	2775	0.29	3503	0.79
			Average	0.71
			Std. Dev.	0.15
			Maximum	0.91
			Minimum	0.57

Table 4-13: Summary of Guide Specifications Flexural Capacities and Statistics

The following two sets of example calculations illustrate the use of the Guide Specifications for determining the flexural resistance of a non-compact compression flange section and of a compact compression flange section. These calculations are usually an iterative process. The last iteration of this process is presented in Section 4.1.1 for brevity.

4.2.1 Non-Compact Compression Flange Example

Bending component B1 was chosen for these example calculations.

- **B1 properties**

F_{yc} = yield stress of the compression flange = 408.5 MPa

F_{yw} = yield stress of the web = 445.4 MPa

L_b = unbraced arc length of the flange = 4772 mm

R = minimum girder radius within the panel = 63,630 mm

b_{fc} = compression flange width = 443.7 mm

D = web depth = 1211 mm

D_c = depth of web in compression = 604.9 mm

t_{fc} = compression flange thickness = 19.48 mm

t_w = web thickness = 8.230 mm

S_{xc} = section modulus referred to the compression flange = 12.41×10^6 mm^3

f_{l1} = 1st order analysis lateral flange bending stress = 69.64 MPa

f_{bu} = 1st order analysis flange stress from vertical bending = 217.6 MPa

- **Check flange compactness**

B1 was designed to be non-compact. To be defined as non-compact, the compression flange must meet the following criterion:

$$\frac{b_{fc}}{t_{fc}} \le 1.02\sqrt{\frac{E}{\left|\left(f_{bu} + f_{l1}\right)\right|}} \le 23$$

$$\frac{b_{fc}}{t_{fc}} = \frac{443.7}{19.48} = 22.8 \le 1.02\sqrt{\frac{204000}{\left|\left(217.6 + 69.64\right)\right|}} = 27.2$$

$\frac{b_{fc}}{t_{fc}} = 22.8 \le 23$ Therefore, the flange is non-compact.

- **Solve for the critical flange stress, F_{cr}**

The critical flange stress is the lesser of a flange stress that, when amplified with the ρ-factors, will cause lateral torsional buckling in unbraced length, or the flange yield strength reduced by the lateral flange bending stress.

The lateral torsional buckling stress is:

$$F_{bs} = F_{yc}\left(1 - 3\left(\frac{L_b}{0.9b_{fc}}\right)^2 \frac{F_{yc}}{\pi^2 E}\right)$$

$$F_{bs} = 408.5\left(1 - 3\left(\frac{4772}{0.9(443.7)}\right)^2 \frac{408.5}{\pi^2(204000)}\right) = 373.0MPa$$

The non-compact flange ρ-factors are:

$$\rho_b = \frac{1}{1 + \frac{L_b}{R}\frac{L_b}{b_{fc}}}$$

$$\rho_b = \frac{1}{1 + \left(\frac{4772}{63{,}630}\right)\left(\frac{4772}{443.7}\right)} = 0.554$$

$$\rho_{w1} = \frac{1}{1 - \frac{f_{l1}}{f_{bu}}\left(1 - \frac{L_b}{75b_{fc}}\right)}$$

$$\rho_{w1} = \frac{1}{1 - \frac{69.64}{217.6}\left(1 - \frac{4772}{75(443.7)}\right)} = 1.378$$

$$\rho_{w2} = \frac{0.95 + \frac{\frac{L_b}{b_{fc}}}{30 + 8{,}000\left(0.1 - \frac{L_b}{R}\right)^2}}{1 + 0.6\left(\frac{f_{l1}}{f_{bu}}\right)}$$

$$\rho_{w2} = \frac{0.95 + \frac{\frac{4772}{443.7}}{30 + 8{,}000\left(0.1 - \frac{4772}{63{,}630}\right)^2}}{1 + 0.6\left(\frac{69.64}{217.6}\right)} = 1.055$$

Because $\frac{f_{l1}}{f_{bu}} \geq 0$, $\rho_w = \min(\rho_{w1}, \rho_{w2}) = 1.055$.

Having determined the ρ-factors, solve for the critical flange stress.

$$F_{cr1} = F_{bs}\rho_b\rho_w$$

$$F_{cr1} = (373.0)(0.554)(1.055) = 218.0MPa$$

$$F_{cr2} = F_y - |f_l|$$

$$F_{cr2} = 408.5 - |69.64| = 338.9MPa$$

$$F_{cr} = \min(F_{cr1}, F_{cr2}) = 218.0i \approx f_b = 217.6MPa$$

- **Check the web stress criterion**

k = bend-buckling coefficient = $9.0\left(\frac{D}{D_c}\right)^2$

$$k = 9.0\left(\frac{1211}{604.9}\right)^2 = 36.07$$

$$F_{cr}(web) = \frac{0.9Ek}{\left(\frac{D}{t_w}\right)^2} \le F_{yw}$$

$$F_{cr}(web) = \frac{0.9(204000)(36.07)}{\left(\frac{1211}{8.230}\right)^2} = 305.9MPa$$

Because the critical web stress, 305.9 *MPa* (44.367 *ksi*) is greater than the vertical bending stress in the section 217.6 *MPa* (31.560 *ksi*) the web condition is acceptable.

- **Determine the equivalent vertical bending moment**

$$M_n = f_{bu}S_{xc}$$

$$M_n = 217.6(12.41x10^6) = 2700x10^6\,N-mm = 2700kN-m$$

Please refer to Table 4-17 to see how this capacity compares to the experimental measurement.

4.2.2 Compact Compression Flange Example

Bending component B5 was chosen for these example calculations.

- **B5 properties**

F_{yc} = compression flange yield strength = 395.0 MPa

F_{yw} = web plate yield strength = 445.2 MPa

L_b = unbraced arc length of the flange = 4772 mm

R = minimum girder radius within the panel = 63,630 mm

b_{fc} = compression flange width = 419.1 mm

D = web depth = 1215 mm

D_c = depth of web in compression = 607.3 mm

t_{fc} = compression flange thickness = 24.66 mm

t_w = web thickness = 8.458 mm

S_{xc} = section modulus referred to the compression flange = 14.56×10^6 mm^3

f_{l1} = 1st order analysis lateral flange bending stress = 105.3 MPa

f_{bu} = 1st order analysis flange stress from vertical bending = 329.0 MPa

- **Check the flange compactness**

B5 was designed to have a compact compression flange. To be defined as compact, the compression flange must meet the following criterion:

$$\frac{b_{fc}}{t_{fc}} \leq 18$$

$\frac{b_{fc}}{t_{fc}} = \frac{419.1}{24.66} = 17.0 \le 18$ Therefore, the flange is compact.

- **Solve for the critical flange stress, F_{cr}**

The critical flange stress is the lesser of a flange stress that, when amplified with the ρ-factors, will cause lateral torsional buckling in unbraced length, or the flange yield strength reduced by the lateral flange bending stress.

The lateral torsional buckling stress is:

$$F_{bs} = F_{yc}\left(1 - 3\left(\frac{L_b}{0.9b_{fc}}\right)^2 \frac{F_{yc}}{\pi^2 E}\right)$$

$$F_{bs} = 395.0\left(1 - 3\left(\frac{4772}{0.9(419.1)}\right)^2 \frac{395.0}{\pi^2(204000)}\right) = 357.8MPa$$

The compact flange ρ-factors are:

$$\overline{\rho}_b = \frac{1}{1 + \frac{L_b}{b_{fc}}\left(1 + \frac{L_b}{6b_{fc}}\right)\left(\frac{L_b}{R} - 0.01\right)^2}$$

$$\overline{\rho}_b = \frac{1}{1 + \frac{4772}{419.1}\left(1 + \frac{4772}{6(419.1)}\right)\left(\frac{4772}{63{,}630} - 0.01\right)^2} = 0.878$$

$$\overline{\rho}_w = 0.95 + 18\left(0.1 - \frac{L_b}{R}\right)^2 + \frac{f_{l1}}{f_{bu}} \frac{\left(0.3 - 0.1\frac{L_b}{R}\frac{L_b}{b_{fc}}\right)}{\overline{\rho}_b\left(\frac{F_{bs}}{F_{yc}}\right)}$$

$$\overline{\rho}_w = 0.95 + 18\left(0.1 - \frac{4772}{63{,}630}\right)^2 + \frac{105.3}{329.0} \frac{\left[0.3 - 0.1\left(\frac{4772}{63{,}630}\right)\left(\frac{4772}{419.1}\right)\right]}{0.878\left(\frac{357.8}{395.0}\right)} = 1.048$$

$$\overline{\rho_b}\,\overline{\rho_w} = 0.878(1.048) = 0.920 < 1.0$$

Having determined the ρ-factors, solve for the critical flange stress.

$$F_{cr1} = F_{bs}\,\overline{\rho}_b\,\overline{\rho}_w$$

$$F_{cr1} = 357.8(0.920) = 329.2MPa$$

$$F_{cr2} = F_y - \frac{|f_{l1}|}{3}$$

$$F_{cr2} = 395.0 - \frac{|105.3|}{3} = 359.9MPa$$

$$F_{cr} = \min(F_{cr1}, F_{cr2}) = 329.2MPa > f_{bu} = 329.0MPa$$

- **Check the web stress criterion**

k = bend-buckling coefficient = $9.0\left(\frac{D}{D_c}\right)^2$

$$k = 9.0\left(\frac{1215}{607.3}\right)^2 = 36.02$$

$$F_{cr}(web) = \frac{0.9Ek}{\left(\frac{D}{t_w}\right)^2} \le F_{yw}$$

$$F_{cr}(web) = \frac{0.9(204000)(36.02)}{\left(\frac{1215}{8.458}\right)^2} = 320.5MPa < f_{bu} = 329.0MPa$$

Because the critical web compressive stress is less than the vertical bending stress in the flange, determine the vertical bending stress based on the critical web stress.

$$F_{cr}(web) \ge \left[\frac{D_c}{D_c + t_{fc}}\right] f_{bu}$$

$$F_{cr}(web) \geq \left[\frac{607.3}{607.3+24.66}\right](329.0) = 316.1MPa < 320.5MPa \text{ okay}$$

Therefore this design meets the critical web stress criterion.

- **Determine the equivalent vertical bending moment**

$$M_n = f_{bu} S_{xc}$$

$$M_n = 329.0\left(14.56x10^6\right) = 4790x10^6\, N-mm = 4790kN-m$$

Please refer to Table 4-17 to see how this capacity compares to the experimental measurement.

4.3 Unified Design Method Predictions

The estimated capacities derived by using the Unified Design Method for the entire suite of bending components can be seen in the top section of Table 4-14. These capacities, M_n, have been determined by using a 1st order analysis with the suggested lateral flange stress amplification factor, and by using a 2nd order analysis. Similar to with the Guide Specification results, each calculated capacity has been normalized by the appropriate experimental result, M_x^{test}, from Chapter 3 to produce the performance ratios in the far right column of each section of Table 4-14. The lower section of this table contains a statistical summary of the performance ratios for each analysis method.

For the 1st order analysis results, the average performance ratio was 0.85, or roughly 15% conservative. This average was associated with a standard deviation of 0.03 or approximately 4% of the mean. The range of results extended from 10% conservative to 19% conservative.

The statistics for the 2nd order analysis results are very similar to the statistical results for the 1st order analysis results. The average performance ratio was 0.84 or 16%

conservative with an associated standard deviation of 0.03 or 4%. The range of results tightened slightly extending from 12% conservative to 18% conservative.

Component	M_x^{test}	1st Order Analysis			2nd Order Analysis		
		M_n	$AF(f_l/f_b)$	M_n/M_x^{test}	M_n	f_l/f_b	M_n/M_x^{test}
	(kN-m)	(kN-m)			(kN-m)		
B1	4339	3908	0.37	0.90	3835	0.33	0.88
B2	4730	4022	0.38	0.85	3944	0.34	0.83
B3	4834	4006	0.42	0.83	3942	0.43	0.82
B4	4880	3967	0.36	0.81	4007	0.28	0.82
B5	5278	4618	0.38	0.87	4590	0.34	0.87
B6	6400	5512	0.37	0.86	5316	0.43	0.83
B7	3503	2919	0.29	0.83	2928	0.28	0.84
			Average	0.85		Average	0.84
			Std. Dev.	0.03		Std. Dev.	0.03
			Maximum	0.90		Maximum	0.88
			Minimum	0.81		Minimum	0.82

Table 4-14: Summary of Unified Design Method Flexural Capacities and Statistics

The following two sets of example calculations illustrate the use of the Unified Design Method for determining the flexural resistance of a discretely braced non-compact compression flange section and of a discretely braced compact compression flange section using the results of a 1st order analysis. Appendix B.2 contains a summary of the Unified Design Method provisions for non-composite I-girders.

4.3.1 Non-Compact Compression Flange Example

As before, bending component B1 was chosen for these example calculations. The B1 section properties listed in Section 4.1.1 still apply. However, the unique set of coincidental loads from the 1st order analysis that are needed for these calculations are listed here:

f_{l1} = 1st order analysis lateral flange bending stress = 100.8 MPa

f_{bu} = 1st order analysis flange stress from vertical bending = 314.9 MPa

- **Check the flange compactness**

B1 was designed to be non-compact. To be defined as compact, the compression flange slenderness must meet the following criterion:

$$\lambda_{pf} = 0.38\sqrt{\frac{E}{F_{yc}}}$$

$$\lambda_{pf} = 0.38\sqrt{\frac{204000}{408.5}} = 8.49$$

$$\lambda_f = \frac{b_{fc}}{2t_{fc}}$$

$$\lambda_f = \frac{443.7}{2(19.48)} = 11.39 > \lambda_{pf} = 8.49$$

Because $\lambda_f > \lambda_{pf}$, the flange is non-compact.

- **Determine critical flange local buckling stress**

Because the flange is non-compact, first determine the critical flange stress that will cause local buckling of the flange.

$$F_{yr} = \min\left[0.7F_{yc}, F_{yw}\right] > 0.5F_{yc}$$

$$F_{yr} = \min\left[0.7(408.5) = 286.0, 445.4\right] = 286.0MPa > 0.5F_{yc} = 204.3MPa$$

$$\lambda_{rf} = 0.56\sqrt{\frac{E}{F_{yr}}}$$

$$\lambda_{rf} = 0.56\sqrt{\frac{204000}{286.0}} = 14.96$$

Because $F_{yc} < F_{yw}$ the hybrid web reduction factor, R_h, is taken as 1.0.

Determine the web load shedding factor, R_b.

If $\frac{2D_c}{t_w} \le 5.76\sqrt{\frac{E}{F_{yr}}}$, then $R_b = 1.0$

$$\frac{2(604.9)}{8.230} = 147.0 \le 5.76\sqrt{\frac{204000}{286.0}} = 153.8 \qquad \text{Therefore } R_b = 1.0$$

$$F_{nc(FLB)} = \left[1 - \left(1 - \frac{F_{yr}}{R_h F_{yc}}\right)\left(\frac{\lambda_f - \lambda_{pf}}{\lambda_{rf} - \lambda_{pf}}\right)\right] R_b R_h F_{yc}$$

$$F_{nc(FLB)} = \left[1 - \left(1 - \frac{286.0}{408.5}\right)\left(\frac{11.39 - 8.49}{14.96 - 8.49}\right)\right] 408.5 = 353.6 MPa$$

- **Determine the critical lateral torsional buckling stress**

The critical lateral torsional buckling stress is based on the unbraced length of the compression flange.

$$r_t = \frac{b_{fc}}{\sqrt{12\left(1 + \frac{1}{3}\frac{D_c t_w}{b_{fc} t_{fc}}\right)}}$$

$$r_t = \frac{443.7}{\sqrt{12\left(1 + \left(\frac{1}{3}\right)\frac{604.9(8.230)}{443.7(19.48)}\right)}} = 117.3 mm$$

$$L_p = 1.0 r_t \sqrt{\frac{E}{F_{yc}}}$$

$$L_p = 1.0(117.3)\sqrt{\frac{204000}{408.5}} = 2621 mm$$

$$L_r = \pi r_t \sqrt{\frac{E}{F_{yr}}}$$

$$L_r = \pi(117.3)\sqrt{\frac{204000}{286.0}} = 9842 mm$$

Because $L_p < L_b \le L_r$, the unbraced length is non-compact.

$$F_{yr} = \min\left[0.7F_{yc}, F_{yw}\right] \ge 0.5F_{yc} = 286.0MPa$$

C_b = 1.0 for constant vertical bending moment

$$F_{nc(LTB)} = C_b\left[1-\left(1-\frac{F_{yr}}{R_hF_{yc}}\right)\left(\frac{L_b-L_p}{L_r-L_p}\right)\right]R_bR_hF_{yc} \le R_bR_hF_{yc}$$

$$F_{nc(LTB)} = 1.0\left[1-\left(1-\frac{286.0}{408.5}\right)\left(\frac{4772-2621}{9842-2621}\right)\right]408.5 = 372.0MPa$$

- **Determine the vertical bending moment capacity using the 1/3 rule**

$$F_{nc} = \min\left[F_{nc(FLB)}, F_{nc(LTB)}\right] = 353.6MPa$$

Because f_{l1} is from a 1st order analysis, apply the recommended amplification factor, AF, to account for the 2nd order geometric effects on lateral flange bending, f_l.

$$AF = \left[\frac{0.85}{1-\frac{f_{bu}}{F_{cr}}}\right]$$

where F_{cr} is the flange elastic lateral-torsional buckling stress.

$$F_{cr} = \frac{C_bR_b\pi^2E}{\left(\frac{L_b}{r_t}\right)^2}$$

$$F_{cr} = \frac{(1.0)(1.0)\pi^2(204000)}{\left(\frac{4772}{117.3}\right)^2} = 1217MPa$$

$$AF = \left[\frac{0.85}{1-\frac{314.9}{1217}}\right] = 1.147$$

$$f_l = AF(f_{l1})$$

$$f_l = 1.147(100.8) = 115.6MPa$$

Apply the 1/3rd rule to determine the vertical bending capacity.

$\varphi_f = 1.00$

$$\phi_f F_n \geq f_{bu} + \frac{1}{3} f_l$$

$$\phi_f F_n = 353.6MPa$$

$$353.6MPa \geq 314.9 + \frac{1}{3}(115.6) = 353.4MPa$$

Therefore f_{bu} = 314.9MPa is acceptable and the equivalent vertical bending moment is:

$$M_n = f_{bu} S_{xc}$$

$$M_n = 314.9(12.41x10^6) = 3908x10^6 N - mm = 3908kN - m$$

Please refer to Table 4-18 to see how this capacity compares to the experimental measurement.

4.3.2 Compact Compression Flange Example

The properties for bending component B5 are listed in Section 4.1.2. The 1st order loads for appropriate for this set of calculations are:

f_{l1} = 1st order analysis lateral flange bending stress = 101.5 MPa

f_{bu} = 1st order analysis flange stress from vertical bending = 317.2 MPa

- **Check the flange compactness**

B5 was designed to have a compact compression flange. Therefore it must meet the following slenderness limit.

$$\lambda_{pf} = 0.38\sqrt{\frac{E}{F_{yc}}}$$

$$\lambda_{pf} = 0.38\sqrt{\frac{204000}{395.0}} = 8.64$$

$$\lambda_f = \frac{b_{fc}}{2t_{fc}}$$

$$\lambda_f = \frac{419.1}{2(24.66)} = 8.50 < \lambda_{pf} = 8.64$$

Because $\lambda_f \le \lambda_{pf}$, the flange is compact.

- **Determine the critical flange local buckling stress**

Because the compression flange is compact, $F_{nc(FLB)} = R_b R_h F_{yc}$.

Determine the hybrid girder reduction factor, R_h.

$F_{yc} < F_{yw}$ Therefore $R_h = 1.0$

Determine the web load shedding factor, R_b.

$$F_{yr} = \min\left[0.7F_{yc}, F_{yw}\right] = 276.5MPa \ge 0.5F_{yc}$$

If $\frac{2D_c}{t_w} \le 5.76\sqrt{\frac{E}{F_{yr}}}$, then $R_b = 1.0$

$\frac{2(607.3)}{8.458} = 143.6 \le 5.76\sqrt{\frac{204000}{276.5}} = 156.4$ Therefore $R_b = 1.0$

$$F_{nc(FLB)} = R_b R_h F_{yc} = 1.0(1.0)395.0 = 395.0MPa$$

- **Determine the critical lateral torsional buckling stress**

$$r_t = \frac{b_{fc}}{\sqrt{12\left(1 + \frac{1}{3}\frac{D_c t_w}{b_{fc} t_{fc}}\right)}}$$

$$r_t = \frac{419.1}{\sqrt{12\left(1+\left(\frac{1}{3}\right)\frac{607.3(8.458)}{419.1(24.66)}\right)}} = 112.1mm$$

$$L_p = 1.0 r_t \sqrt{\frac{E}{F_{yc}}}$$

$$L_p = 1.0(112.1)\sqrt{\frac{204000}{395.0}} = 2548mm$$

$$L_r = \pi r_t \sqrt{\frac{E}{F_{yr}}}$$

$$L_r = \pi(112.1)\sqrt{\frac{204000}{276.5}} = 9566mm$$

Because $L_p < L_b \le L_r$, the unbraced length is non-compact.

C_b = 1.0 for constant vertical bending moment

$$F_{nc(LTB)} = C_b\left[1-\left(1-\frac{F_{yr}}{R_h F_{yc}}\right)\left(\frac{L_b - L_p}{L_r - L_p}\right)\right]R_b R_h F_{yc} \le R_b R_h F_{yc}$$

$$F_{nc(LTB)} = 1.0\left[1-\left(1-\frac{276.5}{395.0}\right)\left(\frac{4772-2548}{9566-2548}\right)\right]395.0 = 357.4MPa \le 395.0MPa$$

- **Determine the vertical bending moment capacity using the 1/3 rule**

$$F_{nc} = \min\left\lfloor F_{nc(FLB)}, F_{nc(LTB)}\right\rfloor = 357.4MPa$$

Determine the lateral flange stress amplification factor, *AF*.

$$AF = \left[\frac{0.85}{1-\frac{f_{bu}}{F_{cr}}}\right]$$

where F_{cr} is the flange elastic lateral-torsinal buckling stress.

$$F_{cr} = \frac{C_b R_b \pi^2 E}{\left(\frac{L_b}{r_t}\right)^2}$$

$$F_{cr} = \frac{(1.0)(1.0)\pi^2(204000)}{\left(\frac{4772}{112.1}\right)^2} = 1111MPa$$

$$AF = \left[\frac{0.85}{1-\frac{314.9}{1111}}\right] = 1.186$$

$$f_l = AF(f_{l1})$$

$$f_l = 1.186(101.5) = 120.4MPa$$

Apply the 1/3rd rule to determine the vertical bending capacity.

$\varphi_f = 1.00$

$$\phi_f F_n \geq f_{bu} + \frac{1}{3} f_l$$

$$\phi_f F_n = 357.4MPa$$

$$357.4MPa \geq 317.2 + \frac{1}{3}(120.4) = 357.3MPa$$

Therefore, the design is acceptable and the equivalent vertical bending moment is:

$$M_n = f_{bu} S_{xc}$$

$$M_n = 317.2\left(14.56x10^6\right) = 4618N - mm = 4618kN - m$$

Please refer to Table 4-18 to see how this capacity compares to the experimental measurement.

4.4 Summary of Predictions

Table 4-15 includes a summary of the predicted vertical bending capacities for each of the bending components as determined with the finite element model in Section 4.1, the Guide Specifications in Section 4.2, and the Unified Design Method in Section 4.3. The performance of each family of results is interpreted by the statistics in the middle and lower sections of this table. The middle section contains a statistical summary of the performance ratios for all bending components by prediction type. Because the B7 finite element prediction was shown to be very sensitive to geometric imperfections (White et al., 2001) that are not a part of this study, and the parameters of B7 fall outside the scope of either set of design provisions, the statistics in the lower section of Table 4-15 exclude the B7 performance data.

The statistics in either the middle or lower section show that the finite element model very accurately and consistently predicted the behavior of the physical experiments. The statistics also show that using either a 1^{st} order analysis or a 2^{nd} order analysis, the Unified Design Method predictions of the physical behavior are approximately 15% conservative but nearly as consistent as the finite element predictions. Finally, the statistics for the Guide Specification predictions indicate the poorest performance of the methods used. The Guide Specifications predicted the physical behavior approximately 30% conservative. However this family of data had a standard deviation of nearly 24% of the mean that indicates a poor consistency of calculation.

Component	Experiment	Finite Element Model		Guide Specifications		Unified Design Method			
						1st Order Analysis		2nd Order Analysis	
	kN-m	kN-m		kN-m		kN-m		kN-m	
	[a]	[b]	[b]/[a]	[c]	[c]/[a]	[d]	[d]/[a]	[e]	[e]/[a]
B1	4539	4574	1.01	2702	0.60	3910	0.86	3835	0.84
B2	4730	4775	1.01	2778	0.59	4022	0.85	3944	0.83
B3	4834	4778	0.99	2748	0.57	4006	0.83	3942	0.82
B4	4880	4718	0.97	2900	0.59	3967	0.81	4007	0.82
B5	5278	5255	1.00	4860	0.92	4621	0.88	4590	0.87
B6	6400	6258	0.98	5813	0.91	5512	0.86	5316	0.83
B7	3503	3993	1.14	2775	0.79	2919	0.83	2928	0.84
Including B7									
Average			1.01		0.71		0.85		0.84
Standard Deviation			0.06		0.16		0.02		0.02
Maximum			1.14		0.92		0.88		0.87
Minimum			0.97		0.57		0.81		0.82
Excluding B7									
Average			0.99		0.70		0.85		0.84
Standard Deviation			0.02		0.17		0.02		0.02
Maximum			1.01		0.92		0.88		0.87
Minimum			0.97		0.57		0.81		0.82

Table 4-15: Summary of Predicted Vertical Bending Moments

Chapter 5. Conclusions

5.1 Summary

Tests were conducted on seven steel I-girders that were horizontally curved. The objective of the tests was to determine the ultimate vertical bending capacity of these I-girders within the frame of a full-scale, single span, three-girder bridge. Each of these test girders or components had an approximate length of 7.62 m (25 ft) long, a radius along its web centerline of 63.63 m (208.75 ft), and a unique combination of flange slenderness, web slenderness and web stiffening. Ultimate capacity was defined as the point at which the component began to shed vertical bending moment to the remainder of the test frame. This condition was always associated with a lateral mechanism within the compression flange of the component. This lateral mechanism consisted of through thickness yielding and of a flange local buckle on the inside half of the compression flange. Both strong-axis (vertical) bending and torsion were additive at this location within the cross-section.

The experimental data from each component test were reduced using both the direct and indirect methods within the elastic range to prove the indirect technique. In the inelastic range, the indirect method of analysis was solely used. The physical test ultimate vertical bending capacities were determined using three sets of data; the installation strains, the self-weight strains and the applied-load effects generated with the indirect method.

In all cases, except for B6, first yield in the component was reached at mid-span on the inside tip of the compression flange. Although direct evidence does not exist, there is strong support that yield was first reached within the compression flange of B6 at the

cross-frame locations. However, this was shortly followed by yielding, and eventually the same half-flange local buckle at mid-span that was apparent in the remaining experiments.

The analytical predictions were produced using a finite element model that was fully nonlinear. This model was virtually constructed with ABAQUS general purpose software using the recommendations of White et al. (2001). The model was created using as-built plate dimensions and individual plate material behavior curves that were generated with the results of a large suite of material tests. Adjustments were also made to the model so that the effects of residual stress from fabrication would impact the results.

The predictor equations of both the AASHTO Guide Specifications and the Unified Design Method were also used to evaluate the vertical bending capacity of each of the bending components. The Guide Specifications requires the use of a 1st order analysis to determine capacity. The Unified Design Method can make use of results from either a 1st order or 2nd order analysis to determine capacity.

5.2 Findings

In general, all of the test results support the use of the Unified Design Method for the design of horizontally curved steel I-girder bridges. The Unified Design Method retains the strength of the Guide Specifications, which is the use of a first order analysis to determine vertical bending capacity of horizontally curved steel I-girders. This method also eliminates the step discontinuity that existed in the Guide Specifications between the behavior of compact and non-compact flanges. Finally, the Unified Design Method provisions reduce the design equations for straight girders as the radius of curvature becomes larger. This reduction brings cohesiveness to the entirety of the I-girder design

for steel bridges. For all of these reasons, the use of the Unified Design Method will be a constructive and positive change for the design consultant community and for bridge owners.

In addition, the experimental testing and analytical modeling yielded the following specific findings:

- Installation strains had a small but significant effect on the ultimate vertical bending capacity of these components. However, the installation process used in these experiments was difficult and not typical to bridge construction.
- Web slenderness and transverse stiffener spacing had a negligible effect on the ultimate vertical bending capacity of these sections.
- Compression flange slenderness did affect ultimate vertical bending capacity with normalized performance decreasing as slenderness rose. Also, post-peak behavior of the compact flanged sections was stable while the non-compact flanged sections experienced a dramatic drop in capacity.
- Predictions of a fully nonlinear finite element model that incorporated actual plate geometry and material properties agreed exceptionally well with the physical behavior for all specimens, with the exception of B7. The very slender flange of B7 was shown by others (White et al., 2001) to be sensitive to geometric imperfections that were not a part of this study.
- Regardless of whether a first or second order analysis was used to determine the vertical and lateral flange bending stress, the Unified Design Method provided a more accurate, consistent and robust determination of vertical bending capacity compared with the Guide Specifications.

5.3 Research Needs

Extensive experimental and analytical work have recently been conducted in the area of horizontally curved steel I-girders through the FHWA CSBRP. However, some topics still need further investigation.

- Hybrid girders. The use of horizontally curved hybrid sections is currently not permitted by either AASHTO Specification. These sections have become more widely used in straight girder design since the introduction of high performance steels. DOTs in several states have reported cost savings when using hybrid sections in negative moment regions. However, an experimental investigation of the effect of hybrid girder web yielding at the strength limit state has never been conducted.
- Cross-frame forces. Additional work performed on the experimental data generated during the CSBRP should result in guidance for the design of cross-frames for horizontally curved bridges. Design forces for these primary members are difficult to determine with the currently available tools.
- Fatigue issues. Moving to the Unified Design Method removes much of the conservatism from the stress ranges that are predicted using the Guide Specifications. The effects of a realized increase in stress range and any accompanying sectional distortion on fatigue need to be investigated.
- Systematic collapse. The test frame of the CSBRP was designed to withstand the load shedding of a bending component as it failed. However, the current practice will not necessarily result in such a design. An analytical investigation could determine

whether additional precautions are needed to prevent a systematic collapse due to progressive load shedding that begins with a failing exterior girder.

Appendix A. Steel Properties Data

Determining the mechanical properties of the materials used in structural experiments insures proper interpretation of the results and supports any analytical evaluation performed using the finite element method. The body of this dissertation deals exclusively with the bending component tests that were a part of the much larger Curved Steel Bridge Research Project (CSBRP). However, material property testing was conducted on samples taken from all steel plates used in the fabrication of the test-frame and the additional component test series; high-shear low-moment components and high-shear high-moment components. Also, tension testing was conducted on samples taken from the structural steel tubes that make up the individual members of the cross-frames and diaphragms. The results of the tension, compression and Young's modulus tests for the entire program are reported in this appendix. When appropriate, the family of data is reduced to those specific tests that affect the analysis of the bending component tests.

While a limited number of compression and Young's modulus tests were conducted, most material property tests performed were tension tests. Web plates were sampled at six locations, flange plates at three locations. Each coupon, or sample, produced as many as three individual results.

A.1 Plate Coupon Locations

Figure A-1 shows a plan view of the test-frame and the individual components. This figure also indicates the limits of the section marks used to identify where individual steel plates where used in fabricating each item. Figures A-2 through A-36 show the location

and orientation of each coupon with respect to either a corresponding girder flange or web.

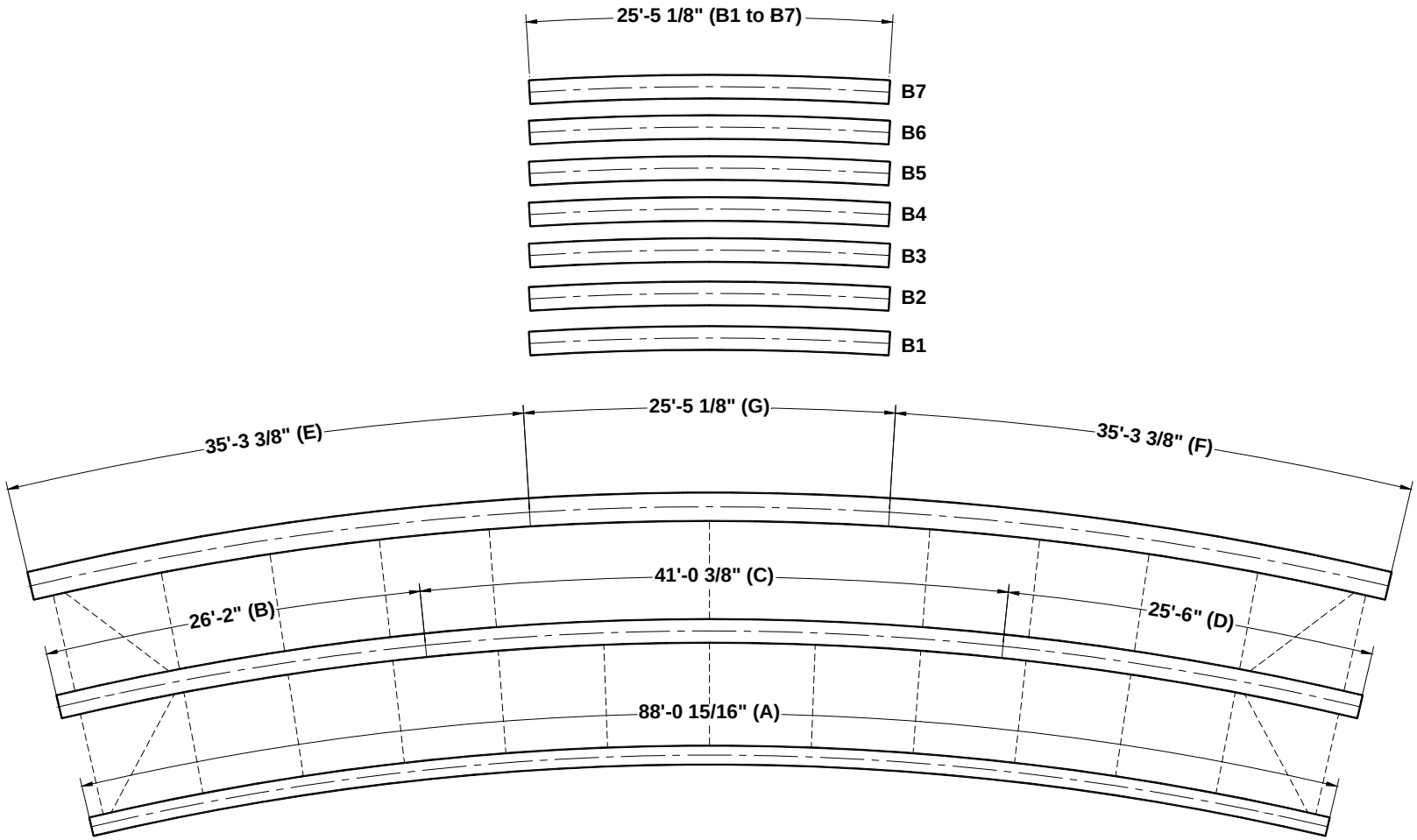

Figure A-1. Layout of Cutting Plates in Full Scale Test of Curve Girders Bridge (See Table 1 for Cutting Schedule)

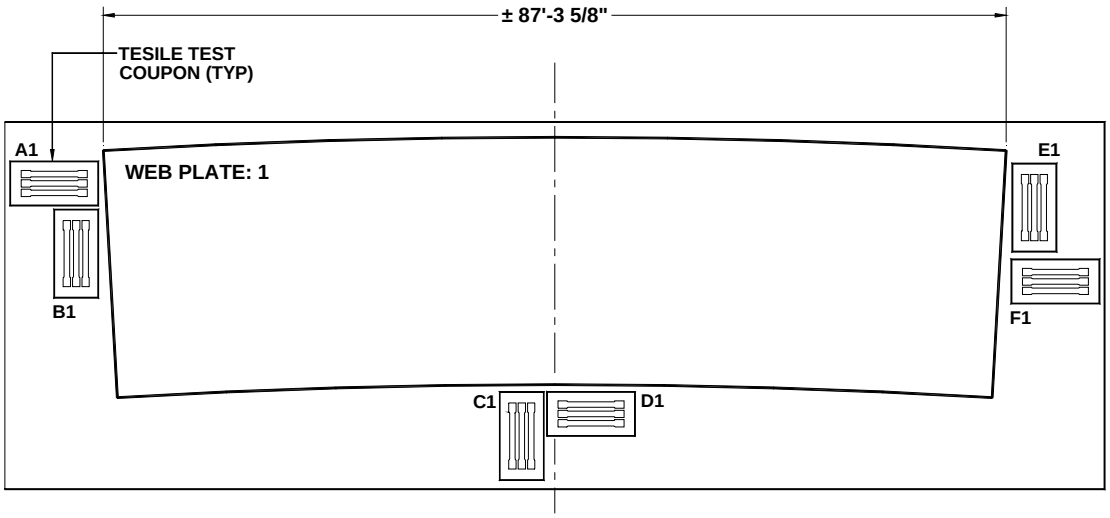

Figure A-2. Location of Tensile Coupons on Plate: 1

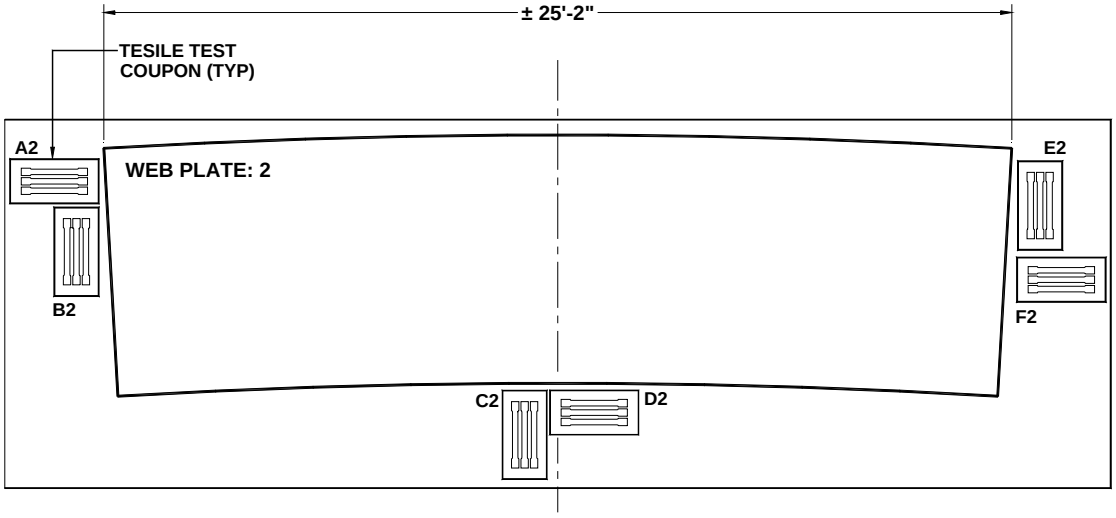

Figure A-3. Location of Tensile Coupons on Plate: 2

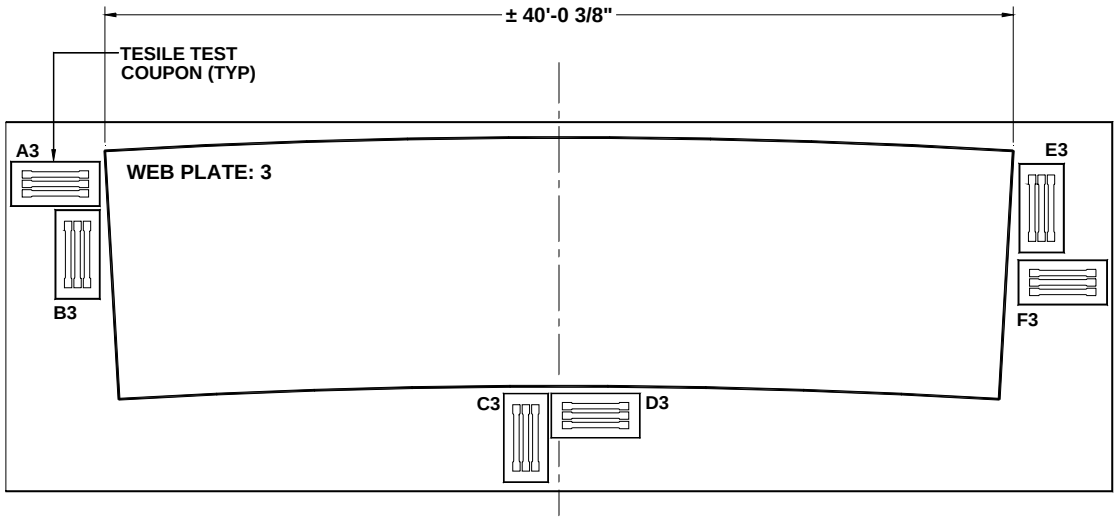

Figure A-4. Location of Tensile Coupons on Plate: 3

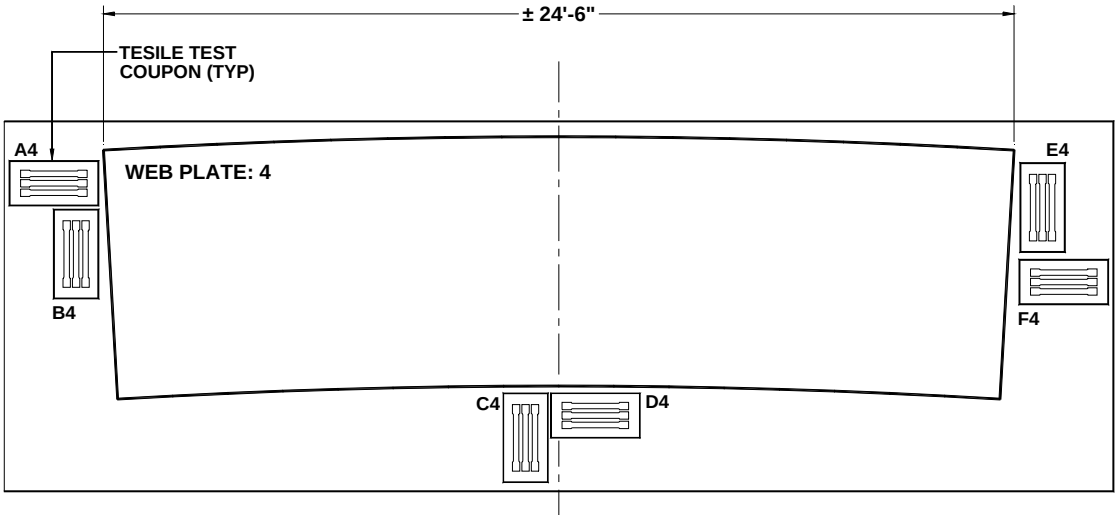

Figure A-5. Location of Tensile Coupons on Plate: 4

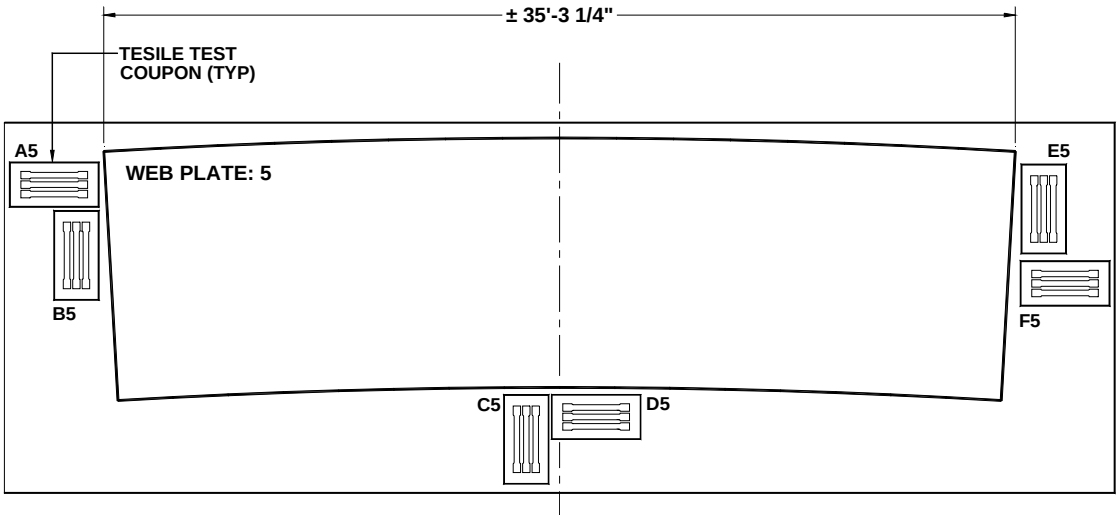

Figure A-6. Location of Tensile Coupons on Plate: 5

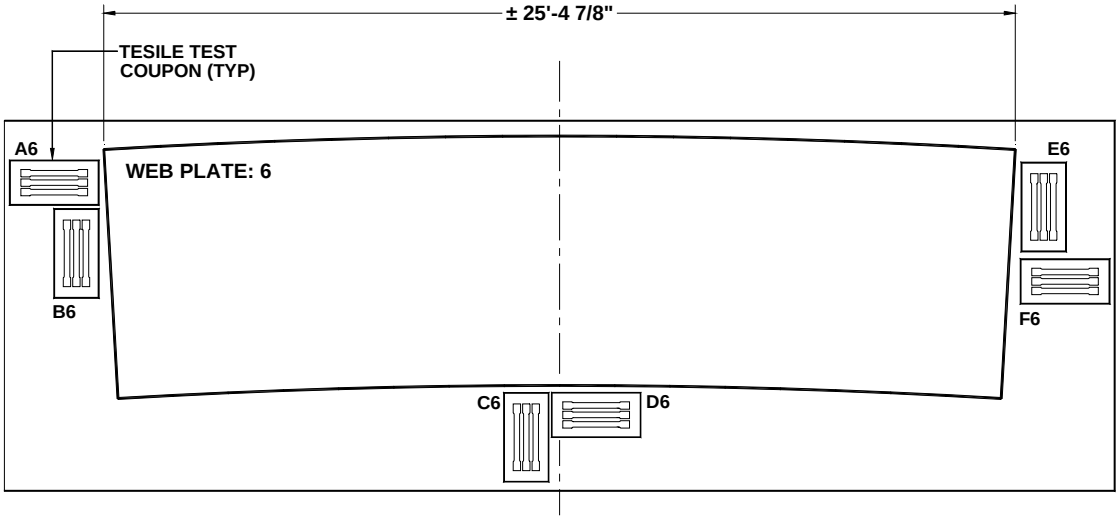

Figure A-7. Location of Tensile Coupons on Plate: 6

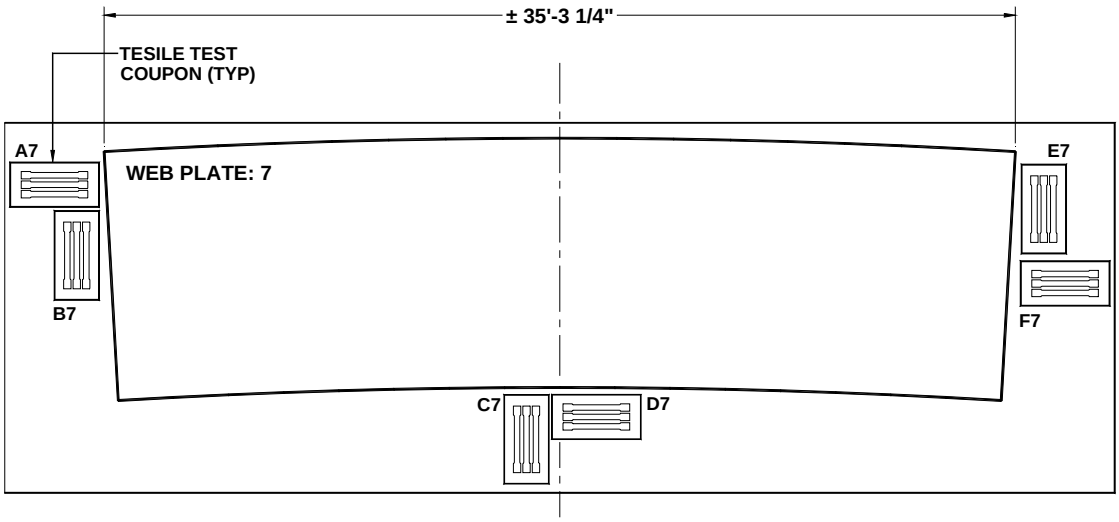

Figure A-8. Location of Tensile Coupons on Plate: 7

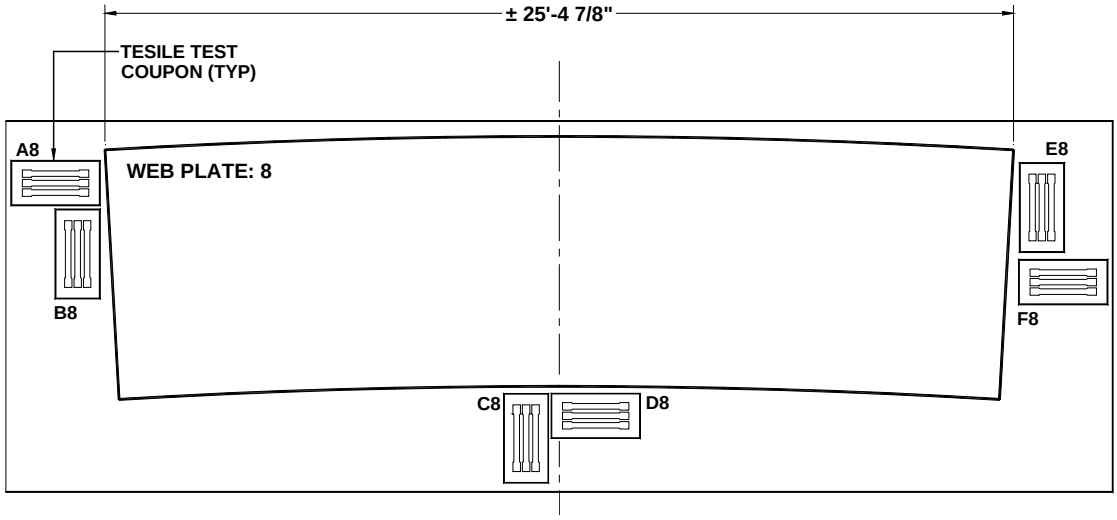

Figure A-9. Location of Tensile Coupons on Plate: 8

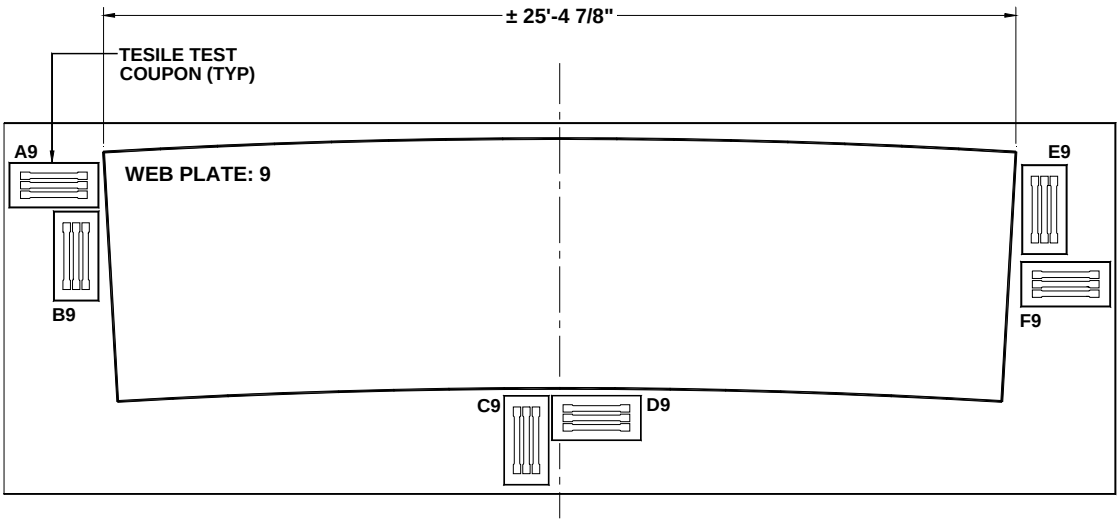

Figure A-10. Location of Tensile Coupons on Plate: 9

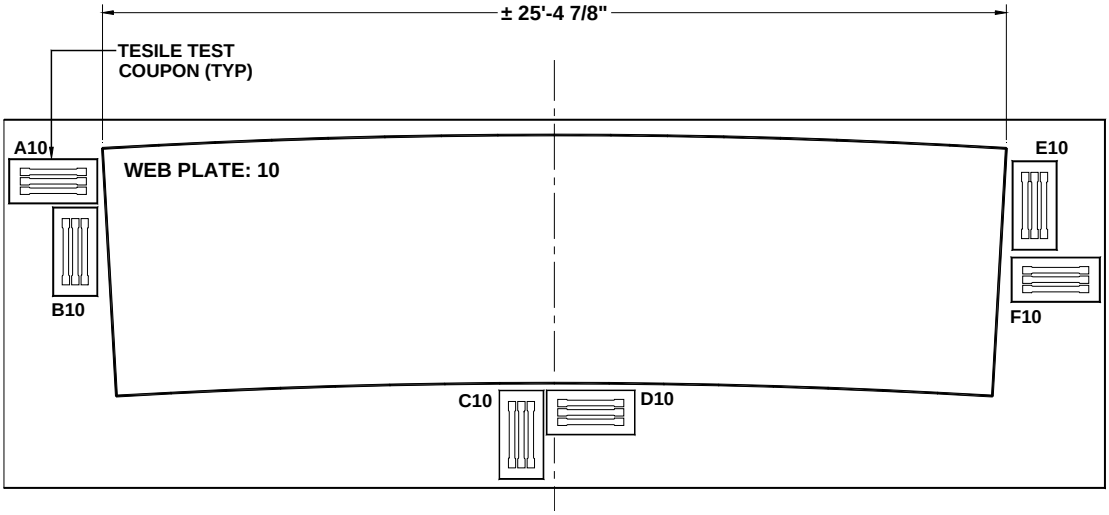

Figure A-11. Location of Tensile Coupons on Plate: 10

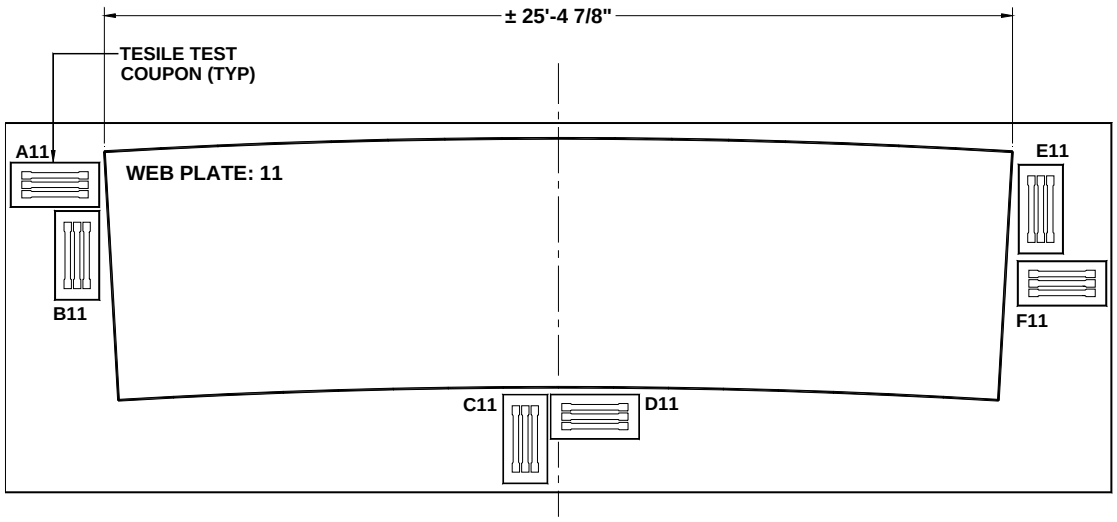

Figure A-12. Location of Tensile Coupons on Plate: 11

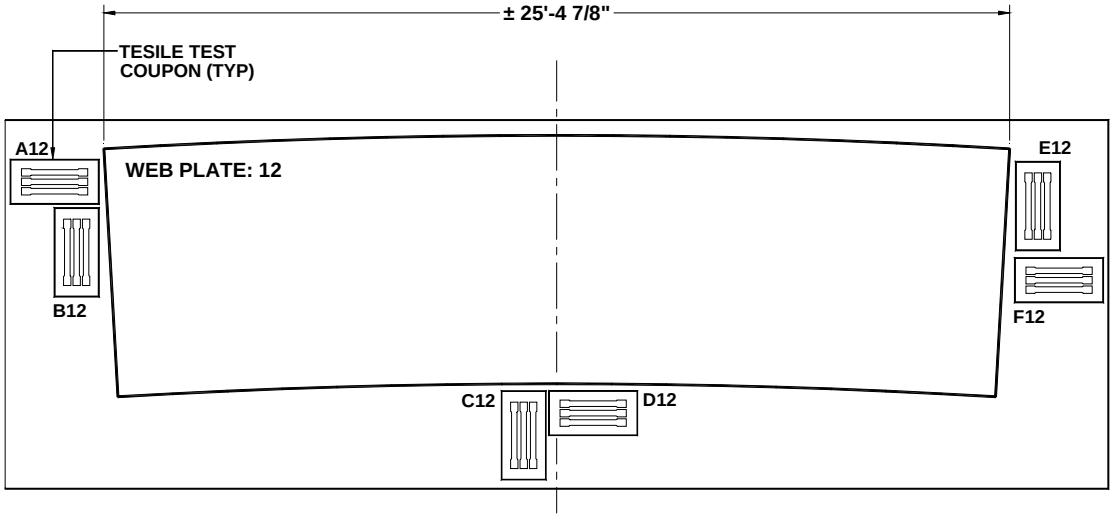

Figure A-13. Location of Tensile Coupons on Plate: 12

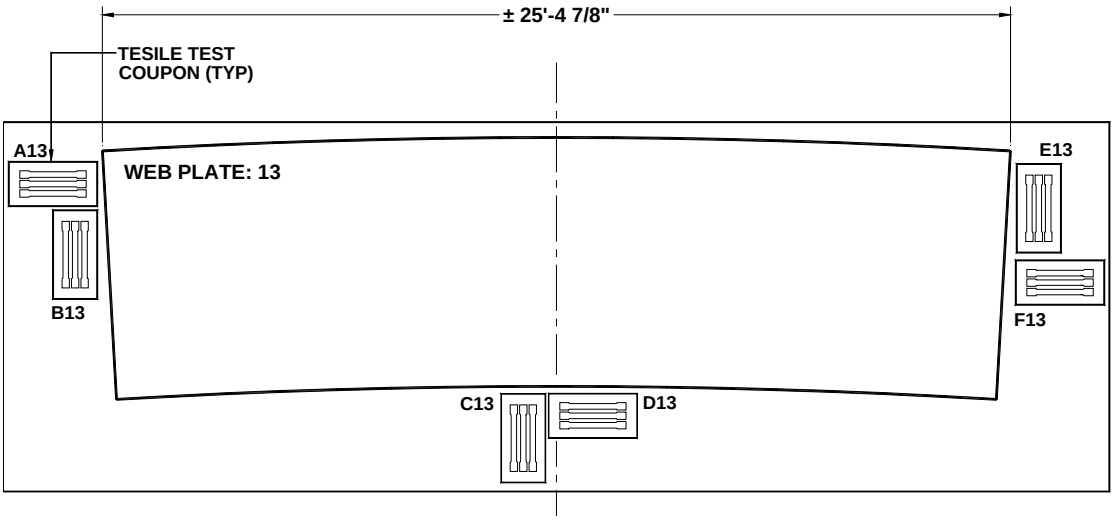

Figure A-14. Location of Tensile Coupons on Plate: 13

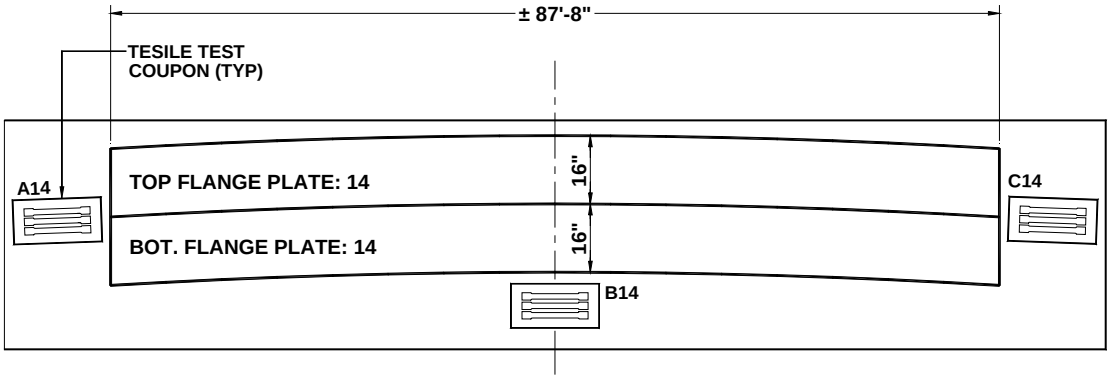

Figure A-15. Location of Tensile Coupons on Plate: 14

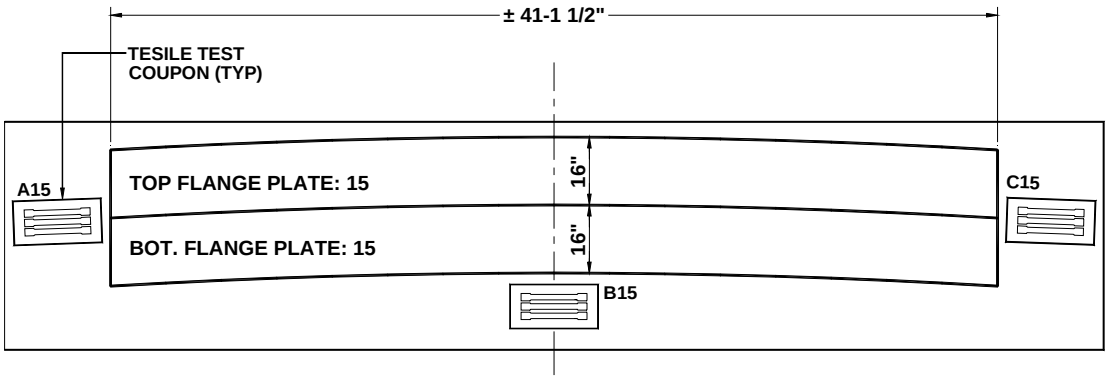

Figure A-16. Location of Tensile Coupons on Plate: 15

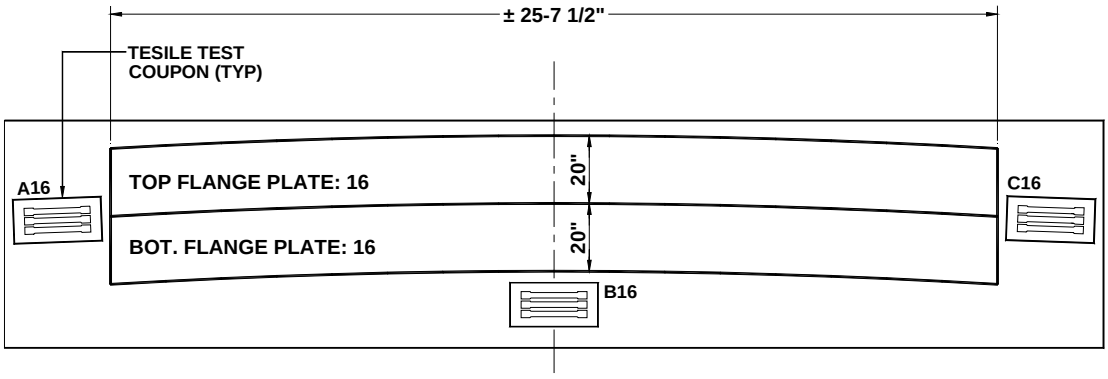

Figure A-17. Location of Tensile Coupons on Plate: 16

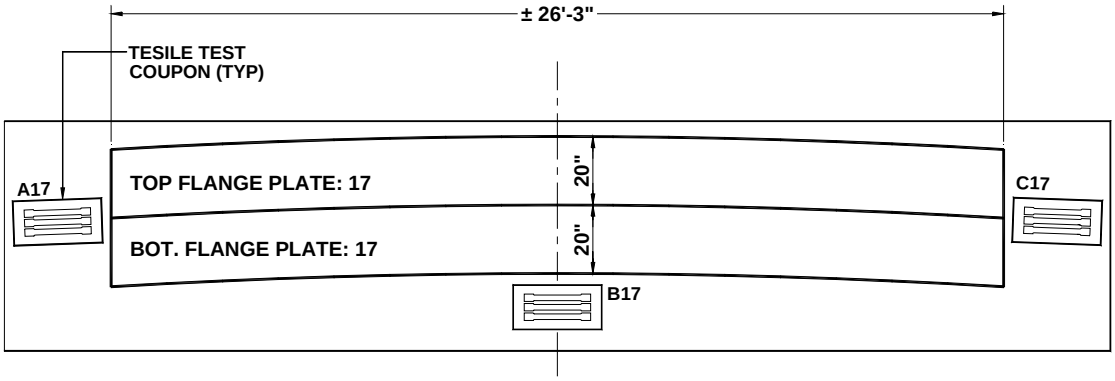

Figure A-18. Location of Tensile Coupons on Plate: 17

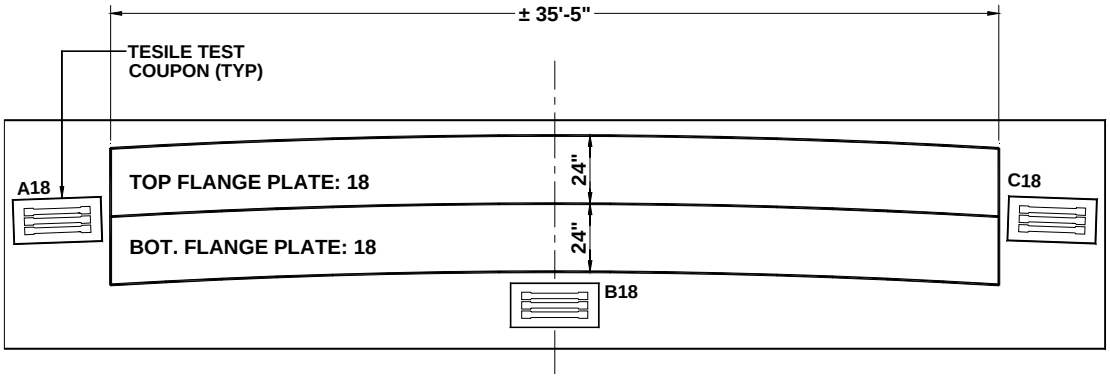

Figure A-19. Location of Tensile Coupons on Plate: 18

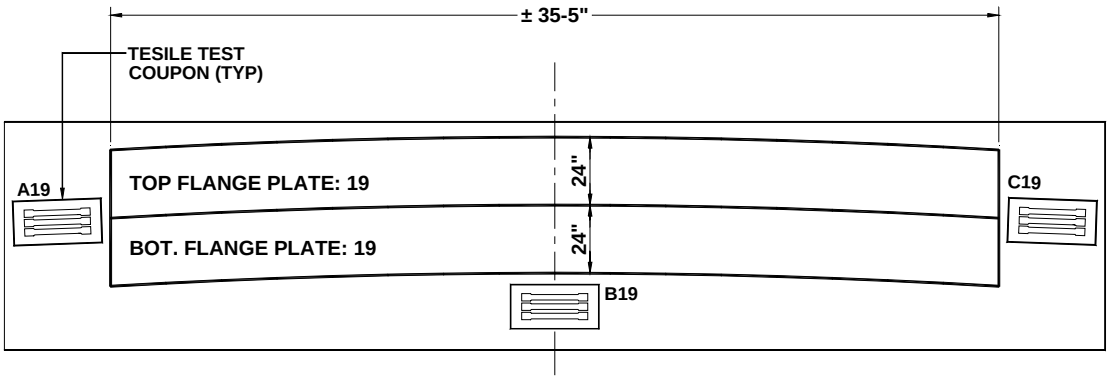

Figure A-20. Location of Tensile Coupons on Plate: 19

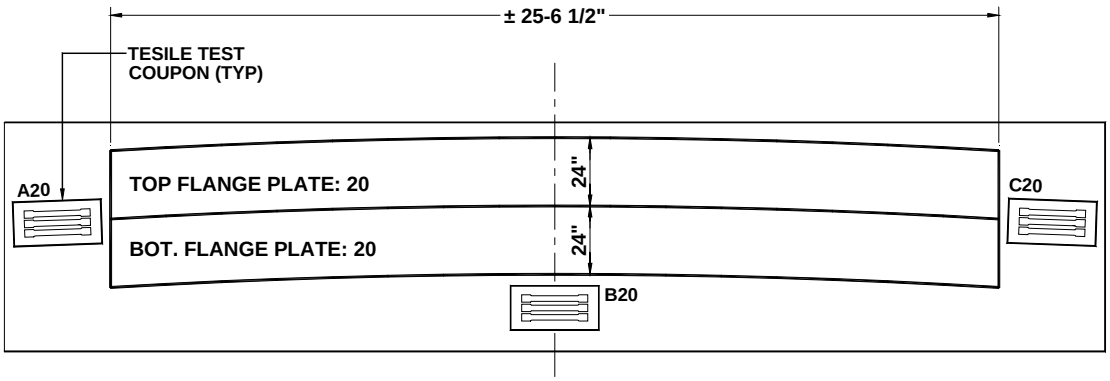

Figure A-21. Location of Tensile Coupons on Plate: 20

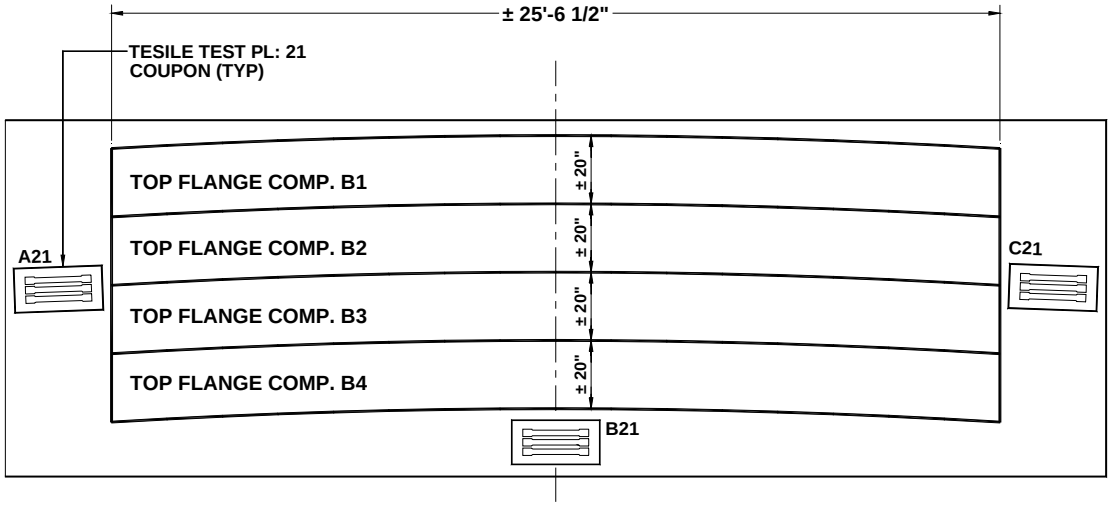

Figure A-22. Location of Tensile Coupons on Plate: 21

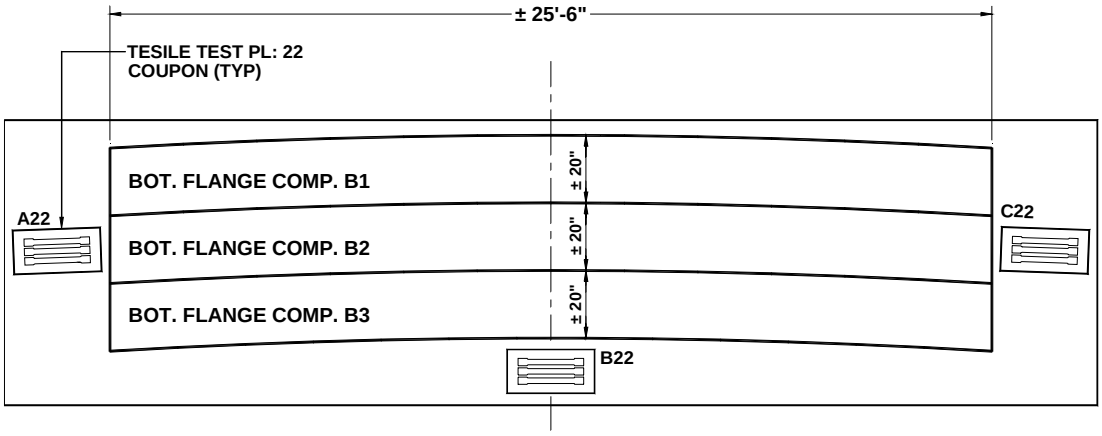

Figure A-23. Location of Tensile Coupons on Plate: 22

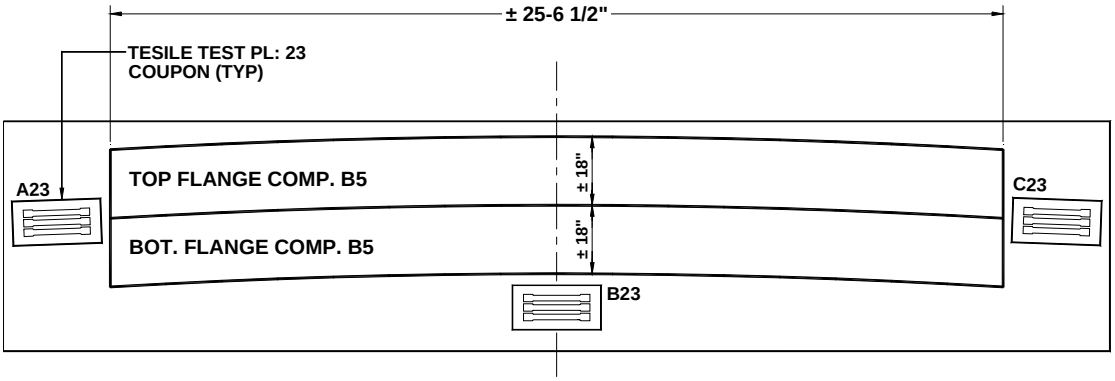

Figure A-24. Location of Tensile Coupons on Plate: 23

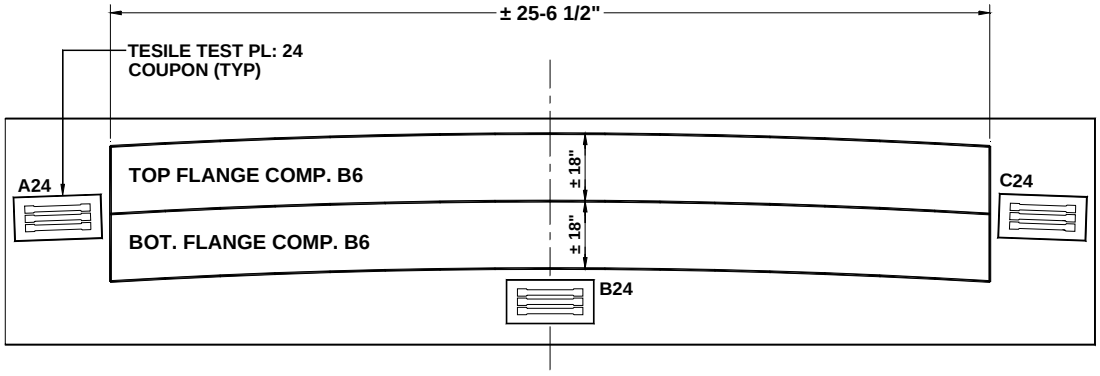

Figure A-25. Location of Tensile Coupons on Plate: 24

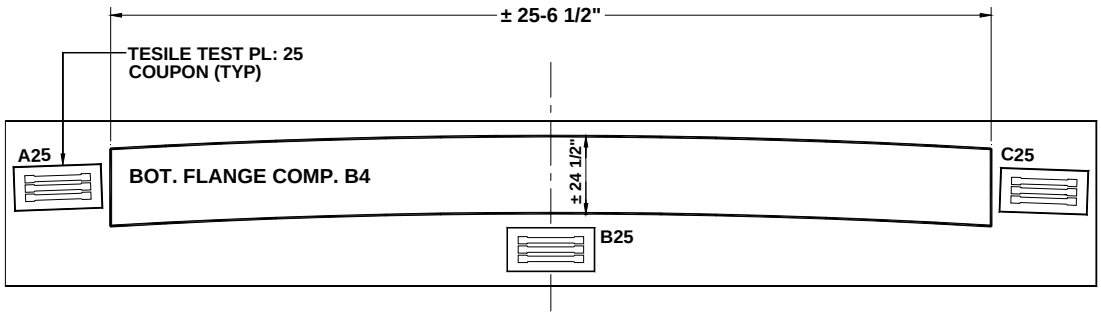

Figure A-26. Location of Tensile Coupons on Plate: 25

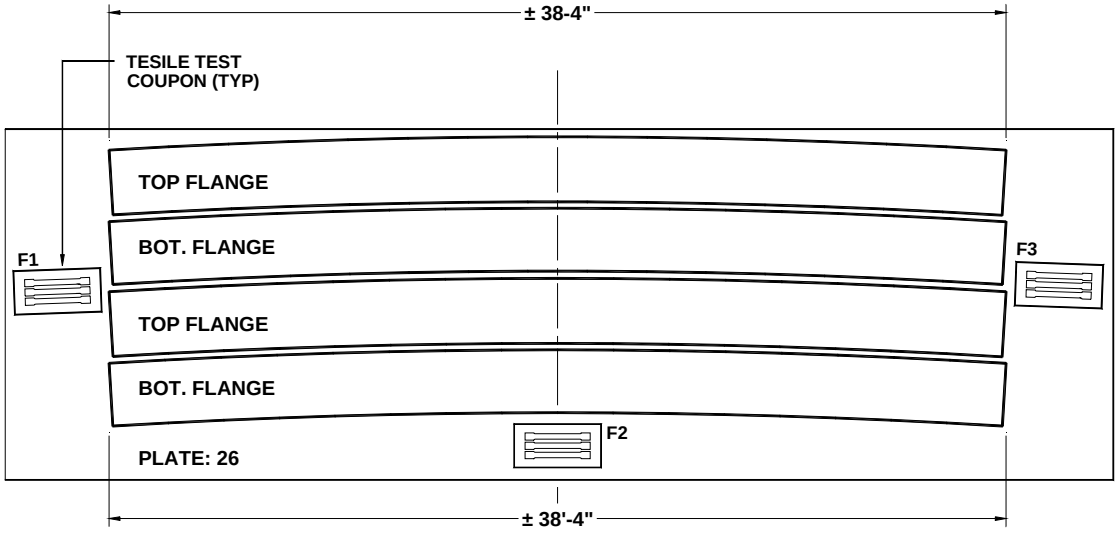

Figure A-27. Location of Tensile Coupons on Plate: 26

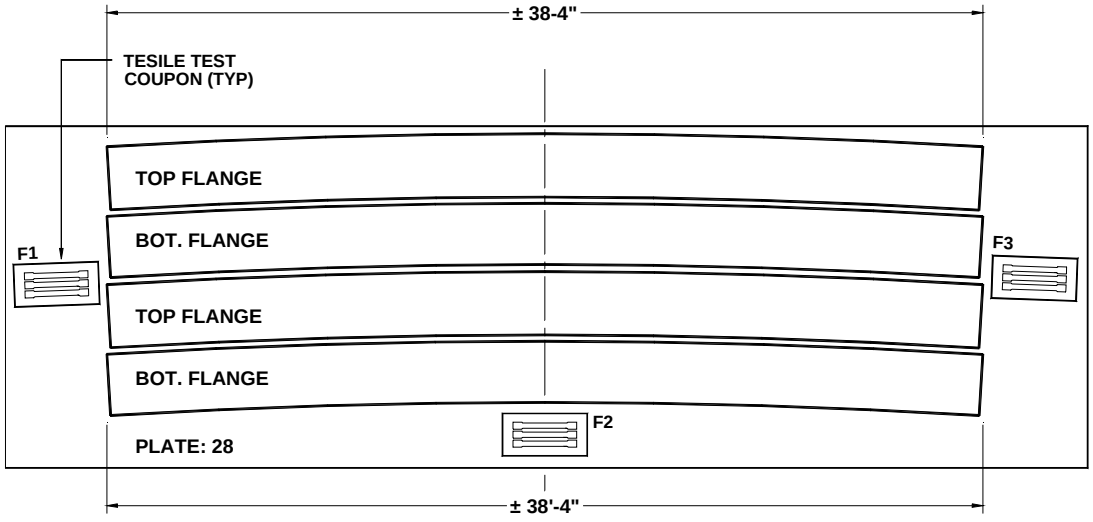

Figure A-28. Location of Tensile Coupons on Plate: 28

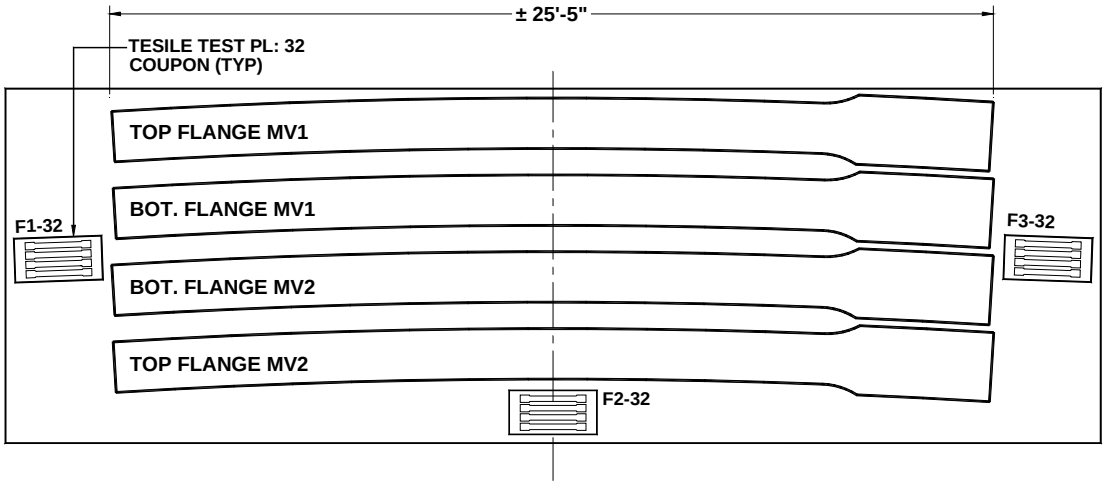

Figure A-29. Location of Tensile Coupons on Plate: 32

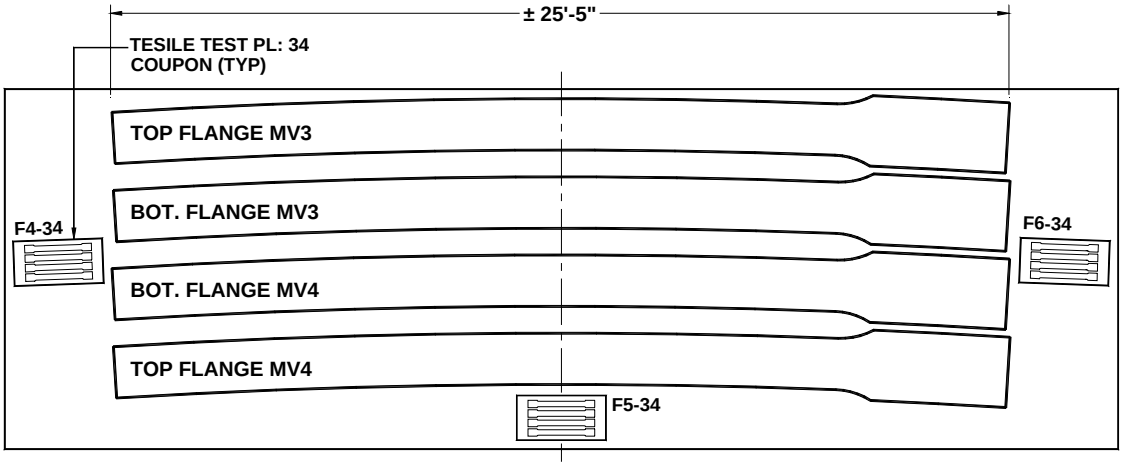

Figure A-30. Location of Tensile Coupons on Plate: 34

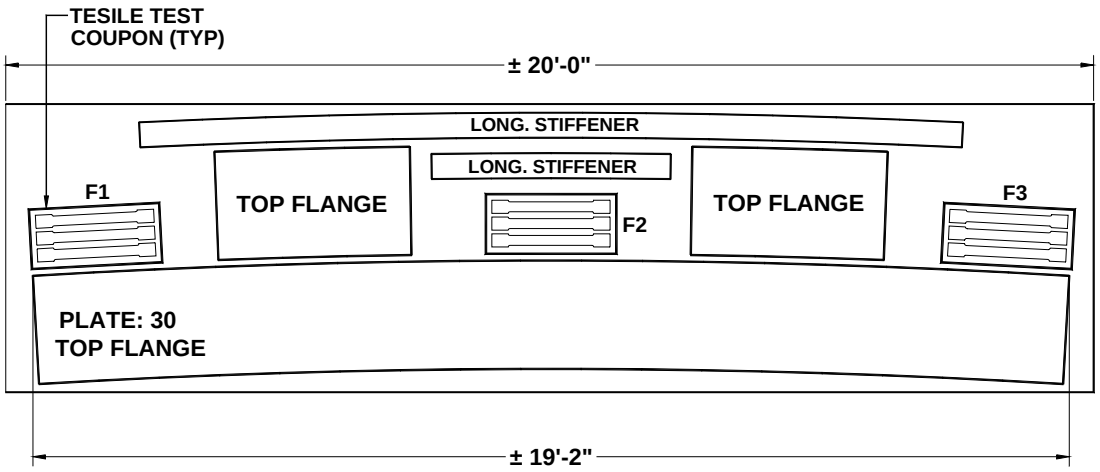

Figure A-31. Location of Tensile Coupons on Plate: 30

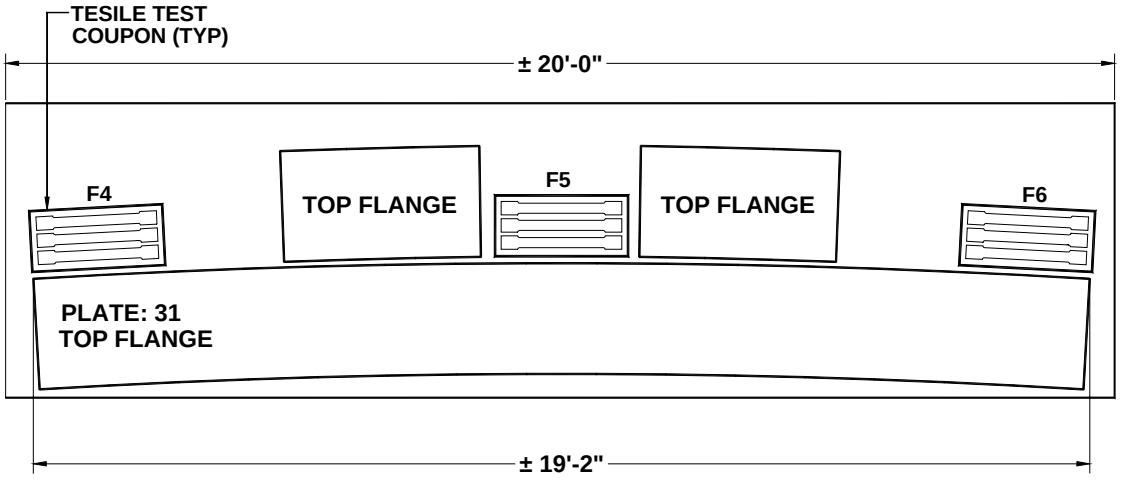

Figure A-32. Location of Tensile Coupons on Plate: 31

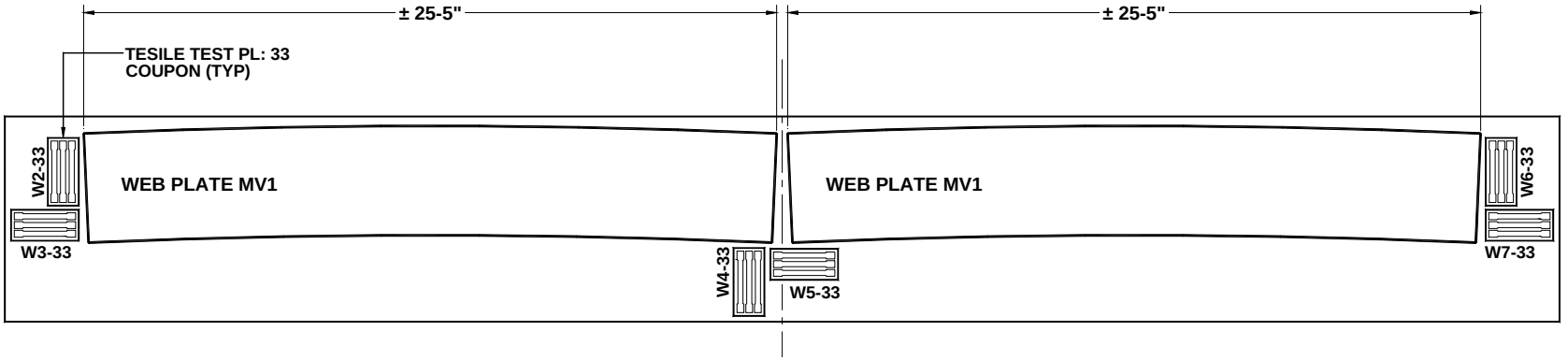

Figure A-33. Location of Tensile Coupons on Plate: 33

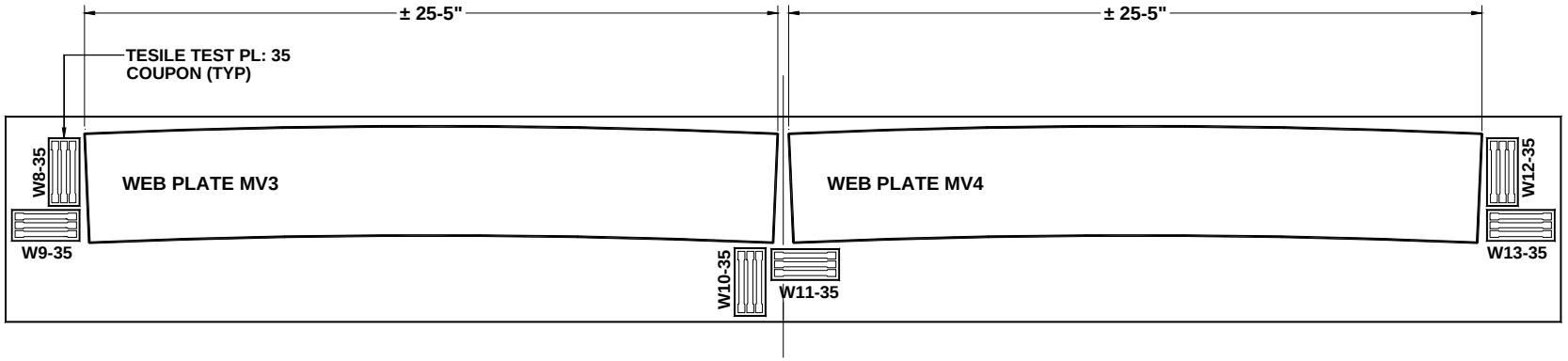

Figure A-34. Location of Tensile Coupons on Plate: 35

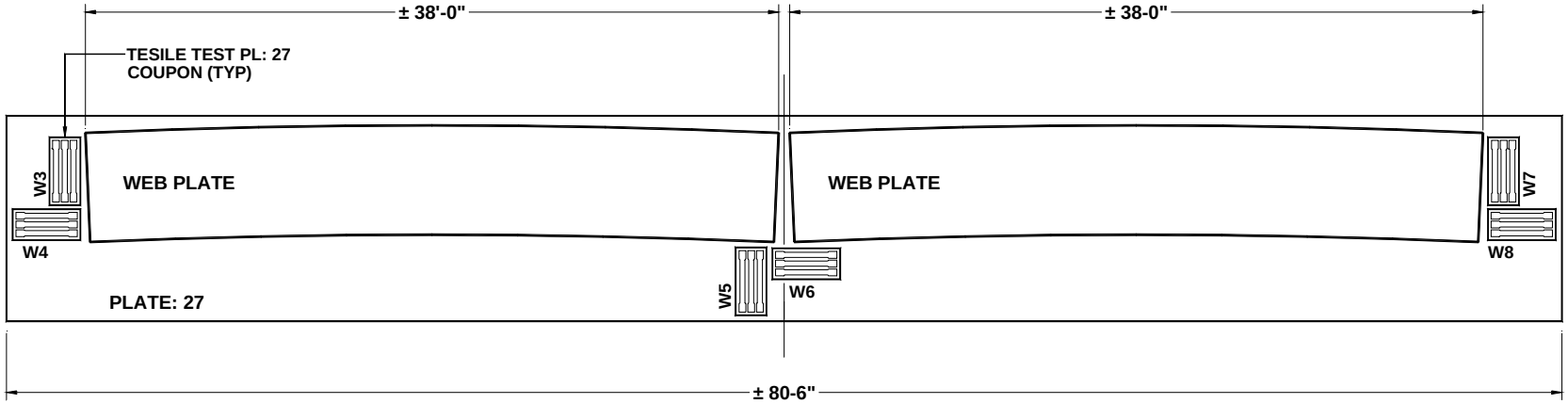

Figure A-35. Location of Tensile Coupons on Plate: 27

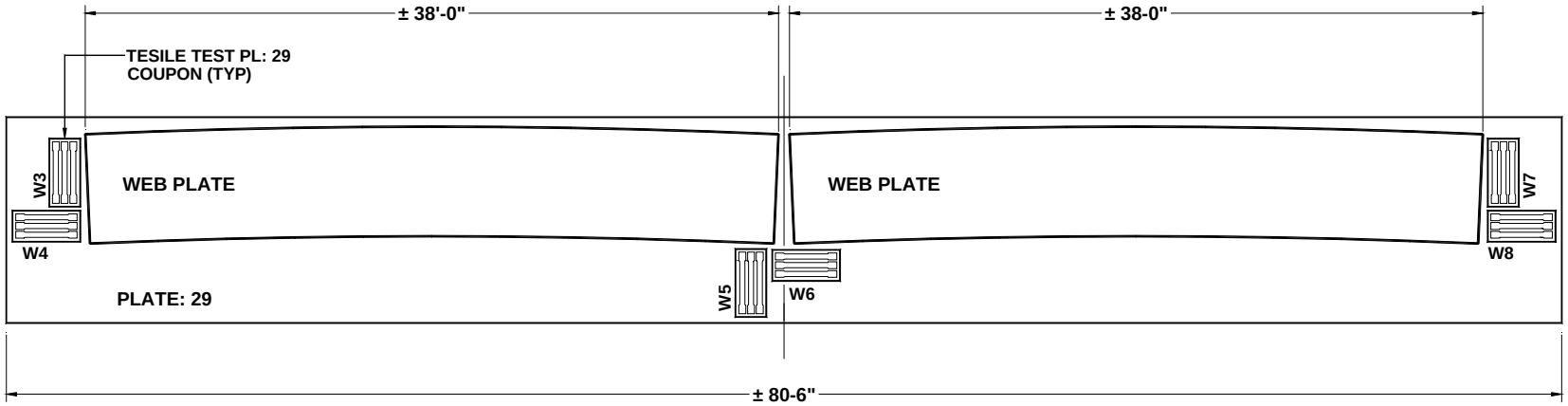

Figure A-36. Location of Tensile Coupons on Plate: 29

A.2 Tension Testing

The tensile tests were performed in accordance with the ASTM E8, *Standard Test Methods for Tension Testing of Metallic Materials*. In most cases, the E8 procedures were supplemented with the Structural Stability Research Council's (SSRC) *Technical Memorandum No. 7: Tension Testing* in order to generate consistent and uniform static yield strength levels. The E8 methods and procedures are designed to specifically determine yield strength, yield point elongation, and tensile strength. In this document the definition of these terms is consistent with those definitions provided in the E8 Standard.

With few exceptions, standard plate-type rectangular test specimens of full plate thickness were used for the tension testing. These specimens are 450mm (18 in.) long, have a reduced section of 225mm (9 in.) by 38mm (1½ in.), and have a 200mm (8 in.) gage length. A maximum taper of 0.15% was used to reduce the cross-sectional area of the specimen to a minimum at the middle of the gage length. This taper is permitted by E8 to insure that rupture occurs within the gage length. The E8 Standard contains a complete set of dimensions for the rectangular tension test specimens.

The remainder of the tension testing was conducted on standard round specimens. These specimens (referred to as Specimen 1 in the E8 Standard) are 125mm (5 in.) long, have a reduced section of approximately 75mm (3 in.), a radius of 12.7mm (½ in.), and a 50mm (2 in.) gage length. Only three (3) tension tests in this program utilized standard round specimens. These test specimens were machined from Plate 34 and are identified as 34-F6-1-1R, 34-F6-1-2R and 34-F6-1-3R.

The SSRC procedure requires that once a specimen reaches yield as defined by a 0.2% elastic modulus offset, the testing should be interrupted and a constant strain

maintained until the load stabilizes but for no longer than 5 minutes. This interruption process should occur at least two more times at 0.005 increments of strain prior to the onset of strain hardening. Once strain hardening of the material begins, the interruption processed should be terminated. Completion of this process will produce the necessary data to determine static yield strength for the material tested by one of two methods outlined in the SSRC memorandum.

The steels used for this program had nominal yield strengths between 345 MPa (50 ksi) and 485 MPa (70 ksi). The ASTM A572 Gr. 345 steel generally exhibited a well defined yield strength and extended yield plateau prior to the onset of strain hardening during tension testing. The ASTM A852 steel generally produced a round-house curve without a well defined yield point.

Tension tests were conducted on 292 specimens taken from 34 steel plates and 17 specimens taken from 3 structural steel tubes. This appendix focuses on the plate steel tension tests. Tables A-1 through A-34 summarize the tension test results for all steel plates used in this program.

A summary of the structural steel tube tension test results is contained in Tables A-35 through A-37. These results have been previously discussed by Linzell (1999).

Plate Number	Section Mark	Location	Steel Type	Nominal Strength (MPa)	Nominal Thickness (mm)	Mill Certificate Properties F_y (MPa)	F_u (MPa)	Elongation (%)
1	A (G1)	Web	A572	345	11.113	390	540	24

Specimen ID	Young's Mod.	Upper Yield		Lower Yield		0.2% Offset Yield		Static Yield		Strain Hardening			Tensile Strength		Gage Length
	E (GPa)	ε (%)	σ (MPa)	ε (%)	σ (MPa)	ε (%)	σ (MPa)	ε (%)	σ (MPa)	ε_{st} (%)	$\varepsilon_{apparent}$ (%)	E_{st} (GPa)	ε (%)	σ (MPa)	(mm)
	Tension Tests (L direction: longitudinal axis in the direction of rolling)														
A1-2	205.4	0.191	405.8	0.832	387.4	0.392	394.2	0.388	386.0	1.811	2.041	2.701	12.25	515.1	203.2
A1-3	205.5	0.191	405.2	0.184	386.1	0.391	391.8	0.388	385.6	1.754	2.118	2.602	12.13	513.4	203.2
D1-1	213.7	0.195	401.0	0.333	389.0	0.384	392.1	0.378	380.1	1.086	1.466	3.102	15.58	531.4	50.8
D1-2	218.7	0.188	403.9	0.261	384.8	0.379	388.5	0.374	377.0	1.120	1.405	3.121	15.47	530.5	50.8
F1-1	204.3	0.165	390.4	0.270	381.1	0.399	385.4	0.392	371.3	1.213	1.412	3.265	15.87	524.3	50.8
F1-2	203.8	0.165	387.9	0.347	376.2	0.386	379.6	0.381	370.1	1.087	1.336	3.385	17.31	522.2	50.8
	Tension Tests (LT direction: longitudinal axis normal to the direction of rolling)														
B1-2	204.6	0.158	397.1	0.221	387.7	0.389	391.7	0.383	378.0	1.180	1.788	2.749	16.11	526.2	50.8
C1-1	199.3	0.175	395.2	0.253	384.2	0.394	388.6	0.388	376.2	0.960	1.474	2.616	16.26	526.1	50.8
C1-2	187.0	0.170	393.1	0.253	379.6	0.398	381.5	0.394	374.0	0.987	1.483	2.951	15.75	525.8	50.8
E1-1	204.8	0.174	394.4	0.210	379.5	0.395	382.1	0.388	366.8	0.907	1.398	3.193	16.44	525.2	50.8
E1-2	185.5	0.175	391.3	0.251	381.3	0.395	380.2	0.391	373.2	0.975	1.427	2.844	17.28	524.9	50.8
Statistics															
Mean	203.0	0.177	396.8	0.310	383.4	0.391	386.9	0.386	376.2	1.189	1.577	2.957	15.50	524.1	
Standard Deviation	9.8	0.012	6.3	0.179	4.1	0.006	5.3	0.006	6.1	0.308	0.275	0.273	1.74	5.5	
Range	33.2	0.037	17.9	0.647	12.7	0.020	14.6	0.020	19.2	0.904	0.782	0.782	5.18	18.0	
Minimum	185.5	0.158	387.9	0.184	376.2	0.379	379.6	0.374	366.8	0.907	1.336	2.602	12.13	513.4	
Maximum	218.7	0.195	405.8	0.832	389.0	0.399	394.2	0.394	386.0	1.811	2.118	3.385	17.31	531.4	
Count	11	11	11	11	11	11	11	11	11	11	11	11	11	11	

Table A-1: Summary of Plate 1 Tension Test Results

Plate Number	Section Mark	Location	Steel Type	Nominal Strength (MPa)	Nominal Thickness (mm)	Mill Certificate Properties		
						F_y (MPa)	F_u (MPa)	Elongation (%)
2	B (G2)	Web	A852	485	12.700	614	722	26

Specimen ID	Young's Mod.	0.2% Offset Yield		Static Yield		Strain Hardening			Tensile Strength		Gage Length
	E (GPa)	ε (%)	σ (MPa)	ε (%)	σ (MPa)	ε_{st} (%)	$\varepsilon_{apparent}$ (%)	E_{st} (GPa)	ε (%)	σ (MPa)	(mm)
	Tension Tests (L direction: longitudinal axis in the direction of rolling)										
A2-1	196.5	0.519	669.1	0.515	661.9	0.519	0.519	4.859	6.556	765.4	203.2
A2-2	202.1	0.532	675.4	0.529	668.3	0.532	0.532	3.971	6.541	765.3	203.2
F2-1	205.2	0.540	700.4	0.533	686.1	0.540	0.540	1.653	6.065	774.2	50.8
F2-2	208.8	0.518	662.7	0.509	644.4	0.518	0.518	3.235	6.815	755.1	50.8
	Tension Tests (LT direction: longitudinal axis normal to the direction of rolling)										
B2-1	202.4	0.536	684.8	0.529	670.3	0.521	0.690	1.579	8.234	768.3	50.8
B2-2	205.3	0.520	699.4	0.513	685.5	0.424	0.597	1.275	7.929	778.0	50.8
E2-1	193.4	0.559	697.2	0.551	681.7	0.769	0.781	1.232	8.033	772.7	50.8
E2-2	207.3	0.537	705.6	0.527	683.9	0.552	0.688	1.314	7.487	780.6	50.8
	Statistics										
Mean	202.6	0.533	686.8	0.526	672.8	0.547	0.608	2.390	7.21	770.0	
Standard Deviation	5.3	0.014	16.2	0.013	14.6	0.098	0.100	1.427	0.82	8.2	
Range	15.4	0.041	42.9	0.042	41.7	0.345	0.263	3.627	2.17	25.5	
Minimum	193.4	0.518	662.7	0.509	644.4	0.424	0.518	1.232	6.06	755.1	
Maximum	208.8	0.559	705.6	0.551	686.1	0.769	0.781	4.859	8.23	780.6	
Count	8	8	8	8	8	8	8	8	8	8	

Table A-2: Summary of Plate 2 Tension Test Results

Plate Number	Section Mark	Location	Steel Type	Nominal Strength (MPa)	Nominal Thickness (mm)	Mill Certificate Properties		
						F_y (MPa)	F_u (MPa)	Elongation (%)
3	C (G2)	Web	A852	485	12.700	535	672	36

Specimen ID	Young's Mod.	0.2% Offset Yield		Static Yield		Strain Hardening			Tensile Strength		Gage Length
	E (GPa)	ε (%)	σ (MPa)	ε (%)	σ (MPa)	ε_{st} (%)	$\varepsilon_{apparent}$ (%)	E_{st} (GPa)	ε (%)	σ (MPa)	(mm)
	Tension Tests (L direction: longitudinal axis in the direction of rolling)										
A3-1	206.6	0.566	758.8	0.554	733.4	0.566	0.566	7.938	4.285	855.6	203.2
A3-2	202.6	0.589	796.0	0.577	772.1	0.589	0.589	8.058	3.823	883.5	203.2
D3-1	198.6	0.573	743.8	0.568	733.9	0.573	0.573	10.754	3.618	849.3	203.2
D3-2	201.3	0.595	798.3	0.588	784.6	0.595	0.595	7.279	4.925	891.0	203.2
F3-1	199.9	0.571	747.8	0.564	733.3	0.571	0.571	10.296	3.360	849.1	203.2
F3-2	202.4	0.542	736.9	0.534	720.6	0.542	0.542	7.300	4.724	845.3	203.2
	Tension Tests (LT direction: longitudinal axis normal to the direction of rolling)										
B3-1	204.2	0.568	754.1	0.561	739.7	0.568	0.568	10.491	2.812	847.3	203.2
B3-2	202.6	0.554	764.3	0.546	747.4	0.554	0.554	9.602	3.267	857.5	203.2
C3-1	204.5	0.579	776.0	0.571	759.9	0.579	0.579	8.225	4.588	877.0	203.2
C3-2	202.9	0.593	780.7	0.586	767.6	0.593	0.593	7.507	4.060	870.8	203.2
E3-1	198.8	0.560	715.2	0.553	700.3	0.560	0.560	7.915	4.313	821.3	203.2
E3-2	199.9	0.566	733.5	0.558	717.4	0.566	0.566	9.497	3.085	831.4	203.2
	Statistics										
Mean	202.0	0.571	758.8	0.563	742.5	0.571	0.571	8.739	3.905	856.6	
Standard Deviation	2.4	0.016	25.5	0.016	24.7	0.016	0.016	1.302	0.686	20.7	
Range	8.0	0.053	83.2	0.055	84.2	0.053	0.053	3.475	2.113	69.7	
Minimum	198.6	0.542	715.2	0.534	700.3	0.542	0.542	7.279	2.812	821.3	
Maximum	206.6	0.595	798.3	0.588	784.6	0.595	0.595	10.754	4.925	891.0	
Count	12	12	12	12	12	12	12	12	12	12	

Table A-3: Summary of Plate 3 Tension Test Results

Plate Number	Section Mark	Location	Steel Type	Nominal Strength (MPa)	Nominal Thickness (mm)	Mill Certificate Properties		
						F_y (MPa)	F_u (MPa)	Elongation (%)
4	D (G2)	Web	A852	485	12.700	614	722	26

Specimen ID	Young's Mod.	0.2% Offset Yield		Static Yield		Strain Hardening			Tensile Strength		Gage Length
	E (GPa)	ε (%)	σ (MPa)	ε (%)	σ (MPa)	ε_{st} (%)	$\varepsilon_{apparent}$ (%)	E_{st} (GPa)	ε (%)	σ (MPa)	(mm)
	Tension Tests (L direction: longitudinal axis in the direction of rolling)										
A4-1	205.5	0.521	681.7	0.514	666.9	0.521	0.521	4.946	5.721	770.3	203.2
A4-2	198.2	0.543	679.7	0.536	665.3	0.543	0.543	3.915	5.872	768.7	203.2
D4-1	197.4	0.554	684.0	0.547	671.0	0.554	0.554	3.589	6.413	771.1	203.2
D4-2	193.0	0.570	677.5	0.563	663.9	0.570	0.570	2.719	6.940	765.4	203.2
F4-1	200.7	0.535	675.3	0.529	663.5	0.535	0.535	3.737	5.847	762.0	203.2
F4-2	201.4	0.542	692.3	0.539	684.6	0.542	0.542	3.955	6.873	778.3	203.2
	Tension Tests (LT direction: longitudinal axis normal to the direction of rolling)										
B4-1	198.7	0.535	698.9	0.528	683.7	0.535	0.535	2.624	6.659	781.0	203.2
B4-2	200.8	0.543	707.6	0.537	695.4	0.543	0.543	2.033	6.924	786.5	203.2
C4-1	202.3	0.511	632.4	0.502	613.8	0.511	0.511	4.878	5.449	724.4	203.2
C4-2	194.3	0.535	651.9	0.530	642.9	0.535	0.535	4.075	7.290	751.1	203.2
E4-1	200.9	0.549	699.5	0.542	686.4	0.549	0.549	2.660	7.087	781.7	203.2
E4-2	202.0	0.556	715.9	0.550	704.8	0.556	0.556	2.434	7.024	796.1	203.2
Statistics											
Mean	199.6	0.541	683.1	0.535	670.2	0.541	0.541	3.464	6.508	769.7	
Standard Deviation	3.5	0.016	23.2	0.016	24.4	0.016	0.016	0.959	0.627	18.6	
Range	12.5	0.058	83.6	0.060	91.0	0.058	0.058	2.914	1.841	71.7	
Minimum	193.0	0.511	632.4	0.502	613.8	0.511	0.511	2.033	5.449	724.4	
Maximum	205.5	0.570	715.9	0.563	704.8	0.570	0.570	4.946	7.290	796.1	
Count	12	12	12	12	12	12	12	12	12	12	

Table A-4: Summary of Plate 4 Tension Test Results

Plate Number	Section Mark	Location	Steel Type	Nominal Strength (MPa)	Nominal Thickness (mm)	Mill Certificate Properties F_y (MPa)	F_u (MPa)	Elongation (%)
5	E (G3)	Web	A572	345	12.700	409	541	42

Specimen ID	Young's Mod.	Upper Yield		Lower Yield		0.2% Offset Yield		Static Yield		Strain Hardening			Tensile Strength		Gage Length
	E (GPa)	ε (%)	σ (MPa)	ε (%)	σ (MPa)	ε (%)	σ (MPa)	ε (%)	σ (MPa)	ε_{st} (%)	$\varepsilon_{apparent}$ (%)	E_{st} (GPa)	ε (%)	σ (MPa)	(mm)
	Tension Tests (L direction: longitudinal axis in the direction of rolling)														
A5-1	199.9	0.200	408.0	0.847	395.6	0.400	398.8	0.398	395.1	1.092	1.343	3.261	12.26	537.2	203.2
A5-2	202.4	0.207	417.3	0.653	396.2	0.397	398.5	0.395	394.2	1.081	1.363	3.168	12.06	536.0	203.2
D5-1	215.0	0.185	403.7	0.247	384.5	0.379	385.1	0.374	373.9	1.248	1.446	4.040	15.97	528.1	50.8
D5-2	205.6	0.172	402.2	0.340	385.0	0.387	388.5	0.381	375.0	1.050	1.372	3.276	16.27	529.3	50.8
F5-2	203.3	0.174	399.4	0.299	384.6	0.391	389.6	0.384	375.0	0.953	1.299	3.330	15.69	529.6	50.8
	Tension Tests (LT direction: longitudinal axis normal to the direction of rolling)														
B5-1	199.9	0.170	395.2	0.299	386.8	0.393	389.2	0.387	376.7	0.971	1.289	3.295	15.19	530.3	50.8
B5-2	208.0	0.174	395.7	0.266	381.7	0.386	383.3	0.380	372.3	1.034	1.273	3.503	15.44	527.8	50.8
C5-1	204.5	0.182	409.8	0.266	391.2	0.390	393.1	0.384	379.3	1.131	1.470	3.095	15.34	533.8	50.8
C5-2	213.9	0.187	411.5	1.037	391.8	0.383	394.6	0.377	381.0	1.038	1.427	2.938	15.64	532.2	50.8
E5-1	208.1	0.167	399.9	0.280	389.7	0.387	390.8	0.380	374.9	1.017	1.458	3.150	15.42	529.6	50.8
E5-2	203.5	0.176	401.0	0.231	386.8	0.381	389.9	0.375	377.6	1.123	1.343	3.594	15.64	527.9	50.8
	Statistics														
Mean	205.8	0.181	404.0	0.433	388.5	0.389	391.0	0.383	379.5	1.067	1.371	3.332	14.99	531.1	
Standard Deviation	5.0	0.013	6.9	0.280	4.7	0.007	4.9	0.008	7.9	0.082	0.070	0.297	1.43	3.3	
Range	15.1	0.040	22.1	0.806	14.5	0.021	15.5	0.024	22.8	0.295	0.197	1.102	4.20	9.5	
Minimum	199.9	0.167	395.2	0.231	381.7	0.379	383.3	0.374	372.3	0.953	1.273	2.938	12.06	527.8	
Maximum	215.0	0.207	417.3	1.037	396.2	0.400	398.8	0.398	395.1	1.248	1.470	4.040	16.27	537.2	
Count	11	11	11	11	11	11	11	11	11	11	11	11	11	11	

Table A-5: Summary of Plate 5 Tension Test Results

Plate Number	Section Mark	Location	Steel Type	Nominal Strength (MPa)	Nominal Thickness (mm)	Mill Certificate Properties F_y (MPa)	F_u (MPa)	Elongation (%)
6	G (G3)	Web	A572	345	12.700	432	557	25

Specimen ID	Young's Mod.	Upper Yield		Lower Yield		0.2% Offset Yield		Static Yield		Strain Hardening			Tensile Strength		Gage Length
	E (GPa)	ε (%)	σ (MPa)	ε (%)	σ (MPa)	ε (%)	σ (MPa)	ε (%)	σ (MPa)	ε_{st} (%)	$\varepsilon_{apparent}$ (%)	E_{st} (GPa)	ε (%)	σ (MPa)	(mm)
	Tension Tests (L direction: longitudinal axis in the direction of rolling)														
A6-1	193.0	0.188	404.8	0.453	391.6	0.404	397.0	0.397	383.6	1.452	1.768	3.637	16.78	539.9	50.8
A6-2	194.5	0.183	401.1	0.304	389.2	0.404	391.3	0.398	379.6	1.185	1.728	3.009	16.29	535.8	50.8
D6-1	195.4	0.169	393.2	0.300	384.8	0.383	386.9	0.376	372.5	0.908	1.304	3.468	16.06	543.1	50.8
D6-2	213.5	0.182	398.6	0.268	386.1	0.364	386.3	0.357	372.8	0.897	1.173	3.647	15.53	545.1	50.8
F6-1	219.0	0.173	407.6	0.283	401.0	0.374	401.4	0.369	391.4	1.417	2.058	2.659	16.02	532.7	50.8
F6-2	204.2	0.203	414.4	0.278	397.5	0.399	402.5	0.393	389.8	1.621	2.018	2.881	15.87	533.9	50.8
	Tension Tests (LT direction: longitudinal axis normal to the direction of rolling)														
B6-1	205.7	0.178	408.3	0.219	393.1	0.393	398.8	0.388	387.6	1.254	1.262	3.594	15.51	540.5	50.8
B6-2	195.6	0.176	393.0	0.303	379.4	0.390	384.1	0.384	371.6	1.386	1.538	3.907	16.17	536.8	50.8
C6-1	208.4	0.189	401.2	0.285	387.9	0.377	388.9	0.371	378.1	0.936	1.299	3.479	15.34	541.6	50.8
C6-2	205.8	0.176	387.3	0.252	377.0	0.380	379.8	0.372	363.9	0.997	1.313	3.505	16.03	530.3	50.8
E6-1	200.1	0.193	414.9	0.344	393.6	0.397	398.5	0.391	386.4	1.545	1.960	2.881	17.07	531.0	50.8
E6-2	197.1	0.176	410.2	0.251	391.1	0.395	395.6	0.389	383.4	1.581	2.062	3.098	16.45	529.2	50.8
	Statistics														
Mean	202.7	0.182	402.9	0.295	389.4	0.388	392.6	0.382	380.1	1.265	1.624	3.314	16.09	536.7	
Standard Deviation	8.2	0.010	8.8	0.059	6.9	0.013	7.4	0.013	8.5	0.274	0.347	0.390	0.51	5.3	
Range	26.1	0.034	27.6	0.234	24.0	0.041	22.7	0.040	27.5	0.724	0.888	1.248	1.73	15.9	
Minimum	193.0	0.169	387.3	0.219	377.0	0.364	379.8	0.357	363.9	0.897	1.173	2.659	15.34	529.2	
Maximum	219.0	0.203	414.9	0.453	401.0	0.404	402.5	0.398	391.4	1.621	2.062	3.907	17.07	545.1	
Count	12	12	12	12	12	12	12	12	12	12	12	12	12	12	

Table A-6: Summary of Plate 6 Tension Test Results

Plate Number	Section Mark	Location	Steel Type	Nominal Strength (MPa)	Nominal Thickness (mm)	Mill Certificate Properties F_y (MPa)	F_u (MPa)	Elongation (%)
7	F (G3)	Web	A572	345	12.700	409	541	42

Specimen ID	Young's Mod.	Upper Yield		Lower Yield		0.2% Offset Yield		Static Yield		Strain Hardening			Tensile Strength		Gage Length
	E (GPa)	ε (%)	σ (MPa)	ε (%)	σ (MPa)	ε (%)	σ (MPa)	ε (%)	σ (MPa)	ε_{st} (%)	$\varepsilon_{apparent}$ (%)	E_{st} (GPa)	ε (%)	σ (MPa)	(mm)
	Tension Tests (L direction: longitudinal axis in the direction of rolling)														
A7-1	200.1	0.200	396.7	1.057	376.7	0.386	389.3	0.378	372.7	0.969	1.057	3.767	15.79	530.8	50.8
A7-2	193.3	0.173	395.2	1.068	384.5	0.397	386.4	0.392	377.7	1.001	1.155	3.895	16.68	530.0	50.8
F7-1	214.4	0.161	402.1	0.219	387.1	0.376	391.1	0.371	380.0	1.185	1.307	3.673	16.09	528.7	50.8
F7-2	191.0	0.184	399.0	0.278	382.7	0.432	387.4	0.426	374.8	1.014	1.413	3.174	15.98	525.0	50.8
	Tension Tests (LT direction: longitudinal axis normal to the direction of rolling)														
B7-1	201.6	0.173	394.8	0.350	383.4	0.409	386.9	0.404	376.1	1.003	1.219	3.763	14.87	527.2	50.8
B7-2	196.7	0.174	390.1	0.420	381.4	0.393	381.5	0.386	368.0	1.119	1.266	3.542	16.04	525.6	50.8
E7-1	207.3	0.168	399.9	0.324	388.5	0.389	393.5	0.383	379.3	1.184	1.407	3.514	16.09	529.7	50.8
E7-2	199.1	0.177	397.6	0.243	387.6	0.414	389.0	0.409	379.3	0.917	1.444	2.965	15.75	529.8	50.8
Statistics															
Mean	200.4	0.176	396.9	0.495	384.0	0.400	388.1	0.394	376.0	1.049	1.284	3.536	15.91	528.3	
Standard Deviation	7.6	0.012	3.7	0.356	3.9	0.018	3.6	0.018	4.1	0.101	0.136	0.318	0.51	2.2	
Range	23.4	0.039	12.0	0.849	11.7	0.056	12.0	0.055	12.0	0.268	0.387	0.930	1.81	5.9	
Minimum	191.0	0.161	390.1	0.219	376.7	0.376	381.5	0.371	368.0	0.917	1.057	2.965	14.87	525.0	
Maximum	214.4	0.200	402.1	1.068	388.5	0.432	393.5	0.426	380.0	1.185	1.444	3.895	16.68	530.8	
Count	8	8	8	8	8	8	8	8	8	8	8	8	8	8	

Table A-7: Summary of Plate 7 Tension Test Results

Plate Number	Section Mark	Location	Steel Type	Nominal Strength (MPa)	Nominal Thickness (mm)	Mill Certificate Properties F_y (MPa)	F_u (MPa)	Elongation (%)
8	B1, B7	Web	A572	345	7.938	434	554	27

Specimen ID	Young's Mod.	Upper Yield		Lower Yield		0.2% Offset Yield		Static Yield		Strain Hardening			Tensile Strength		Gage Length
	E (GPa)	ε (%)	σ (MPa)	ε (%)	σ (MPa)	ε (%)	σ (MPa)	ε (%)	σ (MPa)	ε_{st} (%)	$\varepsilon_{apparent}$ (%)	E_{st} (GPa)	ε (%)	σ (MPa)	(mm)
	Tension Tests (L direction: longitudinal axis in the direction of rolling)														
A8-1	169.2	0.358	465.9	0.496	445.2	0.472	454.2	0.461	436.1	1.683	1.678	2.731	17.04	600.6	50.8
A8-2	187.6	0.224	473.2	0.320	459.6	0.463	461.8	0.459	452.7	2.146	2.624	2.942	17.85	592.4	50.8
D8-1	164.0	0.486	470.9	1.687	454.0	0.486	470.9	0.471	446.3	2.038	2.330	3.155	15.91	591.9	203.2
D8-2	187.0	0.299	469.8	1.406	455.7	0.446	459.3	0.439	445.5	1.886	2.398	3.105	15.69	595.5	50.8
D8-3	203.5	0.255	464.2	1.403	453.1	0.424	459.2	0.418	448.1	1.983	2.164	3.649	15.53	588.7	50.8
	Tension Tests (LT direction: longitudinal axis normal to the direction of rolling)														
B8-1	189.6	0.221	474.7	0.271	454.6	0.441	459.7	0.435	448.2	2.230	2.681	3.296	16.99	591.0	50.8
B8-2	206.7	0.215	481.2	0.265	463.5	0.425	466.9	0.418	453.8	2.123	2.707	2.749	16.03	587.7	50.8
C8-1	204.0	0.247	459.2	0.333	443.0	0.420	449.2	0.412	433.4	1.714	2.152	3.499	16.46	594.1	50.8
C8-2	210.3	0.215	478.1	0.296	458.1	0.437	459.5	0.430	444.3	2.001	2.522	2.864	15.95	588.2	50.8
	Statistics														
Mean	191.3	0.3	470.8	0.7	454.1	0.446	460.1	0.438	445.4	1.978	2.362	3.110	16.38	592.2	
Standard Deviation	16.5	0.1	6.9	0.6	6.5	0.023	6.3	0.021	6.8	0.188	0.329	0.325	0.77	4.1	
Range	46.3	0.3	22.0	1.4	20.5	0.066	21.7	0.058	20.3	0.547	1.029	0.918	2.32	12.9	
Minimum	164.0	0.2	459.2	0.3	443.0	0.420	449.2	0.412	433.4	1.683	1.678	2.731	15.53	587.7	
Maximum	210.3	0.5	481.2	1.7	463.5	0.486	470.9	0.471	453.8	2.230	2.707	3.649	17.85	600.6	
Count	9	9	9	9	9	9	9	9	9	9	9	9	9	9	

Table A-8: Summary of Plate 8 Tension Test Results

Plate Number	Section Mark	Location	Steel Type	Nominal Strength (MPa)	Nominal Thickness (mm)	Mill Certificate Properties F_y (MPa)	F_u (MPa)	Elongation (%)
9	B2	Web	A572	345	9.525	414	535	27

Specimen ID	Young's Mod.	Upper Yield		Lower Yield		0.2% Offset Yield		Static Yield		Strain Hardening			Tensile Strength		Gage Length
	E (GPa)	ε (%)	σ (MPa)	ε (%)	σ (MPa)	ε (%)	σ (MPa)	ε (%)	σ (MPa)	ε_{st} (%)	$\varepsilon_{apparent}$ (%)	E_{st} (GPa)	ε (%)	σ (MPa)	(mm)
	Tension Tests (L direction: longitudinal axis in the direction of rolling)														
A9-1	203.5	0.203	430.4	0.412	414.6	0.405	414.6	0.400	405.2	2.282	2.602	3.074	16.31	552.4	50.8
A9-2	201.4	0.220	423.9	1.159	410.2	0.424	412.1	0.418	400.3	2.094	2.413	3.091	16.20	545.5	50.8
D9-1	198.0	0.180	406.5	0.766	392.2	0.400	397.8	0.393	384.5	. . .	2.556	. . .	3.13	427.2	50.8
D9-2	200.7	0.180	413.1	0.270	400.6	0.407	403.0	0.402	393.0	2.060	2.461	3.023	17.84	532.4	50.8
F9-1	190.0	0.192	405.3	0.350	394.7	0.406	397.8	0.401	389.5	2.140	2.439	3.181	18.02	532.2	50.8
F9-2	200.2	0.201	412.7	0.593	396.2	0.419	400.0	0.412	387.6	2.158	2.184	3.420	17.20	529.7	50.8
	Tension Tests (LT direction: longitudinal axis normal to the direction of rolling)														
B9-1	192.3	0.267	438.0	1.208	417.0	0.423	431.0	0.411	408.1	0.171	2.326	4.182	16.61	564.7	50.8
B9-2	200.3	0.190	444.0	0.251	424.6	0.412	429.1	0.407	419.3	2.177	2.392	3.556	16.93	566.4	50.8
C9-1	190.6	0.172	394.2	2.044	377.7	0.400	382.9	0.394	370.5	2.023	2.615	2.985	17.18	516.4	50.8
C9-2	202.1	0.182	410.2	0.219	396.1	0.394	397.5	0.389	388.3	2.018	2.478	2.673	17.29	527.5	50.8
E9-1	199.9	0.187	415.6	0.457	403.8	0.399	403.6	0.393	391.9	2.263	2.539	3.038	18.67	535.1	50.8
E9-2	204.5	0.191	405.8	1.978	382.1	0.392	397.0	0.386	385.4	1.966	1.978	2.925	17.97	534.1	50.8
	Statistics														
Mean	198.6	0.197	416.6	0.809	400.8	0.407	405.5	0.401	393.6	1.941	2.415	3.195	16.11	530.3	
Standard Deviation	4.9	0.026	14.7	0.651	14.0	0.011	13.9	0.010	12.8	0.596	0.183	0.403	4.15	35.8	
Range	14.5	0.095	49.8	1.824	46.9	0.032	48.1	0.032	48.7	2.111	0.637	1.508	15.54	139.1	
Minimum	190.0	0.172	394.2	0.219	377.7	0.392	382.9	0.386	370.5	0.171	1.978	2.673	3.13	427.2	
Maximum	204.5	0.267	444.0	2.044	424.6	0.424	431.0	0.418	419.3	2.282	2.615	4.182	18.67	566.4	
Count	12	12	12	12	12	12	12	12	12	11	12	11	12	12	

Table A-9: Summary of Plate 9 Tension Test Results

Plate Number	Section Mark	Location	Steel Type	Nominal Strength (MPa)	Nominal Thickness (mm)	Mill Certificate Properties F_y (MPa)	F_u (MPa)	Elongation (%)
10	B3	Web	A572	345	9.525	414	535	27

Specimen ID	Young's Mod.	Upper Yield		Lower Yield		0.2% Offset Yield		Static Yield		Strain Hardening			Tensile Strength		Gage Length
	E (GPa)	ε (%)	σ (MPa)	ε (%)	σ (MPa)	ε (%)	σ (MPa)	ε (%)	σ (MPa)	ε_{st} (%)	$\varepsilon_{apparent}$ (%)	E_{st} (GPa)	ε (%)	σ (MPa)	(mm)
	Tension Tests (L direction: longitudinal axis in the direction of rolling)														
A10-1	201.2	0.195	429.8	0.320	412.8	0.400	415.7	0.395	404.8	2.057	2.461	3.400	16.16	558.6	50.8
A10-2	201.2	0.195	429.8	0.320	412.8	0.409	415.0	0.403	403.1	2.046	2.480	3.359	17.07	560.6	50.8
F10-1	175.7	0.248	405.5	0.331	393.8	0.422	398.3	0.414	383.3	1.904	2.024	2.499	17.38	530.6	50.8
F10-2	198.2	0.177	414.9	0.230	397.8	0.401	404.6	0.397	395.4	2.499	2.976	2.756	17.90	533.2	50.8
	Tension Tests (LT direction: longitudinal axis normal to the direction of rolling)														
B10-1	194.1	0.229	434.5	1.728	414.6	0.414	421.3	0.410	412.5	2.312	2.492	3.164	14.84	550.9	50.8
B10-2	201.7	0.189	421.0	0.272	399.2	0.420	409.6	0.414	398.1	2.164	2.695	2.937	15.83	537.8	50.8
E10-1	201.8	0.176	411.1	0.295	396.8	0.385	399.5	0.381	390.3	2.076	2.547	3.137	17.06	530.8	50.8
E10-2	204.3	0.184	412.2	2.392	382.5	0.393	398.3	0.386	383.1	2.306	2.392	3.946	18.69	522.3	50.8
Statistics															
Mean	197.3	0.199	419.8	0.736	401.3	0.406	407.8	0.400	396.3	2.171	2.509	3.149	16.87	540.6	
Standard Deviation	9.2	0.026	10.5	0.837	11.3	0.013	8.9	0.013	10.5	0.191	0.269	0.441	1.22	14.3	
Range	28.7	0.072	29.0	2.162	32.1	0.037	23.1	0.033	29.4	0.595	0.952	1.447	3.85	38.3	
Minimum	175.7	0.176	405.5	0.230	382.5	0.385	398.3	0.381	383.1	1.904	2.024	2.499	14.84	522.3	
Maximum	204.3	0.248	434.5	2.392	414.6	0.422	421.3	0.414	412.5	2.499	2.976	3.946	18.69	560.6	
Count	8	8	8	8	8	8	8	8	8	8	8	8	8	8	

Table A-10: Summary of Plate 10 Tension Test Results

Plate Number	Section Mark	Location	Steel Type	Nominal Strength (MPa)	Nominal Thickness (mm)	Mill Certificate Properties F_y (MPa)	F_u (MPa)	Elongation (%)
11	B4, B8	Web	A572	345	7.938	434	554	27

Specimen ID	Young's Mod.	Upper Yield		Lower Yield		0.2% Offset Yield		Static Yield		Strain Hardening			Tensile Strength		Gage Length
	E (GPa)	ε (%)	σ (MPa)	ε (%)	σ (MPa)	ε (%)	σ (MPa)	ε (%)	σ (MPa)	ε_{st} (%)	$\varepsilon_{apparent}$ (%)	E_{st} (GPa)	ε (%)	σ (MPa)	(mm)
	Tension Tests (L direction: longitudinal axis in the direction of rolling)														
D11-1	176.1	0.439	462.2	1.458	445.1	0.461	454.3	0.453	439.0	1.945	2.091	3.531	13.54	579.5	203.2
D11-2	172.5	0.348	464.5	1.126	448.9	0.467	461.1	0.455	441.0	2.124	2.636	2.908	15.61	585.9	50.8
D11-3	181.2	0.352	469.7	0.450	454.3	0.506	460.0	0.499	447.9	2.111	2.680	2.809	17.09	592.9	50.8
F11-1	176.7	0.370	474.9	0.524	457.7	0.462	463.3	0.454	447.8	1.990	2.439	2.923	17.26	593.2	50.8
F11-2	182.1	0.343	468.3	0.446	454.0	0.451	455.2	0.448	449.8	2.069	2.619	2.866	17.73	585.5	50.8
	Tension Tests (LT direction: longitudinal axis normal to the direction of rolling)														
C11-1	200.8	0.201	475.2	0.287	455.6	0.429	459.1	0.423	447.3	2.083	2.903	2.589	16.06	587.5	50.8
C11-2	197.1	0.206	477.6	0.275	463.2	0.434	467.9	0.426	453.0	2.334	2.738	2.921	16.79	588.8	50.8
E11-1	187.0	0.219	461.2	0.348	442.8	0.425	442.7	0.420	434.0	2.525	2.936	2.628	18.13	564.5	50.8
E11-2	193.0	0.208	475.1	0.249	455.0	0.434	456.9	0.429	446.8	2.459	2.784	2.932	16.35	583.6	50.8
	Statistics														
Mean	185.2	0.299	469.9	0.574	452.9	0.452	457.8	0.445	445.2	2.182	2.647	2.901	16.51	584.6	
Standard Deviation	9.9	0.090	6.2	0.426	6.4	0.026	7.0	0.025	6.0	0.206	0.258	0.269	1.37	8.7	
Range	28.3	0.238	16.4	1.209	20.4	0.081	25.2	0.079	19.0	0.580	0.845	0.942	4.59	28.8	
Minimum	172.5	0.201	461.2	0.249	442.8	0.425	442.7	0.420	434.0	1.945	2.091	2.589	13.54	564.5	
Maximum	200.8	0.439	477.6	1.458	463.2	0.506	467.9	0.499	453.0	2.525	2.936	3.531	18.13	593.2	
Count	9	9	9	9	9	9	9	9	9	9	9	9	9	9	

Table A-11: Summary of Plate 11 Tension Test Results

Plate Number	Section Mark	Location	Steel Type	Nominal Strength (MPa)	Nominal Thickness (mm)	Mill Certificate Properties F_y (MPa)	F_u (MPa)	Elongation (%)
12	B5	Web	A572	345	7.938	434	554	27

Specimen ID	Young's Mod.	Upper Yield		Lower Yield		0.2% Offset Yield		Static Yield		Strain Hardening			Tensile Strength		Gage Length
	E (GPa)	ε (%)	σ (MPa)	ε (%)	σ (MPa)	ε (%)	σ (MPa)	ε (%)	σ (MPa)	ε_{st} (%)	$\varepsilon_{apparent}$ (%)	E_{st} (GPa)	ε (%)	σ (MPa)	(mm)
	Tension Tests (L direction: longitudinal axis in the direction of rolling)														
A12-2	185.6	0.287	461.4	0.342	444.2	0.449	445.2	0.445	436.4	2.029	2.452	3.135	16.12	579.4	50.8
D12-1	178.8	0.469	466.6	0.788	452.2	0.462	466.6	0.447	440.6	2.183	2.308	3.045	14.48	592.6	203.2
D12-2	186.6	0.318	458.5	0.699	443.0	0.440	449.5	0.431	432.9	2.239	2.339	3.533	14.34	583.4	50.8
D12-3	184.3	0.283	464.5	0.564	454.2	0.475	454.1	0.466	437.8	2.067	2.431	3.142	14.79	589.9	50.8
	Tension Tests (LT direction: longitudinal axis normal to the direction of rolling)														
B12-2	200.9	0.207	464.9	0.430	451.3	0.425	452.1	0.420	443.5	2.077	2.525	2.873	15.96	582.2	50.8
C12-1	181.7	0.333	469.3	0.747	447.8	0.452	460.5	0.440	437.6	1.974	2.569	2.834	14.36	582.2	50.8
C12-2	193.8	0.215	474.7	0.261	458.1	0.434	461.3	0.428	448.2	2.056	2.701	2.787	16.12	589.3	50.8
Statistics															
Mean	187.4	0.302	465.7	0.547	450.1	0.448	455.6	0.439	439.6	2.089	2.475	3.050	15.17	585.6	
Standard Deviation	7.6	0.088	5.3	0.208	5.4	0.017	7.5	0.015	5.1	0.091	0.136	0.257	0.86	4.9	
Range	22.1	0.262	16.3	0.527	15.1	0.050	21.4	0.046	15.3	0.266	0.393	0.745	1.78	13.2	
Minimum	178.8	0.207	458.5	0.261	443.0	0.425	445.2	0.420	432.9	1.974	2.308	2.787	14.34	579.4	
Maximum	200.9	0.469	474.7	0.788	458.1	0.475	466.6	0.466	448.2	2.239	2.701	3.533	16.12	592.6	
Count	7	7	7	7	7	7	7	7	7	7	7	7	7	7	

Table A-12: Summary of Plate 12 Tension Test Results

Plate Number	Section Mark	Location	Steel Type	Nominal Strength (MPa)	Nominal Thickness (mm)	Mill Certificate Properties F_y (MPa)	F_u (MPa)	Elongation (%)
13	B6	Web	A572	345	7.938	434	554	27

Specimen ID	Young's Mod.	Upper Yield		Lower Yield		0.2% Offset Yield		Static Yield		Strain Hardening			Tensile Strength		Gage Length
	E (GPa)	ε (%)	σ (MPa)	ε (%)	σ (MPa)	ε (%)	σ (MPa)	ε (%)	σ (MPa)	ε_{st} (%)	$\varepsilon_{apparent}$ (%)	E_{st} (GPa)	ε (%)	σ (MPa)	(mm)
	Tension Tests (L direction: longitudinal axis in the direction of rolling)														
D13-1	171.8	0.489	462.8	1.055	447.9	0.468	462.3	0.453	436.8	2.105	2.250	3.381	15.76	588.5	203.2
D13-2	185.9	0.439	462.7	0.901	452.9	0.448	460.8	0.437	440.6	1.825	2.320	3.182	16.61	591.5	50.8
D13-3	172.6	0.441	461.6	0.305	442.0	0.468	461.1	0.452	434.8	1.817	2.138	3.214	16.39	586.5	50.8
F13-1	179.7	0.307	458.6	0.446	441.3	0.436	442.5	0.430	432.1	1.941	2.541	2.858	16.99	580.2	50.8
F13-2	190.7	0.299	460.9	0.423	449.8	0.426	448.9	0.420	438.6	2.239	2.628	2.980	17.89	580.0	50.8
	Tension Tests (LT direction: longitudinal axis normal to the direction of rolling)														
C13-1	200.7	0.237	480.5	0.295	460.3	0.429	459.1	0.425	450.8	2.170	2.590	2.806	16.75	590.8	50.8
C13-2	190.0	0.215	479.8	0.428	459.7	0.441	460.7	0.435	449.2	2.088	2.553	2.833	16.60	588.9	50.8
E13-2	193.7	0.237	463.8	0.295	444.2	0.429	443.1	0.424	434.5	2.170	2.590	2.708	16.75	570.2	50.8
Statistics															
Mean	185.6	0.333	466.3	0.519	449.8	0.443	454.8	0.435	439.7	2.044	2.451	2.995	16.72	584.6	
Standard Deviation	10.2	0.108	8.7	0.294	7.4	0.017	8.5	0.012	6.9	0.163	0.187	0.238	0.60	7.3	
Range	28.8	0.274	21.9	0.761	19.0	0.042	19.9	0.033	18.7	0.422	0.490	0.673	2.13	21.2	
Minimum	171.8	0.215	458.6	0.295	441.3	0.426	442.5	0.420	432.1	1.817	2.138	2.708	15.76	570.2	
Maximum	200.7	0.489	480.5	1.055	460.3	0.468	462.3	0.453	450.8	2.239	2.628	3.381	17.89	591.5	
Count	8	8	8	8	8	8	8	8	8	8	8	8	8	8	

Table A-13: Summary of Plate 13 Tension Test Results

Plate Number	Section Mark	Location	Steel Type	Nominal Strength (MPa)	Nominal Thickness (mm)	Mill Certificate Properties F_y (MPa)	F_u (MPa)	Elongation (%)
14	A (G1)	Both Flanges	A572	345	26.988	430	583	16

Specimen ID	Young's Mod.	Upper Yield		Lower Yield		0.2% Offset Yield		Static Yield		Strain Hardening			Tensile Strength		Gage Length
	E (GPa)	ε (%)	σ (MPa)	ε (%)	σ (MPa)	ε (%)	σ (MPa)	ε (%)	σ (MPa)	ε_{st} (%)	$\varepsilon_{apparent}$ (%)	E_{st} (GPa)	ε (%)	σ (MPa)	(mm)
	Tension Tests (L direction: longitudinal axis in the direction of rolling)														
A14-1	214.2	. . .	. . .	. . .	. . .	0.405	440.1	. . .	. . .	0.405	0.405	10.030	9.77	639.7	50.8
A14-2	210.5	. . .	. . .	. . .	. . .	0.405	434.4	. . .	. . .	0.405	0.405	10.395	10.08	634.6	50.8
B14-1	203.8	0.252	436.6	0.349	432.9	0.414	435.6	. . .	. . .	0.435	0.551	4.981	12.43	614.2	50.8
B14-2	202.4	0.322	431.4	0.393	428.1	0.384	429.9	. . .	. . .	0.384	0.384	7.456	12.06	622.6	50.8
C14-1	205.1	0.197	423.5	0.601	412.2	0.405	419.0	0.397	403.5	0.553	0.601	4.751	13.05	583.7	50.8
C14-2	210.6	0.199	424.8	0.663	412.7	0.397	418.8	. . .	. . .	0.558	0.663	4.567	12.90	583.5	50.8
	Statistics														
Mean	207.8	0.242	429.1	0.501	421.4	0.402	429.6	0.397	403.5	0.456	0.501	7.030	11.71	613.1	
Standard Deviation	4.7	0.059	6.1	0.154	10.6	0.010	8.9	. . .	. . .	0.078	0.119	2.682	1.44	24.5	
Range	11.9	0.124	13.0	0.314	20.7	0.031	21.3	. . .	. . .	0.174	0.279	5.827	3.29	56.2	
Minimum	202.4	0.197	423.5	0.349	412.2	0.384	418.8	0.397	403.5	0.384	0.384	4.567	9.77	583.5	
Maximum	214.2	0.322	436.6	0.663	432.9	0.414	440.1	0.397	403.5	0.558	0.663	10.395	13.05	639.7	
Count	6	4	4	4	4	6	6	1	1	6	6	6	6	6	

Table A-14: Summary of Plate 14 Tension Test Results

Plate Number	Section Mark	Location	Steel Type	Nominal Strength (MPa)	Nominal Thickness (mm)	Mill Certificate Properties		
						F_y (MPa)	F_u (MPa)	Elongation (%)
15	C (G2)	Both Flanges	A852	485	30.163	598	713	48

Specimen ID	Young's Mod.	0.2% Offset Yield		Static Yield		Strain Hardening			Tensile Strength		Gage Length
	E (GPa)	ε (%)	σ (MPa)	ε (%)	σ (MPa)	ε_{st} (%)	$\varepsilon_{apparent}$ (%)	E_{st} (GPa)	ε (%)	σ (MPa)	(mm)
	Tension Tests (L direction: longitudinal axis in the direction of rolling)										
A15-1	210.9	0.512	635.5	0.504	619.0	0.573	0.929	3.958	7.56	754.7	203.2
A15-2	213.0	0.498	634.2	0.490	619.0	0.713	0.761	4.446	7.09	754.4	203.2
B15-1	209.7	0.502	633.6	0.493	613.8	0.517	0.748	4.056	7.73	754.0	203.2
B15-2	209.8	0.496	621.7	0.488	604.7	0.326	0.359	4.358	6.65	745.8	203.2
C15-1	209.3	0.514	657.1	0.504	637.3	0.524	0.601	5.367	7.05	784.6	203.2
C15-2	202.2	0.507	627.2	0.501	613.1	0.507	0.507	8.681	5.51	764.3	203.2
	Statistics										
Mean	209.1	0.505	634.9	0.497	617.8	0.527	0.651	5.144	6.93	759.6	
Standard Deviation	3.7	0.007	12.1	0.007	10.9	0.124	0.204	1.803	0.80	13.6	
Range	10.9	0.017	35.5	0.016	32.6	0.387	0.570	4.723	2.22	38.8	
Minimum	202.2	0.496	621.7	0.488	604.7	0.326	0.359	3.958	5.51	745.8	
Maximum	213.0	0.514	657.1	0.504	637.3	0.713	0.929	8.681	7.73	784.6	
Count	6	6	6	6	6	6	6	6	6	6	

Table A-15: Summary of Plate 15 Tension Test Results

Plate Number	Section Mark	Location	Steel Type	Nominal Strength (MPa)	Nominal Thickness (mm)	Mill Certificate Properties		
						F_y (MPa)	F_u (MPa)	Elongation (%)
16	D (G2)	Both Flanges	A852	485	30.163	629	755	18

Specimen ID	Young's Mod.	0.2% Offset Yield		Static Yield		Strain Hardening			Tensile Strength		Gage Length
	E (GPa)	ε (%)	σ (MPa)	ε (%)	σ (MPa)	ε_{st} (%)	$\varepsilon_{apparent}$ (%)	E_{st} (GPa)	ε (%)	σ (MPa)	(mm)
	Tension Tests (L direction: longitudinal axis in the direction of rolling)										
A16-1	215.4	0.510	668.4	0.502	650.4	0.510	0.510	6.005	6.839	800.1	203.2
A16-2	210.7	0.497	668.7	0.489	651.9	0.431	0.694	5.082	6.834	800.0	203.2
B16-1	205.3	0.530	638.9	0.521	620.5	0.743	0.853	3.947	7.652	754.7	203.2
B16-2	210.8	0.509	651.1	0.501	635.3	0.377	0.601	4.345	6.410	772.6	203.2
C16-1	210.3	0.507	646.1	0.499	628.9	0.562	0.574	5.584	6.340	775.5	203.2
C16-2	210.0	0.502	654.5	0.494	637.5	0.590	0.686	4.585	5.649	779.2	203.2
	Statistics										
Mean	210.4	0.509	654.6	0.501	637.4	0.536	0.653	4.924	6.621	780.4	
Standard Deviation	3.2	0.011	12.0	0.011	12.2	0.129	0.120	0.779	0.667	17.4	
Range	10.1	0.033	29.8	0.032	31.3	0.366	0.342	2.058	2.003	45.4	
Minimum	205.3	0.497	638.9	0.489	620.5	0.377	0.510	3.947	5.649	754.7	
Maximum	215.4	0.530	668.7	0.521	651.9	0.743	0.853	6.005	7.652	800.1	
Count	6	6	6	6	6	6	6	6	6	6	

Table A-16: Summary of Plate 16 Tension Test Results

Plate Number	Section Mark	Location	Steel Type	Nominal Strength (MPa)	Nominal Thickness (mm)	Mill Certificate Properties F_y (MPa)	F_u (MPa)	Elongation (%)
18	E (G3)	Both Flanges	A572	345	57.150	396	590	23

Specimen ID	Young's Mod.	Upper Yield		Lower Yield		0.2% Offset Yield		Static Yield		Strain Hardening			Tensile Strength		Gage Length
	E (GPa)	ε (%)	σ (MPa)	ε (%)	σ (MPa)	ε (%)	σ (MPa)	ε (%)	σ (MPa)	ε_{st} (%)	$\varepsilon_{apparent}$ (%)	E_{st} (GPa)	ε (%)	σ (MPa)	(mm)
	Tension Tests (L direction: longitudinal axis in the direction of rolling)														
A18-1	214.8	0.201	372.4	0.200	359.2	0.362	362.3	0.357	352.1	0.503	0.623	4.750	12.73	546.5	50.8
A18-2	237.5	0.182	369.0	0.187	358.0	0.353	363.1	0.349	353.3	0.671	0.680	4.938	13.85	545.3	50.8
B18-1	174.3	. . .	. . .	. . .	. . .	0.419	374.8	0.416	369.2	0.680	0.718	4.830	12.14	565.9	50.8
B18-2	105.4	. . .	. . .	. . .	. . .	0.559	371.2	0.543	353.9	0.508	0.548	5.415	11.68	557.8	50.8
C18-1	201.1	0.303	370.7	0.401	368.6	0.381	368.8	0.376	358.4	0.635	0.684	5.070	14.37	556.7	50.8
C18-2	203.5	0.204	386.0	0.697	377.3	0.389	380.2	0.370	342.6	0.670	0.833	4.712	12.67	562.2	50.8
	Statistics														
Mean	189.4	0.222	374.5	0.371	365.8	0.411	370.1	0.402	354.9	0.611	0.681	4.952	12.91	555.7	
Standard Deviation	46.0	0.055	7.8	0.238	9.0	0.076	6.9	0.073	8.7	0.083	0.095	0.261	1.02	8.3	
Range	132.1	0.121	17.0	0.511	19.3	0.206	17.8	0.194	26.7	0.177	0.285	0.702	2.69	20.6	
Minimum	105.4	0.182	369.0	0.187	358.0	0.353	362.3	0.349	342.6	0.503	0.548	4.712	11.68	545.3	
Maximum	237.5	0.303	386.0	0.697	377.3	0.559	380.2	0.543	369.2	0.680	0.833	5.415	14.37	565.9	
Count	6	4	4	4	4	6	6	6	6	6	6	6	6	6	

Table A-17: Summary of Plate 18 Tension Test Results

Plate Number	Section Mark	Location	Steel Type	Nominal Strength (MPa)	Nominal Thickness (mm)	Mill Certificate Properties F_y (MPa)	F_u (MPa)	Elongation (%)
19	F (G3)	Both Flanges	A572	345	57.150	400	596	25

Specimen ID	Young's Mod.	Upper Yield		Lower Yield		0.2% Offset Yield		Static Yield		Strain Hardening			Tensile Strength		Gage Length
	E (GPa)	ε (%)	σ (MPa)	ε (%)	σ (MPa)	ε (%)	σ (MPa)	ε (%)	σ (MPa)	ε_{st} (%)	$\varepsilon_{apparent}$ (%)	E_{st} (GPa)	ε (%)	σ (MPa)	(mm)
	Tension Tests (L direction: longitudinal axis in the direction of rolling)														
A19-1	139.1	. . .	. . .	. . .	. . .	0.467	384.6	0.456	367.5	0.453	0.660	4.391	10.27	566.7	50.8
A19-2	171.3	0.495	383.0	0.352	378.6	0.403	381.9	0.382	342.9	0.670	0.678	5.225	11.47	567.0	50.8
B19-2	226.2	. . .	. . .	0.300	382.5	0.360	385.0	0.356	375.1	0.497	0.530	4.977	12.55	579.4	50.8
C19-1	214.8	. . .	. . .	. . .	. . .	0.375	378.2	0.370	368.0	0.540	0.573	5.048	12.89	570.8	50.8
C19-2	216.3	. . .	. . .	. . .	. . .	0.374	379.5	0.368	367.6	0.409	0.567	4.528	13.68	570.6	50.8
	Statistics														
Mean	193.6	0.495	383.0	0.326	380.5	0.396	381.8	0.386	364.2	0.514	0.601	4.834	12.17	570.9	
Standard Deviation	37.1	. . .	. . .	0.037	2.8	0.043	3.0	0.040	12.3	0.100	0.064	0.357	1.33	5.1	
Range	87.1	. . .	. . .	0.052	3.9	0.107	6.8	0.100	32.2	0.261	0.148	0.834	3.41	12.7	
Minimum	139.1	0.495	383.0	0.300	378.6	0.360	378.2	0.356	342.9	0.409	0.530	4.391	10.27	566.7	
Maximum	226.2	0.495	383.0	0.352	382.5	0.467	385.0	0.456	375.1	0.670	0.678	5.225	13.68	579.4	
Count	5	1	1	2	2	5	5	5	5	5	5	5	5	5	

Table A-18: Summary of Plate 19 Tension Test Results

Plate Number	Section Mark	Location	Steel Type	Nominal Strength (MPa)	Nominal Thickness (mm)	Mill Certificate Properties F_y (MPa)	F_u (MPa)	Elongation (%)
20	G (G3)	Both Flanges	A572	345	57.150	385	602	33

Specimen ID	Young's Mod.	Upper Yield		Lower Yield		0.2% Offset Yield		Static Yield		Strain Hardening			Tensile Strength		Gage Length
	E (GPa)	ε (%)	σ (MPa)	ε (%)	σ (MPa)	ε (%)	σ (MPa)	ε (%)	σ (MPa)	ε_{st} (%)	$\varepsilon_{apparent}$ (%)	E_{st} (GPa)	ε (%)	σ (MPa)	(mm)
	Tension Tests (L direction: longitudinal axis in the direction of rolling)														
A20-1	199.6	. . .	. . .	. . .	. . .	0.389	375.5	0.385	368.4	0.211	0.321	4.921	13.95	574.2	50.8
A20-2	136.6	. . .	. . .	. . .	. . .	0.484	373.3	0.478	365.6	0.484	0.484	4.553	17.46	572.9	50.8
B20-1	190.4	0.278	374.0	0.304	369.7	0.387	369.9	0.382	359.1	0.424	0.433	5.215	12.49	561.3	50.8
B20-2	188.8	. . .	. . .	. . .	. . .	0.399	374.2	0.394	365.2	0.509	0.449	5.238	12.80	563.0	50.8
C20-2	245.3	. . .	. . .	. . .	. . .	0.348	376.0	0.344	365.9	0.504	0.498	4.800	14.05	561.0	50.8
	Statistics														
Mean	192.2	0.278	374.0	0.304	369.7	0.401	373.8	0.397	364.9	0.426	0.437	4.946	14.15	566.5	
Standard Deviation	38.7	. . .	. . .	. . .	. . .	0.050	2.4	0.049	3.4	0.125	0.070	0.289	1.97	6.5	
Range	108.7	. . .	. . .	. . .	. . .	0.136	6.1	0.134	9.3	0.299	0.178	0.685	4.97	13.2	
Minimum	136.6	0.278	374.0	0.304	369.7	0.348	369.9	0.344	359.1	0.211	0.321	4.553	12.49	561.0	
Maximum	245.3	0.278	374.0	0.304	369.7	0.484	376.0	0.478	368.4	0.509	0.498	5.238	17.46	574.2	
Count	5	1	1	1	1	5	5	5	5	5	5	5	5	5	

Table A-19: Summary of Plate 20 Tension Test Results

Plate Number	Section Mark	Location	Steel Type	Nominal Strength (MPa)	Nominal Thickness (mm)	Mill Certificate Properties F_y (MPa)	F_u (MPa)	Elongation (%)
21	B1, B2, B3, B4	Comp. Flange	A572	345	19.050	434	592	26

Specimen ID	Young's Mod. E (GPa)	Upper Yield ε (%)	Upper Yield σ (MPa)	Lower Yield ε (%)	Lower Yield σ (MPa)	0.2% Offset Yield ε (%)	0.2% Offset Yield σ (MPa)	Static Yield ε (%)	Static Yield σ (MPa)	Strain Hardening ε_{st} (%)	Strain Hardening $\varepsilon_{apparent}$ (%)	Strain Hardening E_{st} (GPa)	Ultimate Strength ε (%)	Ultimate Strength σ (MPa)	Gage Length (mm)
Tension Tests (L direction: longitudinal axis in the direction of rolling)															
A21-1	188.7	0.283	431.2	0.559	413.8	0.407	415.5	0.401	403.3	1.611	1.716	4.594	15.45	577.8	50.8
A21-2	192.1	0.271	435.4	1.434	423.4	0.426	430.2	0.418	414.8	1.428	1.434	4.996	15.88	592.4	50.8
B21-1	194.5	0.442	429.3	0.892	417.7	0.428	429.3	0.416	407.0	1.543	1.654	3.894	15.43	581.1	203.2
B21-2	190.5	0.385	433.0	0.993	415.4	0.422	432.3	0.410	408.9	1.165	1.588	2.927	18.78	584.2	50.8
B21-3	184.3	0.313	433.6	0.882	419.5	0.425	425.0	0.417	410.8	1.440	1.545	4.609	15.75	585.4	50.8
C21-1	194.8	0.246	424.6	1.237	418.2	0.415	422.3	0.408	409.9	1.567	1.735	3.885	14.47	579.8	50.8
C21-2	201.5	0.250	427.7	0.532	415.2	0.408	421.1	0.400	405.1	1.547	1.701	4.288	15.38	577.5	50.8
	Statistics														
Mean	192.3	0.313	430.7	0.933	417.6	0.419	425.1	0.410	408.5	1.472	1.625	4.170	15.88	582.6	
Standard Deviation	5.4	0.074	3.8	0.330	3.2	0.009	5.9	0.008	3.8	0.151	0.109	0.680	1.36	5.3	
Range	17.1	0.196	10.8	0.902	9.6	0.021	16.8	0.018	11.5	0.446	0.300	2.070	4.31	14.9	
Minimum	184.3	0.246	424.6	0.532	413.8	0.407	415.5	0.400	403.3	1.165	1.434	2.927	14.47	577.5	
Maximum	201.5	0.442	435.4	1.434	423.4	0.428	432.3	0.418	414.8	1.611	1.735	4.996	18.78	592.4	
Count	7	7	7	7	7	7	7	7	7	7	7	7	7	7	
Compression Tests															
B21-1	195.5	0.354	458.4	1.132	440.9	0.435	454.8	. . .	. . .	1.498	1.355	6.873			50.8
B21-2	199.4	0.347	459.8	1.173	442.4	0.425	449.9	. . .	. . .	1.507	1.493	6.116			50.8
B21-3	195.9	0.340	458.0	0.498	439.2	0.428	451.0	0.414	422.7	1.485	1.493	5.881			50.8
	Statistics														
Mean	196.9	0.347	458.7	0.934	440.9	0.430	451.9	0.414	422.7	1.497	1.447	6.290			
Standard Deviation	2.1	0.007	0.9	0.379	1.6	0.005	2.6	. . .	. . .	0.011	0.080	0.518			
Range	3.9	0.014	1.8	0.675	3.3	0.010	4.9	. . .	. . .	0.022	0.138	0.991			
Minimum	195.5	0.340	458.0	0.498	439.2	0.425	449.9	0.414	422.7	1.485	1.355	5.881			
Maximum	199.4	0.354	459.8	1.173	442.4	0.435	454.8	0.414	422.7	1.507	1.493	6.873			
Count	3	3	3	3	3	3	3	1	1	3	3	3			

Table A-20: Summary of Plate 21 Tension and Compression Test Results

Plate Number	Section Mark	Location	Steel Type	Nominal Strength (MPa)	Nominal Thickness (mm)	Mill Certificate Properties F_y (MPa)	F_u (MPa)	Elongation (%)
22	B1, B2, B3	Ten. Flange	A572	345	19.050	443	597	27

Specimen ID	Young's Mod.	Upper Yield		Lower Yield		0.2% Offset Yield		Static Yield		Strain Hardening			Tensile Strength		Gage Length
	E (GPa)	ε (%)	σ (MPa)	ε (%)	σ (MPa)	ε (%)	σ (MPa)	ε (%)	σ (MPa)	ε_{st} (%)	$\varepsilon_{apparent}$ (%)	E_{st} (GPa)	ε (%)	σ (MPa)	(mm)
	Tension Tests (L direction: longitudinal axis in the direction of rolling)														
A22-1	189.9	0.189	432.2	0.703	417.1	0.413	417.5	0.407	406.7	1.790	2.080	4.292	16.16	576.2	50.8
A22-2	187.2	0.190	428.4	0.880	410.3	0.420	412.1	0.417	406.4	1.444	1.953	3.108	16.75	572.8	50.8
B22-1	190.1	0.196	439.1	0.809	423.4	0.432	430.7	0.425	417.5	1.884	2.108	3.678	15.35	582.9	203.2
B22-2	205.2	0.196	424.8	0.671	415.9	0.403	417.1	0.399	408.5	1.658	1.966	3.692	16.02	577.9	50.8
C22-1	187.7	0.190	417.4	0.749	406.7	0.418	411.3	0.410	396.8	1.671	1.980	3.806	16.68	569.7	50.8
C22-2	193.7	0.210	437.1	0.532	414.4	0.413	415.9	0.408	405.4	1.819	2.096	4.072	16.12	571.3	50.8
	Statistics														
Mean	192.3	0.195	429.8	0.724	414.6	0.416	417.4	0.411	406.9	1.711	2.030	3.775	16.18	575.2	
Standard Deviation	6.8	0.008	8.1	0.120	5.8	0.010	7.0	0.009	6.6	0.157	0.071	0.404	0.51	4.9	
Range	18.1	0.021	21.7	0.348	16.7	0.030	19.4	0.027	20.8	0.440	0.155	1.184	1.40	13.2	
Minimum	187.2	0.189	417.4	0.532	406.7	0.403	411.3	0.399	396.8	1.444	1.953	3.108	15.35	569.7	
Maximum	205.2	0.210	439.1	0.880	423.4	0.432	430.7	0.425	417.5	1.884	2.108	4.292	16.75	582.9	
Count	6	6	6	6	6	6	6	6	6	6	6	6	6	6	
	Compression Tests														
B22-1	206.4	0.235	478.5	0.450	447.2	0.417	450.0	0.409	431.9	2.077	2.012	7.253			50.8
B22-2	205.5	0.240	472.4	0.914	451.4	0.423	459.2	0.415	442.5	1.947	1.990	6.511			50.8
B22-3	207.2	0.233	479.8	0.583	450.3	0.418	452.5	0.410	436.9	1.823	1.784	5.566			50.8
	Statistics														
Mean	147.9	1.018	330.7	1.387	314.6	1.160	318.4	1.155	307.5	2.231	2.286	4.845			
Standard Deviation	93.2	2.198	217.7	2.045	207.8	2.139	209.5	2.141	201.5	1.752	1.774	2.127			
Range	201.2	5.979	473.8	5.652	445.4	5.970	453.2	5.973	436.5	5.560	5.845	6.069			
Minimum	6.0	0.021	6.0	0.348	6.0	0.030	6.0	0.027	6.0	0.440	0.155	1.184			
Maximum	207.2	6.000	479.8	6.000	451.4	6.000	459.2	6.000	442.5	6.000	6.000	7.253			
Count	7	7	7	7	7	7	7	7	7	7	7	7			

Table A-21: Summary of Plate 22 Tension and Compression Test Results

Plate Number	Section Mark	Location	Steel Type	Nominal Strength (MPa)	Nominal Thickness (mm)	Mill Certificate Properties F_y (MPa)	F_u (MPa)	Elongation (%)
23	B5	Both Flanges	A572	345	23.813	419	571	27

Specimen ID	Young's Mod.	Upper Yield		Lower Yield		0.2% Offset Yield		Static Yield		Strain Hardening			Tensile Strength		Gage Length
	E (GPa)	ε (%)	σ (MPa)	ε (%)	σ (MPa)	ε (%)	σ (MPa)	ε (%)	σ (MPa)	ε_{st} (%)	$\varepsilon_{apparent}$ (%)	E_{st} (GPa)	ε (%)	σ (MPa)	(mm)
Tension Tests (L direction: longitudinal axis in the direction of rolling)															
A23-1	190.1	0.273	432.1	1.011	409.2	0.410	409.7	0.404	398.0	1.787	1.915	4.713	15.49	575.8	50.8
A23-2	214.2	0.194	413.9	0.214	399.6	0.389	398.6	0.384	387.5	1.721	1.986	3.921	17.31	565.5	50.8
B23-1	165.4	0.221	433.1	1.421	413.5	0.441	422.0	0.434	409.6	1.492	2.085	3.675	15.62	579.0	203.2
B23-2	196.0	0.190	411.2	1.865	395.1	0.405	402.0	0.401	393.8	1.789	1.831	4.564	16.84	566.2	50.8
B23-3	207.0	0.206	425.4	1.527	393.4	0.401	401.5	0.396	392.0	1.453	1.534	4.046	16.63	569.8	50.8
C23-1	211.4	0.182	414.8	1.347	401.2	0.392	403.5	0.387	393.9	1.505	1.796	3.782	15.79	569.3	50.8
C23-2	202.9	0.193	415.4	0.372	399.5	0.395	399.1	0.390	389.9	1.675	1.991	4.077	15.12	567.4	50.8
Statistics															
Mean	198.1	0.209	420.8	1.108	401.6	0.405	405.2	0.399	395.0	1.632	1.877	4.111	16.11	570.4	
Standard Deviation	16.7	0.031	9.2	0.613	7.3	0.018	8.3	0.017	7.3	0.145	0.181	0.389	0.81	5.1	
Range	48.8	0.091	22.0	1.651	20.1	0.052	23.4	0.050	22.1	0.336	0.552	1.038	2.19	13.6	
Minimum	165.4	0.182	411.2	0.214	393.4	0.389	398.6	0.384	387.5	1.453	1.534	3.675	15.12	565.5	
Maximum	214.2	0.273	433.1	1.865	413.5	0.441	422.0	0.434	409.6	1.789	2.085	4.713	17.31	579.0	
Count	7	7	7	7	7	7	7	7	7	7	7	7	7	7	
	Compression Tests														
B23-1	206.7	0.226	455.3	0.776	428.1	0.412	439.8	0.401	416.8	1.626	1.766	5.745			50.8
B23-2	205.7	0.230	445.1	0.368	432.9	0.410	432.5	0.402	416.6	1.727	1.673	6.273			50.8
B23-3	207.8	0.252	455.4	1.765	429.6	0.412	438.9	0.404	422.6	1.634	1.775	6.172			50.8
Statistics															
Mean	206.7	0.236	451.9	0.970	430.2	0.411	437.1	0.403	418.7	1.662	1.738	6.063			
Standard Deviation	1.0	0.014	5.9	0.718	2.5	0.001	4.0	0.001	3.4	0.056	0.057	0.280			
Range	2.1	0.026	10.2	1.397	4.8	0.002	7.3	0.003	6.0	0.101	0.102	0.528			
Minimum	205.7	0.226	445.1	0.368	428.1	0.410	432.5	0.401	416.6	1.626	1.673	5.745			
Maximum	207.8	0.252	455.4	1.765	432.9	0.412	439.8	0.404	422.6	1.727	1.775	6.273			
Count	3	3	3	3	3	3	3	3	3	3	3	3			

Table A-22: Summary of Plate 23 Tension and Compression Test Results

Plate Number	Section Mark	Location	Steel Type	Nominal Strength (MPa)	Nominal Thickness (mm)	Mill Certificate Properties F_y (MPa)	F_u (MPa)	Elongation (%)
24	B6	Both Flanges	A572	345	30.163	447	575	26

Specimen ID	Young's Mod.	Upper Yield		Lower Yield		0.2% Offset Yield		Static Yield		Strain Hardening			Tensile Strength		Gage Length
	E (GPa)	ε (%)	σ (MPa)	ε (%)	σ (MPa)	ε (%)	σ (MPa)	ε (%)	σ (MPa)	ε_{st} (%)	$\varepsilon_{apparent}$ (%)	E_{st} (GPa)	ε (%)	σ (MPa)	(mm)
Tension Tests (L direction: longitudinal axis in the direction of rolling)															
A24-1	206.9	0.193	415.9	1.243	393.8	0.388	395.1	0.379	375.7	1.529	1.951	3.552	17.17	558.2	50.8
A24-2	201.0	0.215	416.9	0.352	398.5	0.395	398.6	0.392	391.5	1.787	1.950	4.298	15.73	562.3	50.8
B24-1	198.9	0.192	427.6	0.713	405.9	0.408	413.1	0.401	399.3	1.729	2.027	3.691	15.98	566.4	203.2
B24-2	214.8	0.202	425.0	1.167	400.1	0.389	403.7	0.383	391.4	1.876	2.192	3.195	17.82	559.6	50.8
B24-3	236.5	0.207	416.5	1.375	396.1	0.372	399.6	0.367	387.2	1.630	1.989	3.962	17.23	556.2	50.8
C24-1	209.9	0.208	414.0	0.855	396.5	0.390	397.8	0.384	383.2	1.607	2.022	3.062	16.57	548.5	50.8
C24-2	204.0	0.174	408.6	0.443	399.0	0.396	399.4	0.390	388.7	1.772	1.940	4.103	16.25	558.5	50.8
Statistics															
Mean	210.3	0.199	417.8	0.878	398.6	0.391	401.1	0.385	388.1	1.704	2.010	3.695	16.68	558.5	
Standard Deviation	12.8	0.014	6.5	0.399	3.9	0.011	5.9	0.011	7.4	0.120	0.088	0.461	0.75	5.5	
Range	37.6	0.041	19.0	1.023	12.1	0.036	18.0	0.035	23.6	0.347	0.253	1.236	2.08	17.9	
Minimum	198.9	0.174	408.6	0.352	393.8	0.372	395.1	0.367	375.7	1.529	1.940	3.062	15.73	548.5	
Maximum	236.5	0.215	427.6	1.375	405.9	0.408	413.1	0.401	399.3	1.876	2.192	4.298	17.82	566.4	
Count	7	7	7	7	7	7	7	7	7	7	7	7	7	7	
Compression Tests															
B24-1	209.7	0.228	452.0	1.489	423.7	0.406	433.9	0.396	412.4	1.768	1.600	6.573			50.8
B24-2	210.5	0.217	452.8	0.893	424.8	0.402	427.4	0.396	414.5	1.516	1.360	4.531			50.8
B24-3	207.9	0.224	451.2	1.504	415.6	0.406	429.9	0.397	411.4	1.535	1.516	5.824			50.8
Statistics															
Mean	209.4	0.223	452.0	1.295	421.4	0.405	430.4	0.396	412.7	1.606	1.492	5.643			
Standard Deviation	1.4	0.005	0.8	0.349	5.0	0.002	3.3	0.001	1.6	0.140	0.122	1.033			
Range	2.6	0.011	1.5	0.611	9.2	0.004	6.5	0.002	3.1	0.252	0.240	2.042			
Minimum	207.9	0.217	451.2	0.893	415.6	0.402	427.4	0.396	411.4	1.516	1.360	4.531			
Maximum	210.5	0.228	452.8	1.504	424.8	0.406	433.9	0.397	414.5	1.768	1.600	6.573			
Count	3	3	3	3	3	3	3	3	3	3	3	3			

Table A-23: Summary of Plate 24 Tension and Compression Test Results

Plate Number	Section Mark	Location	Steel Type	Nominal Strength (MPa)	Nominal Thickness (mm)	Mill Certificate Properties F_y (MPa)	F_u (MPa)	Elongation (%)
25	B4	Ten. Flange	A572	345	31.750	460	606	27

Specimen ID	Young's Mod.	Upper Yield		Lower Yield		0.2% Offset Yield		Static Yield		Strain Hardening			Tensile Strength		Gage Length
	E (GPa)	ε (%)	σ (MPa)	ε (%)	σ (MPa)	ε (%)	σ (MPa)	ε (%)	σ (MPa)	ε_{st} (%)	$\varepsilon_{apparent}$ (%)	E_{st} (GPa)	ε (%)	σ (MPa)	(mm)
Tension Tests (L direction: longitudinal axis in the direction of rolling)															
A25-1	209.0	0.224	424.0	1.351	401.9	0.394	405.2	0.387	391.0	1.780	1.995	3.983	17.59	565.0	50.8
A25-2	198.9	0.213	413.0	1.927	390.1	0.397	395.6	0.392	384.2	1.702	1.932	4.396	17.81	558.0	50.8
B25-1	214.8	0.277	420.5	0.488	404.7	0.390	410.0	0.383	394.5	1.871	2.017	4.092	15.57	568.4	203.2
B25-2	179.0	0.231	417.6	1.533	401.8	0.428	403.2	0.421	390.4	1.720	2.020	4.194	16.72	564.7	50.8
B25-3	221.1	0.291	421.6	0.907	398.6	0.387	406.8	0.378	388.2	1.597	1.928	3.453	17.09	566.2	50.8
C25-1	219.9	0.203	414.7	0.450	401.9	0.393	402.6	0.386	389.7	1.770	1.972	3.860	15.36	564.0	50.8
C25-2	222.0	0.209	425.6	0.465	406.0	0.390	407.5	0.384	395.7	1.831	2.022	3.913	16.08	566.7	50.8
Statistics															
Mean	209.2	0.236	419.6	1.017	400.7	0.397	404.4	0.390	390.5	1.753	1.984	3.984	16.60	564.7	
Standard Deviation	15.6	0.035	4.7	0.595	5.2	0.014	4.6	0.014	3.9	0.090	0.041	0.297	0.96	3.3	
Range	43.0	0.088	12.6	1.477	15.9	0.041	14.4	0.043	11.5	0.273	0.093	0.943	2.45	10.4	
Minimum	179.0	0.203	413.0	0.450	390.1	0.387	395.6	0.378	384.2	1.597	1.928	3.453	15.36	558.0	
Maximum	222.0	0.291	425.6	1.927	406.0	0.428	410.0	0.421	395.7	1.871	2.022	4.396	17.81	568.4	
Count	7	7	7	7	7	7	7	7	7	7	7	7	7	7	
Compression Tests															
B25-1	206.3	0.252	444.8	1.232	414.1	0.410	433.7	0.398	409.0	1.680	1.630	6.095			50.8
B25-2	205.8	0.287	445.4	1.542	414.9	0.413	438.8	0.397	405.0	1.607	1.544	6.447			50.8
B25-3	205.6	0.216	428.2	0.309	414.8	0.391	413.7	0.386	403.3	1.642	1.710	5.712			50.8
Statistics															
Mean	205.9	0.252	439.5	1.028	414.6	0.405	428.7	0.393	405.8	1.643	1.628	6.085			
Standard Deviation	0.3	0.036	9.8	0.642	0.4	0.012	13.3	0.007	3.0	0.037	0.083	0.368			
Range	0.7	0.072	17.3	1.233	0.7	0.022	25.1	0.012	5.8	0.073	0.166	0.735			
Minimum	205.6	0.216	428.2	0.309	414.1	0.391	413.7	0.386	403.3	1.607	1.544	5.712			
Maximum	206.3	0.287	445.4	1.542	414.9	0.413	438.8	0.398	409.0	1.680	1.710	6.447			
Count	3	3	3	3	3	3	3	3	3	3	3	3			

Table A-24: Summary of Plate 25 Tension and Compression Test Results

Plate Number	Section Mark	Location	Steel Type	Nominal Strength (MPa)	Nominal Thickness (mm)	Mill Certificate Properties F_y (MPa)	F_u (MPa)	Elongation (%)
26	S1, S1-S	Both Flanges	A572	345	22.225	412	560	28

Specimen ID	Young's Mod.	Upper Yield		Lower Yield		0.2% Offset Yield		Static Yield		Strain Hardening			Tensile Strength		Gage Length
	E (GPa)	ε (%)	σ (MPa)	ε (%)	σ (MPa)	ε (%)	σ (MPa)	ε (%)	σ (MPa)	ε_{st} (%)	$\varepsilon_{apparent}$ (%)	E_{st} (GPa)	ε (%)	σ (MPa)	(mm)
	Tension Tests (L direction: longitudinal axis in the direction of rolling)														
26-F1-1	194.9	0.349	399.4	0.462	386.4	0.403	394.3	0.395	380.0	1.890	1.954	3.570	12.31	539.1	203.2
26-F1-2	189.2	0.369	401.0	0.479	385.7	0.410	397.1	0.401	381.1	1.934	1.932	3.570	12.37	540.7	203.2
26-F1-3	193.5	0.343	402.3	0.478	384.8	0.406	397.9	0.397	381.1	1.920	2.007	3.480	12.40	539.7	203.2
26-F2-1	178.0	0.431	388.7	0.545	385.3	0.403	387.7	0.395	372.3	1.003	1.012	2.999	12.46	539.0	203.2
26-F2-2	173.6	0.427	386.7	0.503	382.8	0.418	385.9	0.410	371.3	1.232	1.234	3.454	12.34	536.7	203.2
26-F2-3	172.1	0.443	384.1	0.553	382.1	0.421	383.9	0.414	372.2	1.200	1.204	3.394	12.40	535.4	203.2
26-F3-1	182.7	0.373	390.6	1.187	383.7	0.406	389.6	0.397	372.6	1.288	1.239	3.912	12.47	542.0	203.2
26-F3-3	194.0	0.327	390.1	1.027	380.5	0.400	388.8	0.393	375.3	1.561	1.640	3.717	12.26	539.9	203.2
	Statistics														
Mean	184.8	0.383	392.9	0.654	383.9	0.408	390.6	0.400	375.7	1.504	1.528	3.512	12.38	539.1	
Standard Deviation	9.4	0.044	7.0	0.285	2.0	0.008	5.2	0.008	4.3	0.373	0.402	0.265	0.07	2.1	
Range	22.8	0.115	18.3	0.725	5.9	0.021	14.0	0.021	9.8	0.931	0.995	0.913	0.20	6.6	
Minimum	172.1	0.327	384.1	0.462	380.5	0.400	383.9	0.393	371.3	1.003	1.012	2.999	12.26	535.4	
Maximum	194.9	0.443	402.3	1.187	386.4	0.421	397.9	0.414	381.1	1.934	2.007	3.912	12.47	542.0	
Count	8	8	8	8	8	8	8	8	8	8	8	8	8	8	

Table A-25: Summary of Plate 26 Tension Test Results

Plate Number	Section Mark	Location	Steel Type	Nominal Strength (MPa)	Nominal Thickness (mm)	Mill Certificate Properties F_y (MPa)	F_u (MPa)	Elongation (%)
27	S1, S1-S	Web	A572	345	7.938	430	565	23

Specimen ID	Young's Mod.	Upper Yield		Lower Yield		0.2% Offset Yield		Static Yield		Strain Hardening			Tensile Strength		Gage Length
	E (GPa)	ε (%)	σ (MPa)	ε (%)	σ (MPa)	ε (%)	σ (MPa)	ε (%)	σ (MPa)	ε_{st} (%)	$\varepsilon_{apparent}$ (%)	E_{st} (GPa)	ε (%)	σ (MPa)	(mm)
	Tension Tests (L direction: longitudinal axis in the direction of rolling)														
27-W4-1	207.5	0.229	442.9	1.551	418.1	0.407	425.3	0.397	405.2	2.015	2.349	3.297	12.17	565.5	203.2
27-W4-2	210.5	0.240	446.8	0.562	427.0	0.409	432.9	0.398	410.2	2.141	2.400	3.308	12.39	567.0	203.2
27-W6-1	207.4	0.238	448.3	0.516	426.6	0.411	432.8	0.403	415.9	1.969	2.354	3.273	12.28	573.0	203.2
27-W6-2	210.4	0.243	449.4	0.933	429.5	0.408	434.3	0.401	417.7	1.996	2.356	3.379	12.23	573.2	203.2
27-W8-1	203.0	0.224	413.1	0.278	393.5	0.396	399.4	0.392	389.8	1.968	2.168	3.475	11.29	556.2	203.2
27-W8-2	228.0	0.226	409.7	0.366	386.9	0.377	388.1	0.374	381.9	2.090	2.224	3.403	11.04	548.4	203.2
	Tension Tests (LT direction: longitudinal axis normal to the direction of rolling)														
27-W3-1	207.9	0.229	453.2	0.819	423.7	0.407	428.5	0.399	412.3	2.104	2.415	3.267	12.22	567.5	203.2
27-W3-2	210.1	0.233	446.6	1.352	424.2	0.407	432.8	0.400	418.5	2.107	2.408	3.272	12.40	566.6	203.2
27-W5-1	208.7	0.235	447.2	1.038	424.5	0.417	428.3	0.409	412.6	2.015	2.366	3.352	12.16	566.3	203.2
27-W5-2	210.8	0.235	452.3	1.166	428.2	0.406	430.8	0.400	418.8	2.013	2.425	3.250	12.20	571.1	203.2
27-W7-2	206.8	0.221	432.2	0.784	407.2	0.402	417.0	0.392	394.8	1.967	2.075	3.622	. . .	564.1	203.2
27-W7-3	216.2	0.233	422.4	0.783	401.7	0.395	407.8	0.389	395.3	1.591	1.859	3.851	12.49	561.1	203.2
	Statistics														
Mean	210.6	0.232	438.7	0.846	415.9	0.404	421.5	0.396	406.1	1.998	2.283	3.396	12.08	565.0	
Standard Deviation	6.3	0.007	15.4	0.387	14.8	0.010	15.2	0.009	12.6	0.142	0.173	0.179	0.47	7.1	
Range	25.0	0.022	43.5	1.273	42.6	0.040	46.3	0.035	36.8	0.550	0.565	0.600	1.46	24.8	
Minimum	203.0	0.221	409.7	0.278	386.9	0.377	388.1	0.374	381.9	1.591	1.859	3.250	11.04	548.4	
Maximum	228.0	0.243	453.2	1.551	429.5	0.417	434.3	0.409	418.8	2.141	2.425	3.851	12.49	573.2	
Count	12	12	12	12	12	12	12	12	12	12	12	12	11	12	

Table A-26: Summary of Plate 27 Tension Test Results

Plate Number	Section Mark	Location	Steel Type	Nominal Strength (MPa)	Nominal Thickness (mm)	Mill Certificate Properties F_y (MPa)	F_u (MPa)	Elongation (%)
28	S2, S2-S	Both Flanges	A572	345	22.225	412	560	28

Specimen ID	Young's Mod.	Upper Yield		Lower Yield		0.2% Offset Yield		Static Yield		Strain Hardening			Tensile Strength		Gage Length
	E (GPa)	ε (%)	σ (MPa)	ε (%)	σ (MPa)	ε (%)	σ (MPa)	ε (%)	σ (MPa)	ε_{st} (%)	$\varepsilon_{apparent}$ (%)	E_{st} (GPa)	ε (%)	σ (MPa)	(mm)
	Tension Tests (L direction: longitudinal axis in the direction of rolling)														
28-F1-1	197.3	0.330	426.9	0.457	407.8	0.411	417.7	. . .	. . .	1.990	2.198	3.686	12.30	559.5	203.2
28-F1-2	200.2	0.337	427.1	1.109	406.9	0.414	423.8	. . .	. . .	1.845	2.111	3.706	12.40	560.9	203.2
28-F1-3	201.5	0.294	426.3	0.453	406.3	0.408	413.4	0.401	398.8	1.999	2.122	3.695	12.31	559.5	203.2
28-F2-1	203.6	0.346	423.0	0.440	404.3	0.405	415.6	. . .	. . .	1.901	2.059	3.624	12.19	558.7	203.2
28-F2-2	201.5	0.364	423.9	1.803	400.6	0.410	422.6	. . .	. . .	1.682	1.814	3.945	12.36	561.0	203.2
28-F2-3	199.3	0.338	422.4	0.484	401.6	0.412	418.6	0.398	391.2	1.945	2.019	3.667	12.39	559.5	203.2
28-F3-1	204.2	0.282	420.7	0.389	402.2	0.398	402.8	. . .	. . .	1.915	2.130	3.635	12.39	555.9	203.2
28-F3-2	203.9	0.295	420.9	0.379	401.9	0.400	406.3	. . .	. . .	1.918	2.056	3.743	12.42	558.1	203.2
28-F3-3	208.9	0.267	420.1	0.318	403.3	0.396	407.1	0.390	394.4	1.951	2.109	3.666	12.49	556.2	203.2
	Statistics														
Mean	202.3	0.317	423.5	0.648	403.9	0.406	414.2	0.396	394.8	1.905	2.069	3.708	12.36	558.8	
Standard Deviation	3.4	0.033	2.7	0.492	2.6	0.007	7.4	0.006	3.8	0.096	0.109	0.096	0.09	1.8	
Range	11.6	0.098	7.0	1.485	7.1	0.018	21.1	0.011	7.6	0.317	0.385	0.321	0.30	5.1	
Minimum	197.3	0.267	420.1	0.318	400.6	0.396	402.8	0.390	391.2	1.682	1.814	3.624	12.19	555.9	
Maximum	208.9	0.364	427.1	1.803	407.8	0.414	423.8	0.401	398.8	1.999	2.198	3.945	12.49	561.0	
Count	9	9	9	9	9	9	9	3	3	9	9	9	9	9	

Table A-27: Summary of Plate 28 Tension Test Results

Plate Number	Section Mark	Location	Steel Type	Nominal Strength (MPa)	Nominal Thickness (mm)	Mill Certificate Properties F_y (MPa)	F_u (MPa)	Elongation (%)
29	S2, S2-S	Web	A572	345	7.938	430	565	23

Specimen ID	Young's Mod.	Upper Yield		Lower Yield		0.2% Offset Yield		Static Yield		Strain Hardening			Tensile Strength		Gage Length
	E (GPa)	ε (%)	σ (MPa)	ε (%)	σ (MPa)	ε (%)	σ (MPa)	ε (%)	σ (MPa)	ε_{st} (%)	$\varepsilon_{apparent}$ (%)	E_{st} (GPa)	ε (%)	σ (MPa)	(mm)
	Tension Tests (L direction: longitudinal axis in the direction of rolling)														
29-W4-1	195.3	0.295	428.2	0.667	411.4	0.415	418.0	. . .	. . .	2.216	2.497	3.235	12.18	555.9	203.2
29-W4-2	194.9	0.277	433.4	0.414	409.4	0.412	413.5	. . .	. . .	2.355	2.624	2.915	12.25	554.8	203.2
29-W4-3	208.3	0.314	428.7	0.406	410.2	0.401	414.7	0.396	404.2	2.135	2.204	3.453	12.34	557.2	203.2
29-W6-1	185.0	0.348	418.6	0.553	406.1	0.424	411.6	. . .	. . .	1.614	1.665	3.880	12.32	559.8	203.2
29-W6-2	198.8	0.363	430.5	0.500	412.4	0.416	428.6	. . .	. . .	1.827	1.950	3.511	12.22	562.0	203.2
29-W6-3	200.2	0.334	429.8	1.547	407.3	0.411	419.7	0.400	397.2	1.452	1.852	3.522	12.04	562.4	203.2
29-W8-1	174.9	0.393	425.4	0.961	411.5	0.442	423.6	. . .	. . .	1.663	1.926	3.420	12.26	565.6	203.2
29-W8-2	195.1	0.376	438.1	0.469	421.8	0.421	433.7	. . .	. . .	1.834	2.152	3.241	12.28	565.5	203.2
29-W8-3	202.7	0.342	435.1	0.445	416.4	0.413	427.8	0.405	412.0	1.916	2.104	3.183	12.31	564.1	203.2
	Tension Tests (LT direction: longitudinal axis normal to the direction of rolling)														
29-W3-1	195.3	0.286	441.2	0.386	412.9	0.418	422.0	. . .	. . .	1.923	2.509	3.133	12.24	556.1	203.2
29-W3-2	204.1	0.248	446.8	1.498	418.0	0.412	429.1	. . .	. . .	2.251	2.544	3.175	. . .	560.8	203.2
29-W3-3	210.5	0.230	445.7	0.708	424.7	0.407	432.2	0.399	414.5	2.373	2.455	3.219	12.15	562.8	203.2
29-W5-1	200.9	0.279	442.1	0.368	408.1	0.412	419.3	. . .	. . .	1.682	1.976	3.302	12.21	557.7	203.2
29-W5-2	190.3	0.261	432.9	0.353	408.1	0.418	415.5	. . .	. . .	1.657	1.970	3.157	11.90	551.0	203.2
29-W5-3	206.9	0.266	442.7	0.336	416.6	0.406	424.4	0.400	410.8	1.634	1.847	3.598	12.16	566.8	203.2
29-W7-1	204.8	0.275	457.9	0.385	428.6	0.413	435.2	. . .	. . .	2.096	2.392	2.986	12.25	564.3	203.2
29-W7-2	200.2	0.263	449.8	1.334	417.3	0.416	431.2	. . .	. . .	2.075	2.385	2.826	12.26	556.8	203.2
29-W7-3	215.5	0.252	445.0	0.910	426.5	0.403	434.1	0.393	412.3	2.096	2.352	2.989	12.30	564.0	203.2
	Statistics														
Mean	199.1	0.300	437.3	0.680	414.8	0.415	424.1	0.399	408.5	1.933	2.189	3.264	12.22	560.4	
Standard Deviation	9.5	0.048	9.9	0.404	6.9	0.009	7.7	0.004	6.5	0.279	0.289	0.265	0.11	4.5	
Range	40.7	0.163	39.4	1.211	22.5	0.041	23.6	0.012	17.2	0.921	0.959	1.054	0.45	15.8	
Minimum	174.9	0.230	418.6	0.336	406.1	0.401	411.6	0.393	397.2	1.452	1.665	2.826	11.90	551.0	
Maximum	215.5	0.393	457.9	1.547	428.6	0.442	435.2	0.405	414.5	2.373	2.624	3.880	12.34	566.8	
Count	18	18	18	18	18	18	18	6	6	18	18	18	17	18	

Table A-28: Summary of Plate 29 Tension Test Results

Plate Number	Section Mark	Location	Steel Type	Nominal Strength (MPa)	Nominal Thickness (mm)	Mill Certificate Properties F_y (MPa)	F_u (MPa)	Elongation (%)
30	B7	Comp. Flange	A572	345	15.875	389	531	24

Specimen ID	Young's Mod.	Upper Yield		Lower Yield		0.2% Offset Yield		Static Yield		Strain Hardening			Tensile Strength		Gage Length
	E (GPa)	ε (%)	σ (MPa)	ε (%)	σ (MPa)	ε (%)	σ (MPa)	ε (%)	σ (MPa)	ε_{st} (%)	$\varepsilon_{apparent}$ (%)	E_{st} (GPa)	ε (%)	σ (MPa)	(mm)
Tension Tests (L direction: longitudinal axis in the direction of rolling)															
30-F1-1	209.1	0.217	402.8	1.595	375.8	0.387	389.5	. . .	. . .	1.365	1.595	3.621	12.27	527.2	203.2
30-F1-2	210.2	0.197	408.0	0.210	382.3	0.384	390.3	. . .	. . .	1.265	1.634	3.230	. . .	531.4	203.2
30-F1-3	217.3	0.205	407.6	0.266	379.8	0.379	389.7	0.373	376.9	1.394	1.486	3.509	12.44	530.3	203.2
30-F2-1	213.7	0.210	411.9	0.284	375.5	0.381	387.1	. . .	. . .	1.144	1.533	3.299	12.33	530.9	203.2
30-F2-2	210.2	0.211	412.2	0.252	385.0	0.386	389.4	. . .	. . .	1.351	1.579	3.616	12.44	531.5	203.2
30-F3-1	216.9	0.220	410.9	0.299	385.1	0.381	388.1	. . .	. . .	1.211	1.590	3.363	12.30	529.1	203.2
30-F3-2	211.7	0.214	410.0	0.318	380.5	0.384	387.9	. . .	. . .	1.263	1.556	3.378	12.39	529.1	203.2
30-F3-3	208.0	0.208	417.7	1.594	386.8	0.393	399.4	0.383	379.6	1.335	1.594	3.359	. . .	534.3	203.2
Statistics															
Mean	212.1	0.210	410.1	0.602	381.4	0.384	390.2	0.378	378.3	1.291	1.571	3.422	12.36	530.5	
Standard Deviation	3.5	0.007	4.3	0.613	4.2	0.004	3.9	0.007	1.9	0.085	0.045	0.144	0.07	2.1	
Range	9.3	0.023	14.9	1.385	11.3	0.013	12.3	0.010	2.7	0.250	0.148	0.391	0.17	7.0	
Minimum	208.0	0.197	402.8	0.210	375.5	0.379	387.1	0.373	376.9	1.144	1.486	3.230	12.27	527.2	
Maximum	217.3	0.220	417.7	1.595	386.8	0.393	399.4	0.383	379.6	1.394	1.634	3.621	12.44	534.3	
Count	8	8	8	8	8	8	8	2	2	8	8	8	6	8	
Compression Tests															
30-F2-3-1	202.0	0.206	414.8	1.067	395.6	0.397	399.9	0.391	386.2	0.996	1.067	4.692			50.8
30-F2-3-2	201.7	0.202	415.9	0.766	392.4	0.384	397.0	0.377	383.2	1.392	1.504	5.667			50.8
30-F2-3-3	204.2	0.202	423.8	0.577	389.6	0.382	398.4	0.375	382.4	1.136	1.263	5.080			50.8
Statistics															
Mean	202.6	0.203	418.2	0.803	392.5	0.388	398.4	0.381	383.9	1.174	1.278	5.146			
Standard Deviation	1.4	0.002	4.9	0.247	3.0	0.008	1.4	0.009	2.0	0.201	0.219	0.491			
Range	2.5	0.004	9.0	0.490	6.0	0.015	2.9	0.016	3.9	0.397	0.437	0.975			
Minimum	201.7	0.202	414.8	0.577	389.6	0.382	397.0	0.375	382.4	0.996	1.067	4.692			
Maximum	204.2	0.206	423.8	1.067	395.6	0.397	399.9	0.391	386.2	1.392	1.504	5.667			
Count	3	3	3	3	3	3	3	3	3	3	3	3			

Table A-29: Summary of Plate 30 Tension and Compression Test Results

Plate Number	Section Mark	Location	Steel Type	Nominal Strength (MPa)	Nominal Thickness (mm)	Mill Certificate Properties F_y (MPa)	F_u (MPa)	Elongation (%)
31	B8	Comp. Flange	A572	345	19.050	378	526	26

Specimen ID	Young's Mod.	Upper Yield		Lower Yield		0.2% Offset Yield		Static Yield		Strain Hardening			Tensile Strength		Gage Length
	E (GPa)	ε (%)	σ (MPa)	ε (%)	σ (MPa)	ε (%)	σ (MPa)	ε (%)	σ (MPa)	ε_{st} (%)	$\varepsilon_{apparent}$ (%)	E_{st} (GPa)	ε (%)	σ (MPa)	(mm)
Tension Tests (L direction: longitudinal axis in the direction of rolling)															
31-F4-1	212.5	0.206	395.3	0.307	363.5	0.379	380.0	. . .	. . .	1.335	1.574	3.376	12.30	515.1	203.2
31-F4-2	207.0	0.200	396.5	0.228	367.2	0.383	377.4	. . .	. . .	1.368	1.526	3.623	12.32	514.6	203.2
31-F5-1	206.1	0.209	392.2	0.527	365.6	0.385	376.3	. . .	. . .	1.440	1.650	3.667	12.23	513.4	203.2
31-F5-2	211.4	0.205	400.2	0.228	370.0	0.381	378.0	. . .	. . .	1.285	1.617	3.295	12.40	516.7	203.2
31-F5-3	207.2	0.200	393.6	0.238	364.3	0.381	374.4	. . .	. . .	1.347	1.578	3.410	12.35	516.6	203.2
31-F6-1	208.3	0.195	400.8	1.477	365.7	0.381	378.3	. . .	. . .	1.187	1.477	3.395	12.05	516.3	203.2
31-F6-2	205.6	0.200	389.1	1.560	366.6	0.384	377.9	. . .	. . .	1.302	1.560	3.326	12.02	513.7	203.2
31-F6-3	208.0	0.201	401.2	0.883	370.2	0.381	376.1	0.374	361.6	1.456	1.639	3.612	12.38	514.1	203.2
Statistics															
Mean	208.3	0.202	396.1	0.681	366.6	0.382	377.3	0.374	361.6	1.340	1.578	3.463	12.26	515.1	
Standard Deviation	2.5	0.004	4.4	0.563	2.4	0.002	1.7	. . .	. . .	0.086	0.058	0.147	0.15	1.3	
Range	6.9	0.014	12.0	1.332	6.7	0.006	5.6	. . .	. . .	0.269	0.173	0.372	0.38	3.3	
Minimum	205.6	0.195	389.1	0.228	363.5	0.379	374.4	0.374	361.6	1.187	1.477	3.295	12.02	513.4	
Maximum	212.5	0.209	401.2	1.560	370.2	0.385	380.0	0.374	361.6	1.456	1.650	3.667	12.40	516.7	
Count	8	8	8	8	8	8	8	1	1	8	8	8	8	8	
Compression Tests															
31-F4-3-1	204.9	0.207	399.0	1.239	372.5	0.374	378.3	0.366	362.6	1.116	1.239	4.990			50.8
31-F4-3-2	205.2	0.211	395.3	1.216	370.6	0.363	378.3	0.358	367.2	1.119	1.228	5.033			50.8
31-F4-3-3	201.4	0.211	390.4	1.266	367.5	0.384	375.8	0.378	362.6	1.185	1.266	5.358			50.8
Statistics															
Mean	203.8	0.210	394.9	1.241	370.2	0.374	377.4	0.367	364.1	1.140	1.244	5.127			
Standard Deviation	2.1	0.002	4.3	0.025	2.5	0.010	1.4	0.010	2.6	0.039	0.020	0.201			
Range	3.8	0.004	8.6	0.050	5.0	0.021	2.5	0.020	4.6	0.070	0.038	0.367			
Minimum	201.4	0.207	390.4	1.216	367.5	0.363	375.8	0.358	362.6	1.116	1.228	4.990			
Maximum	205.2	0.211	399.0	1.266	372.5	0.384	378.3	0.378	367.2	1.185	1.266	5.358			
Count	3	3	3	3	3	3	3	3	3	3	3	3			

Table A-30: Summary of Plate 31 Tension and Compression Test Results

Table 7.1-32: Summary of Plate 32 Tension Test Results

Plate Number	Section Mark	Location	Steel Type	Nominal Strength (MPa)	Nominal Thickness (mm)	Mill Certificate Properties F_y (MPa)	F_u (MPa)	Elongation (%)
32	MV1, MV2	Both Flanges	A572	345	19.050	458	620	21

Specimen ID	Young's Mod.	Upper Yield		Lower Yield		0.2% Offset Yield		Static Yield		Strain Hardening			Tensile Strength		Gage Length
	E (GPa)	ε (%)	σ (MPa)	ε (%)	σ (MPa)	ε (%)	σ (MPa)	ε (%)	σ (MPa)	ε_{st} (%)	$\varepsilon_{apparent}$ (%)	E_{st} (GPa)	ε (%)	σ (MPa)	(mm)
	Tension Tests (L direction: longitudinal axis in the direction of rolling)														
32-F1-3	213.5	0.240	484.4	0.305	447.2	0.411	452.1	0.406	442.5	1.110	1.351	4.511	11.72	622.2	203.2
32-F1-4	218.3	0.260	477.3	0.315	449.6	0.405	451.0	0.401	443.0	1.033	0.993	4.971	8.19	615.6	203.2
32-F2-1	209.6	0.273	452.5	0.317	434.5	0.416	433.4	0.413	428.0	0.897	0.953	5.238	11.76	612.6	203.2
32-F2-2	205.4	0.293	448.8	0.342	429.4	0.407	432.5	0.402	423.1	0.849	0.896	5.307	11.75	611.2	203.2
32-F3-1	222.5	0.228	466.5	0.279	438.0	0.397	441.2	0.393	432.0	0.851	1.032	4.976	11.75	619.6	203.2
32-F3-2	228.8	0.226	468.3	0.283	438.6	0.392	440.4	0.389	432.5	0.908	1.012	5.242	11.73	620.3	203.2
	Statistics														
Mean	216.3	0.3	466.3	0.3	439.5	0.4	441.8	0.4	433.5	0.9	1.0	5.0	11.2	616.9	
Standard Deviation	8.6	0.0	13.8	0.0	7.6	0.0	8.4	0.0	7.9	0.1	0.2	0.3	1.4	4.5	
Range	23.4	0.1	35.6	0.1	20.2	0.0	19.6	0.0	19.9	0.3	0.5	0.8	3.6	11.1	
Minimum	205.4	0.2	448.8	0.3	429.4	0.4	432.5	0.4	423.1	0.8	0.9	4.5	8.2	611.2	
Maximum	228.8	0.3	484.4	0.3	449.6	0.4	452.1	0.4	443.0	1.1	1.4	5.3	11.8	622.2	
Count	6	6	6	6	6	6	6	6	6	6	6	6	6	6	

Table A-31: Summary of Plate 32 Tension Test Results

Plate Number	Section Mark	Location	Steel Type	Nominal Strength (MPa)	Nominal Thickness (mm)	Mill Certificate Properties F_y (MPa)	F_u (MPa)	Elongation (%)
33	MV1, MV2	Web	A572	345	7.938	425	506	36

Specimen ID	Young's Mod.	Upper Yield		Lower Yield		0.2% Offset Yield		Static Yield		Strain Hardening			Tensile Strength		Gage Length
	E (GPa)	ε (%)	σ (MPa)	ε (%)	σ (MPa)	ε (%)	σ (MPa)	ε (%)	σ (MPa)	ε_{st} (%)	$\varepsilon_{apparent}$ (%)	E_{st} (GPa)	ε (%)	σ (MPa)	(mm)
	Tension Tests (L direction: longitudinal axis in the direction of rolling)														
33-W3-1	213.5	0.200	422.6	1.196	393.1	0.388	401.0	0.384	392.9	2.402	2.963	1.789	12.42	472.8	203.2
33-W3-2	214.1	0.205	430.4	2.262	396.8	0.377	401.0	0.374	394.1	2.684	2.960	2.170	12.34	476.7	203.2
33-W5-1	214.0	0.210	446.1	1.572	407.5	0.392	412.5	0.388	403.3	2.305	2.446	2.484	12.49	491.4	203.2
33-W5-2	214.5	0.206	439.6	1.573	408.9	0.392	410.9	0.388	402.4	2.422	2.646	2.233	. . .	493.9	203.2
33-W7-1	215.1	0.202	434.4	1.614	408.1	0.392	412.4	0.388	404.3	2.527	3.168	1.745	12.32	481.5	203.2
33-W7-2	214.6	0.205	438.4	2.644	404.8	0.392	411.7	0.388	403.9	2.569	2.913	2.132	. . .	485.3	203.2
	Tension Tests (LT direction: longitudinal axis normal to the direction of rolling)														
33-W2-1	216.0	0.197	419.7	0.579	394.6	0.386	400.9	0.382	393.2	2.829	3.301	1.562	12.22	474.1	203.2
33-W2-2	214.6	0.193	419.5	0.263	396.2	0.385	397.5	0.382	389.9	2.956	3.269	1.875	11.06	473.4	203.2
33-W4-1	215.3	0.207	444.9	0.524	408.7	0.390	409.5	0.387	401.6	2.150	2.725	1.919	. . .	492.8	203.2
33-W4-2	214.1	0.211	449.1	0.791	409.8	0.393	414.2	0.390	406.5	2.290	2.680	2.050	12.19	492.0	203.2
33-W6-1	218.8	0.205	447.6	2.623	411.2	0.381	418.2	0.377	410.1	2.061	2.623	1.951	12.26	492.8	203.2
33-W6-2	216.2	0.207	448.7	2.593	401.7	0.412	415.7	0.409	407.6	2.241	2.589	2.178	12.14	492.5	203.2
	Statistics														
Mean	215.1	0.204	436.7	1.519	403.4	0.390	408.8	0.386	400.8	2.453	2.857	2.007	12.16	485.0	
Standard Deviation	1.4	0.005	11.3	0.868	6.6	0.009	6.9	0.009	6.6	0.271	0.282	0.251	0.43	8.7	
Range	5.3	0.018	29.6	2.381	18.1	0.035	20.7	0.035	20.2	0.894	0.855	0.922	1.43	21.1	
Minimum	213.5	0.193	419.5	0.263	393.1	0.377	397.5	0.374	389.9	2.061	2.446	1.562	11.06	472.8	
Maximum	218.8	0.211	449.1	2.644	411.2	0.412	418.2	0.409	410.1	2.956	3.301	2.484	12.49	493.9	
Count	12	12	12	12	12	12	12	12	12	12	12	12	9	12	

Table A-32: Summary of Plate 33 Tension Test Results

Plate Number	Section Mark	Location	Steel Type	Nominal Strength (MPa)	Nominal Thickness (mm)	Mill Certificate Properties F_y (MPa)	F_u (MPa)	Elongation (%)
34	MV3, MV4	Both Flanges	A572	345	23.813	396	545	23

Specimen ID	Young's Mod.	Upper Yield		Lower Yield		0.2% Offset Yield		Static Yield		Strain Hardening			Tensile Strength		Gage Length
	E (GPa)	ε (%)	σ (MPa)	ε (%)	σ (MPa)	ε (%)	σ (MPa)	ε (%)	σ (MPa)	ε_{st} (%)	$\varepsilon_{apparent}$ (%)	E_{st} (GPa)	ε (%)	σ (MPa)	(mm)
	Tension Tests (L direction: longitudinal axis in the direction of rolling)														
34-F6-2a	206.1	0.355	394.7	0.510	388.6	0.390	389.7	0.384	377.2	0.712	0.830	4.026	12.488	546.7	203.2
34-F6-1-1R	219.0	0.183	380.1	0.241	361.5	0.368	368.6	0.363	356.3	0.584	0.741	4.221	13.065	535.9	50.8
34-F6-1-2R	214.9	0.191	380.7	0.241	363.3	0.382	369.5	0.377	358.6	0.614	0.675	4.322	13.561	536.8	50.8
34-F6-1-3R	207.8	0.197	375.2	0.245	360.9	0.363	366.7	0.358	356.7	0.533	0.662	4.521	12.423	537.9	50.8
	Statistics														
Mean	212.0	0.2	382.7	0.3	368.6	0.4	373.6	0.4	362.2	0.6	0.7	4.3	12.9	539.4	
Standard Deviation	6.1	0.1	8.4	0.1	13.4	0.0	10.8	0.0	10.1	0.1	0.1	0.2	0.5	5.0	
Range	12.9	0.2	19.5	0.3	27.7	0.0	23.0	0.0	20.9	0.2	0.2	0.5	1.1	10.8	
Minimum	206.1	0.2	375.2	0.2	360.9	0.4	366.7	0.4	356.3	0.5	0.7	4.0	12.4	535.9	
Maximum	219.0	0.4	394.7	0.5	388.6	0.4	389.7	0.4	377.2	0.7	0.8	4.5	13.6	546.7	
Count	4	4	4	4	4	4	4	4	4	4	4	4	4	4	

Table A-33: Summary of Plate 34 Tension Test Results

Plate Number	Section Mark	Location	Steel Type	Nominal Strength (MPa)	Nominal Thickness (mm)	Mill Certificate Properties F_y (MPa)	F_u (MPa)	Elongation (%)
35	MV3, MV4	Web	A572	345	7.938	425	506	36

Specimen ID	Young's Mod.	Upper Yield		Lower Yield		0.2% Offset Yield		Static Yield		Strain Hardening			Tensile Strength		Gage Length
	E (GPa)	ε (%)	σ (MPa)	ε (%)	σ (MPa)	ε (%)	σ (MPa)	ε (%)	σ (MPa)	ε_{st} (%)	$\varepsilon_{apparent}$ (%)	E_{st} (GPa)	ε (%)	σ (MPa)	(mm)
	Tension Tests (L direction: longitudinal axis in the direction of rolling)														
35-W9-1	218.2	0.192	419.0	1.258	397.7	0.384	402.3	0.381	395.1	2.249	3.152	1.557	12.18	473.7	203.2
35-W9-2	213.8	0.194	415.6	0.202	388.6	0.383	391.5	0.381	386.5	2.680	3.127	2.047	12.47	466.7	203.2
35-W11-1	218.1	0.211	451.5	0.273	411.4	0.379	413.6	0.375	404.8	1.773	2.560	1.883	12.21	499.2	203.2
35-W11-2	214.6	0.208	444.0	0.734	407.0	0.392	411.1	0.388	402.4	2.041	2.485	1.943	12.27	492.4	203.2
35-W13-1	213.5	0.215	452.7	1.078	415.4	0.396	419.2	0.393	411.5	2.528	2.816	1.758	12.28	493.2	203.2
35-W13-3	213.2	0.211	450.2	1.492	413.2	0.395	416.9	0.390	406.0	2.003	3.124	1.427	. . .	490.8	203.2
	Tension Tests (LT direction: longitudinal axis normal to the direction of rolling)														
35-W8-1	215.6	0.207	447.2	1.569	412.6	0.393	416.0	0.390	409.2	2.128	2.741	2.060	12.27	493.5	203.2
35-W8-2	215.8	0.206	449.3	0.910	410.6	0.391	413.7	0.387	405.4	2.293	2.536	2.337	12.25	494.5	203.2
35-W10-1	213.3	0.211	448.7	0.268	409.4	0.392	410.1	0.389	403.1	2.052	2.478	1.934	11.72	493.1	203.2
35-W10-2	213.2	0.210	441.3	0.372	407.4	0.391	408.1	0.386	397.9	2.014	2.491	1.933	11.71	492.7	203.2
35-W12-1	216.3	0.213	459.9	0.238	423.9	0.399	430.8	0.396	422.8	1.445	2.826	1.363	12.13	502.2	203.2
35-W12-2	215.0	0.217	466.3	0.291	431.7	0.403	436.6	0.398	425.9	2.257	2.680	2.135	. . .	509.5	203.2
	Statistics														
Mean	215.1	0.208	445.5	0.724	410.7	0.392	414.2	0.388	405.9	2.122	2.751	1.865	12.15	491.8	
Standard Deviation	1.8	0.008	14.7	0.521	11.0	0.007	11.8	0.006	10.9	0.324	0.262	0.291	0.24	11.5	
Range	5.1	0.025	50.7	1.367	43.1	0.024	45.1	0.023	39.3	1.235	0.674	0.974	0.76	42.8	
Minimum	213.2	0.192	415.6	0.202	388.6	0.379	391.5	0.375	386.5	1.445	2.478	1.363	11.71	466.7	
Maximum	218.2	0.217	466.3	1.569	431.7	0.403	436.6	0.398	425.9	2.680	3.152	2.337	12.47	509.5	
Count	12	12	12	12	12	12	12	12	12	12	12	12	10	12	

Table A-34: Summary of Plate 35 Tension Test Results

Sturctual Steel Tube ID	Location	Outside Diameter (mm)	Steel Type	Nominal Strength (MPa)	Nominal Thickness (mm)	Mill Certificate Properties		
						F_y (MPa)	F_u (MPa)	Elongation (%)
674	Cross-Frames	127.0	A513 Grade 1026	448	6.350	555	666	18.0

Specimen ID	Young's Mod.	0.2% Offset Yield		Static Yield		Strain Hardening			Tensile Strength		Gage Length
	E (GPa)	ε (%)	σ (MPa)	ε (%)	σ (MPa)	ε_{st} (%)	$\varepsilon_{apparent}$ (%)	E_{st} (GPa)	ε (%)	σ (MPa)	(mm)
	Tension Tests (L direction: longitudinal axis in the direction of rolling)										
674-J1-1	205.4	0.425	492.8	0.419	478.7	0.425	0.425	15.975	6.33	645.6	50.8
674-J1-2	231.5	0.421	570.6	0.417	561.0	0.421	0.421	6.969	5.88	666.9	50.8
674-J2-1	235.7	0.428	561.5	0.424	551.3	0.428	0.428	4.993	5.96	657.3	50.8
674-J2-2	217.6	0.387	477.9	0.379	456.2	0.387	0.387	18.093	5.93	647.1	50.8
674-J3-1	170.1	0.500	528.8	0.476	486.3	0.500	0.500	11.984	5.60	655.7	50.8
674-J3-2	215.4	0.409	484.9	0.403	471.0	0.409	0.409	17.128	6.19	649.5	50.8
	Statistics										
Mean	212.6	0.428	519.4	0.420	500.7	0.428	0.428	12.524	5.98	653.7	
Standard Deviation	23.6	0.038	40.3	0.032	44.2	0.038	0.038	5.513	0.25	8.0	
Range	65.6	0.113	92.7	0.097	104.8	0.113	0.113	13.100	0.73	21.2	
Minimum	170.1	0.387	477.9	0.379	456.2	0.387	0.387	4.993	5.60	645.6	
Maximum	235.7	0.500	570.6	0.476	561.0	0.500	0.500	18.093	6.33	666.9	
Count	6	6	6	6	6	6	6	6	6	6	

Table A-35: Summary of Structural Steel Tube 674 Tension Test Results

Sturctual Steel Tube ID	Location	Outside Diameter (mm)	Steel Type	Nominal Strength (MPa)	Nominal Thickness (mm)	Mill Certificate Properties		
						F_y (MPa)	F_u (MPa)	Elongation (%)
811	Cross-Frames	127.000	A513 Grade 1026	448	6.350	584	679	19.0

Specimen ID	Young's Mod.	0.2% Offset Yield		Static Yield		Strain Hardening			Tensile Strength		Gage Length
	E (GPa)	ε (%)	σ (MPa)	ε (%)	σ (MPa)	ε_{st} (%)	$\varepsilon_{apparent}$ (%)	E_{st} (GPa)	ε (%)	σ (MPa)	(mm)
	Tension Tests (L direction: longitudinal axis in the direction of rolling)										
811-J1-1	234.1	0.399	529.1	0.394	513.9	0.399	0.399	6.465	6.85	634.8	50.8
811-J1-2	237.7	0.392	513.6	0.385	494.3	0.392	0.392	12.646	6.69	656.2	50.8
811-J2-2	268.6	0.359	504.5	0.353	483.5	0.359	0.359	10.503	6.85	628.8	50.8
811-J3-1	193.9	0.427	474.4	0.415	448.9	0.427	0.427	16.727	6.46	634.6	50.8
811-J3-2	205.8	0.439	531.5	0.430	512.8	0.439	0.439	8.327	6.52	647.0	50.8
Statistics											
Mean	228.0	0.403	510.6	0.395	490.7	0.403	0.403	10.934	6.67	640.3	
Standard Deviation	29.3	0.031	23.1	0.030	26.6	0.031	0.031	3.983	0.18	11.1	
Range	74.7	0.079	57.0	0.078	65.0	0.079	0.079	10.262	0.39	27.4	
Minimum	193.9	0.359	474.4	0.353	448.9	0.359	0.359	6.465	6.46	628.8	
Maximum	268.6	0.439	531.5	0.430	513.9	0.439	0.439	16.727	6.85	656.2	
Count	5	5	5	5	5	5	5	5	5	5	

Table A-36: Summary of Structural Steel Tube 811 Tension Test Results

Sturctual Steel Tube ID	Location	Outside Diameter (mm)	Steel Type	Nominal Strength (MPa)	Nominal Thickness (mm)	Mill Certificate Properties		
						F_y (MPa)	F_u (MPa)	Elongation (%)
871	Cross-Frames	127.0	A513 Grade 1026	448	6.350			

Specimen ID	Young's Mod.	0.2% Offset Yield		Static Yield		Strain Hardening			Tensile Strength		Gage Length
	E (GPa)	ε (%)	σ (MPa)	ε (%)	σ (MPa)	ε_{st} (%)	$\varepsilon_{apparent}$ (%)	E_{st} (GPa)	ε (%)	σ (MPa)	(mm)
	Tension Tests (L direction: longitudinal axis in the direction of rolling)										
871-J1-1	202.3	0.462	555.6	0.457	546.0	0.462	0.462	9.400	5.27	669.1	50.8
871-J1-2	216.5	0.404	486.3	0.395	466.5	0.404	0.404	17.916	5.86	643.9	50.8
871-j2-1	228.8	0.447	546.9	0.436	522.0	0.447	0.447	15.255	6.07	684.8	50.8
871-J2-2	202.3	0.431	553.4	0.423	533.0	0.431	0.431	12.813	5.85	673.9	50.8
871-J3-1	282.6	0.359	510.1	0.349	478.6	0.359	0.359	18.814	6.07	674.0	50.8
871-J3-2	195.7	0.484	546.8	0.471	520.9	0.484	0.484	12.510	6.00	671.3	50.8
	Statistics										
Mean	221.4	0.431	533.2	0.422	511.2	0.431	0.431	14.451	5.85	669.5	
Standard Deviation	32.3	0.045	28.4	0.044	31.5	0.045	0.045	3.568	0.30	13.6	
Range	86.9	0.125	69.4	0.122	79.5	0.125	0.125	9.414	0.80	40.8	
Minimum	195.7	0.359	486.3	0.349	466.5	0.359	0.359	9.400	5.27	643.9	
Maximum	282.6	0.484	555.6	0.471	546.0	0.484	0.484	18.814	6.07	684.8	
Count	6	6	6	6	6	6	6	6	6	6	

Table A-37: Summary of Structural Steel Tube 871 Tension Test Results

The matrix of tension test results was intended to include the following variables: steel grade, plate thickness and specimen orientation. However, due to the volume of tension testing additional variables were introduced into the results. These parameters include steel manufacturer, testing laboratory/load frame and data acquisition instrument gage length. These additional parameters are discussed when their effect is manifested in the test results.

A.2.1 Yield Strength Results

Modifying the E8 Standard by SSRC Technical Memorandum No. 7 permits the determination of up to four individual yield strengths from each test record. The offset yield strength is determined by the intersection of the stress-strain record with a line parallel to the exhibited initial modulus but offset 0.2% in strain. The upper yield strength is the first maximum stress associated with discontinuous yielding. The lower yield strength is the minimum stress recorded during discontinuous yielding neglecting any transient effects. Finally, the static yield strength is determined by essentially eliminating the loading rate effect on specimen behavior.

A.2.1.1 Offset Yield Strength

The offset yield strength mean and standard deviation for all A572 and A852 tension tests were 410.6 ± 25.7 MPa (59.55 ± 3.73 ksi) and 693.9 ± 47.9 MPa (100.64 ± 6.95 ksi), respectively. As expected for both steel grades, the thicker flange plates displayed lower yield strengths than the thinner web plates. Test specimen orientation, either in the direction of plate rolling (longitudinal) or normal to the direction of plate rolling (transverse) did not influence test results. A summary of these results is contained in Tables A-38 and A-39

Strength	Sample Description	All Plates	Web Plates (thickness ≤ 12.7 mm)		Flange Plates
	Specimen Orientation		Longitudinal	Transverse	Longitudinal
	Statistic				
Offset Yield	Mean (MPa)	410.6	416.5	417.8	400.7
	Standard Deviation (MPa)	25.7	25.9	26.3	21.7
	Number of Tests	248	72	77	99
Upper Yield	Mean (MPa)	425.7	430.8	433.1	415.0
	Standard Deviation (MPa)	26.8	25.4	28.8	22.8
	Number of Tests	236	77	72	87
Lower Yield	Mean (MPa)	406.3	412.4	411.7	396.6
	Standard Deviation (MPa)	25.0	24.9	25.7	21.5
	Number of Tests	237	77	72	88
Static Yield	Mean (MPa)	398.3	404.9	403.6	387.4
	Standard Deviation (MPa)	25.9	25.0	26.5	22.6
	Number of Tests	212	71	66	75
Tensile	Mean (MPa)	551.2	545.3	542.3	562.1
	Standard Deviation (MPa)	32.5	35.2	31.5	27.8
	Number of Tests	247	76	72	99

Table A-38: A572 Steel Tension Testing Statistics

Strength	Sample Description	All Plates	Web Plates (thickness ≤ 12.7 mm)		Flange Plates
	Specimen Orientation		Longitudinal	Transverse	Longitudinal
	Statistic				
Offset Yield	Mean (MPa)	693.9	711.2	713.6	644.7
	Standard Deviation (MPa)	47.9	45.7	41.0	15.4
	Number of Tests	44	16	16	12
Static Yield	Mean (MPa)	678.8	697.1	698.8	627.6
	Standard Deviation (MPa)	47.9	43.0	40.9	15.0
	Number of Tests	44	16	16	12
Tensile	Mean (MPa)	793.5	803.1	801.6	770.0
	Standard Deviation (MPa)	42.7	49.0	44.4	18.4
	Number of Tests	44	16	16	12

Table A-39: A852 Steel Tension Testing Statistics

The average yield strength for all A572 tension tests, 410.6 MPa, was very near the average yield strength of 420 MPa reported on the mill certificates that accompanied the steel plate from the producer and represents a consistent 19% over-strength when normalized by the nominal specified yield strength for this material. However, the average yield strength for all A852 tension tests, 693.9 MPa, was well in excess of an average mill certification reported value of 598 MPa. The A852 over-strength apparent in all tension tests averages 43%. This strength level is significantly greater than the over-strength expected based on the mill certification data. The mill certification data suggests an average over-strength of approximately 23% which is much more consistent with the

A572 over-strength results. No explanation as to the considerable difference between the physical test data and the mill certification test data which were both produced in accordance with the same testing standard is available.

A.2.1.2 Upper Yield Strength

Upper yield strength is defined by the E8 Standard as the first stress maximum associated with discontinuous yielding prior to the onset of strain hardening. Figure A-37 shows a typical tension test records for the A572 and A852 steel specimens tested as a part of this program as well as typical tension test records for HPS 485W and HPS 690W steels. The A572 and HPS steels exhibit well defined yield plateaus which are clearly evident in the figure. For steels that inelastically deform in this manner it is possible to determine upper and lower yield strengths that will permit engineers to better understand the materials behavior.

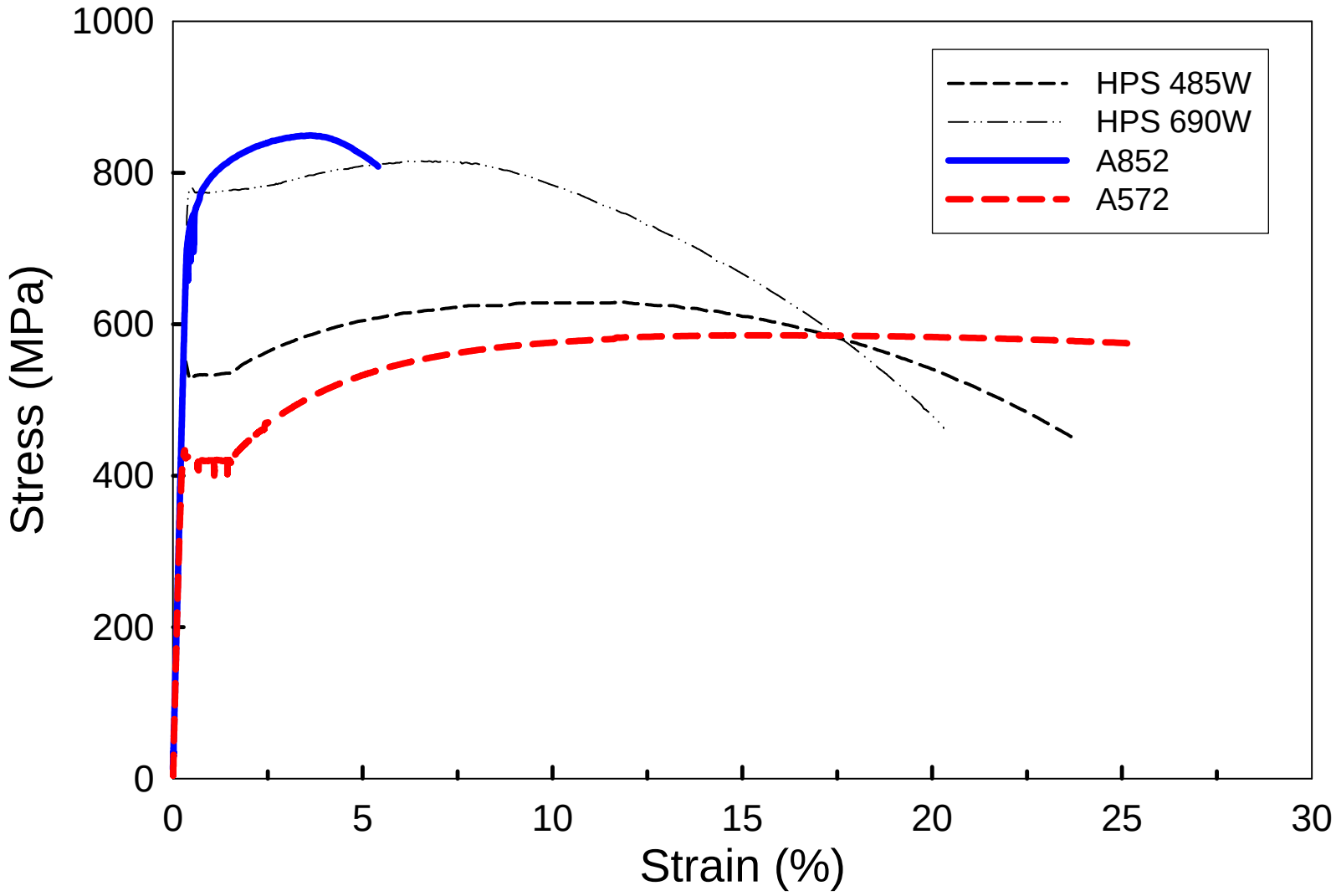

Figure A-37: Typical Tension Test Records

For the A572 specimens tested in this program the average upper yield strength was 425.7 MPa (61.74 ksi) which is approximately a 4% increase compared to the offset yield strength. All of the conclusions and trends reported for the offset yield strength results also apply to the A572 upper yield strength values.

The A852 specimens exhibited the round-house type curve shown in Figure A-37. With sufficient scrutiny of the results, upper yield strength can sometimes be identified in the A852 test records. However, these initial instances of discontinuous yielding are associated with very slight load reductions and are immediately followed by strain hardening of the material and therefore it is inappropriate to report these values.

The HPS steel test records are included on Figure A-37 as an aside. The American Association of State Highway and Transportation Officials (AASHTO), which maintains the codes and specifications that govern bridge design in the United States, recently replaced A852 and A514 steels, which have nominal yield strengths of 485MPa and 690MPa respectively, with HPS 485W and HPS 690W as the approved steels for bridge construction at those strength levels. The change was made in part to bring more uniformity to the post yield behavior of steels used to construct bridges.

A.2.1.3 Lower Yield Strength

Lower yield strength is defined by the E8 Standard as the minimum stress recorded during discontinuous yielding, ignoring transient effects. The average lower yield strength for the A572 specimens was 406.3 MPa (58.93 ksi). This strength is generally used to establish the stress level of the yield plateau for stress-strain relationship models for materials of this type.

No lower yield strength results are reported for the A852 test results for the reasons discussed in Section A.1.2.1.2 above.

A.2.1.4 Static Yield Strength

Static Yield Strength is defined by SSRC Technical Memorandum No. 7 as the yield strength of a material absent of any strain-rate effects. Procedures for determining the static yield strength for mild steels that exhibit either a yield plateau or a round-house tensile stress-strain behavior are discussed in the Technical Memorandum.

The A572 specimens had an average static yield strength of 398.3 MPa (57.77 ksi). This strength level is approximately 2% less than the lower yield strengths and approximately 3% less than the offset yield strengths determined for this steel. These reductions account for the strain rate effect that is inherent to the lower and offset yield strength results.

The A852 specimens displayed an average static yield strength of 678.8 MPa (98.45 ksi) which was only 2% less than the average offset yield strength for this material.

No functional relationship between individual test strain-rate and the static yield/offset yield or static yield/lower yield ratio was evident from the test data.

A.2.2 Yield Point Elongation Results

Yield Point Elongation is defined by the E8 Standard as the strain, expressed in percent, separating the stress-strain curve's first point of zero slope from the point of transition from discontinuous yielding to uniform strain hardening. Simply, this is the strain capacity of the yield plateau. The A572 specimens had an average yield point elongation of 1.42%. As discussed previously, the A852 specimens did not exhibit a yield plateau.

A.2.3 Tensile Strength Results

Tensile Strength is defined by the E8 Standard as the maximum stress recorded during a tension test. The average tensile strength for A572 specimens was 551.2 MPa (79.94 ksi) which was produced at a strain of approximately 14.38%. The average offset yield-to-tensile strength ratio for this material was 0.75. This ratio was very consistent and had an associated standard deviation of 0.04.

The average tensile strength for the A852 specimens was 793.5 MPa (115.09 ksi) which occurred at approximately 6.00% strain. The average offset yield-to-tensile strength ratio for the A852 specimens was more consistent but a significantly higher value of 0.87 (standard deviation of 0.02).

A.3 Compression Testing

Compression testing was conducted in accordance with ASTM E9, *Standard Test Methods of Compression Testing of Metallic Materials at Room Temperature*. These tests were limited to specimens taken from the steel plates that where used in the fabrication of the CSBRP bending test component compression flanges. Three specimens from each of seven plates of A572 steel were tested for a total of twenty-one compression tests.

The test data obtained using the E9 Standard may be used to determine yield strength, yield point elongation and compressive strength. However, since the steels used in this program do not fail in compression by shattering, the compressive strength is a value that is dependent on concurrent strain and specimen geometry. Selection of this point from the stress-strain record is arbitrary and therefore results for compressive strength are not presented in this report.

As defined by the E9 Standard, medium-length cylindrical specimens were used for the compression testing. Medium-length specimens have an approximate length-to-diameter ratio of 3.0 and are generally used to determine the compressive strength properties of steels. The diameter of each specimen was kept as near as possible, with allowances for machining, to the full thickness of the plate from which it was cut. Compression test specimens in this program had nominal thicknesses of 19mm (3/4 in.).

Although SSRC Technical Memorandum No. 7 was developed to modify the E8 Standard in order to eliminate the strain rate effects from tension test yield strength results, it was also successfully employed during the compression testing for the same purpose. Plate specific static yield strength results, and all other individual compression test results can be see on Tables A-21 through A-25 and Tables A-30 and A-31. A summary of the compression test data appears on Table A-40.

Strength	Statistic	
Offset Yield	Mean (MPa)	425.4
	Standard Deviation (MPa)	27.0
	Number of Tests	21
Upper Yield	Mean (MPa)	441.7
	Standard Deviation (MPa)	26.3
	Number of Tests	21
Lower Yield	Mean (MPa)	417.1
	Standard Deviation (MPa)	26.4
	Number of Tests	21
Static Yield	Mean (MPa)	404.7
	Standard Deviation (MPa)	24.3
	Number of Tests	19

Table A-40: A572 Steel Compression Testing Statistics.

A significant assumption of the structural engineering community is that the steels commonly used for the design and construction of buildings and bridges behave

similarly, if not identically, within the tension and compression stress-strain domains. The purpose of these compression tests within this program was to either validate this assumption, or to provide sufficient data to adequately construct the compressive stress-strain relationship for A572 steel plate for use in the analysis of the data and finite element modeling.

A.3.1 Yield Strength Results

Since these results, like the tension test results, are engineering stress-strain quantities, small increases in all strength categories are expected. These increases account for the difference in cross-sectional area of a necking tension test specimen and a barreling compression test specimen. However, once these properties are converted to a true stress-strain relationship the differences become slight as is demonstrated in Section 4 of this dissertation.

A.3.1.1 Offset Yield Strength

The offset yield strength for compression tests were determined using a 0.2% initial modulus strain offset. The average offset yield strength for the compression tests was 425.4 MPa (61.70 ksi) which represents approximately a 3.6% increase compared to the appropriate tension test result.

A.3.1.2 Upper Yield Strength

The average upper yield strength of the compression tests was 441.7 MPa (64.06 ksi). This strength level is 3.8% greater than the tension test result for upper yield strength.

A.3.1.3 Lower Yield Strength

The average compression test lower yield strength is 417.1 MPa (60.49 ksi). This strength represents a small, 2.6%, increase over the average tension test lower yield strength reported as 406.3 MPa (58.93 ksi).

A.3.1.4 Static Yield Strength

Static yield strengths produced during the compression tests averaged 404.7 MPa (58.70 ksi). This represents only a slight 1.6% increase strength increase when compared to the tension test results.

A.3.2 Yield Point Elongation Results

Yield point elongation averaged 1.28% for the compression tests. This property was the most effected by the difference in test method between tension and compression testing. The tension test result of 1.42% represents an increase of almost 11% in strain capacity prior to strain hardening.

A.4 Young's Modulus Testing

The Young's Modulus testing was conducted in accordance with ASTM E111, *Standard Test Method for Young's Modulus, Tangent Modulus, and Chord Modulus*. Ten (10) Young's modulus tests were conducted as a part of this program. Parameters include steel grade and plate thickness. The E111 Standard was used without modification to conduct the testing. Standard plate-type tension specimens as described in Section A.1.2 were selected as the test specimens since the testing was performed in the tension stress-strain domain.

Two independent methods of acquiring uniaxial test specimen deformation were used. On one side of each plate-type specimen was place a 6.35mm (1/4 inch) long electrical resistance strain gage. The strain gage data averages or smears the behavior of the steel under the length of the gage. On the opposite side of the test specimen a clip gage with a 50.8mm (2 inch) gage length was used. This device also reports the average behavior of the specimen but now over a length 8 times as long as the strain gage.

Three (3) sets of loadings and unloadings were recorded during each test. The results are shown in Table A-41.

Sample Description	Data Acquisition Device	Data Source	Young's Modulus		
			Mean (GPa)	Standard Deviation (GPa)	Number of Results
All	Clip Gage	Initial Slope	200.9	5.5	10
		Unloading Slope	209.4	4.4	10
	Strain Gage	Initial Slope	204.7	0.6	10
		Unloading Slope	205.0	0.6	10
A572 Steel	Clip Gage	Initial Slope	200.2	6.2	6
		Unloading Slope	210.1	4.3	6
	Strain Gage	Initial Slope	204.9	0.7	6
		Unloading Slope	205.3	0.7	6
A852 Steel	Clip Gage	Initial Slope	202.1	4.8	4
		Unloading Slope	208.4	5.2	4
	Strain Gage	Initial Slope	204.4	0.5	4
		Unloading Slope	204.7	0.2	4

Table A-41: Young's Modulus Testing Statistics

Qualified Young's modulus results can also be obtained from both tension testing and compression testing. These results are summarized in Table A-42

.

Sample Description	Specimen Orientation	Girder Component	Modulus (GPa)	Standard Deviation (GPa)	Number of Tests
Tension Tests	All		201.5	14.4	292
A572 Tension Tests	All		201.2	15.5	248
	Longitudinal	All	200.2	17.5	176
		Webs	198.7	14.4	77
		Flanges	201.4	19.5	99
	Transverse	All	203.5	8.8	72
A852 Tension Tests	All		203.6	5.3	44
	Longitudinal	All	204.9	5.7	28
		Webs	201.3	4.0	16
		Flanges	209.8	3.4	12
	Transverse	All	201.3	3.7	16
Compression Tests	All		204.5	4.0	21
Note: Web plate thicknesses are less than or equal to 12.7mm (1/2 inch).					

Table A-42: Young's Modulus Statistics from Tension and Compression Testing

A.4.1 Young's Modulus Testing Results

If the initial slope and unloading slope from each set of test data is averaged then the mean Young's modulus for all tests performed is 205.2 GPa (29,762 ksi) from the clip gage data and 204.9 GPa (29,718 ksi) from the strain gage data. Table A-41 shows that the average results for steel type differ insignificantly from the average for the entire body of data.

A.4.2 Young's Modulus from Tension Testing

Determining Young's modulus from a tension test is permitted by the E111 Standard as long as the result is reported as being produced during such a test. The reason that the

result must be qualified is that specimen deformation during the single loading cycle of a tension test is often affected by the flatness of the specimen, the alignment of the data acquisition device, the alignment of the grips, and the seating of the specimen within the test frame.

The average Young's modulus determined from tension testing is 201.5 GPa (29,225 ksi) and the associated standard deviation is 14.4 GPa (2089 ksi). Table A-42 illustrates that neither steel type, plate thickness [web plate thicknesses are less than or equal to 12.7 mm (1/2 in.)] nor specimen orientation significantly effected the test results.

A.4.3 Young's Modulus from Compression Testing

The average Young's modulus determined during the compression testing was 204.5 GPa (29,660 ksi).

A.5 True Stress-Strain

In order to elevate the accuracy of their predictions, finite element programs require true stress-strain relationships be constructed for the materials they are modeling. True stress-strain relationships are produced by modifying engineering stress-strain relationships that result from tension or compression testing for the necking or barreling of the specimen, respectively, as they undergo plastic deformation. It is particularly important to incorporate true stress-strain relationships into analytical models when materials will be loaded significantly beyond their proportional limit since a material's cross-sectional dimensions can experience substantial changes from its original state.

By their nature, the tension and compression tests described in Sections A.1.2 and A.1.3 and conducted as a part of this program produce engineering stress-strain

relationships. Conversion of those characteristics to true stress-strain was accomplished using the relationships derived in the following sections.

A.5.1 True Strain

Engineering strain, ε_e, is classically defined as a non-dimensionalized change in length that relates the new length, L_i, of a material to the original length, L_o, with the following equation:

$$\varepsilon_e = \frac{L_i - L_o}{L_o} = \frac{L_i}{L_o} - 1 \qquad \text{Equation A-1}$$

True strain, ε_t, is defined by the following differential:

$$d\varepsilon_t = \frac{dL}{L} \qquad \text{Equation A-2}$$

where the material's length, L, is measured in the direction of the strain. The true strain in any direction results from integrating Equation A-2 over the change in length experienced by a material in that direction.

$$\varepsilon_t = \int_{L_o}^{L_i} \frac{dL}{L} = \ln\left(\frac{L_i}{L_o}\right) \qquad \text{Equation A-3}$$

Solving Equation A-1 for $\frac{L_i}{L_o}$ and substituting the result into Equation A-3 produces the following relationship for converting engineering strain, ε_e, to true strain, ε_t.

$$\varepsilon_t = \ln(\varepsilon_e + 1) \qquad \text{Equation A-4}$$

A.5.2 True Stress

Engineering stress, σ_e, in a material is classically defined as the total load at any point, P, acting over the undeformed cross-sectional area, A_o, of material normal to that force at that point. This relationship is represented by the following equation:

$$\sigma_e = \frac{P}{A_o}$$ Equation A-5

True stress, σ_t, is determined by distributing the same load, P, over the deformed area, A_i.

$$\sigma_t = \frac{P}{A_i}$$ Equation A-6

As metallic materials exceed their yield strengths they plastically deform with negligible change in overall volume, V. During a tension test increases in length are offset by decreases in cross-sectional area. Likewise, during a compression test decreases in length are offset by increases in cross-sectional area. If an material's volume remains constant and can be expressed as its cross-sectional area, A, times its concurrent length, L, then

$$V_o = V_i \rightarrow A_o L_o = A_i L_i$$ Equation A-7

Solving Equation A-5 for the load P and Equation A-7 for the area A_i, and then substituting for those expressions in Equation A-6 results in the following equation:

$$\sigma_t = \sigma_e \left(\frac{L_i}{L_o} \right)$$ Equation A-8

Again solving Equation A-1 for the ratio $\frac{L_i}{L_o}$ and substituting the result into Equation A-8 produces the following relationship for converting engineering stress, σ_e, to true stress, σ_t.

$$\sigma_t = \sigma_e (\varepsilon_e + 1)$$ Equation A-9

Appendix B. Design Equations

B.1 A Summary of the Guide Specification Provisions for the Design of Non-Composite I-Girders in Flexure

The following section summarizes the Guide Specification provisions for determining critical flange and web longitudinal stresses, F_{cr}, in singly symmetric horizontally curved I-girders.

B.1.1 I-Girder Flanges

The Guide Specification provisions are valid for I-girder flanges that meet the following criteria:

$$f_{l1} \le 0.5F_{yc}$$

if $f_{bu} \ge \min(0.33F_{yc},\ 117MPa)$ then $\left|\frac{f_{l1}}{f_{bu}}\right| \le 0.5$

$$L_b \le 25b_{fc}$$

$$L_b \le \frac{R}{10}$$

$$b_{fc} \ge 0.15D$$

$$t_{fc} \ge 1.5t_w$$

where:

f_{l1} = total factored lateral flange bending stress at the section under consideration

f_{bu} = largest computed factored average flange stress at the section under consideration

F_{yc} = yield strength of the compression flange

L_b = unbraced arc length of the flange

b_f = minimum flange width in the panel

R = minimum girder radius within the panel

b_{fc} = compression flange width at section under consideration

D = web depth at section under consideration

t_{fc} = compression flange thickness at section under consideration

t_w = web thickness at section under consideration

B.1.1.1 Partially Braced Compression Flanges

- Compact Flanges

For flanges that meet the following criteria:

$$\frac{b_{fc}}{t_{fc}} \leq 18$$

$$F_{yc} \leq 345Mpa$$

the critical compressive longitudinal stress, F_{cr}, is the smaller of F_{cr1} or F_{cr2}:

$$F_{cr1} = F_{bs}\overline{\rho}_b\overline{\rho}_w \qquad \text{Equation B-1}$$

$$F_{cr2} = F_{yc} - \frac{|f_{l1}|}{3} \qquad \text{Equation B-2}$$

where:

$$F_{bs} = F_{yc}\left(1 - 3\left(\frac{L_b}{0.9b_{fc}}\right)^2 \frac{F_{yc}}{\pi^2 E}\right)$$ Equation B-3

$$\overline{\rho}_b = \frac{1}{1 + \frac{L_b}{b_{fc}}\left(1 + \frac{L_b}{6b_{fc}}\right)\left(\frac{L_b}{R} - 0.01\right)^2}$$ Equation B-4

$$\overline{\rho}_w = 0.95 + 18\left(0.1 - \frac{L_b}{R}\right)^2 + \frac{f_{l1}}{f_{bu}} \frac{\left(0.3 - 0.1\frac{L_b}{R}\frac{L_b}{b_{fc}}\right)}{\overline{\rho}_b\left(\frac{F_{bs}}{F_{yc}}\right)}$$ Equation B-5

and $\overline{\rho}_b \overline{\rho}_w \leq 1.0$.

- Non-Compact Flanges

For flanges that meet the following slenderness criteria:

$$\frac{b_{fc}}{t_{fc}} \leq 1.02\sqrt{\frac{E}{|(f_{bu} + f_{l1})|}} \leq 23$$ Equation B-6

the critical compressive longitudinal stress, F_{cr} is the smaller of F_{cr1} or F_{cr2}:

$$F_{cr1} = F_{bs}\rho_b\rho_w$$ Equation B-7

$$F_{cr2} = F_{yc} - |f_{l1}|$$ Equation B-8

where F_{bs} is given in Equation B-3 above and:

$$\rho_b = \frac{1}{1 + \frac{L_b}{R}\frac{L_b}{b_{fc}}}$$ Equation B-9

$$\rho_{w1} = \frac{1}{1 - \frac{f_{l1}}{f_{bu}}\left(1 - \frac{L_b}{75 b_{fc}}\right)}$$ Equation B-10

$$\rho_{w2} = \frac{0.95 + \frac{\frac{L_b}{b_{fc}}}{30 + 8{,}000\left(0.1 - \frac{L_b}{R}\right)^2}}{1 + 0.6\left(\frac{f_{l1}}{f_{bu}}\right)}$$ Equation B-11

and, if $\frac{f_{l1}}{f_{bu}} \geq 0$, then $\rho_w = \min(\rho_{w1}, \rho_{w2})$. Otherwise $\rho_w = \rho_{w1}$.

B.1.1.2 Partially Braced Tension Flanges

For flanges that meet the following slenderness criteria:

$$\frac{b_{fc}}{t_{fc}} \leq 1.02\sqrt{\frac{E}{|(f_{bu} + f_{l1})|}} \leq 23$$ Equation B-12

the critical compressive longitudinal stress, F_{cr} is the smaller of F_{cr1} or F_{cr2} where:

$$F_{cr1} = F_y \overline{\rho}_b \overline{\rho}_w$$ Equation B-13

and where $\overline{\rho}_b$, $\overline{\rho}_w$ and F_{cr2} are given by Equations B-4, B-5 and B-2, respectively.

B.1.2 I-Girder Webs

B.1.2.1 Unstiffened Webs

For unstiffened webs that meet the following slenderness criteria:

for $R \leq 213m$

$$\frac{D}{t_w} \le 100$$

for $R > 213m$

$$\frac{D}{t_w} \le 100 + 0.125(R - 213) \le 150$$

the critical compressive longitudinal stress, F_{cr}, is:

$$F_{cr} = \frac{0.9Ek}{\left(\frac{D}{t_w}\right)^2} \le F_{yc} \qquad \text{Equation B-14}$$

where:

k = bend-buckling coefficient = $7.2\left(\frac{D}{D_c}\right)^2$

D_c = depth of web in compression

B.1.2.2 Transversely Stiffened Webs

For transversely stiffened webs that meet the following slenderness and stiffener spacing criteria:

$$\frac{D}{t_w} \le 150$$

for $R \le 213m$

$$d_o \le D$$

for $R > 213m$

$$d_o \le \left(1.0 + 0.00506(R - 213)\right)D \le 3D$$

the critical compressive longitudinal stress, F_{cr}, is given by Equation B-14 above but where:

k = bend-buckling coefficient = $9.0\left(\frac{D}{D_c}\right)^2$

B.1.2.3 Transversely and Longitudinally Stiffened Webs

For transversely and longitudinally stiffened webs that meet the transverse stiffener spacing requirements of Section B.1.2.2 and the following slenderness criteria:

$$\frac{D}{t_w} \leq 300$$

the critical compressive longitudinal stress is given by Equation B-14 above but where the bend-buckling coefficient is:

$$k = 5.17\left(\frac{D}{t_s}\right)^2 \text{ for } \frac{d_s}{D_c} \geq 0.4$$

or

$$k = 11.64\left(\frac{D}{D_c - d_s}\right)^2 \text{ for } \frac{d_s}{D_c} < 0.4$$

where:

d_s = distance along web between longitudinal stiffener and compression flange

B.2 A Summary of the Unified Design Method Equations for the Design of Non-Composite I-Girders in Flexure

The Unified Design Method provisions to determine the flange longitudinal stress limit, $\phi_f F_n$, are valid for I-Girders that meet the following criteria:

Compression flanges width, b_f, shall be at least 30% of the depth of the web in compression, D_c.

Tension flanges shall meet the following slenderness requirement:

$$\frac{b_{ft}}{2t_{ft}} \le 12.0$$

Webs shall meet the following slenderness requirements:

For unstiffened or transversely stiffened webs

$$\frac{D}{t_w} \le 150$$

For longitudinally stiffened webs

$$\frac{D}{t_w} \le 300$$

For all strength limit state load combinations the governing design equation for longitudinal flange stress is:

$$\phi_f F_n \ge f_{bu} + \frac{1}{3} f_l \qquad \text{Equation B-15}$$

where

$$f_l \le 0.6F_y$$

$\varphi_f = 1.00$

and F_n is determined for either the compression flange, F_{nc}, or the tension flange, F_{nt}, by the provisions outlined below.

B.2.1 Discretely Braced Compression Flanges

The longitudinal compressive stress limit, $\phi_f F_{nc}$, is the smaller of $\phi_f F_{nc(FLB)}$ or $\phi_f F_{nc(LTB)}$ determined from the Flange Local Buckling and Lateral Torsional Buckling limits.

B.2.1.1 Flange Local Buckling

If $\lambda_f \le \lambda_{pf}$, then the flange is compact and

$$F_{nc(FLB)} = R_b R_h F_{yc}$$ Equation B-16

where

$$\lambda_f = \frac{b_{fc}}{2t_{fc}}$$

$$\lambda_{pf} = 0.38\sqrt{\frac{E}{F_{yc}}}$$

If $\lambda_f > \lambda_{pf}$, then the flange is non-compact and

$$F_{nc(FLB)} = \left[1 - \left(1 - \frac{F_{yr}}{R_h F_{yc}}\right)\left(\frac{\lambda_f - \lambda_{pf}}{\lambda_{rf} - \lambda_{pf}}\right)\right] R_b R_h F_{yc}$$ Equation B-17

where

$$F_{yr} = \min\left[0.7F_{yc}, F_{yw}\right] > 0.5F_{yc}$$

$$\lambda_{rf} = 0.56\sqrt{\frac{E}{F_{yr}}}$$

B.2.1.2 Lateral Torsional Buckling

If $L_b \le L_p$, then compact unbraced length and

$$F_{nc(LTB)} = R_b R_h F_{yc}$$ Equation B-18

where

$$r_t = \frac{b_{fc}}{\sqrt{12\left(1 + \frac{1}{3}\frac{D_c t_w}{b_{fc} t_{fc}}\right)}}$$

$$L_p = 1.0 r_t \sqrt{\frac{E}{F_{yc}}}$$

If $L_p < L_b \le L_r$, then non-compact unbraced length and

$$F_{nc(LTB)} = C_b\left[1-\left(1-\frac{F_{yr}}{R_h F_{yc}}\right)\left(\frac{L_b - L_p}{L_r - L_p}\right)\right]R_b R_h F_{yc} \le R_b R_h F_{yc} \qquad \text{Equation B-19}$$

where

$$F_{yr} = \min\left[0.7F_{yc}, F_{yw}\right] \ge 0.5F_{yc}$$

$$L_r = \pi r_t \sqrt{\frac{E}{F_{yr}}}$$

If $L_b > L_r$, then slender unbraced length and

$$F_{nc(LTB)} = F_{cr} \le R_b R_h F_{yc} \qquad \text{Equation B-20}$$

where

$$F_{cr} = \frac{C_b R_b \pi^2 E}{\left(\frac{L_b}{r_t}\right)^2}$$

B.2.2 Discretely Braced Tension Flanges

The longitudinal tensile stress limit, $\phi_f F_{nt}$, is

$$\phi_f F_{nt} = R_h F_{yt} \qquad \text{Equation B-21}$$

References

AASHTO, 2004. LRFD Bridge Design Specifications, American Association of State Highway and Transportation Officials, 3rd Edition with 2005 Interim Provisions, Washington, DC.

AASHTO, 2003. Guide Specifications for Horizontally Curved Steel Girder Highway Bridges. American Association of State Highway and Transportation Officials, Washington, DC.

Adams, P.F., Lay, M.G. and Galambos, T.V., 1964. "Experiments on High Strength Steel Members", Fritz Engineering Laboratory Report No. 297.8, Lehigh University.

Brennan, P.J. and Mandel, J.A., 1971. "Analysis of Seekonk River Bridge Small Scale Structure Through Three Dimensional Mathematical Method and Structural Testing," Syracuse University Report, Research Project HPR-2(111), Syracuse, NY.

Brennan, P.J. and Mandel, J.A., 1974. "Analysis of Small Scale Structure of Ramp P Over Interstate I291 in Springfield, Massachusetts, Through Three Dimensional Mathematical Method and Structural Testing," Syracuse University Report, Research Project HPR-2(111), Syracuse, NY.

Colville, J., 1972. "Shear Connector Studies on Curved Girders", University of Maryland Civil Engineering Research Report #45, College Park, MD.

Culver, C.G. and Nasir, G., 1970. "Instability of Horizontally Curved Members," Pennsylvania Department of Highways Research Project No. 68-32.

Daniels, J.H., Zettlemoyer, N., Abraham, D., and Batcheler, R.P., 1979. "Fatigue of Curved Steel Bridge Elements – Ultimate Strength Tests of Horizontally Curved Plate and Box Girders," Lehigh University. Pennsylvania Department of Transportation Report No. DOT-FH-11.8198.7.

Donaldson, B.K., 1993. Analysis of Aircraft Structures: An Introduction, McGraw-Hill.

Duwadi, S.R., Grubb, M.A., Yoo, C.H., and Hartmann, J.L., 2000. "Federal Highway Administration's Horizontally Curved Steel Bridge Research Project," Proceedings of the 5th International Bridge Engineering Conference, Transportation Research Board, Paper No. 5B0011, Tampa, FL.

European Convention for Constructional Steelwork (ECCS), 1976. Manual on Stability of Steel Structures, 2nd Edition, Publication No. 22.

Farrar, C.R., and Duffey, T.A., 1998. "Bridge Modal Properties Using Simplified Finite Element Analysis," Journal of Bridge Engineering, American Society of Civil Engineers, Reston, VA.

Frank, K.H., George, D.A., Schluter, C.A., Gealy, S., and Horos, D.R., 1993. "Notch Toughness Variability in Bridge Steel Plates", National Cooperative Highway Research Council Report 355, Washington, DC.

Fukomoto, Y., Itoh, Y., and Kubo, M., 1980. "Strength Variation of Laterally Unsupported Beams," *Journal of the Structural Division*, American Society of Civil Engineers, Vol. 106, No. ST1, Reston, VA.

Galambos, T.V., 1988. Guide to Stability Design Criteria for Metal Structures, 4th Edition, Wiley-Interscience.

Galambos, T.V., 1968. Structural Members and Frames, Prentice-Hall.

Grubb, M.A., and Hall, D.H., *CSBRP work product report to be published*. "Curved Steel Bridge Research Project – Volume II: I-Girder Bending Component Tests," Federal Highway Administration, Report No. FHWA-RD-XX-XXX, Washington, DC.

Grubb, M.A., Yadlosky, J.M., Zureick, A.H., Hall, D.H., Yoo, C.H., and Duwadi, S.R., 1995. "FHWA Curved Steel Bridge Research Project," Proceedings 13th ASCE Structures Congress, American Society of Civil Engineers, Boston, MA.

Hall, D.H., Grubb, M.A., and Yoo, C.H., 1999. "Improved Design Specifications for Horizontally Curved Steel Girder Highway Bridges," NCHRP Report 424, National Cooperative Highway Research Program, Washington, DC.

Heins, C.P., 1975. Bending and Torsional Design in Structural Members, D.C. Heath and Company.

Kuo, J.T.C., and Heins, Jr., C.P., 1971. "Behavior of Composite Beams Subjected to Torsion", University of Maryland Civil Engineering Research Report #39, College Park, MD.

Kollbrunner, C.F., and Basler, K., 1969. Torsion in Structures, Springer-Verlag.

Linzell, D.G., 1999. "Studies of a Full-Scale Horizontally Curved Steel I-Girder Bridge System Under Self-Weight," Ph.D. Thesis, School of Civil and Environmental Engineering, Georgia Institute of Technology, Atlanta, GA.

Mozer, J., Cook, J., and Culver, C.G., 1975. "Horizontally Curved Highway Bridges, Stability of Curved Plate Girders – Report P3," Federal Highway Administration, Report No. FHWA-RD-75-XXX, Washington, DC.

Mozer, J., and Culver, C.G., 1975. "Horizontally Curved Highway Bridges, Stability of Curved Plate Girders – Report P1," Federal Highway Administration, Report No. FHWA-RD-75-XXX, Washington, DC.

Mozer, J., Ohlson, R., and Culver, C.G., 1975. "Horizontally Curved Highway Bridges, Stability of Curved Plate Girders – Report P2," Federal Highway Administration, Report No. FHWA-RD-75-XXX, Washington, DC.

Nakai, H., Kitada, T., and Ohminami R., 1985. "Experimental Study on Buckling and Ultimate Strength of Curved Girders Subject to Combined Loads of Bending and Shear," *Proceedings of Japan Society of Civil Engineers*, No. 356/I-3.

Nakai, H., and Kotoguchi, H., 1983. "A Study on Lateral Buckling Strength and Design Aid for Horizontally Curved I-Girder Bridges," *Proceedings of Japan Society of Civil Engineers*, No. 339.

Shanmugam, N.E., Thevendran, V., Liew, J.Y.R., and Tan, L.O.,1995. "Experimental Study on Steel Beams Curved in Plan," *ASCE Journal of Structural Engineering*, V121, N2, pp. 249-259.

Shore, S. and Lapore, J.A., 1975. "Horizontally Curved Highway Bridges – Small Scale Model Tests," Federal Highway Administration, Report No. FHWA-RD-93-133, Washington, DC.

Spates, K.R. and Heins, Jr., C.P., 1968. "The Analysis of Single Curved Girders with Various Loadings and Boundary Conditions," University of Maryland Civil Engineering Research Report #20, College Park, MD.

SSRC, 1991. "Horizontally Curved Girders – A Look to the Future," Report of the Annual Task Group 14 Meeting, Structural Stability Research Council.

Timoshenko, S.P., 1953. Collected Papers, McGraw-Hill.

White, D.W. and Grubb, M.A., 2005. "Unified Resistance Equations for Design of Curved and Tangent Steel Bridge I-Girders," Transportation Research Board, Proceedings of the 84th Annual Meeting, Washington, DC.

White, D.W., Zureick, A.H., Phoawanich, N., and Jung, S.-K., 2001. "Development of Unified Equations for Design of Curved and Straight Steel Bridge I Girders," Final Report to American Iron and Steel Institute Transportation and Infrastructure Committee, Professional Service Industries, Inc. and the Federal Highway Administration, School of Civil and Environmental Engineering, Georgia Institute of Technology, Atlanta, GA.

Zureick, A., Naqib, R., and Yadlosky, J. M., 1994. "Curved Steel Bridge Research Project Report I, Synthesis," Federal Highway Administration, Report No. FHWA-RD-93-129, Washington, DC.